

**A Thesis Submitted for the Degree of PhD at the University of Warwick**

**Permanent WRAP URL:**

<http://wrap.warwick.ac.uk/108022/>

**Copyright and reuse:**

This thesis is made available online and is protected by original copyright.

Please scroll down to view the document itself.

Please refer to the repository record for this item for information to help you to cite it.

Our policy information is available from the repository home page.

For more information, please contact the WRAP Team at: [wrap@warwick.ac.uk](mailto:wrap@warwick.ac.uk)

**A thesis**

**entitled**

**Kinetics and Mechanism of the  
Complexation of Labile Metal  
Ions by Macrocyclic Ligands.**

**by**

**Andrew Mark Wynn, BSc (hons)**

**Submitted to the University of Warwick in  
fulfilment of the requirements for the  
award of the degree of Doctor of Philosophy**

**Department of Chemistry and Molecular Sciences  
University of Warwick  
September 1989**

0812078

## Table of Contents

	Page
List of Figures.	
List of Tables.	
Acknowledgements.	
Declaration.	
Summary.	
Abbreviations.	
Dedication.	
 Chapter 1.	
1.1 Introduction.	1
1.2 Substitution Reactions of Labile Metal Ions; Monodentate Ligands.	2
1.3 Substitution Reactions of Labile Metal Ions; Bidentate Ligands.	7
1.4 Substitution Reactions of Labile Metal Ions; Multidentate Ligands.	12
1.5 Substitution Reactions of Labile Metal Ions; Macrocyclic Ligands.	15
(a) Macrocycles reacting at rates comparable to open-chain ligands.	15
(b) Effect of ring size.	17
(c) Effect of alkylation.	19
(d) Effect of rigidity.	22
(e) Effect of protonation.	25
(f) Effect of number of donors.	27
(g) Effect of mixed donor atoms.	27
(h) Macrocyclic polythiaethers.	28

	Page
(i) Macrocyclic polyethers.	30
(j) Macrobicyclic ligands.	32
1.6 Dissociation Reactions of Macrocyclic Complexes.	34
1.7 The Thermodynamics of Macrocyclic Complexes; "The Macrocyclic Effect."	46

**Chapter 2. The Kinetics of Complexation of 1,4,8,11-tetra-azacyclotetradecane and 1,4,7-triazacyclotetradecane with  $Ni^{2+}$ ,  $Co^{2+}$ , and  $Cu^{2+}$  Ions in Dimethyl Sulphoxide Solution.**

2.1 Introduction.	56
2.2 Experimental.	58
2.2.1 Materials and Syntheses.	58
2.2.2 Kinetic Measurements.	61
2.3 Results.	62
2.3.1 The Complexation Reaction between $Ni^{2+}$ and Cyclam in dmso.	62
2.3.2 The Complexation Reaction between $Ni^{2+}$ and [9]ane $N_3$ in dmso.	64
2.3.3 The Complexation Reaction between $Cu^{2+}$ and Cyclam in dmso.	65
2.3.4 The Complexation Reaction between $Cu^{2+}$ and [9]ane $N_3$ in dmso.	65
2.3.5 The Complexation Reaction between $Co^{2+}$ and Cyclam in dmso.	66
2.3.6 The Complexation Reaction between $Co^{2+}$ and [9]ane $N_3$ in dmso.	67
2.4 Discussion.	68

**Chapter 3. Rates and Mechanism of Co-ordination of Labile Metal Ions with Tri- and Tetra-aza Macrocycles Functionalised with a Single Pendent Co-ordinating 2,2'-Bipyridyl-6-yl-methyl Arm.**

3.1 Introduction.	80
3.2 Experimental.	85
3.3 Results.	85

	Page
3.3.1 The Complexation Reaction between $Ni^{2+}$ and 1-(2,2'-bipyridyl-6-yl-methyl)-1,4,8,11-tetraazacyclotetradecane in dms0.	85
3.3.2 The Complexation Reaction between $Ni^{2+}$ and 1-(2,2'-bipyridyl-6-yl-methyl)-1,4,7-triazacyclononane in dms0.	86
3.3.3 The Complexation reaction between $Co^{2+}$ and 1-(2,2'-bipyridyl-6-yl-methyl)-1,4,8,11-tetraazacyclotetradecane in dms0.	87
3.3.4 The Complexation reaction between $Co^{2+}$ and 1-(2,2'-bipyridyl-6-yl-methyl)-1,4,7-triazacyclononane in dms0.	87
3.3.5 The Complexation Reaction between $Cu^{2+}$ and 1-(2,2'-bipyridyl-6-yl-methyl)-1,4,8,11-tetraazacyclotetradecane in dms0.	88
3.3.6 The Complexation Reaction between $Cu^{2+}$ and 1-(2,2'-bipyridyl-6-yl-methyl)-1,4,7-triazacyclononane in dms0.	88
3.3.7 The Complexation Reaction between $Zn^{2+}$ and 1-(2,2'-bipyridyl-6-yl-methyl)-1,4,8,11-tetraazacyclotetradecane in dms0.	89
3.3.8 The Complexation Reaction between $Zn^{2+}$ and 1-(2,2'-bipyridyl-6-yl-methyl)-1,4,7-triazacyclononane in dms0.	90
3.3.9 The Complexation Reactions between $Mn^{2+}$ and 1-(2,2'-bipyridyl-6-yl-methyl)-1,4,8,11-tetraazacyclotetradecane and 1-(2,2'-bipyridyl-6-yl-methyl)-1,4,7-triazacyclononane in dms0.	90
3.4 Discussion.	91

Chapter 4. Rates and Mechanism of Co-ordination of Labile Transition Metal Ions with Tetra-aza Macrocycles Containing a Pyridine Group.

4.1 Introduction.	104
4.2 Experimental.	104
4.3 Results.	105
4.3.1 The Complexation Reaction between $Ni^{2+}$ and $PyN_3$ in dms0.	105
4.3.2 The Complexation Reaction between $Ni^{2+}$ and $Me-PyN_3$ in dms0.	105

	Page
4.3.3 The Complexation Reaction between $\text{Ni}^{2+}$ and $\text{Me}_3\text{-PyN}_3$ in dmso.	106
4.3.4 The Complexation Reaction between $\text{Co}^{2+}$ and $\text{PyN}_3$ in dmso.	106
4.3.5 The Complexation Reaction between $\text{Co}^{2+}$ and $\text{Me-PyN}_3$ in dmso.	107
4.3.6 The Complexation Reaction between $\text{Co}^{2+}$ and $\text{Me}_3\text{-PyN}_3$ in dmso.	108
4.3.7 The Complexation Reaction between $\text{Cu}^{2+}$ and $\text{PyN}_3$ in dmso.	108
4.3.8 The Complexation Reaction between $\text{Cu}^{2+}$ and $\text{Me-PyN}_3$ in dmso.	109
4.3.9 The Complexation Reaction between $\text{Cu}^{2+}$ and $\text{Me}_3\text{-PyN}_3$ in dmso.	110
4.4 Discussion.	110
 Chapter 5. A Study of Amine Modified Silica Gels.	
5.1 Introduction.	122
5.1.1 Silica Gel:- Surface Structure and Metal Binding.	122
5.1.2 Modified Silica Gels:- Syntheses and Metal Binding.	129
5.1.3 Macrocycles Bonded to Silica Gel.	140
5.1.4 Introduction to the Present Study.	143
5.2 Experimental.	143
5.2.1 Materials and Syntheses.	143
5.2.2 Metal Uptake Studies.	146
5.3 Results and Discussion.	147
 Appendix 1.	
Appendix 2.	167
Appendix 3.	172
References.	177

### List of Figures

	Page or Following Page
1.1 The I. C. B. mechanism for $Ni^{2+}$ and ethylenediamine.	10
1.2 Stepwise substitution of an $N_4$ macrocycle with $Cu^{2+}$ .	15
1.3 Penta-co-ordinate intermediate in the reactions of $Ni^{2+}$ and $Cu^{2+}$ with $N_4$ macrocycles.	21
1.4 Proposed structures of $Cu^{2+}$ / diamide $N_4$ macrocycle complexes.	24
1.5 Ring size effects for $Cu^{2+}$ / tetrathiaether complexes.	28
1.6 Non-linear dependence of $k_f$ on reacting metal ionic radius for valinomycin.	31
1.7 Stepwise dissociation mechanism for $[Cu(tet-b)(blue)]^{2+}$ .	36
1.8 Plot of $k_{obs}$ against $[H^+]$ for $Cu^{2+}$ / $N_3$ complexes.	38
1.9 Dissociation mechanism of $Cu^{2+}$ / $N_5$ complexes.	40
1.10 Factors influencing solution stability of complexes.	47
1.11 Formation parameters for formation of $Cu^{2+}$ /polyamine complexes.	50
1.12 Variation of $\log K$ with chelate ring size for $N_4$ macrocyclic complexes.	51
1.13 Ring size effects for $Cu^{2+}$ / tetrathiaether complexes.	54
2.1 Electronic spectra of $Ni^{2+}$ and Cyclam in dmsO.	62
2.2 Typical stopped-flow trace for the reaction of $Ni^{2+}$ and cyclam.	63
2.3 First-order plot for the initial step in the reaction of $Ni^{2+}$ and cyclam.	63
2.4 The first-order dependence of $k_{obs}$ on $[Ni^{2+}]$ for step 1.	63
2.5 Eyring plot for step 1 in the reaction of $Ni^{2+}$ and cyclam.	63
2.6 Fit of $Ni^{2+}$ /cyclam kinetic data to consecutive first-order kinetics.	64
2.7 Electronic spectra of $Ni^{2+}$ and $[9]aneN_3$ in dmsO.	64
2.8 The first-order dependence of $k_{obs}$ on $[Ni^{2+}]$ for step 1.	64
2.9 Eyring plot for step 1 in the reaction of $Ni^{2+}$ and $[9]aneN_3$ .	64
2.10 Electronic spectra of $Cu^{2+}$ and cyclam in dmsO.	65

	Page or Following Page
2.11 Typical stopped-flow trace for the $\text{Cu}^{2+}$ / cyclam reaction.	65
2.12 The first-order dependence of $k_{\text{obs}}$ on $[\text{Cu}^{2+}]$ for step 1.	65
2.13 Eyring plot for step 1 in the reaction of $\text{Cu}^{2+}$ and cyclam.	65
2.14 Eyring plot for step 2 in the reaction of $\text{Cu}^{2+}$ and cyclam.	65
2.15 Electronic spectra of $\text{Cu}^{2+}$ and [9]ane $\text{N}_3$ in dmsO.	65
2.16 The first-order dependence of $k_{\text{obs}}$ on $[\text{Cu}^{2+}]$ for step 1.	66
2.17 Eyring plot for step 1 in the reaction of $\text{Cu}^{2+}$ and [9]ane $\text{N}_3$ .	66
2.18 Electronic spectra of $\text{Co}^{2+}$ and cyclam in dmsO.	66
2.19 Typical stopped-flow traces for the $\text{Co}^{2+}$ / cyclam reaction.	66
2.20 The first-order dependence of $k_{\text{obs}}$ on $[\text{Co}^{2+}]$ for step 1.	66
2.21 Eyring plot for step 1 in the reaction of $\text{Co}^{2+}$ and cyclam.	67
2.22 Plot showing non-first-order kinetics for 3rd stage in the $\text{Co}^{2+}$ /cyclam 67 reaction.	
2.23 Linear fit of data for 3rd stage to 2nd order kinetics in the reaction of 67 $\text{Co}^{2+}$ and cyclam.	
2.24 Electronic spectra of $\text{Co}^{2+}$ and [9]ane $\text{N}_3$ in dmsO.	67
2.25 The first-order dependence of $k_{\text{obs}}$ on $[\text{Co}^{2+}]$ for step 1.	68
2.26 Eyring plot for step 1 in the reaction of $\text{Co}^{2+}$ and [9]ane $\text{N}_3$ .	68
3.1 Electronic spectra of $\text{Ni}^{2+}$ and Cyclam-Bipy in dmsO.	85
3.2 The first-order dependence of $k_{\text{obs}}$ on $[\text{Ni}^{2+}]$ for step 1.	86
3.3 Eyring plot for step 1 in the reaction of $\text{Ni}^{2+}$ and Cyclam-Bipy.	86
3.4 Linear first-order plot of data for the 2nd step in the reaction between 86 $\text{Ni}^{2+}$ and Cyclam-Bipy.	
3.5 Electronic spectra of $\text{Ni}^{2+}$ and [9]ane $\text{N}_3$ -Bipy in dmsO.	86
3.6 Typical stopped-flow trace for the $\text{Ni}^{2+}$ and [9]ane $\text{N}_3$ -Bipy reaction.	86
3.7 The first-order dependence of $k_{\text{obs}}$ on $[\text{Ni}^{2+}]$ for step 1.	86
3.8 Eyring plot for step 1 in the reaction of $\text{Ni}^{2+}$ and [9]ane $\text{N}_3$ -Bipy.	86

	Page or Following Page
3.9 Electronic spectra of $\text{Co}^{2+}$ and Cyclam-Bipy in dmsO.	87
3.10 The first-order dependence of $k_{\text{obs}}$ on $[\text{Co}^{2+}]$ for step 1.	87
3.11 Eyring plot for step 1 in the reaction of $\text{Co}^{2+}$ and Cyclam-Bipy.	87
3.12 Electronic spectra of $\text{Co}^{2+}$ and [9]aneN <sub>3</sub> in dmsO.	87
3.13 The first-order dependence of $k_{\text{obs}}$ on $[\text{Co}^{2+}]$ for step 1.	88
3.14 Eyring plot for step 1 in the reaction of $\text{Co}^{2+}$ and [9]aneN <sub>3</sub> -Bipy.	88
3.15 Electronic spectra of $\text{Cu}^{2+}$ and Cyclam-Bipy in dmsO - U. V. region.	88
3.16 Electronic spectra of $\text{Cu}^{2+}$ and Cyclam-Bipy in dmsO - visible region.	88
3.17 Electronic spectra of $\text{Cu}^{2+}$ and [9]aneN <sub>3</sub> -Bipy in dmsO/visible region.	88
3.18 Electronic spectra of $\text{Cu}^{2+}$ and Cyclam-Bipy in dmsO - U. V. region.	89
3.19 The first-order dependence of $k_{\text{obs}}$ on $[\text{Cu}^{2+}]$ for step 1.	89
3.20 Electronic spectra of $\text{Zn}^{2+}$ and Cyclam-Bipy in dmsO.	89
3.21 The first-order dependence of $k_{\text{obs}}$ on $[\text{Zn}^{2+}]$ for step 1.	89
3.22 Eyring plot for step 1 in the reaction of $\text{Zn}^{2+}$ and Cyclam-Bipy - forward reaction.	89
3.23 Eyring plot for step 1 in the reaction of $\text{Zn}^{2+}$ and Cyclam-Bipy - reverse reaction.	89
3.24 Eyring plot for step 2 in the reaction of $\text{Zn}^{2+}$ and Cyclam-Bipy.	90
3.25 Electronic spectra of $\text{Zn}^{2+}$ and [9]aneN <sub>3</sub> -Bipy in dmsO.	90
3.26 The first-order dependence of $k_{\text{obs}}$ on $[\text{Zn}^{2+}]$ for step 1.	90
3.27 Eyring plot for step 1 in the reaction of $\text{Zn}^{2+}$ and [9]aneN <sub>3</sub> -Bipy - forward reaction.	90
3.28 Eyring plot for step 1 in the reaction of $\text{Zn}^{2+}$ and [9]aneN <sub>3</sub> -Bipy - reverse reaction.	90
3.29 Eyring plot for step 2 in the reaction of $\text{Zn}^{2+}$ and [9]aneN <sub>3</sub> -Bipy.	90
3.30 Electronic spectra of $\text{Mn}^{2+}$ and [9]aneN <sub>3</sub> -Bipy in dmsO.	91
3.31 Crystal structures of some [9]aneN <sub>3</sub> -Bipy complexes.	101

	Page or Following Page
4.1 Electronic spectra of $\text{Ni}^{2+}$ and $\text{PyN}_3$ in dmsu.	105
4.2 Typical stopped-flow trace for the reaction of $\text{Ni}^{2+}$ and $\text{PyN}_3$ .	105
4.3 The first-order dependence of $k_{\text{obs}}$ on $[\text{Ni}^{2+}]$ for step 1.	105
4.4 Eyring plot for step 1 in the reaction of $\text{Ni}^{2+}$ and $\text{PyN}_3$ .	105
4.5 Electronic spectra of $\text{Ni}^{2+}$ and $\text{Me-PyN}_3$ in dmsu.	105
4.6 Non-linear first-order fit of the whole data set for the reaction of $\text{Ni}^{2+}$ and $\text{Me-PyN}_3$ .	105
4.7 The first-order dependence of $k_{\text{obs}}$ on $[\text{Ni}^{2+}]$ for step 1.	106
4.8 Eyring plot for step 1 in the reaction of $\text{Ni}^{2+}$ and $\text{Me-PyN}_3$ .	106
4.9 Electronic spectra of $\text{Ni}^{2+}$ and $\text{Me}_3\text{-PyN}_3$ in dmsu - visible region.	106
4.10 The first-order dependence of $k_{\text{obs}}$ on $[\text{Ni}^{2+}]$ for step 1.	106
4.11 Eyring plot for step 1 in the reaction of $\text{Ni}^{2+}$ and $\text{Me}_3\text{-PyN}_3$ .	106
4.12 Electronic spectra for $\text{Ni}^{2+}$ and $\text{Me}_3\text{-PyN}_3$ in dmsu - U. V. region.	106
4.13 Electronic spectra of $\text{Co}^{2+}$ and $\text{PyN}_3$ in dmsu.	106
4.14 The first-order dependence of $k_{\text{obs}}$ on $[\text{Co}^{2+}]$ for step 1.	107
4.15 Eyring plot for step 1 in the reaction of $\text{Co}^{2+}$ and $\text{PyN}_3$ .	107
4.16 Electronic spectra of $\text{Co}^{2+}$ and $\text{Me-PyN}_3$ in dmsu.	107
4.17 Stopped-flow trace showing consecutive first-order kinetics.	107
4.18 Non-linear first-order fit of whole data set in the reaction of $\text{Co}^{2+}$ and $\text{Me-PyN}_3$ .	107
4.19 The first-order dependence of $k_{\text{obs}}$ on $[\text{Co}^{2+}]$ for step 1.	107
4.20 Eyring plot for step 1 in the reaction of $\text{Co}^{2+}$ and $\text{Me-PyN}_3$ .	107
4.21 Eyring plot for step 2 in the reaction of $\text{Co}^{2+}$ and $\text{Me-PyN}_3$ .	108
4.22 Electronic spectra of $\text{Co}^{2+}$ and $\text{Me}_3\text{-PyN}_3$ in dmsu.	108
4.23 The first-order dependence of $k_{\text{obs}}$ on $[\text{Co}^{2+}]$ for step 1.	108
4.24 Eyring plot for step 1 in the reaction of $\text{Co}^{2+}$ and $\text{Me}_3\text{-PyN}_3$ .	108
4.25 Electronic spectra of $\text{Cu}^{2+}$ and $\text{PyN}_3$ in dmsu.	108

	Page or Following Page
4.26 The first-order dependence of $k_{\text{obs}}$ on $[\text{Cu}^{2+}]$ for step 1.	109
4.27 Electronic spectra of $\text{Cu}^{2+}$ and $\text{Me-PyN}_3$ in dmsO.	109
4.28 Stopped-flow trace showing consecutive first-order kinetics at 568 nm.	109
4.29 Stopped-flow trace showing consecutive first-order kinetics at 700 nm.	109
4.30 The first-order dependence of $k_{\text{obs}}$ on $[\text{Cu}^{2+}]$ for step 1.	109
4.31 Eyring plot for step 1 in the reaction of $\text{Cu}^{2+}$ and $\text{Me-PyN}_3$ - forward reaction.	109
4.32 Eyring plot for step 1 in the reaction of $\text{Cu}^{2+}$ and $\text{Me-PyN}_3$ - reverse reaction.	109
4.33 Electronic spectra of $\text{Cu}^{2+}$ and $\text{Me}_3\text{-PyN}_3$ in dmsO.	110
4.34 The first-order dependence of $k_{\text{obs}}$ on $[\text{Cu}^{2+}]$ for step 1.	110
4.35 Eyring plot for step 1 in the reaction of $\text{Cu}^{2+}$ and $\text{Me}_3\text{-PyN}_3$ - forward reaction.	110
4.36 Eyring plot for step 1 in the reaction of $\text{Cu}^{2+}$ and $\text{Me}_3\text{-PyN}_3$ - reverse reaction.	110
4.37 Variation of $k_f$ for initial reaction on ligand methylation.	119
4.38 Crystal structure of free ligand related to $\text{PyN}_3$ .	119
5.1 I. R. spectra of heat treated silica gel.	123
5.2 CP / MAS $^{29}\text{Si}$ nmr spectrum of Fisher S-157 silica gel.	123
5.3 187 MHz $^1\text{H}$ CRAMPS spectra of Fisher S-679 silica gel.	123
5.4 Quantitative $^{29}\text{Si}$ MAS nmr spectra of surface treated silica gel.	124
5.5 Average structure of Fisher S-157 silica gel.	124
5.6 Bulk hydroxyl density as a function of temperature.	126
5.7 DeBoer and Vleeskins model of the surface of silica gel.	126
5.8 Hockey model of the surface of silica gel.	126
5.9 Peri and Hensley model of the surface of silica gel.	127
5.10 Sindorf and Maciel model of the surface of silica gel.	127

	Page or Following Page
5.11 Metal extraction onto silica gel as a function of pH.	127
5.12 Adsorption of $\text{Cu}^{2+}$ and $\text{SiO}^-$ concentration as a function of pH.	128
5.13 Proposed structure of $\text{Cu}(\text{bipy})_2(\text{SiO}^-)_2$ surface complex.	128
5.14 Extraction of $\text{Cu}^{2+}$ onto various functionalised silica gels.	133
5.15 CP / MAS $^{29}\text{Si}$ nmr spectra of modified silica gels.	135
5.16 CP / MAS $^{29}\text{Si}$ nmr spectra of silica gel reacted with $\text{Si}(\text{CH}_3)_2\text{Cl}_2$ .	136
5.17 $^{13}\text{C}$ nmr spectrum of a diamine modified silica gel.	139
5.18 Metal adsorption for a modified silica gel.	140
5.19 $^{13}\text{C}$ CP / MAS nmr spectra of modified silica gels.	152
5.20 Metal uptake for cyclam modified silica gel.	153
5.21 Linear fit of $\text{Co}^{2+}$ uptake onto gel 5 to the Langmuir isotherm.	157
5.22 Anti-Langmuirian characteristics of $\text{Cu}^{2+}$ uptake onto gel 6.	158

### List of Tables

	Page or Following Page
1.1 Values of $K_{\text{eq}}$ calculated for various solvents.	4
1.2 Resolved rate constants for the Ni(II) / alkylamine reaction systems.	5
1.3 Resolved rate constants and $K_{\text{eq}}$ for the formation of $\text{Ni}^{2+}$ complexes.	6
1.4 Resolved rate constants for the reactions of Ni(II) with N-alkyl substituted ethylenediamines.	9
1.5 Rate constants relating to the SCS mechanism for formation of chelate complexes.	11
1.6 Rates of water exchange for various Ni(amine) $_2^{2+}$ complexes.	13
1.7 Rate constants for the reaction of $\text{Ni}^{2+}$ with various ligands.	13
1.8 Resolved rate constants for the reaction of $\text{Cu}(\text{OH})_2$ (II) species with 16 various polyamines.	16
1.9 Resolved rate constants for the reaction of $\text{Ni}^{2+}$ with various ligands.	17
1.10 Rate constants for the reaction of various macrocycles with $\text{Cu}^{2+}$ .	18
1.11 Rate constants for the reaction of $\text{Cu}^{2+}$ with $\text{N}_3$ macrocycles.	19
1.12 Rate constants for the reactions of Cu(II) species with $\text{N}_5$ macrocycles.	19
1.13 Rate constants for the reactions of $\text{Ni}^{2+}$ , $\text{Cu}^{2+}$ , $\text{Co}^{2+}$ and $\text{Zn}^{2+}$ with 20 $\text{N}_4$ macrocycles.	20
1.14 Rate constants for the reactions of $\text{Ni}^{2+}$ and $\text{Cu}^{2+}$ with methylated cyclams.	21
1.15 Rate constants for the reaction of $\text{Cu}^{2+}$ with various ligands.	22
1.16 Rate constants for the reaction of $\text{Cu}(\text{O}_2\text{CMe})^+$ with various ligands.	25
1.17 Protonation constants for various polyamines.	26
1.18 Rate constants for the reactions of $\text{Cu}^{2+}$ with polythiaethers.	30
1.19 Rate constants for the reaction of 18-crown-6 with various cations.	32
1.20 Observed first-order rate constants for the dissociation of various	35

	Page or Following Page
Cu(II) species.	
1.21 Resolved rate constants for the dissociation and isomerisation of [Cu(tet-a)(blue)] <sup>2+</sup> .	36
1.22 Rate constants for the dissociation of Ni <sup>2+</sup> / N <sub>3</sub> complexes.	37
1.23 Rate constants for the dissociation of various Cu <sup>2+</sup> complexes.	39
1.24 Variation in acid dissociation rate constant with ring size.	41
1.25 Acid dissociation rate constants for Ni <sup>2+</sup> and Cu <sup>2+</sup> complexes.	42
1.26 Rate constants for the dissociation of Ni <sup>2+</sup> / N <sub>2</sub> O <sub>2</sub> complexes.	44
1.27 Calculated rate constants for the dissociation of Cu <sup>2+</sup> / S <sub>x</sub> complexes.	45
1.28 Stability constants for various Cu <sup>2+</sup> / N <sub>4</sub> complexes.	48
1.29 Stability constants and enthalpies and entropies of formation for various Ni <sup>2+</sup> complexes.	49
1.30 Stability constants and enthalpies and entropies of formation for Cu <sup>2+</sup> / polyamine complexes.	53
1.31 Stability constants and thermodynamic parameters for Cu <sup>2+</sup> / N <sub>2</sub> S <sub>2</sub> complex formation.	54
2.1 Measured rate constants for the reaction of various macrocyclic ligands with labile transition metals.	69
2.2 Calculated values for n.	72
2.3 Activation parameters for the reactions in table 2.1.	74
3.1 Formation rate constants of metal ions with various ligands.	82
3.2 Measured rate constants for the reactions of various pendent arm ligands with labile transition metal ions.	92
3.3 Comparison of rate constants for various Ni <sup>2+</sup> and Co <sup>2+</sup> reactions.	92
3.4 Calculated values of n.	93
3.5 Comparison of logK <sub>1</sub> for bipy and bipy/macrocycle species.	96
3.6 Comparison of forward rate constants for various Zn <sup>2+</sup> reactions.	98

	Page or Following Page
3.7 Comparison of reverse rate constants for various $Zn^{2+}$ reactions.	98
3.8 Activation parameters for the reactions of two single pendent arm macrocycles with labile transition metal ions.	99
3.9 Comparison of Activation enthalpies for various $Ni^{2+}$ and $Co^{2+}$ reactions.	101
4.1 Rate constants and activation parameters for the reactions of $Co^{2+}$ with $PyN_3$ 's.	111
4.2 Rate constants and activation parameters for the reactions of $Ni^{2+}$ with $PyN_3$ 's	114
4.3 Rate constants and activation parameters for the reactions of $Cu^{2+}$ with $PyN_3$ 's	117
5.1 Elemental analyses for gels 1 - 6.	148
5.2 Comparison of observed and calculated C / N ratios.	149
5.3 Calculated surface density and silanol coverage.	151
5.4 Metal uptake data for gel 5.	154
5.5 Maximum uptake of $Cu^{2+}$ in gels 1 - 6.	155
5.6 $Cu^{2+}$ capacity of various modified silica gels.	156
5.7 Data calculated from the Langmuir isotherm equation.	157
5.8 U. V. / visible diffuse reflectance data.	158

### Acknowledgements

I would like to take this opportunity to thank my supervisor, Dr. Peter Moore, for his helpful advice throughout the course of this work, and for introducing me to macrocycles and kinetics.

I would also like to thank the members of Peter Moore's research group for useful discussions, Dr. Fiona McLaren for the gift of the ligands in Chapter 3, Mr Eric Burgess for repairing the fragile glassware of the stopped-flow apparatus and to Dr. Mark E. Smith for obtaining the  $^{13}\text{C}$  CP MAS solid state n.m.r. spectra in the final chapter. I would particularly like to thank my wife, Joanne, for drawing all the illustrations and for helping me when things got tough.

The work described in this thesis was carried out in the Department of Chemistry and Molecular Sciences between October 1986 and September 1989, the facilities of which are gratefully acknowledged. I also wish to acknowledge the Science and Engineering Research Council and my industrial sponsors the United Kingdom Atomic Energy Authority (Winfrith) for their funding of my work.

### Declaration

To the best of my knowledge, the work described in this thesis is original. Part of this work has been published in the scientific literature, with the following reference:

F. McLaren, P. Moore, and A. M. Wynn;  
J. Chem. Soc., Chem. Commun., 1989, 798.

Though further publications are in preparation.

### Summary

The kinetics of complexation of labile transition metal ions with three classes of macrocyclic N-donor ligands have been studied in dmsO solution using pseudo-first-order conditions and employing the stopped-flow technique, with observation of U. V. / visible absorbance changes on reaction. All reactions studied displayed biphasic, consecutive first-order kinetics with an initial, rapid step which was first-order in both metal and ligand, followed by a second, slower step which was independent of the metal concentration.

The unsubstituted macrocycles cyclam and [9]aneN<sub>9</sub> reacted via a dissociative interchange mechanism with the formation of an unstable intermediate which isomerises to the stable product. This intermediate is proposed to involve full co-ordination of the macrocycles to the metal ions with one or more N atoms co-ordinated in an unstable configuration.

For the same macrocycles, each containing a single, pendent co-ordinating 2,2'-bipyridyl-6-yl-methyl arm, the complexation reactions occurred via an intermediate which involved co-ordination of the metal ions to the bipyridyl moiety, the ensuing slower reaction involving co-ordination of the macrocyclic moiety. This presents the most clear-cut evidence so far that pendent arm macrocycles react initially by co-ordination to the pendent arm.

For N<sub>4</sub> macrocycles, with a pyridine group substituted for a secondary amine, the reactions occur by initial attack at the secondary amines adjacent to the pyridine moiety. With the tri-methylated form of the macrocycle Ni<sup>2+</sup> ions react more rapidly than do Co<sup>2+</sup> ions, which is very unusual. This behaviour is explained by proposing a different reaction mechanism for each ion with Me<sub>3</sub>-PyN<sub>4</sub> as the final products are of different geometries. With Cu<sup>2+</sup> an unstable intermediate is formed involving formation of only one Cu-N bond.

The properties of silica gels modified with open-chain and macrocyclic polyamines were also studied. The less bulky and least sterically hindered polyamines were bound to the surfaces in greater quantities, although pretreatment involving heating at high temperatures significantly improved the binding of cyclam to the surfaces. An investigation of the uptake of transition metal ions from aqueous solutions illustrated the important role that the surface structure has to play on the activity of the binding sites. A gel modified with cyclam displayed a high degree of selectivity for Cu<sup>2+</sup> over Co<sup>2+</sup> and Ni<sup>2+</sup> illustrating the potentially important application of such systems in ion selective waste water treatments.

### List of Abbreviations

dmf	dimethylformamide
dmsO	dimethylsulphoxide
F.T.	Fourier Transform
U.V.	Ultra-Violet
I.R.	Infra-Red
S.F.	Stopped Flow
nmr	nuclear magnetic resonance
ppm	parts per million
C.P.	Cross Polarization
MAS	Magic Angle Spinning
CRAMPS	Combined rotation and multiple-pulse spectroscopy
HOQ	8-hydroxyquinoline
esr	electron spin resonance
fac	facial
mer	meridional
sh	shoulder in peak
$\Delta H^\ddagger$	enthalpy of activation
$\Delta S^\ddagger$	entropy of activation
$\Delta G^\ddagger$	free energy of activation
$M^{n+}$	metal ion (n valent)
S	solvent or sulphur
L	ligand
en	ethylene-1,2-diamine
dien	diethylenetriamine
trien	triethylenetetramine
tetren	tetraethylenepentamine
py	pyridine

bipy	2,2'-bipyridine
terpy	2,2':6',2''-terpyridine
cyclam	1,4,8,11-tetraazacyclotetradecane
tmc	1,4,8,11-tetramethyl-1,4,8,11-tetraazacyclotetradecane
tmbc	tetramethyldibenzocyclam
isocyclam	1,4,7,11-tetraazacyclotetradecane
2,2,2-tet	N,N'-Bis(2-aminoethyl)ethylenediamine
2,3,2-tet	N,N'-Bis(2-aminoethyl)-1,3-propanediamine
3,2,3-tet	N,N'-Bis(3-aminopropyl)ethylenediamine
3,3,3-tet	N,N'-Bis(3-aminopropyl)-1,3-propanediamine
[9]aneN <sub>3</sub>	1,4,7-triazacyclononane / znn
[10]aneN <sub>3</sub>	1,5,8-triazacyclodecane / zdn
[12]aneN <sub>3</sub>	1,5,9-triazacyclododecane / zdd
mznn	2-methyl-[9]aneN <sub>3</sub>
zud	1,5,9-triazacycloundecane
zaud	1,6,9-triazacycloundecane
zadd	1,7,10-triazacyclododecane
ztd	1,6,10-triazacyclotridecane
zted	1,7,11-triazacyclotetradecane
ccha	cyclohexane-1,3,5-triamine / <i>cis,cis</i> -tach
tpt	3,3-diaminodipropylamine
Cyclam/bipy	1-(2',2''-Bipyridyl-6'-ylmethyl)-1,4,8,11-tetraazacyclotetradecane
[9]aneN <sub>3</sub> /bipy	1-(2',2''-Bipyridyl-6'-ylmethyl)-1,4,7-triazacyclononane
tet-a	ms-(5,12)-7,7,14,14-Me <sub>2</sub> -1,4,8,11-tetraazacyclotetradecane
tet-b	rac-(5,12)-7,7,14,14-Me <sub>2</sub> -1,4,8,11-tetraazacyclotetradecane
18-crown-6	1,4,7,10,13,16-hexaoxacyclooctadecane
benzo-15-crown-5	benzo-1,4,7,10,13-pentaoxacyclopentadeca-2-ene

**To Joanne**

## Chapter 1

### 1.1 Introduction

The structure and chemistry of amine ligands is very varied and thus provides a useful means of subjectively studying the kinetics and thermodynamics of their reactions with transition metals. The effects of only slight changes in the ligand structure such as adding an extra carbon into the ligand backbone or using bulky groups on donor atoms can be investigated. Thus, the synthesis of the particular amine required is of great importance. Many such syntheses can be carried out quite simply, but as the ligands get more and more complicated the synthetic procedures required to make these compounds become more demanding. Some of the most complicated of these ligands are the macrocyclic amines which are useful, interesting and unique species for probing reaction kinetics and thermodynamics.

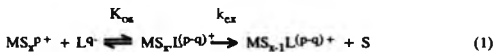
There now exists a whole variety of compounds which are classed as macrocycles, and there are many good books and reviews covering their discovery, synthesis and metal complexes.<sup>1-41</sup>

The work in the first part of this thesis describes a study of the kinetics of complexation of various macrocyclic ligands and shows how the structure of firstly unsubstituted macrocycles, then pendent arm macrocycles, and finally macrocycles containing a pyridine ring affects the reaction kinetics with various divalent first row transition metal ions. The remainder of Chapter 1 is an introduction to these studies, looking at the mechanisms of substitution reactions of amines, and highlighting the significant role synthetic macrocycles have played in this field over the last 20 years.

## 1.2 Substitution Reactions of Labile Metal Ions

### Monodentate Ligands

Labile octahedral metal ions react with monodentate ligands according to the Eigen-Wilkins or interchange mechanism.<sup>42-46</sup>



- M = metal ion (charge p)  
S = solvent  
L = monodentate ligand (charge q)

This two step mechanism involves the initial formation of an outer-sphere complex, the rate of which is diffusion controlled and whose equilibrium constant ( $K_{os}$ ) can thus be calculated using the Fuoss equation:<sup>47</sup>

$$K_{os} = (4/3 \ 000) \pi a^3 N_A e^b \quad (2)$$

$$\text{where } b = Z_a Z_b e_0^2 / 8 \epsilon k T \quad (3)$$

- a = centre to centre distance between the two reaction partners  
at the point of closest approach  
 $N_A$  = Avogadro's Number  
 $Z_a$  &  $Z_b$  = charges on reacting species  
 $K_{os}$  = outer-sphere association constant  
 $e_0$  = electronic charge  
 $\epsilon$  = dielectric constant of medium  
 $k$  = Boltzmann's Constant  
 $T$  = absolute temperature

The second step is the rate determining substitution of the ligand into the coordination sphere of the metal. This step has been found to be dissociative in character for many metals ( $\Delta V^\ddagger$  is positive) and to be independent of the nature of the ligand, and is roughly equal to the rate of exchange of the solvent molecules on the metal ion ( $k_{ex}$ ). All the theory was originally worked out using data from aqueous media, but it has since been found to hold for labile octahedral ions in non-aqueous solvents.<sup>48</sup>

The general rate law for the reaction is:

$$+d[ML^{(p-q)+}]/dt = K_{os}k_{ex}[MP^+][L^q]/(1 + K_{os}[L^q]) \quad (4)$$

but under usual experimental conditions, where  $[MP^+] > [L^q]$ :

$$+d[ML^{(p-q)+}]/dt = K_{os}k_{ex}[MP^+][L^q] \quad (5)$$

Thus, the rate constant for any reaction of a monodentate ligand with an octahedral metal ion can be calculated using the expression;

$$k_f = K_{os}k_{ex} \quad (6)$$

The value of  $k_{ex}$  will depend on the nature of the metal ion and the solvent, whereas  $K_{os}$  will depend on the charge on the ligand, the reaction medium and most importantly, the distance of closest approach between the centre of the nearest donor atom on the ligand (for multidentate ligands) and the centre of the metal ion. This parameter is the most difficult to estimate for the calculation of  $K_{os}$ , as it depends on the subtle combination of many steric and electronic factors involved in the interaction of the bound solvent molecules with the metal and the ligand.

With unprotonated amines the ligands are uncharged and according to the Fuoss equation as the charge of one of the species approaches zero, then the exponential term approaches unity, and the equation reduces to equation (2);

$$K_{os} = n^3 \times 2.52 \times 10^{21} (n \text{ in cm}) \quad (7)$$

For dipolar ligands, with no formal charge, attempts have been made to apply the Fuoss association theory<sup>49</sup> to take into account the expected association between a cation and a dipolar molecule.

$$K_{\text{on}} = (4/3 \ 000)\pi a^3 N_A e^U \quad (8)$$

$$\text{where } U = e\mu/E(a^2 - d^2) \text{ ref. 50} \quad (9)$$

and  $\mu$  = dipole moment of ligand

$a$  = distance between centre of cation and centre of dipole

$d$  = dipole radius

However, in aqueous solution the value of  $e^U$  makes a negligible difference to the expression. Substituting common values of  $\mu$ ,  $a$  and  $d$  into the equation ( e.g.  $\mu = 4$ ,  $a = 7 \times 10^{-8}$  cm,  $d = 6 \times 10^{-8}$  cm ) gives  $e^U = 1.0000106$ , which is clearly so close to unity that it may be neglected. This is not the case with charged ligands, where such factors play an important role.

The value of  $K_{\text{on}}$  is largely solvent dependent and a list of various values calculated for different solvents is given in Table 1.1.

Table 1.1

Values of  $K_{\text{on}}$  calculated for various solvents.

Solvent	$a/\text{\AA}$	$K_{\text{on}}/\text{dm}^3 \text{ mol}^{-1}$	ref.
water	4.0	0.16	51
water	4.9	0.3	52
water	3.4	0.1	53
methanol	5.0	0.32	54
dmsO	3.4-5.8	0.1-0.5	55
dmf	3.4-5.8	0.1-0.5	55
dmsO	6.0	0.54	56
dmsO	7.0	0.86	57
dmsO	6.1	0.57	58

Clearly, the bulkiness of the solvent molecules is an important factor in establishing the value of the association constant. The bulkier dmsO molecules have a larger value than when the smaller water molecules are used as solvent.

As the ligands become more complicated in structure another factor has to be

taken into account. This is because  $K_{oa}$  does not include the fact that the ligand molecule must be properly oriented in the outer-sphere complex for bonding to occur at the time that the metal-solvent bond breaks. If it is not in the correct position then solvent exchange will take place with no substitution of the solvent molecule by the ligand. This competition between solvent and ligand is displayed in the increasing alkylation of ammonia causing a decrease in the rate constants for reaction with  $Ni^{2+}$  in aqueous solution (see Table 1.2), and also manifesting itself in a destabilisation of the 1:1 complexes.

**Table 1.2**

Resolved rate constants for the Ni(II)/alkylamine reaction systems;<sup>59</sup>  
 25 °C,  $\mu = 1.0 \text{ mol dm}^{-3} (\text{HClO}_4)$ .

Ligand	$k_f \times 10^{-3}$ ( $\text{dm}^3 \text{ mol}^{-1} \text{ s}^{-1}$ )	$k_d$ ( $\text{s}^{-1}$ )	$\log K_1$
$\text{NH}_3$	4.48	7.1	2.80
$\text{MeNH}_2$	1.31	7.7	2.23
$\text{EtNH}_2$	0.865	13.3	1.81
$i\text{-PrNH}_2$	0.605	16.8	1.56
$\text{Me}_2\text{NH}$	0.332	11.3	1.47

One attempt to overcome this problem is by the introduction of a "statistical factor" into the Eigen-Wilkins equation;

$$k_f = nK_{oa}k_{-ca} \quad (10)$$

The value of "n" depends therefore on the nature of the solvent, for many systems n can be taken as unity, but there are also many situations where it is not, and it thus becomes an important variable. For instance, Langford suggested that n would represent the probability that a ligand molecule in the second co-ordination sphere, rather than a solvent molecule, occupies the co-ordination site vacated by the dissociating solvent molecule, this means that n would be determined by the number of

sites in the second co-ordination sphere, and values of 0.1 to 0.2 were suggested.<sup>60</sup> Connick proposed a value of 3/4 for *n* on the basis of steric arguments for octahedrally solvated metal ions in water.<sup>61</sup>

A number of studies have been carried out to determine the values of *n* in various solvents.<sup>54, 62-65</sup>

The Eigen-Wilkins equation was originally found to hold by equating values of  $k_f/K_{os}$  with the solvent exchange rates. This was because  $k_f$  could easily be measured, usually using flow or perturbation techniques for labile ions,  $K_{os}$  could be cal-

**Table 1.3**

Rate constants and  $K_{os}$  for the formation of  $Ni^{2+}$  complexes;<sup>66</sup>  
in aqueous solution at 298.2 K.

Ligand	$k_f$ $10^{-3}(\text{dm}^3 \text{mol}^{-1} \text{s}^{-1})$ (measured)	$K_{os}$ (molar scale) (calculated)	$k_{ex}$ $10^{-3}(\text{s}^{-1})$ (derived)
N-methylimidazole <sup>+</sup>	0.23	0.02	12
ammonia	5	0.15	33
hydrogen fluoride	3	0.15	20
imidazole	2.8-6.4	0.15	19-43
1,10-phenanthroline	4.1	0.15	26
fluoride <sup>-</sup>	8	1	8
acetate <sup>-</sup>	100	3	30
oxalateH <sup>-</sup>	5	2	3
oxalate <sup>2-</sup>	75	13	6
methylphosphate <sup>2-</sup>	290	40	7
pyrophosphate <sup>3-</sup>	2100	88	24
tripolyphosphate <sup>4-</sup>	6800	570	12
cf. water exchange			30

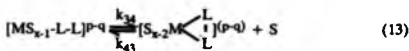
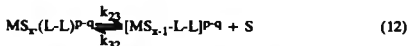
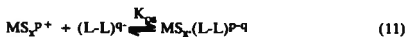
culated from the Fuoss equation, and  $k_{ex}$  was measurable independently usually by nmr techniques. Comparing data for  $k_f/K_{ex}$  with  $k_{ex}$  gave values which were roughly the same, any anomalies require the introduction of the statistical factor. Table 1.3 shows the data for a range of ligands reacting with  $Ni^{2+}$  in aqueous solution.

Once the relationship was established it was then possible to use the equation to determine values of either  $k_f$ ,  $n$ ,  $K_{ex}$  or  $k_{ex}$  using any three of the variables which is of great use in cases where one of the values is not obtainable in other ways or where  $k_{ex}$  for a particular metal has not already been determined in a particular solvent. Thus, the expression can be used to predict solvent exchange rates before they have been measured independently.

### 1.3 Substitution Reactions of Labile Metal Ions

#### Bidentate Ligands

When ligands with two donor atoms react with octahedrally solvated metal ions in solution, the reaction will occur in a similar way to monodentate ligand complexation except that now an extra step is required to close the chelate ring. The mechanism becomes:



Again the first step is diffusion-controlled association of the two reactants. Step 2 is the substitution of one donor atom into the inner co-ordination sphere of the metal ion, and step 3 is the substitution of the second donor atom, closing the chelate ring.

Assuming steady state conditions for the intermediates the rate expression now

becomes:

$$d[X]/dt = K_{08}k_{23}k_{34}[MS_2P^+][(L-L)^9 \cdot ]/(k_{32} + k_{34}) \quad (14)$$

where  $k_{23}$  is equivalent to the solvent exchange rate.

If the rate of chelate ring closure is much faster than the solvent exchange rate of the metal then  $k_{34} \gg k_{32}$  and the expression becomes:

$$d[X]/dt = K_{08}k_{23}[MS_2P^+][(L-L)^9 \cdot ] \quad (15)$$

and since  $k_{23} = k_{ex}$

$$k_f = K_{08}k_{23} \quad (16)$$

This is the same expression as that for monodentate ligands and so many bidentate ligands react at rates comparable to monodentate ligands.

Even for cases where  $k_{34} \approx k_{32}$  the expression will still be:

$$k_f = \frac{1}{2}K_{08}k_{23} \quad (17)$$

and will still approximate to Eigen-Wilkins kinetics.

However if the rate of chelate ring closure becomes much slower than the rate of substitution of the first donor atom, then  $k_{34} \ll k_{32}$  and the expression becomes:

$$k_f = K_{08}k_{23}k_{34}/k_{32} \quad (18)$$

and so the ratio  $k_{34}/k_{32}$  causes the rate constant to be lower than expected by the Eigen-Wilkins mechanism. This mechanism, in which chelate ring closure becomes the rate determining step is generally called the "sterically controlled substitution" or SCS mechanism,<sup>67</sup> though Margerum et al<sup>68</sup> prefer the term "chelation controlled substitution." Thus, it is this ratio of  $k_{34}$  to  $k_{32}$  which controls the kinetics of substitution of bidentate ligands with octahedrally solvated metal ions. In other words, the kinetics are determined by the competition between ring closure and return of a solvent molecule at the point in the mechanism where only one donor atom is bound to the metal ion. This behaviour will be very dependent upon the

geometry and structure of the ligand.

There are some substitution reactions involving bidentate ligands which occur at rates much greater than the Eigen-Wilkins mechanism predicts. This was first seen in the reactions of ethylenediamine and its substituents with  $Ni^{2+}$  in aqueous solution.<sup>69</sup> Table 1.4 shows a comparison of rate constants of complexation of N-alkyl-substituted diamines with  $Ni^{2+}$  (compare with Table 1.2 for the alkylamines).

**Table 1.4**

Resolved rate constants for the reactions of  $Ni^{2+}$  with N-alkyl-substituted diamines;<sup>70</sup> 25.0 °C,  $\mu = 0.1 \text{ mol dm}^{-3}$

Ligand	$k_f(L)$ $\text{dm}^3 \text{ mol}^{-1} \text{ s}^{-1}$	$k_f(HL^+)$ $\text{dm}^3 \text{ mol}^{-1} \text{ s}^{-1}$
en	$\leq 4 \times 10^5$	ca. 200
N,N-diEten	$3.4 \times 10^5$	123
N,N'-diEten	$9.7 \times 10^3$	8.0
TriEten	< 10	-
TeEten	ca. 0	ca. 0
TeMeen	$3.6 \times 10^2$	0.2

The rate of ammonia reacting with  $Ni^{2+}$  is as would be predicted by the dissociative interchange mechanism for a monodentate ligand, i.e.  $k_f = K_{in}k_{ex} = 0.15 \times 3 \times 10^4 = 4.5 \times 10^3 \text{ mol}^{-1} \text{ dm}^3 \text{ s}^{-1}$  (see 1.2). The effect of increasing alkylation can also be seen, in the decreasing values of  $k_f$  (see Table 1.2). However, for the bidentate ligand en the rate constant is now about 90 times faster than a simple monodentate ligand. Again, with increasing alkylation the rate constants decrease until with tetraethyl-en the complex is thermodynamically unfavourable and does not form. Rorabacher<sup>51</sup> suggested that the anomalously high rate for en was due to an increased outer-sphere interaction of the ligand with the hydrated metal ion caused by hydrogen bonding between the basic nitrogen donors and the bound water mole-

cules, thus increasing the value of  $K_{\text{OH}}$ . This is known as the "internal conjugate base (ICB) mechanism" after the conjugate base mechanism (termed  $S_N1$  CB) developed by Basolo and Pearson<sup>71,72</sup> in the 1950's to explain the rapid rate of base induced hydrolysis of halopentamine cobalt(3) complexes in water.

The ICB mechanism is illustrated in Figure 1.1 for the reaction of hexaquo-nickel(2) ion with en. The proposed mechanism consists of five steps; firstly the outer-sphere complex is formed as normal, but then a hydrogen bond is formed between a co-ordinated water molecule and a basic donor atom of the ligand. The metal species thus now has a bound molecule of hydroxyl character and this causes a labilisation of a water molecule in a *cis*-position, promoting rapid substitution of the second donor atom from the same bidentate ligand. Once the first metal-donor bond is established the hydrogen-bond then ruptures, followed by further bonding of the ligand in the normal fashion to close the chelate ring. Thus, the mechanism relies on the basicity and availability of protons on the donor atoms and Turan<sup>73</sup> has observed a linear relationship between the  $pK_a$  of the basic nitrogen atom and the degree of ICB enhancement. This is one reason why in Table 1.4 increasing alkylation causes decreasing rate constants. When there are no protons available for hydrogen bonding, as in the case of tetramethyl- and tetraethyl- en the rates are thus decreased significantly. Steric effects also come into play with these ligands.

It must be stated that this mechanism has been questioned quite convincingly by Jordan<sup>74</sup> who claims that the increased reactivity of the polyamines can be accounted for by normal kinetic effects, and that upholders of the ICB mechanism have neglected important reactions of monoprotonated diamines in the analysis of their results. He suggests that further experiments must be carried out over a wider range of pH than was employed in Rorabacher's studies<sup>75</sup> in order to demonstrate the ICB effect unequivocally and to eliminate possible interferences from a more reactive  $(H_2O)_5NiOH^+$  ion.

Using negative or positively charged ligands will cause an increase and a decrease in rate respectively due to electrostatic attraction/repulsion when reacted

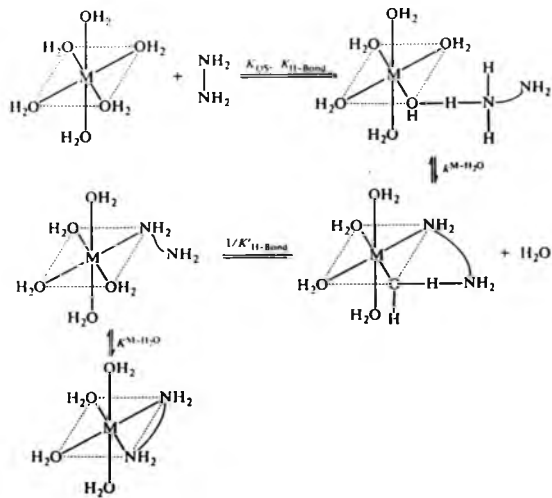


Fig. 1.1 The I. C. B. mechanism for  $\text{Ni}^{2+}$  and ethylenediamine.<sup>68</sup>

with a metal cation. This however, will be taken into account by the outer-sphere association constant term ( $K_{os}$ ) in the Eigen-Wilkins equation, and will not produce anomalous results by themselves.

The main factor which causes a decrease in the expected rate constants for bidentate ligand substitution reactions is steric hindrance. Sterically hindered ligands will destabilise the singly bound species relative to unhindered ligands and will increase the value of  $k_{32}$  in the mechanism. Increasing the ring size also has the same effect, but this time it is due to a reduction in the value of  $k_{34}$ . This is because as the ligand backbone gets longer the likelihood that the free end of the ligand in the singly-bonded intermediate will be in exactly the right position to take advantage of the vacant site on the metal ion during the very short time before an adjacent solvent molecule fills the space will be reduced. Examples of the effect of increasing steric hindrance and ring size are shown in Table 1.5 for various amino acids reacting with divalent transition metal cations.

It has been established that in these amino acids the carboxylate end bonds to the metal first<sup>68,79</sup> where ring closure is the rate determining step due to:

- (a) electrostatic attraction between the  $\text{COO}^-$  group and the positively charged metal ion, and
- (b) the ICB effect causing outer-sphere association between a co-ordinated water molecule and the amino group, speeding up the binding of the carboxylate group.

This causes the  $k_{34}/k_{32}$  ratio to be less than unity, and so the ring closure rates become rate determining. This argument is in contrast to the suggestion of Wilkins<sup>80</sup> who expects the amino group to bond first.

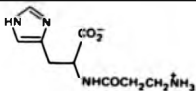
Thus, it has been established that even with relatively simple bidentate ligands the kinetics can be very complicated, and the question always arises, is the rate determining step loss of the first solvent molecule or closing of the chelate ring?

**Table 1.5** Rate constants relating to the SCS mechanism for formation of chelate complexes.<sup>66</sup>

$M^{-1} s^{-1}$ , at 298.2 K in aqueous solution

Cobalt(II)	
water exchange:	$2 \times 10^6$
complex formation with monodentate ligands:	uncharged $\sim 1$ to $3 \times 10^5$ charge 1 $\sim 1$ to $3 \times 10^6$
<b>5-membered rings:</b>	
glycinate <sup>-</sup>	$2 \times 10^6$
$\alpha$ -alaninate <sup>-</sup>	$2 \times 10^6$
$\alpha$ -aminobutyrate <sup>-</sup>	$2.5 \times 10^5$
iminodiacetate <sup>2-</sup>	$1 \times 10^7$
<b>6-membered rings:</b>	
$\beta$ -alaninate <sup>-</sup>	$1 \times 10^5$
$\beta$ -aminobutyrate <sup>-</sup>	$2 \times 10^4$
iminodipropionate <sup>2-</sup>	$3 \times 10^5$
<b>Copper(II)</b>	
water exchange:	$4 \times 10^6$
reaction with:	ammonia pyridine imidazole
	$2$ to $20 \times 10^6$
5-membered-ring: $\alpha$ -alaninate	$10 \times 10^6$
6-membered-ring: $\beta$ -alaninate	$2 \times 10^6$
7-membered-ring: L-carnosine*	$5 \times 10^6$

\*L-carnosine =



This simple question is sometimes difficult to answer from experimental data, and it is often the case that a smaller  $k_f$  value for comparable reactions is the only evidence for a shift in the rate determining step to chelate ring closure. However, steric effects must always be considered in first bond formation, though other factors such as the ICB effect can offset this.

For the rate determining step to be first bond formation a bidentate ligand must have two strong donors, no steric hindrance, be relatively flexible and have the donor groups in good proximity. This ideal is matched by very few ligands, and so deviations will arise in many cases.

#### 1.4 Substitution Reactions of Labile Metal Ions

##### Multidentate Ligands

Ligands with more than two donor atoms do not react in any way fundamentally different to bidentate ligands, except in the fact that an increased number of steps will be required to fully bond the ligand. Indeed, the mechanism given for the substitution reactions of bidentate ligands is still valid for the same reactions with multidentate ligands. The establishment of the first bond, or the first chelate ring for the SCS mechanism, appears to signal rapid successive ring closures with most multidentate ligands, presumably due to labilisation of solvents adjacent to bound donor atoms and the close proximity of the remaining donors (this effect can be seen in Table 1.6 which illustrates the increase in water exchange rate with increasing ammonia co-ordination, and increasing chelation for Ni(amine)<sup>2+</sup> species) and to the extra stability gained from forming the remaining chelate rings (see 1.5).

Such rapid ring closure for the later stages of such a reaction has been shown in a study of the ligand trien bound to Cr<sup>3+</sup> (aq) as a bidentate ligand, which converts to a terdentate ligand simply by leaving at pH 7-8 for less than 5 minutes at 0 °C. Subsequent proton uptake then stabilises the "partially unwrapped" ligand.<sup>85</sup>

Table 1.6

Rates of water exchange for various Ni(amine)<sup>2+</sup> complexes; aqueous solution at 25.0 °C.

Species	$k_{ex} / s^{-1}$	ref.
Ni(H <sub>2</sub> O) <sub>6</sub> <sup>2+</sup>	$3 \times 10^4$	81
Ni(H <sub>2</sub> O) <sub>5</sub> (NH <sub>3</sub> ) <sup>2+</sup>	$2.5 \times 10^5$	82
Ni(H <sub>2</sub> O) <sub>4</sub> (NH <sub>3</sub> ) <sub>2</sub> <sup>2+</sup>	$6.1 \times 10^5$	82
Ni(H <sub>2</sub> O) <sub>3</sub> (NH <sub>3</sub> ) <sub>3</sub> <sup>2+</sup>	$2.5 \times 10^6$	82
Ni(H <sub>2</sub> O)(NH <sub>3</sub> ) <sub>5</sub> <sup>2+</sup>	$4.3 \times 10^6$	81
Ni(H <sub>2</sub> O) <sub>4</sub> (en) <sup>2+</sup>	$4.4 \times 10^5$	83
Ni(H <sub>2</sub> O) <sub>3</sub> (dien) <sup>2+</sup>	$1.2 \times 10^6$	84
Ni(H <sub>2</sub> O) <sub>2</sub> (trien) <sup>2+</sup>	$2.9 \times 10^6$	84

Thus pyridine, bipyridine and terpyridine react at comparable rates in aqueous solution (Table 1.7).

Table 1.7

Rate constants for the reaction of Ni<sup>2+</sup> with various ligands; aqueous solution, 25.0 °C.

Ligand	$10^{-3}k_f$ (dm <sup>3</sup> mol <sup>-1</sup> s <sup>-1</sup> )	ref.
NH <sub>3</sub>	5.0	51
pyridine	ca. 4.0	86
2,2'-bipyridine	1.5	86
2,2',2''-terpyridine	1.4	87

Therefore, even multidentate ligands can react via the Eigen-Wilkins mechanism, at rates comparable to monodentate ligands. However, as with bidentate ligands, steric hindrance may slow down a reaction from first bond formation to clos-

ing of the first chelate ring. Such steric hindrance becomes increasingly important in multidentate ligands which are closed into one or more rings as opposed to the open-chain congeners (e.g. azamacrocycles compared with the linear polyamines such as en, dien, trien, tetren etc.). These cyclic ligands are the so called "macrocyclic ligands" and they are a useful probe of steric effects in reactions. They show many interesting and useful kinetic and thermodynamic effects which have been put to good use in a wide range of applications.<sup>88,89</sup>

With all multidentate ligands complete complexation with a metal ion is accompanied by extensive desolvation. The energy requirements of this process are such that the reaction must take place in a stepwise manner.<sup>69,90,91</sup> However, with cyclic ligands, such as the macrocycles, having no free end means that the twisting and folding process that a ligand has to undergo to complete complexation may become difficult or impossible to achieve in the fashion of linear multidentate ligands. Thus macrocyclic ligands may require some degree of multiple desolvation during complexation. The extra energy required to overcome this step may manifest itself in a slowing down of the reaction, when compared to linear analogues. This rate decrease may be studied in macrocycles by successively increasing ring size, alkylation at donor atoms and on the carbon framework, incorporating more rigid groups into the framework (such as multiple bonds and aromatic groups), protonation and by changing the number or types of donor atoms. All these will be discussed in the next section, largely in relation to synthetic macrocycles containing nitrogen donors, as these are the topic of this thesis. From a biological viewpoint azamacrocycles are the most important of the synthetic macrocycles due to their use as "model systems" for biological systems.<sup>9,14,92</sup>

## 1.5 Substitution Reactions of Labile Metal Ions

### Macrocyclic Ligands

#### (a) Macrocycles reacting at rates comparable to open-chain ligands.

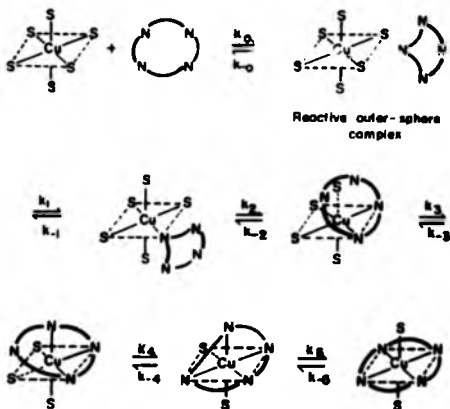
A number of studies have shown that macrocycles follow the normal complexation behaviour explained in the previous sections. This is not possible by simply reacting a metal ion with an N-donor macrocycle in water since large protonation effects control the reaction in the pH range employed in most kinetic studies (see section (e)). In order to study the reactions of the unprotonated ligands other conditions must be used.

Rorabacher et al<sup>93</sup> used strongly basic aqueous media (0.1-2.0 mol dm<sup>-3</sup> NaOH) to ensure the absence of ligand protonation. At high pH the reacting metal ion is present as the hydroxylated species, in their case Cu(OH)<sub>3</sub><sup>-</sup> and Cu(OH)<sub>4</sub><sup>2-</sup>, but as the ligands are neutral, it is assumed that the general effects observed would carry over to the behaviour of fully aquated metal ions. Comparing the kinetic behaviour of the most closely correlated open-chain and cyclic ligands (Et<sub>2</sub>-2,3,2-tet and cyclam) indicates that the macrocycles can react at rates comparable to open-chain ligands (Table 1.8). The effect of alkylation is also seen in this table (see section (c)). The proposed mechanism of complexation is shown in figure 1.2 which illustrates the stepwise substitution of an N<sub>4</sub>-donor macrocycle. For the Cu(OH)<sub>3</sub><sup>-</sup> species Jahn-Teller (tetragonal) inversion following the first bond formation is proposed as the rate determining step. For Cu(OH)<sub>4</sub><sup>2-</sup>, second bond formation is suggested as the rate determining step when reacting with macrocycles and the more sterically hindered open-chain ligands.

Another way in which the problem of ligand protonation has been overcome has been to study the complexation reactions in aprotic solvents, such as dms<sup>55</sup>, dmf<sup>55,94</sup>, and CH<sub>3</sub>CN.<sup>95</sup>

In dms<sup>o</sup> the rate constants for reaction of Ni<sup>2+</sup> with 2,6,9,13-tetraazatetradecane and cyclam were found to be<sup>55</sup>  $2.6 \times 10^3 \text{ dm}^3 \text{ mol}^{-1} \text{ s}^{-1}$

Fig. 1.2 Stepwise substitution of an  $N_4$  macrocycle with  $Cu^{2+}$ ,<sup>93</sup>



Reactive outer-sphere complex

Detailed mechanism for bonding of first and second donor atoms.

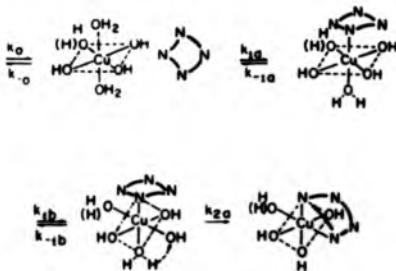




Table 1.8

Resolved rate constants for the reaction of  $\text{Cu}(\text{OH})_x(\text{II})$  species with unprotonated cyclic and open-chain polyamines;<sup>93</sup>

25.0 °C, 0.1-2.0 mol dm<sup>-3</sup> NaOH

Ligand	$k_f(\text{Cu}(\text{OH})_3)$ (dm <sup>3</sup> mol <sup>-1</sup> s <sup>-1</sup> )	$k_f(\text{Cu}(\text{OH})_4)$ (dm <sup>3</sup> mol <sup>-1</sup> s <sup>-1</sup> )
2,3,2-tet	$(1.0 \pm 0.7) \times 10^7$	$(4.3 \pm 0.2) \times 10^6$
Et <sub>7</sub> -2,3,2-tet	$(3.0 \pm 0.3) \times 10^6$	$(2.9 \pm 0.6) \times 10^5$
Cyclam	$(2.7 \pm 0.4) \times 10^6$	$(3.8 \pm 0.9) \times 10^4$
Me <sub>7</sub> -cyclam	$5.6 \times 10^5$	$0.9 \times 10^4$
tet-a	ca. $10^4$	$< 10^2$
Et <sub>4</sub> dien	$4.0 \times 10^5$	$< 10^3$

and  $1.6 \times 10^3 \text{ dm}^3 \text{ mol}^{-1} \text{ s}^{-1}$  respectively, at 25 °C. In dmf the same ligands reacted with rate constants of  $3.2 \times 10^3 \text{ dm}^3 \text{ mol}^{-1} \text{ s}^{-1}$  and  $1.8 \times 10^3 \text{ dm}^3 \text{ mol}^{-1} \text{ s}^{-1}$  respectively<sup>57</sup> at 25 °C. In each solvent the rates were shown to be comparable to the solvent exchange rates of  $\text{Ni}^{2+}$  in the particular solvent, as expected on the basis of the Eigen-Wilkins mechanism.

Studies in  $\text{CH}_3\text{CN}$ <sup>95</sup> established that the rates of incorporation of  $\text{Ni}^{2+}$  into both linear and macrocyclic tetra-amines are essentially identical within experimental error, with a rate constant ca.  $900 \text{ dm}^3 \text{ mol}^{-1} \text{ s}^{-1}$  at 25 °C (see Table 1.9).

In all of these studies of complexations with macrocycles in non-aqueous solvents more than one step is observed (usually two), the later step (or steps) being assigned to the isomerisation via *N*-inversion of a thermodynamically unstable intermediate species to a final, most stable product.

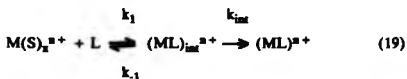


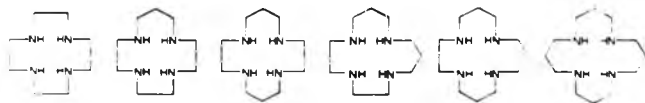
Table 1.9

Resolved rate constants for the reaction of  $\text{Ni}^{2+}$  with various ligands;<sup>95</sup>  
acetonitrile, 25 °C

Ligand	$10^{-2}k_f$ ( $\text{dm}^3 \text{mol}^{-1} \text{s}^{-1}$ )
cyclam	7.6
$\text{Me}_2\text{cyclam}$	7.3
$\text{Me}_4\text{cyclam}$	9.3
tet-a	9.2
tet-b	8.3
3,2,3-tet	10.0
2,3,2-tet	10.0
trien	10.0

(b) Effect of ring size.

The effect of changing the ring size of an  $N_4$  macrocyclic ligand was rigorously studied by Kaden et al.<sup>96</sup> by measuring the rates of complexation of  $\text{Co}^{2+}$ ,  $\text{Ni}^{2+}$ ,  $\text{Cu}^{2+}$  and  $\text{Zn}^{2+}$  with the ligands shown below in water at 25 °C over a range of pH.



[12]ane  $N_4$ , [13]ane  $N_4$ , [14]ane  $N_4$ , [14]ane  $N_4$ , [15]ane  $N_4$ , [16]ane  $N_4$

The rates of reaction follow the order  $\text{Cu}^{2+} > \text{Zn}^{2+} > \text{Co}^{2+} > \text{Ni}^{2+}$  which parallels the sequence of their water exchange rates.<sup>97</sup> The kinetics are largely the reactions of the monoprotonated species. Kaden came to three conclusions from his studies:

(1) Rates of complexation of protonated species of the same charge are slower for cyclic ligands than for the corresponding open chain tetramines

(2) For a given metal ion the complexation rate constants with  $LH^+$  are all in one order of magnitude and do not vary in any regular way with ring size

(3) For  $k(LH_2)$  with  $Cu^{2+}$  the values strongly depend on the macrocycle and generally increase with ring size.

In contrast Kodama and Kimura have carried out a series of polarographic studies to determine the effect of ring size on the kinetics of  $N_4$  donor macrocycles.<sup>98-102</sup> They found that the rate constants for the reaction of the protonated macrocycles with  $Cu^{2+}$  in acetate buffer generally increased with increasing ring size from 12 to 15 members, with the 13 and 14 membered cyclic amines having almost identical rate constants (Table 1.10).

Table 1.10

Rate constants for the reaction of  $Cu^{2+}$  with macrocycles of varying ring size; aqueous solution, acetate buffer (reactive species  $Cu(O_2CMe)^+$ ),  $\mu = 0.2 \text{ mol dm}^{-3}$

Ligand	$k_{LH}$ $\text{dm}^3 \text{ mol}^{-1} \text{ s}^{-1}$	$k_{LH_2}$ $\text{dm}^3 \text{ mol}^{-1} \text{ s}^{-1}$	ref.
[12]ane $N_4$	$1.8 \times 10^6$	0.18	103
[13]ane $N_4$	$5.6 \times 10^6$	10.1	100
[14]ane $N_4$	$6.8 \times 10^6$	$5.3 \times 10^6$	102
[15]ane $N_4$	$4.0 \times 10^8$	-	102

However, a similar study with  $Zn^{2+}$  showed no such trend.<sup>104</sup>

For  $N_3$  macrocyclic ligands the rate constants for reaction of  $Cu^{2+}$  have been studied in water at 25 °C over a range of pH and have been shown to depend greatly on the size of the ring.<sup>105</sup> In the acetate buffer used the reactions can be resolved into the reactions of  $Cu^{2+}$  and  $CuOAc^+$  with the monoprotonated ligands (see Table 1.11).

Table 1.11

Rate constants for the reaction of Cu(II) species with various N<sub>3</sub>-macrocycles;<sup>105</sup> aqueous solution, acetate buffer, 25 °C,  $\mu = 0.5 \text{ mol dm}^{-3}$  (KNO<sub>3</sub>)

Ligands	$k_f(\text{Cu}^{2+}/\text{LH}^+)$ ( $\text{dm}^3 \text{ mol}^{-1} \text{ s}^{-1}$ )	$k_f(\text{CuOAc}^+/\text{LH}^+)$ ( $\text{dm}^3 \text{ mol}^{-1} \text{ s}^{-1}$ )
[9]aneN <sub>3</sub>	$2.4 \times 10^6$	$1 \times 10^7$
[10]aneN <sub>3</sub>	$7.4 \times 10^4$	$8.6 \times 10^5$
[12]aneN <sub>3</sub>	23	$2.8 \times 10^3$

In contrast, with N<sub>3</sub> macrocycles an increase in rate constant with ring size is observed under similar conditions to the N<sub>3</sub> study<sup>106</sup> (see Table 1.12). However, here, the kinetics are largely the reactions of the di- and tri- protonated species. This is because as the ring size becomes smaller the conformational flexibility becomes more pronounced, which lowers the rate of reaction. Also, adding more protons increases the electrostatic repulsion between the ligand and the metal cation, again lowering the rate (see section (c)).

Table 1.12

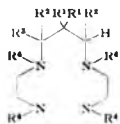
Rate constants for the reactions of Cu(II) species with various N<sub>3</sub> macrocycles;<sup>110</sup> aqueous solution, acetate buffer, 25 °C,  $\mu = 0.5 \text{ mol dm}^{-3}$  (KNO<sub>3</sub>)

Ligand	$k_f(\text{Cu}/\text{LH}_2)$	$k_f(\text{CuOAc}/\text{LH}_2)$	$k_f(\text{Cu}/\text{LH}_3)$	$k_f(\text{Cu}/\text{LH}_3)$
			$k_f / (\text{dm}^3 \text{ mol}^{-1} \text{ s}^{-1})$	
[15]aneN <sub>3</sub>	$1.4 \times 10^6$	$9.7 \times 10^4$	-	-
[16]aneN <sub>3</sub>	$2.4 \times 10^6$	$3.1 \times 10^6$	$5.6 \times 10^2$	ca. 1
[17]aneN <sub>3</sub>	$4.9 \times 10^6$	$8.6 \times 10^6$	$8.7 \times 10^3$	$8.1 \times 10$

(c) Effect of alkylation.

The effect of alkylation of N-donor macrocycles has been studied both in terms of alkylation at the donor atoms and on the carbon framework. Kaden and Stein-

mann were amongst the first to systematically study the effect of substituents on the rates of complexation.<sup>107</sup> The reactions of  $\text{Ni}^{2+}$ ,  $\text{Co}^{2+}$ ,  $\text{Cu}^{2+}$  and  $\text{Zn}^{2+}$  with four different substituted cyclic tetramines were studied over a range of pH. The resolved rate constants are shown in Table 1.13.



- L<sup>1</sup> [13]ane N<sub>4</sub>  
 L<sup>2</sup> R<sup>1</sup> = CH<sub>3</sub>, R<sup>2</sup> = R<sup>3</sup> = R<sup>4</sup> = H  
 L<sup>3</sup> R<sup>2</sup> = CH<sub>3</sub>, R<sup>1</sup> = R<sup>3</sup> = R<sup>4</sup> = H  
 L<sup>4</sup> R<sup>2</sup> = R<sup>3</sup> = CH<sub>3</sub>, R<sup>1</sup> = R<sup>4</sup> = H  
 L<sup>5</sup> R<sup>1</sup> = R<sup>4</sup> = CH<sub>3</sub>, R<sup>2</sup> = R<sup>3</sup> = H

Table 1.13

Rate constants for the reaction of  $\text{Ni}^{2+}$ ,  $\text{Cu}^{2+}$ ,  $\text{Co}^{2+}$  and  $\text{Zn}^{2+}$  with L<sup>1-5</sup>;<sup>107</sup> aqueous solution, 25 °C,  $\mu = 0.5 \text{ mol dm}^{-3}$ ,  $k_{\text{HL}} / (\text{dm}^3 \text{ mol}^{-1} \text{ s}^{-1})$

Ligand	$\text{Ni}^{2+}$	$\text{Cu}^{2+}$	$\text{Co}^{2+}$	$\text{Zn}^{2+}$
	$k_{\text{HL}}$	$k_{\text{HL}}$	$k_{\text{HL}}$	$k_{\text{HL}}$
L <sup>1</sup>	145	$1.1 \times 10^7$	-	-
L <sup>2</sup>	110	$1.2 \times 10^7$	$1.8 \times 10^2$	$8.0 \times 10^4$
L <sup>3</sup>	55	$6.5 \times 10^6$	-	-
L <sup>4</sup>	14	$3.4 \times 10^6$	-	-
L <sup>5</sup>	$4.5 \times 10^{-2}$	$2.2 \times 10^3$	$1.1 \times 10^{-1}$	88

From the results they concluded that substituents in the  $\beta$ -position to a coordinating nitrogen have no effect on the rate of complexation, but that substituents in the  $\alpha$ -position slow down the first step of the reaction.

Buxtorf and Kaden<sup>108</sup> studied the effect of successive N-methylation on the rate of reaction of substituted cyclams with  $\text{Ni}^{2+}$  and  $\text{Cu}^{2+}$  in aqueous solution. The resolved rate constants for the reactions of the monoprotonated ligands with the

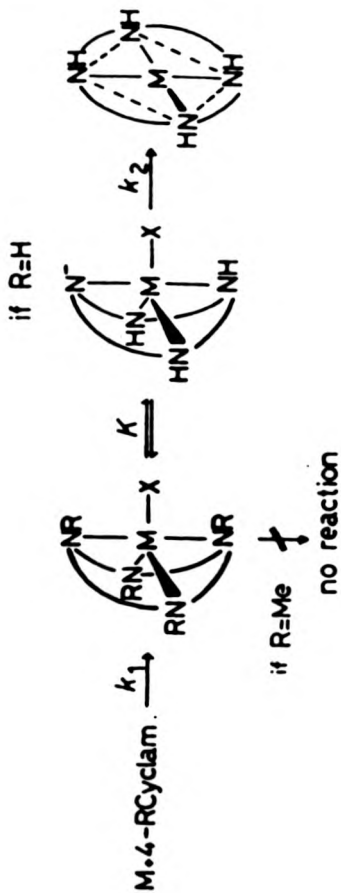


Fig. 1.3 Penta-co-ordinate intermediate in the reactions of  $\text{Ni}^{2+}$  and  $\text{Cu}^{2+}$  with  $\text{N}_4$  macrocycles. 108

metal ions are shown in Table 1.14.

Table 1.14

Rate constants for the reaction of  $\text{Ni}^{2+}$  and  $\text{Cu}^{2+}$  with methylated cyclams;<sup>108</sup> aqueous solution, 25 °C,  $k_{\text{LH}} / (\text{dm}^3 \text{mol}^{-1} \text{s}^{-1})$

Ligand	$k_{\text{LH}} / \text{Cu}^{2+}$	$k_{\text{LH}} / \text{Ni}^{2+}$
cyclam	$2.6 \times 10^5$	7.4
Me-cyclam	$1.2 \times 10^7$	55
Me <sub>2</sub> -cyclam	$2.8 \times 10^6$	10
Me <sub>4</sub> -cyclam	$2.9 \times 10^5$	1.4

For open-chain amines one would expect to see a gradual decrease in rate constant with successive methylation until all the nitrogens are methylated, causing a severe drop in rate.<sup>70</sup> However, with the substituted cyclams this trend is not observed. Thus, the expected decrease in rate may be compensated for by a favourable change in conformation or the rate determining step being different from the open-chain amine reactions. An interesting observation is that for the fully methylated cyclam the product of complexation is a penta-co-ordinate species with an equatorially bound solvent molecule, unlike the square planar species observed with the other ligands. This can be explained by an intermediate being formed in each case which must deprotonate to form the square planar complex, going via the conjugate base (Figure 1.3). This behaviour was also observed by Barefield et al.<sup>109,110</sup>

A similar study carried out in  $\text{dmf}^{94}$  on the reactions of Me-substituted cyclam with  $\text{Ni}^{2+}$  and  $\text{Cu}^{2+}$  show a decrease in rate with successive methylation. In  $\text{dmsO}$  the complexation rate of  $\text{tmc}$  is over 300 times smaller than that observed with cyclam, when reacting with  $\text{Ni}^{2+}$  at 25 °C.<sup>55</sup> The effect of alkylation in the complexation reactions of unprotonated ligands can also be seen in Table 1.8 (section (a)) for the reactions of  $\text{Cu}(\text{OH})_3^-$  and  $\text{Cu}(\text{OH})_4^{2-}$  with various open-chain and cyclic amines. Again successive alkylation causes a decrease in the resolved rate constants.

(d) Effect of rigidity.

In one of the earliest publications on the subject, the effect of increasing rigidity of N-donor ligands on the rate of complex formation with Cu(II) in 0.5 mol dm<sup>-3</sup> NaOH was studied. The basic conditions were required to avoid ligand protonation. The second order rate constants are illustrated in Table 1.15.

The porphyrin ring is the most rigid and will thus have the greatest difficulty in twisting and folding to produce a stepwise desolvation mechanism. Some degree of multiple desolvation is almost certainly required for the complexation process. This may also occur, to a lesser extent, with the unsaturated and saturated cyclic amines, where multiple desolvation may be necessary in the co-ordination of the third or fourth nitrogen donors.

Table 1.15

Rate constants for the reaction of Cu<sup>2+</sup> with various ligands;<sup>111</sup>  
25.0 °C, 0.5 mol dm<sup>-3</sup> NaOH, k<sub>f</sub> / (dm<sup>3</sup> mol<sup>-1</sup> s<sup>-1</sup>)

Ligand	k <sub>f</sub>
2,3,2-tet	ca. 10 <sup>7</sup>
tet-a	1.6 x 10 <sup>3</sup>
tet-b	3.6 x 10 <sup>3</sup>
<i>trans</i> -[14]-diene	5.6 x 10 <sup>3</sup>
hematoporphyrin	2.0 x 10 <sup>-2</sup>

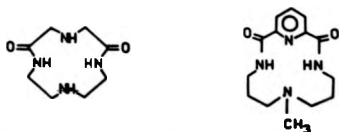
The effect of replacing a secondary amine by a pyridine group in tetra-amine macrocycles was studied by Schultz-Grünow and Kaden.<sup>112</sup> The reactions of the ligands shown with Co<sup>2+</sup>, Ni<sup>2+</sup>, Cu<sup>2+</sup> and Zn<sup>2+</sup> were studied in aqueous solution.



Again the kinetics are resolvable as the reactions of the protonated ligands. On comparison with cyclic amines with no rigidity incorporated, the effect on the reaction rates of introducing a pyridine ring is a reduction of 10-100 times, though it is not clear whether the effect is due to the decreased flexibility of the ligands or to other steric effects.

Klaehn et al<sup>113</sup> studied the rate of reaction of tmbc with  $\text{Cu}^{2+}$  in dmf. They observed a two step reaction, with a rate constant for the initial complexation step of  $k_f = 39.4 \pm 1.2 \text{ dm}^3 \text{ mol}^{-1} \text{ s}^{-1}$  at 25 °C, the slower, metal independent step was considered to be the rearrangement of an unfavourably co-ordinated complex to the final product. At the time there were no other data to compare to this figure, and so the effect of the two benzene rings in the structure could not be determined. However, in a recent publication the value of the rate constant for the reaction of tmc with  $\text{Cu}^{2+}$  in dmf is reported (at -43 °C).<sup>94</sup> By calculating the rate constant at 25 °C from the reported activation parameters using the Eyring equation, a rate constant of  $(9.5 \pm 1.9) \times 10^4 \text{ dm}^3 \text{ mol}^{-1} \text{ s}^{-1}$  is obtained. Thus, the two benzene rings in tmbc reduce the rate some  $2\text{-}3 \times 10^3$  times, which is a considerable decrease. A reduction in rate of only about 20 times is observed in the reaction of tmc with  $\text{Ni}^{2+}$  in dmf compared with cyclam<sup>55</sup> and of 25 times for the reaction of dibenzo cyclam with  $\text{Cu}^{2+}$  in ethanol/water.<sup>114</sup> Thus, the very large rate decrease for tmbc may indicate a change in mechanism compared to tmc and dibenzo cyclam.

The effect of rigidity on the complexation kinetics of macrocycles has also been investigated using dioxo-tetra-aza macrocycles.<sup>115,116</sup> The two ligands shown were compared via their reactions with  $\text{Ni}^{2+}$  and  $\text{Cu}^{2+}$  in aqueous solution.



Protonation is very important in these ligands as the N-donors of amides will not bond to a metal ion until they are deprotonated. Thus, many different species can exist; their relative concentrations dependent on the pH (Figure 1.4).

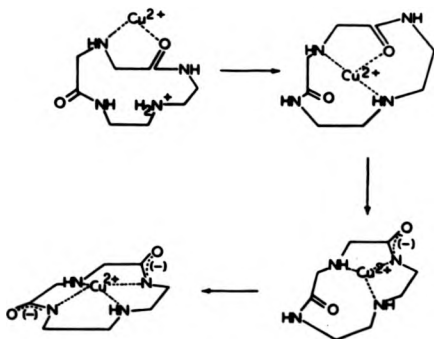


Fig. 1.4 Proposed structures of  $\text{Cu}^{2+}$  / diamide  $\text{N}_4$  macrocycle complexes.<sup>115</sup>

The kinetics of the more flexible ligand 1 resemble those of open-chain ligands, whereas for ligand 2 the increased rigidity considerably reduces the reaction rate to  $1.5 \text{ dm}^3 \text{ mol}^{-1} \text{ s}^{-1}$  for the reaction of unprotonated ligand with  $\text{Cu}^{2+}$  at pH 5.5-5.8 at  $25^\circ\text{C}$ . The similar ligand  $\text{Me}_3\text{PyN}_3$ , which contains no amide groups, reacts with  $\text{Cu}^{2+}$  at  $(2.3 \pm 0.5) \times 10^5 \text{ dm}^3 \text{ mol}^{-1} \text{ s}^{-1}$  even in its monoprotinated form.<sup>112</sup> This illustrates the great effect on rigidity that introducing amido groups into macrocycles can have. Another example is in the comparison of the monoprotinated forms of cyclam, [13]ane $\text{N}_4$ , dioxo-cyclam and dioxo-[13]ane $\text{N}_4$  reacting with  $\text{Cu}(\text{O}_2\text{CMe})^+$  in aqueous solution (Table 1.16).

Table 1.16

Rate constants for the reaction of  $\text{Cu}(\text{O}_2\text{CMe})^+$  with various monoprotonated macrocycles;<sup>116</sup> aqueous solution, 25 °C,  $\mu = 0.2 \text{ mol dm}^{-3}$

Ligand	$k_{\text{HL}} / (\text{dm}^3 \text{ mol}^{-1} \text{ s}^{-1})$
	$5.6 \times 10^6$
	$5.3 \times 10^6$
	$9.5 \times 10^2$
	$3.1 \times 10^3$

(e) Effect of protonation.

Macrocyclic polyamines exist as protonated species in water at the pH ranges used in most kinetic studies. Thus, a constant problem is the resolving of the kinetic data into rate constants for the different species present. In order to do this as wide a range of pH as possible must be studied to determine the effect of  $\text{H}^+$  concentration, and the protonation constants of the ligands must be determined. For open-chain polyamines the protonation constants decrease fairly steadily as each extra proton is added, but for cyclic polyamines the closed structure decreases the distance between the protonated sites on the ligand. For an  $\text{N}_4$  macrocycle, such as cyclam, the second proton will bind in the position *trans* to the first protonation site, but successive protonations become extremely difficult because of the proximity of the donors, thus a large drop in protonation constant is seen in going from  $\text{p}K_2^{\text{H}}$  to  $\text{p}K_3^{\text{H}}$  in cyclam (see Table 1.17).

Table 1.17

Protonation constants for various polyamines, 25 °C

Refs; 69, 96, 104, 117.

Ligand	pK <sub>1</sub>	pK <sub>2</sub>	pK <sub>3</sub>	pK <sub>4</sub>	pK <sub>5</sub>
trien	9.80	9.08	6.55	3.25	-
cyclam	11.83	10.76	< 2	< 2	-
cyclam	11.50	10.30	1.62	0.94	-
tetren	9.78	9.38	8.14	4.83	3.15
[15]aneN <sub>5</sub>	10.85	9.65	6.00	1.74	1.16

This effect decreases as the ring size increases. A lesser effect occurs with N<sub>5</sub> macrocyclic amines, where a drop in pK<sup>H</sup> occurs from pK<sub>3</sub><sup>H</sup> to pK<sub>4</sub><sup>H</sup> (see Table 1.17).

Therefore, the number of possible reactions for M<sup>2+</sup> reacting with an N<sub>4</sub> macrocyclic ligand L can complicate the kinetics:



The slow reactions of macrocycles in aqueous solution are due to electrostatic interactions, since the positive charges of the protonated ligand and the metal cation will be closer together in cyclic ligands than in open-chain ligands. This is why the mono- and di-protonated forms of cyclam react 30,000 times slower with Ni(H<sub>2</sub>O)<sub>6</sub><sup>2+</sup> than do the corresponding species of the open-chain polyamine trien.<sup>118</sup> Intramolecular hydrogen bonding, which occurs in open-chain polyamines, can affect the rate of complexation reactions.<sup>70,75</sup> This effect is magnified in cyclic

amines as hydrogen bonds tend to form within the ring.<sup>119</sup>

To avoid the effects of protonation a number of studies have involved the use of aprotic solvents<sup>55,94,95</sup> and strongly basic aqueous media<sup>93</sup> (see section (a)).

(f) Effect of number of donors.

The effect on reaction rates of changing the number of donor atoms in the macrocyclic ring is a subject which has been little explored. Certainly, if the reactions followed the Eigen-Wilkins mechanism changing the number of donor atoms should not in itself affect the rate of reaction. However, by changing the number of donors the ring size, protonation and solvation of the ligand will also be changed as well. Thus, to determine this effect, studies need to be carried out in conditions which will avoid protonation (e.g. in aprotic solvents), and ideally not affect ring size (e.g. using [12]aneN<sub>3</sub> and [12]aneN<sub>4</sub>).

Certainly for the monoprotonated forms of [9]aneN<sub>3</sub> and [14]aneN<sub>4</sub> reacting with  $\text{Cu}(\text{O}_2\text{CMe})^+$  (at 25 °C,  $l = 0.2 \text{ mol dm}^{-3}$ ) the rate constants are virtually identical,  $(6.8 \pm 0.5) \times 10^6$  and  $(5.3 \pm 0.5) \times 10^6 \text{ dm}^3 \text{ mol}^{-1} \text{ s}^{-1}$  respectively.<sup>102</sup>

(g) Effect of mixed donor atoms.

The incorporation of other types of donor atoms into macrocyclic amines has found some use in probing the mechanisms of complexation of macrocycles. Kallianou and Kaden<sup>120</sup> studied a macrocycle containing 2N and 2S donors in order to shed light on the protonation effects which lower the rate of complexation for N-donor macrocycles compared to analogous open-chain ligands (see section (e)).

The N<sub>2</sub>S<sub>2</sub> ligand allows the relative positions of the protonated site and the site of first bond formation to be known. Introducing S donors into the ring also lowers the stability of the complexes formed (see section 1.7) and thus allows the study of metal-metal exchange and complex dissociation reactions (see section 1.6), which are not easy to carry out with macrocyclic polyamines. The kinetics of the ligand reacting with  $\text{Cu}^{2+}(\text{aq})$  in an acetate buffer were measured over a range of pH. The

rate constant for the reaction of the monoprotonated form of the ligand was resolved as  $29 \text{ dm}^3 \text{ mol}^{-1} \text{ s}^{-1}$ , which is some  $10^5$ - $10^6$  times smaller than the typical values obtained for monoprotonated tetraaza macrocycles (e.g. see Table 1.10). This can be explained in two ways; firstly, attack could occur initially at an S-atom in a *trans*-position to the protonated amine, the relatively weak Cu-S bond<sup>121</sup> causing the rate determining step to shift to second bond formation. Alternatively, the low rate constant could be due to attack at an N-atom *cis* to the protonated site, the rate determining first bond formation being reduced by strong electrostatic interactions between the dipositive cation and the ammonium group. This kind of behaviour is observed with open-chain polyamines, where the monoprotonated species react  $10^4$ - $10^5$  times slower than the free ligand,<sup>122</sup> thus the latter explanation is more appealing.

The complexation kinetics of  $\text{N}_2\text{O}_2$ -macrocycles have also been studied.<sup>123</sup> The reactions of each of two ligands with  $\text{Ni}^{2+}$  in methanol were observed to consist of an initial fast, metal dependent step followed by a slower step which was postulated to involve a rearrangement of the ligand within the nickel(II) co-ordination sphere. The initial step followed the Eigen-Wilkins mechanism, with first bond formation being the rate determining step, the rate being comparable to the rate of exchange of methanol on  $\text{Ni}^{2+}$ , unlike alot of tetraaza macrocycles, where the rate determining step is not controlled by the dissociation of the first co-ordinated solvent molecule.<sup>107,108,118,124-127</sup>

#### (h) Macrocyclic polythiaethers.

The thiaether macrocycles have generally not received as much attention as the polyamines. Like the amines they have been suggested as "models" for biological systems, such as the "blue" copper proteins (e.g. plastocyanin) and the iron containing rubredoxins and ferredoxins.<sup>128</sup> Thus, many of the model system's properties pertaining to these naturally occurring systems have been studied<sup>17</sup> such as their Cu(II)/Cu(I) self-exchange rates.<sup>129</sup> The kinetics of complexation of a range of poly-

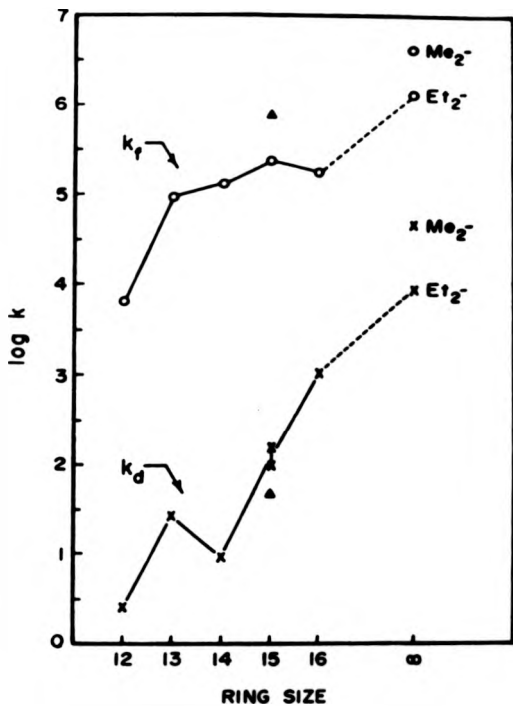
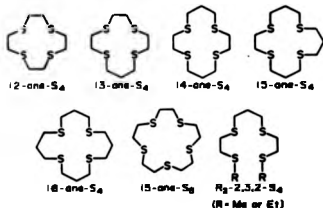


Fig. 1.5 Ring size effects for  $\text{Cu}^{2+}$  / tetraethiaether complexes.<sup>121</sup>

thiaethers have been studied extensively by Rorabacher et al.<sup>121,130</sup>

The studies were carried out in a methanol/water solvent mixture due to ligand solubility difficulties, over a range of 25-95% methanol. These ligands have significant differences to the polyamines. The ligands are free of protonation, and so the large influence of protonation found in the kinetics of polyamines (see section (e)) will have no bearing with these systems. Also, the ligands are not significantly solvated which allows direct examination of the configuration contributions to complex stabilities. With polyamines the high degree of ligand solvation plays an important part in the high stabilities of the complexes (see section 1.7). The weaker complexes of the thiaethers also permit the direct measurement of the dissociation rate constants (see section 1.6).



As the percentage of methanol increases the values for  $k_f$  decreases consistently for all the ligands shown above indicating that the effect of solvent on  $k_f$  is independent of the ligand structure.

The resolved rate constants are shown in Table 1.18. Figure 1.5 shows the variation of formation rate constants with ring size.

The value of  $k_f$  for [15]aneS<sub>4</sub> is greater than that for [16]aneS<sub>4</sub> due to the greater ease in closing five-membered chelate rings compared to six-membered rings.<sup>77,131</sup> 15-ane-S<sub>5</sub> reacts faster than [15]aneS<sub>4</sub> due to the increase in the number of available five membered rings and the extra flexibility gained in introducing another donor atom. As the ring size of the ligands decreases the rate decreases due to a reduction in the flexibility of the ligands. The proposed mechanism for the complex formation between  $\text{Cu}(\text{H}_2\text{O})_6^{2+}$  and the cyclic tetraethers is similar to

Table 1.18

Calculated rate constants for the reaction of  $\text{Cu}^{2+}$  with various polythiaethers;<sup>121</sup> aqueous solution, 25 °C, 0.1 mol dm<sup>-3</sup>  $\text{ClO}_4^-$  ( $\text{HClO}_4$ )

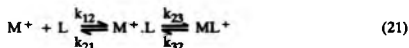
Ligand	$10^{-4} k_f / (\text{dm}^3 \text{mol}^{-1} \text{s}^{-1})$
[12]aneS <sub>4</sub>	0.65
[13]aneS <sub>4</sub>	7.4
[14]aneS <sub>4</sub>	13
[15]aneS <sub>4</sub>	23.5
[16]aneS <sub>4</sub>	17
[15]aneS <sub>5</sub>	75
Et <sub>2</sub> -2,3,2-S <sub>4</sub>	130
Me <sub>2</sub> -2,3,2-S <sub>4</sub>	420

that proposed for the analogous cyclic tetraamines<sup>93</sup> (see Figure 1.2, section 1.5(a)). The rate determining step is concluded to be at the point of second bond formation from conformational and bond strength considerations. To test this hypothesis the kinetics of the reaction of  $\text{Cu}^{2+}$  with [14]aneS<sub>3</sub>N were measured. The extra bond strength in the Cu-N bond compared to a Cu-S should be sufficient to shift the rate determining step back to first bond formation. This would produce a calculated rate constant of  $(3-16) \times 10^6 \text{ dm}^3 \text{ mol}^{-1} \text{ s}^{-1}$  (at 25 °C)<sup>121</sup> if this mechanism occurred. The value of the resolved rate constant of formation was  $3.5 \times 10^6 \text{ dm}^3 \text{ mol}^{-1} \text{ s}^{-1}$  (25 °C, 0.1 M  $\text{NaClO}_4$ ) and so it was concluded that the data fitted the proposed mechanism.

#### (i) Macrocyclic polyethers.

A number of studies of the complexation kinetics of cyclic polyethers reacting with alkali metals have been undertaken. The rates of such reactions are generally much faster than the rates of transition metal complexations with macrocyclic amines, approaching the diffusion limit in many cases (ca.  $10^9-10^{10} \text{ s}^{-1}$ ). This can

occur when the reacting cation has so low a charge density that the rate determining step in the loss of a solvent molecule is the diffusion of that molecule into the bulk solvent. Thus, as with the substitution reactions of metal ions with monodentate ligands (see section 1.2) the simplified complexation reactions can be written as;



where  $K_{ca} = k_{12}/k_{21}$

and  $k_f = K_{ca}k_{23}$ , when  $k_{21} \gg k_{23}$

Linear variations of  $\log k_f$  with ionic radius of the reacting cations are known for many ligands in water, when all the metal ions have the same charge.<sup>45</sup> However, with macrocycles this has been found to be different, as figure 1.6 shows for the naturally occurring macrocycle valinomycin.<sup>132</sup>

This behaviour may be explained by the interaction of a variety of contributing factors, including solvation and chelation effects.<sup>133</sup>

An important factor in the complexation reactions of crown ethers is the presence of conformational equilibria which are set up between different conformational forms of the ligand. These can have a profound effect on the kinetics. For the reaction of dibenzo-30-crown-10 in methanol with a variety of monovalent cations Chock<sup>134</sup> proposed that an immeasurably fast conformational equilibrium was established in the reactions prior to the complexation reaction.



(where  $CR_1$  and  $CR_2$  denote different conformations of the uncomplexed ligand)

Grell et al<sup>132</sup> also suggested the occurrence of such a conformational equilibrium in the reaction of valinomycin with monovalent cations, but this time they proposed the equilibration took place after the rate determining step. These rapid conformational equilibria highlight the flexibility of these ligands. This flexibility is a

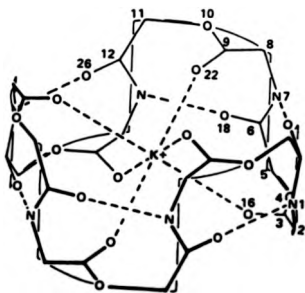
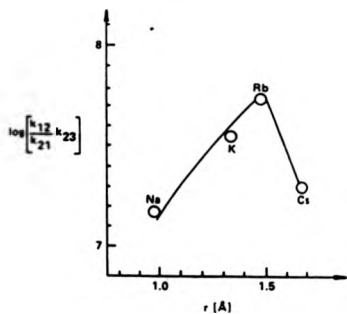


Fig. 1.6 Non-linear dependence of  $k_f$  on reacting metal ionic radius for valinomycin.<sup>7</sup>

necessity for the explanation of the nearly diffusion controlled rate constants for complexation, as more rigid ligands would require the total desolvation of a binding site on a metal ion before complexation could occur, which would significantly reduce the rate as more energy would be required.

Examples of rates of complex formation for the crown ether 18-crown-6 are shown in Table 1.19.

**Table 1.19**

Rate constants for the reaction of 18-crown-6 with various monovalent cations;<sup>135</sup> aqueous solution, 25 °C,  $\mu$  ca. 0.3 mol dm<sup>-3</sup>,  $k_f / (\text{dm}^3 \text{mol}^{-1} \text{s}^{-1})$

Cation	$k_f$
Na <sup>+</sup>	2.2 x 10 <sup>8</sup>
K <sup>+</sup>	4.3 x 10 <sup>8</sup>
Rb <sup>+</sup>	4.4 x 10 <sup>8</sup>
Cs <sup>+</sup>	4.3 x 10 <sup>8</sup>
NH <sub>4</sub> <sup>+</sup>	5.6 x 10 <sup>8</sup>
Ag <sup>+</sup>	11.2 x 10 <sup>8</sup>
Tl <sup>+</sup>	9.0 x 10 <sup>8</sup>

(j) Macrobicyclic ligands.

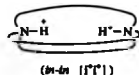
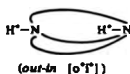
Macrobicyclic ligands, or cryptands, are macrocycles containing two rings. Most cryptands synthesized consist of bridgehead nitrogen atoms with N or O donors present in the interconnecting chains.



$a = b = c = 0$	<b>Cryptand 111</b>
$a = b = 0, c = 1$	<b>Cryptand 211</b>
$a = 0, b = c = 1$	<b>Cryptand 221</b>
$a = b = c = 1$	<b>Cryptand 222</b>

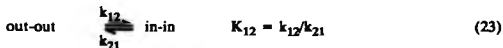
These ligands have been reviewed by Lehn.<sup>20-22,136</sup> As with the crown ethers,

the kinetic studies of cryptands have been largely confined to the alkali metals. Conformational changes in solution are again important for this class of ligands. There are three possible stereoisomers for the ligands shown above;



Simmons and Park found that an equilibrium exists between the [o,o] and [i,i] isomers. The [o,i] isomer is of higher energy due to a nonbonded repulsion effect.<sup>137</sup> Lehn et al suggested that the cryptands and their cryptated cation complexes exist as an equilibrium mixture of all three conformations and observed exchange at the cations in solution.<sup>138</sup> A simple complexation-decomplexation process was favoured over a bimolecular exchange, which is the same as the complexation mechanisms for all the other types of macrocycles.

The complexation rates of cryptands with alkali metals are ca.  $10^6 \text{ dm}^3 \text{ mol}^{-1} \text{ s}^{-1}$  (139) which is slower than the same reactions with the crown ethers (see section (i)). The stability constants of the cryptates are, however, ca.  $10^3$  larger than the crown ether complexes.<sup>138</sup> Unlike the monocyclic macrocycles the stability is not simply dependent on a very slow dissociation rate but also involves contributions from the complexation rate. The observed complexation rates are slower than for a diffusion-controlled process, though this may be the result of a conformational rearrangement equilibrium being set up prior to the complexation process:<sup>140</sup>

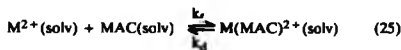


Thus a knowledge of the stability constant for the equilibrium change is required in order to resolve the true complexation rates, which may indeed turn out to be diffusion-controlled (this would require a  $K_{12}$  of ca.  $10^{-5} \text{ s}^{-1}$ ).

### 1.6 Dissociation Reactions of Macrocyclic Complexes

Generally it is difficult to measure the rates of dissociation of macrocyclic complexes at the same time as measuring the rates of formation, as can sometimes be done with complexes of lower dentate ligands. This is because the rates of dissociation are extremely slow for macrocyclic complexes, and the dissociations have to be induced by adding acid, base,  $\text{CN}^-$ ,  $\text{Hg}^{2+}$  or  $\text{Ag}^+$  which increase the dissociation rate. Open-chain polyamines have been shown to dissociate from metals via an "unzipping mechanism".<sup>14</sup> However, cyclic ligands have no free end with which to initiate this mechanism and so the reactions are considerably slowed down. It has been suggested<sup>14</sup> that dissociation in macrocyclic complexes involves initial attack of an appropriate ligand at an axial site in planar  $\text{N}_4$  complexes, followed by a folding of the ligand to remove the donor atom from the bonding. Certainly, evidence exists for the folding of macrocycles being involved in the complexation of such species.<sup>108</sup>

The very slow rates of dissociation of macrocyclic complexes is the kinetic reason for the high stability of these species (see section 1.7). The term "multiple juxtapositional fixedness" was coined by Busch<sup>14</sup> to describe this phenomenon.



Cabbiness and Margerum<sup>111</sup> first discussed this effect and Table 1.20 shows some of their data, comparing the open-chain ligand complex  $\text{Cu}(\text{2,3,2-tet})^{2+}$  with  $\text{Cu}^{2+}$  complexes of macrocyclic ligands. The rate constants were measurable only under conditions of high acidity (6.1 M HCl).



Table 1.21

Resolved rate constants for the dissociation and isomerisation of  
 $[\text{Cu}(\text{tet-a})(\text{blue})]^{2+}$ ,  $\text{H}_2\text{O}$ , 25 °C,  $\mu = 5.0 \text{ mol dm}^{-3} (\text{HNO}_3 + \text{NaNO}_3)^{141}$

$$k_1 = 2.6 (\pm 0.3) \times 10^{-4} \text{ dm}^3 \text{ mol}^{-1} \text{ s}^{-1}$$

$$k_{-1} = 1.4 (\pm 0.1) \times 10^{-3} \text{ s}^{-1}$$

$$k_2 = 2.5 (\pm 0.1) \times 10^{-3} \text{ s}^{-1}$$

$$k_3 = 4.6 (\pm 0.2) \times 10^{-4} \text{ s}^{-1}$$

The rate determining step in the dissociation process is proposed to be the cleavage of the second Cu-N bond, which is in contrast to the mechanism for the dissociation of Cu complexes of the open-chain polyamines, where first bond cleavage is the rate determining step.<sup>68</sup>

A later study of an acid dissociation from the point of view of the  $[\text{Cu}(\text{tet-a})(\text{red})]^{2+}$  species<sup>143</sup> confirmed the original results and added a figure of  $(2.27 \pm 0.10) \times 10^{-8} [\text{H}^+] \text{ dm}^3 \text{ mol}^{-1} \text{ s}^{-1}$  for the slow reaction of  $[\text{Cu}(\text{tet-a})(\text{red})]^{2+}$  to  $[\text{Cu}(\text{Htet-a})]^{3+}$  under the same reaction conditions.

The acid dissociation mechanism of the five co-ordinate folded  $[\text{Cu}(\text{tet-b})(\text{blue})]^{2+}$  complex was also studied,<sup>142</sup> and was found to depend on both protonation and solvent-separation pathways, unlike its (tet-a) analogue. No isomerisation was involved this time. The proposed stepwise dissociation mechanism is illustrated in Figure 1.7.

A study comparing the acid dissociations of  $\text{Cu}(\text{cyclam})^{2+}$  and  $\text{Cu}(3,2,3\text{-tet})^{2+}$  illustrated the relative complexity of the dissociation of a macrocyclic complex compared to an open-chain complex.<sup>145</sup> The authors proposed that cleavage of the first Cu-N bond of  $\text{Cu}(\text{cyclam})^{2+}$  is predominantly via the protonation pathway, whereas for  $\text{Cu}(3,2,3\text{-tet})^{2+}$  it is mainly via the solvation pathway. They suggest it is because the unrestricted donor atoms of 3,2,3-tet are able to move easily out of the first co-ordination sphere and are relatively unaffected by acid.<sup>145</sup> Whereas, the restricted donor atoms of cyclam rely on the acid to strip them from the co-ordination sphere

as the solvent has little effect on this process. The rate determining step for the open-chain ligand is the cleavage of the first Cu-N bond because the leaving donor group can easily rotate away from the metal on dissociation. With the restricted cyclic ligand the solvation of the metal ion and the very close protonated, uncoordinated amine group is sterically hindered, thus shifting the rate determining step to second bond cleavage.

The acid hydrolysis of the Ni(II) and Cu(II) complexes of a number of triaza-macrocycles have been extensively studied.<sup>147-149</sup> The Ni(II) complexes of [12]aneN<sub>3</sub> and [9]aneN<sub>3</sub> show marked similarities in their kinetic behaviour to Ni(c-tach)<sup>2+</sup>.<sup>150</sup> This is perhaps not surprising as all three amines form tridentate complexes which can only co-ordinate facially to metal ions, and all are structurally restricted, so that on bond breaking the N-donor atom cannot be removed very far from the metal. It might be expected that the more flexible [12]aneN<sub>3</sub> ligand would promote an easier unwrapping process, but this is not the case. The Ni[9]aneN<sub>3</sub><sup>2+</sup> complex is probably more strained than the Ni[12]aneN<sub>3</sub><sup>2+</sup><sup>151,152</sup> and thus the rate of dissociation of the [9]aneN<sub>3</sub> complex is greater than for the [12]aneN<sub>3</sub> complex. The argument is backed up by the smaller  $\Delta H^\ddagger$  of hydrolysis of Ni[9]aneN<sub>3</sub><sup>2+</sup> which suggests weaker bonding in the complex compared to Ni[12]aneN<sub>3</sub><sup>2+</sup> (see Table 2.22).

**Table 1.22**

Rate constants for the dissociation of Ni<sup>2+</sup>/N<sub>3</sub> complexes;<sup>149</sup>

aqueous solution

Complex	temp, °C	10 <sup>5</sup> k, s <sup>-1</sup>	10 <sup>5</sup> k <sub>H</sub> , dm <sup>3</sup> mol <sup>-1</sup> s <sup>-1</sup>
Ni[9]aneN <sub>3</sub> <sup>2+</sup>	25	3.25 (± 0.67)	13.0 (± 1.0)
	35	7.6 (± 2.1)	55.8 (± 3.2)
Ni[12]aneN <sub>3</sub> <sup>2+</sup>	30	0.260 (± 0.014)	0.100 (± 0.019)
	40	0.52 (± 0.24)	1.00 (± 0.37)

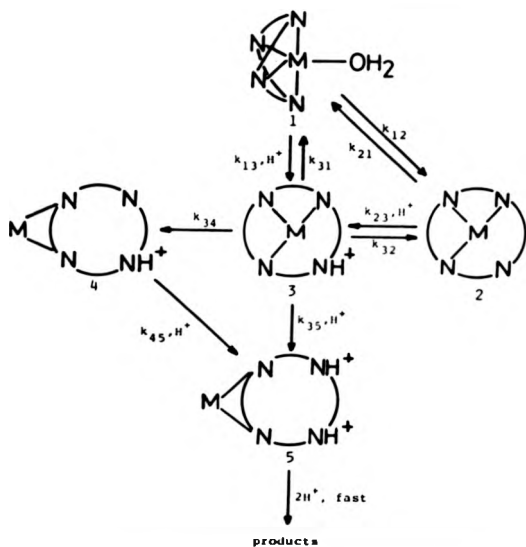
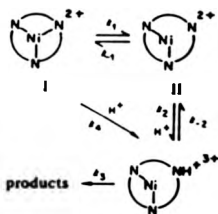


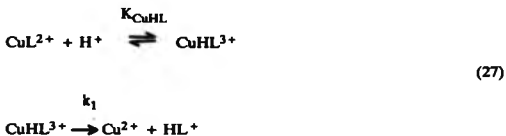
Fig. 1.7 Stepwise dissociation mechanism for  $[\text{Cu}(\text{tet-b})(\text{blue})]^{2+}$ .<sup>142</sup>



A number of  $\text{Cu(II)N}_3$  complexes have been studied, and a variety of kinetic behaviour has been observed.<sup>147,148</sup> Complexes containing the smaller ring sizes,  $\text{Cu(znn)}^{2+}$ ,  $\text{Cu(zdn)}^{2+}$ ,  $\text{Cu(zud)}^{2+}$  and  $\text{Cu(mznn)}^{2+}$  display a first order dependence of dissociation rate with  $[\text{H}]^+$ , whereas the larger ring sizes,  $\text{Cu(zdd)}^{2+}$ ,  $\text{Cu(ztd)}^{2+}$ ,  $\text{Cu(zaud)}^{2+}$ ,  $\text{Cu(zadd)}^{2+}$  and  $\text{Cu(zted)}^{2+}$  show an acid dependence at low  $[\text{H}]^+$  but become independent of acid at higher concentrations. The non-macrocyclic complex  $\text{Cu(ccha)}^{2+}$  also displayed this behaviour (see Figure 1.8).

The rate constants for dissociation are shown in Table 1.23.

Comparing the rates of dissociation of  $\text{Cu(znn)}^{2+}$ ,  $\text{Cu(zdn)}^{2+}$  and  $\text{Cu(zud)}^{2+}$  shows a decrease in rate as the macrocyclic ring size increases. The acid dissociations of the complexes with the larger ring sizes can be accounted for by the mechanism:



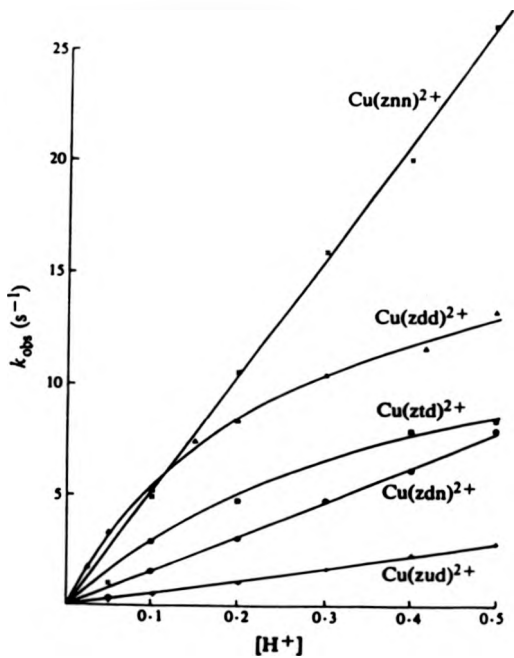


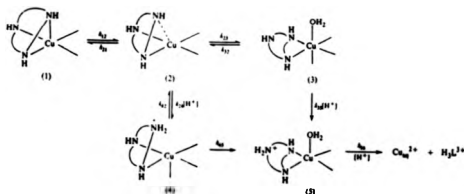
Fig. 1.8 Plot of  $k_{\text{obs}}$  against  $[\text{H}^+]$  for  $\text{Cu}^{2+} / \text{N}_3$  complexes.<sup>147</sup>

Table 1.23

Rate constants for the dissociation of various  $\text{Cu}^{2+}$  complexes;<sup>147,148</sup>  
aqueous solution

Complex	$k_H / (\text{dm}^3 \text{mol}^{-1} \text{s}^{-1})$	$k_1 / (\text{s}^{-1})$
$\text{Cu}(\text{znn})^{2+}$	51	-
$\text{Cu}(\text{mznn})^{2+}$	26	-
$\text{Cu}(\text{zdn})^{2+}$	17	-
$\text{Cu}(\text{zud})^{2+}$	5.6	-
$\text{Cu}(\text{zaud})^{2+}$	-	67
$\text{Cu}(\text{zdd})^{2+}$	-	21
$\text{Cu}(\text{zadd})^{2+}$	-	45
$\text{Cu}(\text{ztd})^{2+}$	-	15
$\text{Cu}(\text{zted})^{2+}$	-	50
$\text{Cu}(\text{ccha})^{2+}$	-	75

The mechanism is displayed graphically below:



The acid-independent pathway is accounted for by the path (1)-(2)-(3)-(5)-products with  $k_{32}$  as the rate determining step, whereas the acid-dependent pathway involves the process (1)-(2)-(4)-(5)-products. All complexes will display both pathways in their dissociation reactions, but since the acid-dependent pathway is generally much faster the other pathway is only observed in special circumstances. General acid catalysis was observed for the acid dissociation of

$\text{Cu}(\text{zdd})^{2+}$  indicating the importance of the direct proton attack,<sup>105</sup> with attack of the acid with concomitant Cu-N bond breaking being the rate determining step.

The acid hydrolysis of the Cu(II) and Ni(II) complexes of the ligand [15]aneN<sub>5</sub> have been studied.<sup>153</sup> A second-order dependence on  $[\text{H}^+]$  was observed for both species, indicating that the transition state of the reaction must involve two protons. This was explained by initial proton attack at an apical nitrogen atom in the  $\text{Cu}^{2+}$  species, since axial Cu-N bonds are weaker due to Jahn-Teller distortion. Attack of a second proton at the equatorial sites would then explain the kinetic behaviour (see Figure 1.9).

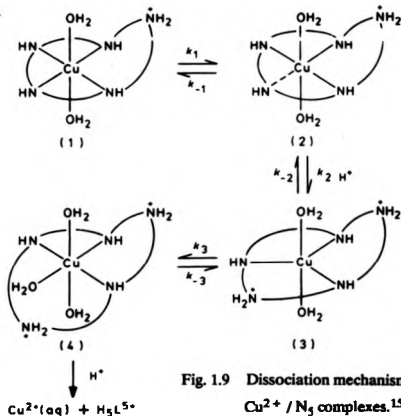


Fig. 1.9 Dissociation mechanism of  $\text{Cu}^{2+} / \text{N}_5$  complexes.<sup>153</sup>

The observed rate law was,  $\text{rate} = k_{\text{H}}[\text{complex}][\text{H}^+]^2$ , with  $k_{\text{H}}$  for  $[\text{CuL}]^{2+}$   $4.9 \times 10^{-2} \text{ dm}^6 \text{ mol}^{-2} \text{ s}^{-1}$  and for  $[\text{NiL}]^{2+}$   $0.63 \text{ dm}^6 \text{ mol}^{-2} \text{ s}^{-1}$  at 25 °C. The mechanism was confirmed by the observation of a third-order dependence on  $[\text{H}^+]$  for the Cu(II) and Ni(II) complexes of the hexadentate ligand 1,4,7,10,13,16-hexa-aza-cyclooctadecane. The same mechanism was observed for the Cu(II) complexes of [16] & [17]-aneN<sub>5</sub>.<sup>154</sup> Table 1.24 illustrates the increase in acid dissociation rate with

increasing ring size.

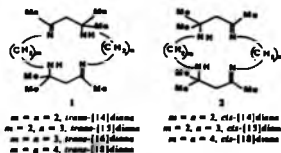
Table 1.24

Variation in acid dissociation rate constant with ring size for a series of Cu(II)/N<sub>5</sub> macrocyclic complexes;<sup>154</sup> (25 °C, aqueous)

Ligand	$k_{14}$ / (dm <sup>6</sup> mol <sup>-2</sup> s <sup>-1</sup> )
[15]aneN <sub>5</sub>	0.049
[16]aneN <sub>5</sub>	4.85
[17]aneN <sub>5</sub>	$1.18 \times 10^3$

The Ni(II) complex of [17]aneN<sub>5</sub> shows only a first-order dependence on [H<sup>+</sup>] ( $k_{14} = 0.23$  dm<sup>3</sup> mol<sup>-1</sup> s<sup>-1</sup> at 25 °C, I = 0.1 mol dm<sup>-3</sup>), so it would appear that only the four equatorial nitrogens are bound to the Ni(II) ion in the pH range studied, the axial N being protonated throughout.<sup>154</sup>

Structural effects on the dissociation rates of macrocyclic complexes have been studied. The kinetics of the acid catalysed dissociation of *trans*- and *cis*-diimine N<sub>4</sub> macrocyclic complexes were studied in order to evaluate the effect of ring unsaturation on the dissociation rates.



On comparison of the rates of acid dissociation for the *trans*-macrocyclic copper(II) complexes a decrease is observed as the ring size decreases from 18 to 16, with a second order dependence on [H<sup>+</sup>]. For the *cis*-macrocycles the rate decreases from 15 to 14, and then increases for the 13 membered monoimine. This indicates that the rate of hydrolysis is a minimum for the 14 membered tetraaza macrocyclic complexes, which is in keeping with the idea that the strain involved in

square planar co-ordination is least for a symmetrical 14 membered macrocycle. The results for the Ni(II) complexes display similar trends, with the rate of  $[\text{Ni}(\text{trans}\text{-}[14]\text{diene})]^{2+}$  dissociation being ca.  $10^{-9} \text{ s}^{-1}$  at 25 °C in 2 mol dm<sup>-3</sup> HCl,<sup>155</sup> see Table 1.25.

The acid catalysed dissociation of the Cu(II) complex of *cis*-[18]diene is known to possess a distorted tetrahedral geometry and this is reflected in the fast dissociation rate (Table 1.25), and is due to the high degree of strain in the structure. In comparison, the analogous *trans*-complex is essentially planar, with few steric problems, and thus dissociates much more slowly in acid. Indeed, the *cis*-complex is so

Table 1.25

Acid dissociation rate constants for Ni<sup>2+</sup> and Cu<sup>2+</sup> complexes of diimine macrocyclic complexes;<sup>155,156</sup> 25 °C

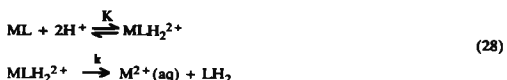
Complex	$k_H / (\text{dm}^3 \text{ mol}^{-1} \text{ s}^{-1})$
$[\text{Cu}(\text{trans}\text{-}[16]\text{diene})]^{2+}$	$9 \times 10^{-3}$
$[\text{Cu}(\text{trans}\text{-}[18]\text{diene})]^{2+}$	$4.8 \times 10^{-3}$
$[\text{Cu}(\text{trans}\text{-Me}_6[14]\text{diene})]^{2+}$	$2 \times 10^{-4}$
$[\text{Cu}(\text{trans}\text{-Me}_6[18]\text{diene})]^{2+}$	$3.6 \times 10^{-2}$
$[\text{Cu}(\text{cis}\text{-Me}_6[18]\text{diene})]^{2+}$	25
$[\text{Ni}(\text{trans}\text{-}[15]\text{diene})]^{2+}$	$3.5 \times 10^{-5}$
$[\text{Ni}(\text{Me}[15]\text{diene})]^{2+}$	$3.8 \times 10^{-6}$
$[\text{Ni}(\text{trans}\text{-}[18]\text{diene})]^{2+}$	$5 \times 10^{-4}$
$[\text{Ni}(\text{trans}\text{-Me}_6[18]\text{diene})]^{2+}$	$6 \times 10^{-4}$

highly strained that it dissociates faster than  $[\text{Cu}(\text{2,3,2-tet})]^{2+}$  which contains an open-chain ligand (Table 1.20).

The increased rigidity of the imine groups makes the macrocycles less flexible than the saturated cyclic tetramines, making the conformational changes required to move a dissociated nitrogen away from the metal more difficult. Kinetic results for

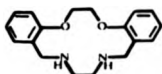
the Cu(II) compounds indicate that the rate determining step may be the breaking of the second Cu-N bond.

Acid dissociations of the Cu(II) and Ni(II) complexes of 5,7-dioxo-cyclam proceed entirely by an acid induced pathway, with no solvolytic pathway detectable. Again, a second order  $[H^+]$  dependence is observed, with a possible kinetic scheme for the dissociation being:

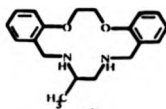


The slow dissociation after initial protonation is the rate determining step. The rate constant for the Cu(II) complex is  $1.15 \pm 0.03 \times 10^7 \text{ dm}^6 \text{ mol}^{-2} \text{ s}^{-1}$  at 25 °C and for the Ni(II) complex it is  $1.23 \pm 0.01 \times 10^5 \text{ dm}^6 \text{ mol}^{-2} \text{ s}^{-1}$ . The diamide macrocycles react much more rapidly than the similar tetraaza macrocyclic complexes, which normally show a first order dependence on  $[H^+]$ .<sup>145</sup> The reason for this is probably an initial attack by protons on the amide oxygen atoms to give the iminol tautomer, followed by intramolecular proton transfer to the nitrogen donors, thus producing a rapid preequilibrium prior to the dissociation. Such protonation behaviour has been observed in acid solutions of  $[Co(NH_3)_4(\text{glyNH})]^{2+}$ <sup>157</sup> and  $[Co(\text{glyglyO})_2]^{+}$ .<sup>158</sup>

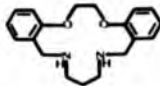
Since macrocyclic polyamines dissociate so slowly mixed-donor macrocycles have often been studied instead, since their lower stabilities make the complexes more amenable to study because they are more labile. To this end the kinetics of acid dissociation of a range of Ni(II) complexes of 14-17 membered  $N_2O_2$ -donor macrocycles were studied.<sup>159</sup>



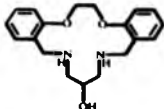
$L^a$



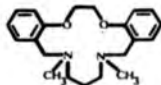
$L^b$



$L^c$



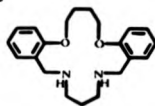
$L^d$



$L^e$



$L^f$



$L^g$

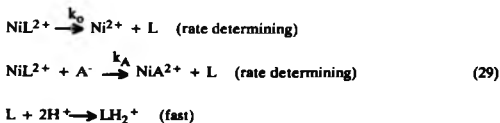
Kinetic data for the dissociations are given in Table 1.26.

Table 1.26

Rate constants for the dissociation of various  $Ni^{2+}/N_2O_2$  macrocyclic complexes;<sup>1,59</sup> aqueous solution (except L<sup>c</sup>, L<sup>f</sup> & L<sup>g</sup> in 90% methanol),  $[H^+] = 1.0 \text{ mol dm}^{-3}$

Macrocyclic	ring size	$k_{obs}$ (25 °C), s <sup>-1</sup>
L <sup>a</sup>	14	$8.8 \times 10^{-1}$
L <sup>b</sup>	14	$1.4 \times 10^{-1}$
L <sup>c</sup>	15	$3.5 \times 10^{-3}$
L <sup>d</sup>	15	$1.7 \times 10^{-2}$
L <sup>e</sup>	15	$3.8 \times 10^{-4}$
L <sup>f</sup>	16	$6.4 \times 10^{-4}$
L <sup>g</sup>	17	> 0.5

Acetic acid was shown to have a strong catalyzing effect on the reactions, unlike other acids tried, and it was suggested that it was the acetate ion that was responsible for this behaviour, though general acid catalysis was not indicated. The reactions are generally independent of the acid concentration and fit the mechanism:



The second step is only important for the acetate ion, and in all other cases the acid only scavenges the free ligand to prevent reformation of the initial complex. Thus, the solvolytic pathway is the rate determining step in these complexes. This almost certainly involves cleavage of the first or second oxygen atom, since similar studies using macrocyclic  $S_2N_2$  complexes show similar kinetic behaviour and both

sets of complexes dissociate quicker than  $N_4$ -donor macrocyclic Ni(II) complexes. An isokinetic correlation supports the existence of a constant mechanism throughout the series of  $N_2O_2$  complexes studied. The rate of dissociation of the unsubstituted macrocycles is very dependent on the ring size, with kinetic labilities following the sequence  $14 > 15 > 16 < 17$ . This suggests that the 16 membered macrocycle provides the best fit for Ni(II) ion, which is in accordance with hole size considerations.<sup>160</sup> C- and N- methylation of the ligands reduces the dissociation rate of the complexes which suggests that a steric barrier is involved in the dissociation of the macrocycle. This is in keeping with the observations of Barefield et al on the N-methylation of  $N_4$  donor macrocycles.<sup>109,161</sup>

The dissociation trends of Cu(II) complexes of the polythiaether macrocycles have been investigated by Rorabacher et al.<sup>121,130</sup> They discovered that the dissociation rates have far more relevance to the stabilities and the macrocyclic effect (see section 1.7) than the complexation rates (see section 1.5 (h)). Acid conditions were not required in these studies as the macrocycles possess S-donors. The measurements of formation and dissociation rate constants and the kinetic stabilities were

**Table 1.27**

Calculated rate constants for the dissociation of various  $Cu^{2+}$ /polythiaether complexes;<sup>121</sup> aqueous solution, 25 °C,  $0.1 \text{ mol dm}^{-3} \text{ ClO}_4^-$  ( $\text{HClO}_4$ )

Ligand	$10^{-1} k_d / (\text{s}^{-1})$
[12]aneS <sub>4</sub>	0.26
[13]aneS <sub>4</sub>	2.7
[14]aneS <sub>4</sub>	0.6
[15]aneS <sub>4</sub>	15.8
[16]aneS <sub>4</sub>	106
[15]aneS <sub>5</sub>	4.9
Et <sub>2</sub> -2,3,2-S <sub>4</sub>	860
Me <sub>2</sub> -2,3,2-S <sub>4</sub>	4500

thus possible at the same time. The rate constants for dissociation of the Cu(II) complexes are shown in Table 1.27.

A large solvent dependence of the rate constants was observed in methanol-water mixtures suggesting that solvation of the partially dissociated ligands greatly aids the dissociation process. The effect of ring size on the dissociation rate is shown in Figure 1.5. The effect of the constrained ligand flexibility is manifested in the large increases in the dissociation rates going from 14 to 16 membered macrocycles and on to the open-chain ligands. The 13 membered macrocyclic complex does not follow this trend as the metal ion is already partially "out" of the ring since it is not coplanar with the donor atoms as in the larger ring structures and so dissociates faster. This effect is balanced by increased rigidity in the  $[\text{Cu}[12]\text{aneS}_4]^{2+}$  complex.

### 1.7 The Thermodynamics of Macrocyclic Complexes

#### "The Macrocyclic Effect."

The term "macrocyclic effect" was originated to describe the greater stabilities observed for aqueous metal complexes with cyclic tetraamines, which are several orders of magnitude more stable than the corresponding complexes with analogous linear amines of the same denticity. Cabiness and Margerum<sup>162</sup> first reported the effect. The macrocyclic effect was seen as an extension of the chelate effect, which refers to the greater stability of a complex containing chelate rings compared to that of an analogous complex which contains fewer or no rings.<sup>163</sup> Thus, for example the complex  $[\text{Ni(en)}_3]^{2+}$ , containing 3 chelate rings, has an overall stability constant of  $\log \beta = 18.28$ , whereas the complex  $[\text{Ni}(\text{NH}_3)_6]^{2+}$ , which has the same number and type of donor but no chelate rings, has an overall stability constant of  $\log \beta = 8.61$ ; which is nearly  $10^{10}$  times less stable than the chelated complex.

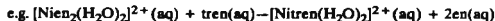
Since;

$$\Delta G^\circ = -RT \ln \beta = \Delta H^\circ - T \Delta S^\circ \quad (30)$$

the factors which contribute to the chelate effect can be split into enthalpy and

entropy contributions (see figure 1.10).

The main contribution always comes from the entropy, whether the enthalpy is favourable or not. Indeed, there are a number of examples of the chelate effect where the enthalpy is actually unfavourable, yet a chelate effect is still observed;



$$\log \beta = 1.88$$

$$\Delta H^\circ = +13.0 \text{ kJ mol}^{-1}, -T\Delta S^\circ = -23.7 \text{ kJ mol}^{-1}, \Delta G^\circ = -10.7 \text{ kJ mol}^{-1}$$

(ref. 165)

The entropy contribution will always be favourable because chelation will cause an increase in the number of unbound molecules (solvent or ligand). The chelate effect generally decreases with increasing size of the chelate ring; thus 1,3-diaminopropane has a smaller chelate effect than 1,2-diaminoethane. This is because when one end of the chelating ligand is bound to the metal the longer the length of the carbon chain, the further away the other donor atom/s of the ligand will be from the metal ion and so the ring will be less likely to close.

Some of these arguments can be used when attempting to explain the macrocyclic effect. It is easy to see how the entropy term will always be favourable for the complexation of a cyclic ligand compared to an open-chain ligand as the cyclic ligand is already restricted in many ways and so will have far less degrees of freedom to lose than the open-chain ligand (assuming that both complexes, with closely analogous ligands have similar entropies). However, the enthalpy term may or may not be favourable and many investigations into the macrocyclic effect have attempted to assign the additional stability of macrocyclic complexes to either entropy, enthalpy or a combination of both factors. The macrocyclic effect can also be explained in kinetic terms and is due to a decreased rate of dissociation in macrocyclic complexes compared to those with open-chain ligands, this is known as "multiple juxtapositional fixedness" (see section 1.6).

Fig. 1.10 Factors influencing solution stability of complexes.<sup>164</sup>

Enthalpy effects	Entropy effects
Variation of bond strength with electronegativities of metal ions and ligand donor atom	Number of chelate rings Size of chelate ring
Ligand field effects	Changes of solvation on complex formation
Steric and electrostatic repulsion between ligand donor groups in the complex	Arrangement of chelate rings Entropy variations in uncoordinated ligands
Enthalpy effects related to the conformation of the uncoordinated ligand	Effects resulting from differences in configurational entropies of the ligand in complex compounds
Other coulombic forces involved in chelate ring formation	<i>Entropy of solution of ligands</i>
<i>Enthalpy of solution of ligands</i>	<i>Entropy of solution of coordinated metal ions</i>
<i>Change of bond strength when ligand is changed (same donor and acceptor atom)</i>	

Cabbiness and Margerum first observed the macrocyclic effect when comparing the stability of a series of 1:1 complexes of tetramines with Cu(II) (Table 1.28). The authors attributed the reduced stability to  $[\text{Cu}(\text{tet-a})(\text{blue})]^{2+}$  compared to the (tet-a)(red) complex because of a folded macrocyclic structure, producing a less stable structure compared to the planar  $[\text{Cu}(\text{tet-a})(\text{red})]^{2+}$ . However, this theory is incorrect, as  $[\text{Cu}(\text{tet-a})(\text{blue})]^{2+}$  has a planar structure as well. The reason for the low stability lies in the unstable chelate ring structure. In  $[\text{Cu}(\text{tet-a})(\text{red})]^{2+}$  the ligand is in its most stable configuration, with both six membered chelate rings in a chair form and both five membered rings in a gauche form.<sup>141,166</sup> However, the authors concluded from the  $[\text{Cu}(\text{tet-a})(\text{red})]^{2+}$  results that the macrocyclic effect was about 10 times larger than could be explained by the chelate effect observed for Cu(II) and amine complexes. The two ligands used for comparison, tet-a and 2,3,2-tet, have many differences in their structure, and so further studies were initiated so as to compare ligands which resembled one another structurally much more closely.

Table 1.28

Stability constants for various 1:1 complexes of  $\text{Cu}^{2+}$ /tetramines;<sup>162</sup>

25.0 °C,  $\mu = 0.1 \text{ mol dm}^{-3}$

Ligand	log K
tpt	13.1
3,3,3-tet	17.3
tren	18.8
trien	20.1
2,3,2-tet	23.9
tet-a(blue)	20
tet-a(red)	28

The first of these investigations was designed to assess the contribution of

ligand solvation on the macrocyclic effect. A series of 1:1 complexes of both macrocyclic and open-chain tetramines with Ni(II) were studied by absorbance and calorimetric measurements (Table 1.29).<sup>167,168</sup>

The stability constant of the Ni(II)[14]aneN<sub>4</sub> complex is more than 10<sup>6</sup> times greater than for Ni(II)(2,3,2-tet). Comparison of the thermodynamic contributions shows that this enhanced stability is due to a more favourable enthalpy contribution for the macrocyclic ligand complex, with the  $\Delta H^\circ$  for Ni([14]aneN<sub>4</sub>)<sup>2+</sup> being 58.8

**Table 1.29**

Stability constants, enthalpies and entropies of formation for various Ni<sup>2+</sup> complexes, aqueous solution, 25 °C,  $\mu = 0.1 \text{ mol dm}^{-3}$ .<sup>169</sup>

Complex	log K <sub>NIL</sub>	$\Delta H^\circ$ (kJ mol <sup>-1</sup> )	$\Delta S^\circ$ (J K <sup>-1</sup> mol <sup>-1</sup> )
Ni(cyclam) <sup>2+</sup>	22.2	-129.7	-8.4
Ni(Me <sub>2</sub> cyclam) <sup>2+</sup>	21.9	-117.2	+33.5
Ni(tet-a) <sup>2+</sup>	ca. 20	-	-
Ni(tet-b)	18.2	-	-
Ni(2,3,2-tet) <sup>2+</sup>	15.8	-81.2	+30.1
Ni(trien) <sup>2+</sup>	13.8	-58.6	+66.9
Ni(2,3,2-tet) <sup>2+</sup> (s.p.)	15.3	-70.3	+57.7
Ni(trien) <sup>2+</sup> (s.p.)	11.9	-44.4	+78.2

kJ mol<sup>-1</sup> more favourable than the Ni(2,3,2-tet)<sup>2+</sup> (only the contribution from the square planar complex is used for comparison, the contributions from the octahedral complex with which it is in equilibrium must be neglected for ideal comparison). This large difference cannot be explained by stronger Ni-N bonding or by more favourable ring contributions (the most favourable arrangement of chelate rings being 5,6,5,6-membered as it holds ring strain to a minimum<sup>169</sup>). It was concluded that the dominant factor responsible for the macrocyclic effect in the tetramine ligands is the lower degree of solvation of the macrocycle compared to the

open-chain ligand. The cyclic nature of [14]aneN<sub>4</sub> physically prevents it from having as large a hydration number as 2,3,2-tet, and data suggest that the macrocycle has at least two fewer water molecules. Thus, the enthalpy was considered to contribute the major factor for the macrocyclic effect in these complexes, with a smaller factor being the lower configurational entropy of the already cyclic ligand. The importance of steric effects was observed in the destabilising influence of the presence of methyl substituents on the 14 membered macrocyclic ring. The effect increasing with increasing the number of methyl groups from two to six.

Much the same conclusions were reached by Dei and Gori in a study of the thermodynamics of the metathesis;



They established that the macrocyclic effect was due to favourable enthalpy contributions in the form of stronger Cu-N bonds in the cyclam complex and to favourable solvation enthalpy.<sup>170</sup>

More recent investigations by Paoletti et al<sup>171-176</sup> have shown that both entropy and enthalpy can make significant contributions to the macrocyclic effect. In a series of calorimetric studies the authors measured the entropies and enthalpies of formation of a number of macrocyclic and non-macrocyclic tetramine Cu(II) and Zn(II) complexes, and were able to assess the relative contributions of each to the macrocyclic effect. Some of their results are plotted in Figure 1.11.

The values for  $\Delta S^\circ$  show that the entropy contribution is always more favourable for the complexes of the macrocyclic ligands than for those of the non-cyclic ligands. Figure 1.11 shows that the enthalpy contribution is greatest for the 14 membered macrocyclic ring with Cu(II), and follows the sequence [14] > [13] > [15] > [12]. This follows the sequence of the relative strengths of the Cu-N interactions, and indicates that the enthalpy contribution to the macrocyclic effect is dependent on the matching of the size of the macrocyclic ligand aperture to that of the metal

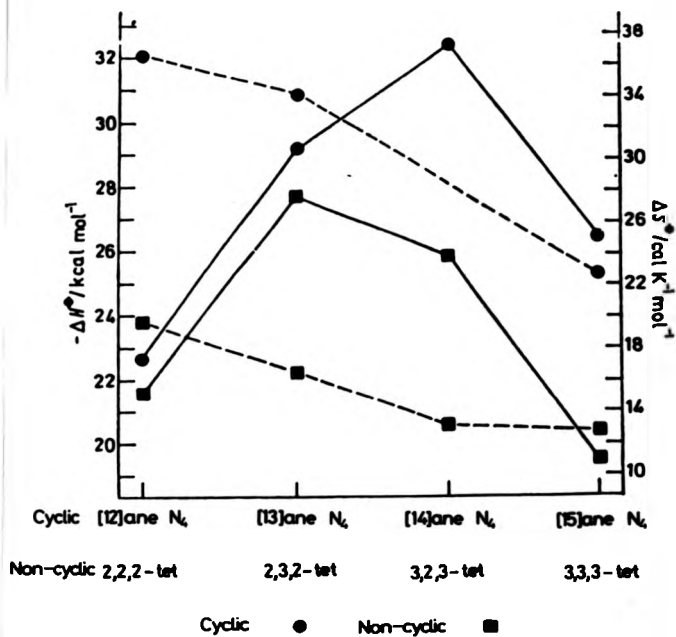


Fig. 1.11 Formation parameters for the formation of  $\text{Cu}^{2+}$  / polyamine complexes.<sup>173</sup>

ion. A reassessment of the macrocyclic effect for  $(\text{Ni}[14]\text{janeN}_4)^{2+}$ <sup>175</sup> compared to  $\text{Ni}(2,3,2\text{-tet})^{2+}$  showed that the enthalpy term was much lower than previously measured (ca. 22 kJ mol<sup>-1</sup>) and so brought this system in line with the theory that the entropy and enthalpy terms can both significantly contribute to the macrocyclic effect. The sequence of the chelate rings was also found to have an effect on the thermodynamics of complexation.<sup>174</sup> It was observed that when unfavourable pre-orientation is present (i.e. anything but 5,6,5,6-membered chelate rings for tetramines) the energy saving due to cyclisation is outbalanced by the formation of weaker and less exothermic Cu-N bonds with respect to analogous open-chain ligands. Thus, isocyclam (1,4,7,11-tetraazacyclotetradecane) has an enthalpy of formation of -27.8 kJ mol<sup>-1</sup> with Cu(II) at 25 °C, whereas cyclam has  $\Delta H^\circ = -32.4$  kJ mol<sup>-1</sup>.

Hancock and Ngwenya also studied the effect of increase of chelate ring size on the stabilities of macrocyclic complexes.<sup>177</sup> They measured the stabilities of four tetraaza macrocyclic complexes which consisted of three five-membered chelate rings plus a fourth chelate ring which varied regularly from five to eight members.

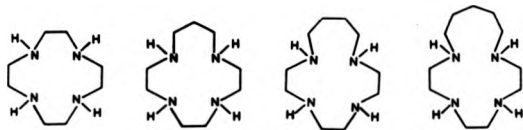


Figure 1.12 illustrates the trends observed, relative to the stability of the first ligand with each metal ion. They observed that the complex stabilities depended little on the size of the macrocyclic ring and that the main factor involved is the size of the chelate ring formed, the particular differentiation in stability being dependent on the size of the particular metal ion used.

Macrocyclic ring size effects in tetramines have also been investigated by Kodama and Kimura.<sup>98-102,104</sup> They measured the equilibria of complex formation of 12, 13, 14 and 15 membered tetramines with Cu(II), Zn(II), Pb(II) and Cd(II) by

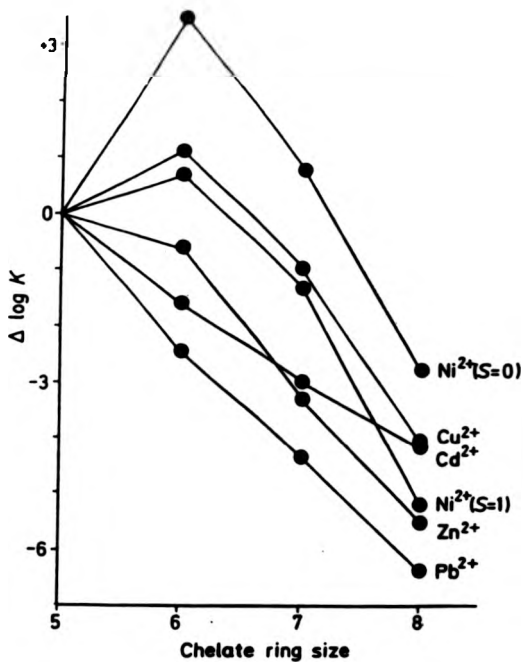


Fig. 1.12 Variation of  $\log K$  with chelate ring size for  $\text{N}_4$  macrocyclic complexes.<sup>177</sup>

polarographic methods, as well as those of their non-macrocyclic analogues.

They observed that for the 12 membered macrocyclic complex with Cu(II), the macrocyclic effect was due to a large positive entropy term which can be explained by the pre-orientation prior to chelation (a favourable ligand conformation); this outweighs the unfavourable enthalpy, which is probably a result of steric constraint in the complex. For the 13 membered macrocycle the entropy contribution to the stability of the Cu(II) complex is somewhat reduced, and the macrocyclic effect is now due to a combination of both enthalpy and entropy terms. The 14 membered macrocyclic complex also exhibits this combination of favourable terms. For the 15 membered macrocyclic Cu(II) complex deciding which term makes the chief contribution to the macrocyclic effect depends on which open-chain ligand it is compared to. If 4,8-diazaundecane-1,11-diamine is used for the comparison the significant term is the  $\Delta H$  contribution. However, if 4,7-diazadecane-1,10-diamine is used, then the  $\Delta S$  term becomes dominant. This illustrates the difficulty in finding macrocyclic and open-chain ligands which are closely analogous. In contrast to these results, the Zn(II) complexes of these macrocyclic ligands show little change in stability with ring size, and the macrocyclic effect, when compared to related complexes of open-chain tetramines, is always due to the favourable entropy changes.<sup>104</sup>

The Cu(II) complexes of triamine macrocycles show no macrocyclic effect,<sup>102,178</sup> with a  $\log K_{CuL}$  for 1,4,7-triazacyclononane of 16.2, and that for 3-azapentane-1,5-diamine being 15.8. The reason for this is that a high degree of steric strain is present in the facially bound cyclic ligands; whereas the open-chain triamine bonds meridionally with no strain, this causes a very unfavourable enthalpy change, which cancels out the favourable entropy contribution from the macrocyclic ligand. In contrast, cyclisation in the Zn(II) complexes produces an increase in complex stability ( $\log K_{CuL} = 11.3$  for the macrocycle and  $\log K_{CuL} = 8.8$  for the open-chain ligand). This is presumably because  $Zn^{2+}$  does not prefer a planar co-ordination like  $Cu^{2+}$  and so the enthalpy term does not suffer, allowing the entropy to become the dominant factor.

With macrocyclic pentamines the Cu(II) complexes again show a macrocyclic effect, but in contrast to the tetramines the enthalpy term is dominant in determining the increased stabilities. Increasing the ring size decreases the stability of the complexes, the entropy term for complex formation varying little (Table 1.30).

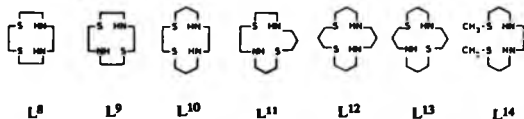
In the Zn(II) complexes the  $\Delta S$  terms are wholly responsible for the increased stability of the macrocyclic systems with the enthalpy terms little affected by ring size, which is in contrast to the Cu(II) complexes, although the same trend of decreasing stability with increasing ring size is still observed. These differences must again reflect the different steric requirements of the two metals. These same trends are observed with the Cd(II), Hg(II) and Pb(II) complexes.<sup>178</sup>

Table 1.30

Stability constants, enthalpies and entropies of  $\text{Cu}^{2+}$ /polyamine complex formation: aqueous solution, 25 °C,  $\mu = 0.2 \text{ mol dm}^{-3}$ ; 106

Ligand	log K	$\Delta H^\circ$ (kJ mol <sup>-1</sup> )	$\Delta S^\circ$ (J K <sup>-1</sup> mol <sup>-1</sup> )
[15]aneN <sub>5</sub>	28.3	-137.7	+ 92.1
[16]aneN <sub>5</sub>	27.1	-136.8	+ 58.6
[17]aneN <sub>5</sub>	23.8	-113.8	+ 75.3

Introducing sulphur atoms into nitrogen donor macrocycles has the effect of reducing the stability of the metal complexes. The thermodynamics of complexation of a series of *cis*- and *trans*-N<sub>2</sub>S<sub>2</sub> donor macrocycles with varying ring size was studied with Cu(II).<sup>179</sup> All the ligands formed [ML]<sup>2+</sup> complexes, although the 12 membered macrocycles and the open-chain ligand also formed hydroxo-species [ML(OH)]<sup>+</sup>.



Both *cis*- and *trans*- macrocycles displayed the trends previously observed for tetraaza macrocycles of maximum stability at 14 membered ligands. The *cis*- ligands are more stable than the *trans*- due to the higher stability of five membered chelate rings with two nitrogens (Table 1.31). The macrocyclic effect is due to a large entropy term, with a smaller contribution from a favourable enthalpy term, this can be seen by comparing the *cis*- 14 membered macrocyclic complex with the open-chain complex. This is also similar to the tetramine macrocyclic complexes.

With polythiaether macrocycles, where all the nitrogens are replaced by sulphur atoms, the Cu(II) complexes are even less stable than in the mixed species.<sup>180</sup> Maximum stability is again observed for the 14 membered macrocycle.

Table 1.31

Stability constants and thermodynamic parameters for Cu<sup>2+</sup> complexes of L<sup>8-14</sup> aqueous solution, 25 °C,  $\mu = 0.5 \text{ mol dm}^{-3}$  (KNO<sub>3</sub>):<sup>179</sup>

Ligand	log K	$-\Delta H^\circ$ (kJ mol <sup>-1</sup> )	$\Delta S^\circ$ (J K <sup>-1</sup> mol <sup>-1</sup> )
L <sup>8</sup>	14.2	59.4	72.8
L <sup>9</sup>	12.0	39.8	96.6
L <sup>10</sup>	16.0	66.1	83.7
L <sup>11</sup>	13.1	58.2	56.5
L <sup>12</sup>	10.6	-	-
L <sup>13</sup>	10.6	-	-
L <sup>14</sup>	11.4	57.7	24.7

The relative contributions of entropy and enthalpy are illustrated in Figure 1.13. All the data can only be interpreted relative to each other as an unfortunate dependence on the perchlorate ion concentration was observed (due to perchlorate bonding to the metal ions), and was only resolved for the Cu([14]aneS<sub>4</sub>)<sup>2+</sup> species, although the dependence was found to be very similar for all the different complexes.<sup>181</sup> The entropy of complexation is seen to decrease with increasing ring size,

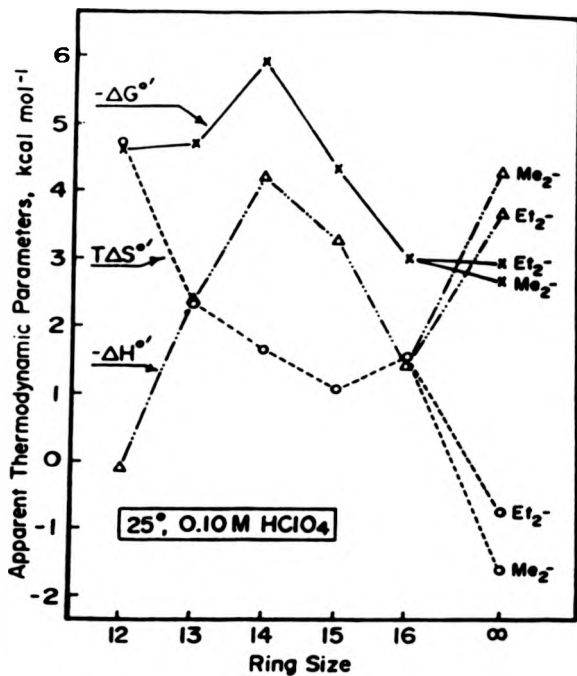


Fig. 1.13 Ring size effects for  $\text{Cu}^{2+}$  / tetraethiaether complexes.<sup>180</sup>

with the [16]aneS<sub>4</sub> complex being slightly anomalous. This is as expected since as the ring size increases greater loss of freedom will occur on complexation if all the complexes are of comparable rigidity. The entropy values for the tetraethiaether complexes are all much less than those of the tetraaza complexes, reflecting the importance of the ligand desolvation in the latter complexes. The enthalpy changes reflect the strength of the Cu-S bonding, with a minimum in enthalpy change for the Cu([14]aneS<sub>4</sub>)<sup>2+</sup> complex. By comparison of the thermodynamic data for the open-chain ligand complexes with the [14]aneS<sub>4</sub> complex, it can be shown that the macrocyclic effect in the polythiaethers is controlled by the favourable entropy of complexation.

Recently, Hancock and Martell<sup>182</sup> published an excellent analysis of the chelate, macrocyclic and cryptate effects, in which they conclude that a number of factors contributed to the increased complex stabilities;

(1) pre-organisation of the ligand so that the donor atoms in the free ligand are correctly oriented prior to complex formation,

(2) desolvation of the donor atoms in the sterically constrained spaces of the ligands,

(3) intrinsic basicity effects, such that greater basicity is induced in donor atoms as ethylene bridges are added to the ligands,

(4) and enforced dipole-dipole repulsion in the ligands, which is relieved on complexation.

## Chapter 2

### The Kinetics of Complexation of 1,4,8,11-tetra-azacyclotetradecane and 1,4,7-triazacyclo-nonane with $\text{Ni}^{2+}$ , $\text{Co}^{2+}$ and $\text{Cu}^{2+}$ Ions in Dimethyl Sulphoxide Solution

#### 2.1 Introduction

The kinetics of complexation of macrocyclic ligands with transition metals are reviewed in Chapter 1. The kinetics in aqueous solutions are significantly affected by protonation effects, which complicates the analysis of the rate data and the establishment of a proposed mechanism, and necessitates measurement of rate data over a range of pH. At low pH the protonated macrocycles are present which react extremely slowly. At high enough pH the macrocycles are present as the free ligands, and studies have been carried out under such conditions for this reason.<sup>93</sup> However, at high pH the metal ions are present as hydroxo species (e.g.  $[\text{Cu}(\text{OH})_3]^-$  and  $[\text{Cu}(\text{OH})_4]^{2-}$  in 0.1 - 2.0 mol  $\text{dm}^{-3}$  NaOH), which will have different reactivities to the hexaquo species present in the mid-pH range. Indeed, in the case of tetraaza macrocycles reacting with  $\text{Cu}^{2+}$  at high pH the two different metal hydroxo species are proposed to react with different rate determining steps.<sup>93</sup> Thus, different complexities are introduced into the data analysis rather than simplification, and working with strong NaOH solutions is not at all convenient.

Unprotonated macrocycles can be studied quite easily in aqueous solution at the normal pH range employed in kinetic studies by using the polythiaether macrocycles, which contain only S-donor atoms which do not protonate, and which are not as strongly solvated as the hydrogen-bonding tetraaza macrocycles. However, the lack of hydrogen-bonding means that the thiaether macrocycles are not very soluble in pure aqueous solvents and experimentally a mixture of solvents must be used. Rorabacher et al used a water/methanol mixture in their studies of the kinetics and

thermodynamics of cyclic polythiaether complexations.<sup>121,130</sup>

If nitrogen donor macrocycles are to be studied then other methods must be used to avoid protonation and hopefully simplify the processes involved in complexation. The simplest method is to carry out the kinetic studies in aprotic solvents, such as acetonitrile, dimethyl formamide and dimethyl sulphoxide,<sup>183,184</sup> where protonation of the aza macrocycles cannot occur. A number of studies using these solvents have been reported.<sup>55,94,95,113</sup> An added advantage of this method is that hydroxo species of the metal ions will not be formed if pure, dry solvents are used. From previous work in these solvents the kinetics of complexation do indeed appear to be simpler in a dipolar aprotic solvent than in water. Studies under pseudo-first order conditions ( $[M^{2+}] \gg [L]$ ) in dimethyl sulphoxide and dimethyl formamide have revealed two reaction steps. These consist of an initial fast step which is dependent on the concentration of the metal ion, and a slower second step which is independent of metal ion concentration. Investigations using  $CH_3CN$  as solvent showed the presence of more than two steps in some cases.<sup>95</sup>

All of the original work reported in this thesis has been carried out using dmsu as solvent. In this chapter the studies concentrate on the complexation reactions of the  $N_4$ -donor macrocycle 1,4,8,11-tetra-azacyclotetradecane (Cyclam) and the  $N_3$ -donor macrocycle 1,4,7-tri-azacyclononane ( $(9)aneN_3$ ) with Ni(II), Co(II) and Cu(II). Attempts were made to establish whether the  $N_4$  and  $N_3$  macrocycles react via the Eigen-Wilkins dissociative interchange mechanism, or if the steric constraints of the cyclic ligands impose restrictions on the mechanism, perhaps causing the first chelate ring closure to become rate determining. If these ligands react via a dissociative interchange mechanism then the rates of reaction should be identical for the two ligands and should be the same as reaction rates for analogous open-chain ligands.

The reaction of  $Ni^{2+}$  with cyclam in dmsu has already been studied<sup>55</sup> and was repeated in this study. Reactions with other metals ions and studies of the  $N_3$  macrocyclic ligand were made to extend the knowledge of the mechanisms of complexation of these simple macrocyclic systems, which can then be used as the basis

for the study of complexation reactions of pendent arm macrocycles (Chapter 3) and more sterically hindered macrocycles (Chapter 4).

## 2.2 Experimental

### 2.2.1 Materials and Syntheses.

Anhydrous  $Mn^{2+}$ ,  $Co^{2+}$ ,  $Ni^{2+}$ ,  $Cu^{2+}$  and  $Zn^{2+}$  dmsO tetrafluoroborate salts were prepared from the commercially available hydrated metal tetrafluoroborate salts (Alfa-Inorganics) using an analogous procedure to the synthesis of the perchlorate salts.<sup>185</sup>

A fairly dry sample of the hydrated salt (ca. 2g), used as supplied, was dissolved in 25 cm<sup>3</sup> of triethyl orthoformate (Aldrich) and stirred in a sealed Schlenk tube for 2 hours under dry nitrogen. Dry dmsO (ca. 5 cm<sup>3</sup>) was then added dropwise via a syringe to precipitate out the dmsO solvates. The suspension was then left to stir for a further hour under nitrogen, before filtration to collect the solids. The product was then washed with a mixture of 9:1 dry ethyl ether and triethyl orthoformate. Recrystallisation was carried out using a minimum amount of a 9:1 dry nitromethane and dmsO mixture. All products were then dried under vacuum or in sealed bottles in a dry nitrogen flushed glove-box.

Hydrated manganese(II) tetrafluoroborate was prepared by reacting manganese metal (BDH) with fluoroboric acid (40%, BDH). After all the metal had dissolved the solution was filtered to remove any insoluble material, then all the solvent was taken off on a rotary evaporator to leave a pale pink solid. This was recrystallised from a minimum amount of water and dried under vacuum overnight. The hexahydrated tetrafluoroborate salt thus formed was then used to prepare the hexa(dmsO) salt in the same way as for the other metals.

All the products were tested for water or tetrafluoroborate co-ordination by examination of their infra-red spectra (4000-200 cm<sup>-1</sup>), recorded as nujol mulls between NaCl plates. All products showed no sign of water or fluoroborate interfer-

ence. The tetra-fluoroborate salts have a distinct advantage over the more frequently used perchlorate salts in that the former are not potentially explosive unlike the perchlorates.<sup>196</sup> The tetra-fluoroborates have also been found to be even weaker co-ordinating anions than the perchlorates e.g. in  $Zn(MeOH)_6^{2+}$  solutions.<sup>197</sup>

The solid complexes are generally held to have the same structures as their analogous perchlorate salts;  $[M(dmsO)_6][BF_4]_2$  (for  $M = Mn, Co, Ni$ ) and  $[M(dmsO)_4][BF_4]_2$  (for  $M = Cu$  and  $Zn$ ).<sup>185-188</sup> The complexes were analysed by metal ion titration <sup>198,199</sup>,  $Mn^{2+}$ ; calculated 7.9%, found 7.8%,  $Co^{2+}$ ; calculated 8.4%, found 8.1%,  $Ni^{2+}$ ; calculated 8.4%, found 8.3%,  $Cu^{2+}$ ; calculated 11.6%, found 11.4%,  $Zn^{2+}$ ; calculated 11.7%, found 11.5%. The structures of the solvated cations in solution are however not as clearly defined. Certainly for  $Mn^{2+}$ ,  $Co^{2+}$  and  $Ni^{2+}$  all evidence points to the standard octahedrally solvated ion seen in many other solvents. For  $Cu^{2+}$  however both square planar<sup>189</sup> and octahedral<sup>190,191</sup> co-ordination have been suggested. Taking into account the Jahn-Teller tetragonally distorted octahedral species found in other solvents the true structure probably lies somewhere in between the two suggested, with axially co-ordinated dmsO molecules lying at long distances from the metal ion compared to the more strongly bound equatorial molecules. The most recent investigation suggests that the formation of  $[Cu(dmsO)_6]^{2+}$  is much less extensive than  $[Cu(dmsO)_4]^{2+}$ ,<sup>192</sup> though both still exist.

For  $Zn^{2+}$  the situation is even less clear cut. In methanol the solvation number of  $Zn^{2+}$  is reported to vary from six at low dilution to four at higher concentrations.<sup>193</sup> Since a low co-ordinate species may well react by an associative mechanism and a higher co-ordinate species by a dissociative mechanism it is clearly important to make the distinction in interpretation of kinetic data. There is evidence that  $Zn^{2+}$  reacts by the standard  $I_d$  mechanism in dmsO,<sup>194</sup> perhaps suggesting the higher co-ordinate species. However, there is significant evidence for the existence of complicating tetrahedral/octahedral conversions during reactions of  $Zn^{2+}$  in solution.<sup>195</sup> Thus the question is still open to debate. It may be that there is more than

one  $Zn^{2+}$  species present in solution thus giving the possibility of more than one reaction occurring with the same ligand.

All stock solutions were prepared using dry dmsO. This was dried by refluxing the dmsO (Fisons) under vacuum over calcium hydride for at least 1 hour, followed by vacuum distillation. Most dmsO dried in this way was used immediately, but if not it was stored over 4Å molecular sieves, previously activated by heating at 300°C in a stream of dry nitrogen in a fluidised sand bath for at least 5 hours.

The ionic strength of the solutions was kept constant at 0.1 mol dm<sup>3</sup> by adding the appropriate amount of sodium tetrafluoroborate (Aldrich) which had been previously dried in an oven at 80 °C. Some solutions were prepared in a dry box under nitrogen without coming into contact with moist air and some were prepared quickly in air. No difference in data was observed with the solutions prepared under different conditions. Indeed, previous kinetic studies carried out in dmsO show little or no change in the results obtained upon addition of small amounts of water.<sup>56,62</sup> However, for kinetic experiments carried out under nitrogen, all solutions were prepared in a nitrogen-flushed glove box.

The metal concentration of each metal solution was determined by direct titration of the solutions using edta.<sup>198,199</sup> The edta solutions used were all aqueous and each aliquot of metal solution analysed (usually 5 cm<sup>3</sup>) was diluted with an equal volume of distilled water. This aided mixing of the edta solution and the metal dmsO solution (fortunately dmsO and water are miscible).  $Co^{2+}$ ,  $Ni^{2+}$  and  $Cu^{2+}$  solutions were analysed using murexide (ammonium purpurate; Fisons) as indicator and aq.  $NH_3/NH_4Cl$  as buffer.  $Mn^{2+}$  and  $Zn^{2+}$  were analysed using Eriochrome Black T (Solochrome Black) as indicator and aq.  $NH_3/NH_4Cl$  as buffer.

The ligands used in the present study, namely cyclam and [9]aneN<sub>3</sub> were prepared using literature methods.<sup>200-202</sup> Purity checks on these ligands were carried out using <sup>1</sup>H and <sup>13</sup>C nmr in CDCl<sub>3</sub> solutions, and mass spectra.

<sup>1</sup>H nmr spectra were recorded on a 220 MHz C.W. Perkin-Elmer R34 spectrometer. <sup>13</sup>C nmr spectra were recorded on a Bruker WH180 Fourier Transform

spectrometer at 45.26 MHz. Infra-red spectra were obtained with a Perkin-Elmer 580B spectrometer. UV-visible spectra of metal, ligand and complex solutions were obtained with either a Shimadzu UV-365 or a Philips-PU8700 spectrophotometer. Mass spectra were obtained on a Kratos MS80 spectrometer.

### 2.2.2 Kinetic Measurements.

The complexation reactions of the transition metal dmsO solutions with the macrocycles in dmsO solution were measured at various temperatures between 20°C (pure dmsO freezes at 18.4 °C) and 40 °C using the stopped-flow method by following the change in absorbance/transmittance with time. The wavelength at which each reaction was studied was determined by searching for a suitable change in absorbance upon complexation. A change from ca. 0.1 to 0.2 absorbance units was usually quite adequate to give clear results. However, since the equipment analysed the transmittance change, which is on a log scale, even smaller changes could be studied as long as the change occurred close enough to "zero" absorbance. Thus, suitable concentrations of reactants had to be used which gave a measurable absorbance change at a suitable wavelength yet which produced a rate of reaction which was within the stopped-flow timescale. For studies in the ultra-violet region a deuterium light source was used, and in the visible region a tungsten light source.

Pseudo-first order kinetics were maintained throughout by ensuring that the concentration of the metal ion is in at least a ten-fold excess over the ligand, in the case of multidentate macrocyclic ligands this also ensures that only the 1:1 complexes are being observed. In certain cases, more useful data can be obtained by maintaining the concentration of the ligand in excess of the metal<sup>56</sup> particularly when two or more ligands can react with a single metal ion, however the time and expense involved in making macrocyclic ligands renders this approach impractical. Ionic strength was maintained at 0.1 mol dm<sup>-3</sup> throughout the studies using NaBF<sub>4</sub>. However, small variations in ionic strength do not significantly affect the rates of reactions involving uncharged ligands, such as the macrocycles involved in these

studies.

Typical concentrations were  $2.5 \times 10^{-4}$  -  $1 \times 10^{-3}$  mol dm<sup>-3</sup> ligand and  $2.5 \times 10^{-3}$  -  $2 \times 10^{-2}$  mol dm<sup>-3</sup> metal. Studies were carried out by varying the metal concentrations and keeping the ligand concentration constant. All first order data were followed for at least 2 to 3 half-lives for best accuracy<sup>203</sup> and each run was repeated at least 3 times, often more. Where required the infinity reading or "end point" was calculated using the method of Swinbourne<sup>204</sup> using a computer program specifically written for the analysis of stopped-flow data. All first order plots were linear for at least 3 half-lives.

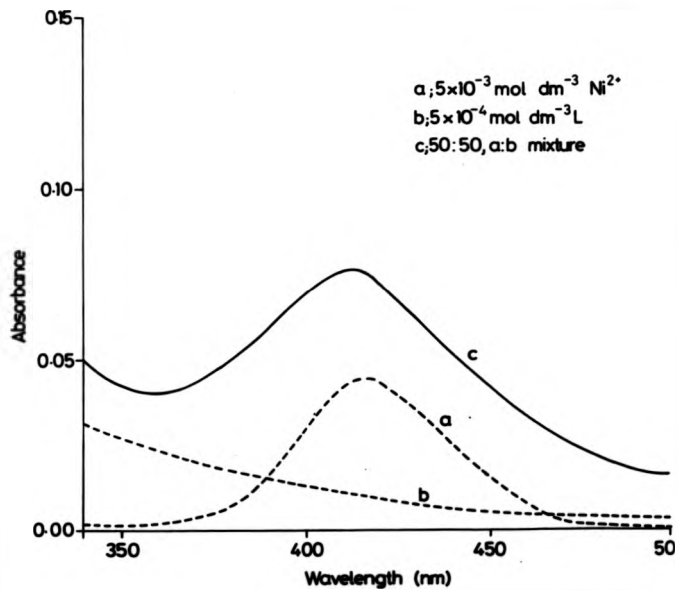
The absorbance/transmittance data was collected by a photomultiplier tube and converted from analog to digital data to be analysed using an Apple II Europlus microcomputer. The program was designed to analyse data in a variety of forms including first order and consecutive first order fits using straight line and curve-fit routines.<sup>205</sup> Metal concentration variation was analysed and temperature dependence data was fitted to the Eyring equation on the same computer using a weighted linear least-squares analysis.<sup>206</sup> All the errors quoted on rate constants are the standard deviations.

## 2.3 Results

### 2.3.1 The Complexation Reaction between Ni<sup>2+</sup> and Cyclam in dmso.

In a previous study of this reaction Kaden and Hertli<sup>25</sup> followed the absorbance changes at 450 nm using the stopped-flow method. The same wavelength was employed in this study as it was found to be the point of optimum absorbance/transmittance change in the UV/visible region. Figure 2.1 shows the change in the electronic spectrum on mixing Ni<sup>2+</sup> and cyclam solutions in dmso. The same range of metal concentrations was also used,  $1.2 \times 10^{-2}$  mol dm<sup>-3</sup> (after mixing). However, Kaden and Hertli used a ligand concentration of  $3.4 \times 10^{-4}$  mol dm<sup>-3</sup>, which certainly ensures pseudo-first order conditions, but only produces a very small

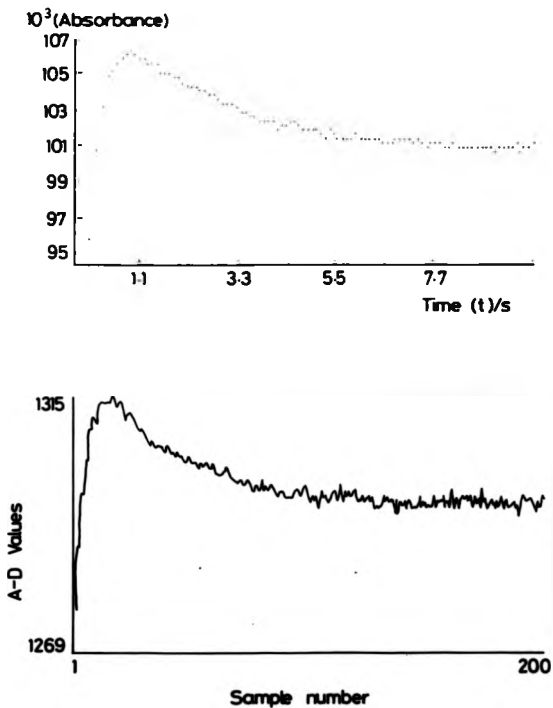
Fig. 2.1 Electronic spectra of  $\text{Ni}^{2+}$  and Cyclam in dmso.



change on mixing, at 450 nm. For more accurate results, whilst still maintaining pseudo-first order conditions, a ligand concentration of  $1 \times 10^{-3} \text{ mol dm}^{-3}$  (after mixing) was used in this study. In agreement with previous studies in dmso a two step, consecutive first order process was observed. Figure 2.2 shows a typical stopped-flow trace. The two steps are clearly observable, the first step proceeding via an increase in absorbance and the second by a decrease in absorbance. Kaden and Hertli described the intermediate as possessing a lower molar absorption coefficient than the product at this wavelength, but the present results show that the opposite is true. The authors did not publish any data to corroborate this point and so the difference cannot be commented on. The rate of the initial step is easily measurable by studying the absorbance change over a suitably short time (in this case, 0.15 s). The observed rate constant ( $k_{\text{obs}}$ ) was determined from the slope of a plot of  $\ln(A_t - A_\infty)$  vs. time. All plots were straight lines, showing first order kinetics, e.g. see figure 2.3. Between 3 and 14 values of  $k_{\text{obs}}$  at each metal concentration and each temperature were obtained. The initial fast step in the kinetics was found to have a first order dependence on the metal concentration. A plot of  $k_{\text{obs}}$  vs.  $[\text{Ni}^{2+}]$  (figure 2.4) shows a straight line of gradient  $k_f$  (bimolecular rate constant) according to the equation for pseudo-first order kinetics;  $K_{\text{obs}} = k_f [\text{M}^{2+}] + k_d$ . The dissociation rate constant ( $k_d$ ) was experimentally indistinguishable from zero in this study.

The value of  $k_f$  at  $25 \pm 0.1 \text{ }^\circ\text{C}$  determined from this study was  $1617 \pm 0.2 \text{ dm}^3 \text{ mol}^{-1} \text{ s}^{-1}$ , which agrees well with the value of  $(1.6 \pm 0.1) \times 10^3 \text{ dm}^3 \text{ mol}^{-1} \text{ s}^{-1}$  obtained by Kaden and Hertli, and shows the greater accuracy involved in the present study. The activation parameters for this process were obtained from an Eyring plot using values of  $k_{\text{obs}}$  measured at different temperatures for a given metal concentration (see figure 2.5). The derived activation parameters for the first step were  $\Delta H^\ddagger = 49.3 \pm 1.2 \text{ kJ mol}^{-1}$  and  $\Delta S^\ddagger = -17.6 \pm 4.0 \text{ J K}^{-1} \text{ mol}^{-1}$  at  $25 \text{ }^\circ\text{C}$ . Again these agree well with the values of Kaden and Hertli who obtained  $\Delta H^\ddagger = 47 \pm 5 \text{ kJ mol}^{-1}$  and  $\Delta S^\ddagger = -25 \pm 17 \text{ J K}^{-1} \text{ mol}^{-1}$ , and again show the greater accuracy in the present study.

Fig. 2.2 Typical stopped-flow trace for the reaction of  $\text{Ni}^{2+}$  and cyclam, top trace shows digitized data, bottom trace shows direct transmittance data.



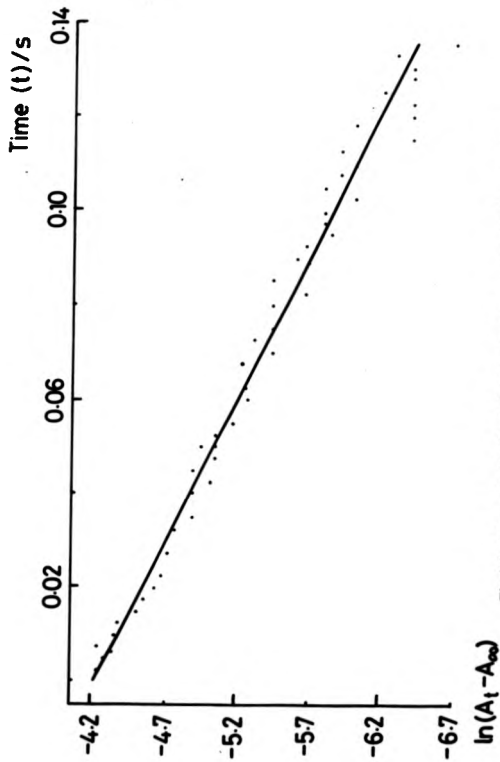


Fig. 2.3 First-order plot for the initial step in the reaction of  $\text{Ni}^{2+}$  and cyclam.

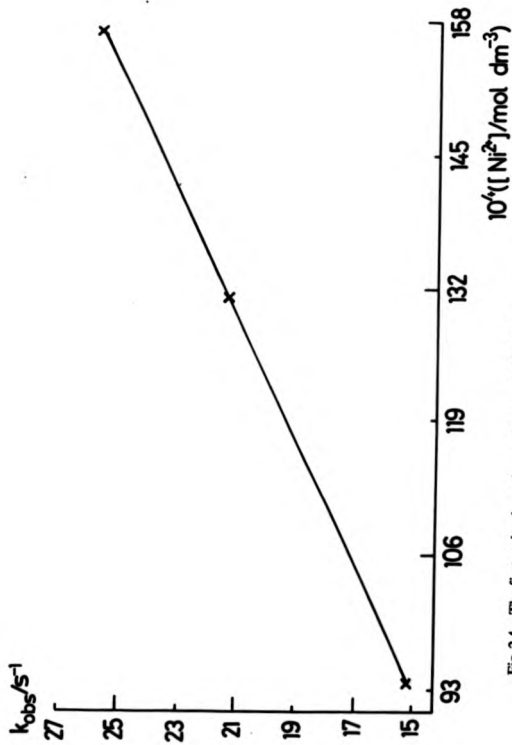
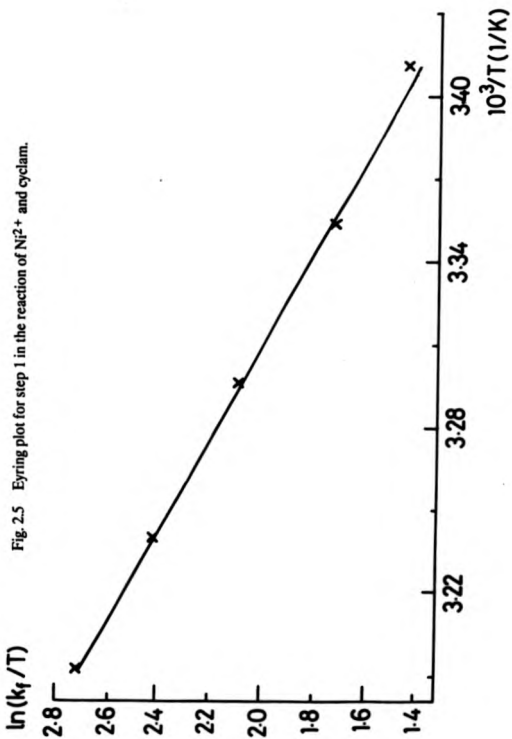


Fig. 2.4 The first-order dependence of  $k_{obs}$  on  $[Ni^{2+}]$  for step 1.



The second step of the reaction could also be followed by studying the absorbance change over a suitable time. Thus, values of  $k_{\text{obs}}$  could be obtained in the same way as for the first step, by following the reaction over 10 s (the data showing first order plots of  $\ln(A_t - A_\infty)$  vs. time), though the smaller absorbance change gave less accurate results. The accuracy of the  $k_{\text{obs}}$  values for the slower second step could be improved by fitting the whole data set to consecutive first order kinetics by a non-linear least square fit using the Newton-Gauss algorithm<sup>207</sup> (see figure 2.6). Both methods gave comparable results, and so a combination of the methods were used to obtain the final values of  $k_{\text{obs}}$ . The observed rate constants of the second step were found to be independent of the metal concentration, which is in agreement with previous studies in these systems. The rate constant for the second step was found to be  $0.531 \pm 0.016 \text{ s}^{-1}$  at 25 °C. This differs greatly from the  $2.3 \pm 0.2 \text{ s}^{-1}$  quoted by Kaden and Hertli. The new value is preferred in this study as it is much more in keeping with the values obtained for similar reaction steps measured previously in dmsO and dmf, which are much slower than Kaden and Hertli's figure.<sup>94,113</sup> The small absorbance change and low  $k_{\text{obs}}$  values for the second stage did not facilitate measurement of activation parameters for this step. All rate data obtained from these studies are listed in Appendix 1.

### 2.3.2 The Complexation Reaction between $\text{Ni}^{2+}$ and [9]aneN<sub>3</sub> in dmsO.

The effect on the electronic spectrum of mixing  $\text{Ni}^{2+}$  with [9]aneN<sub>3</sub> solutions under pseudo-first order conditions is shown in figure 2.7. The point of optimum absorbance change was considered to be at 644 nm. The same concentrations of  $\text{Ni}^{2+}$  and ligand as used for the cyclam study were employed here (see 2.3.1). Similar stopped-flow traces were obtained, with a two step, consecutive first order reaction observed. The first stage was followed over 0.2 s, and the second over 10 s. Analysis as before gave a value of  $k_1 = 1747 \pm 2 \text{ dm}^3 \text{ mol}^{-1} \text{ s}^{-1}$  for the initial, metal dependent step at 25 °C (figure 2.8), with activation parameters of  $\Delta H^\ddagger = 35.4 \pm 1.6 \text{ kJ mol}^{-1}$  and  $\Delta S^\ddagger = -64.3 \pm 5.2 \text{ J K}^{-1} \text{ mol}^{-1}$  at 25 °C (figure 2.9), the dissociation rate

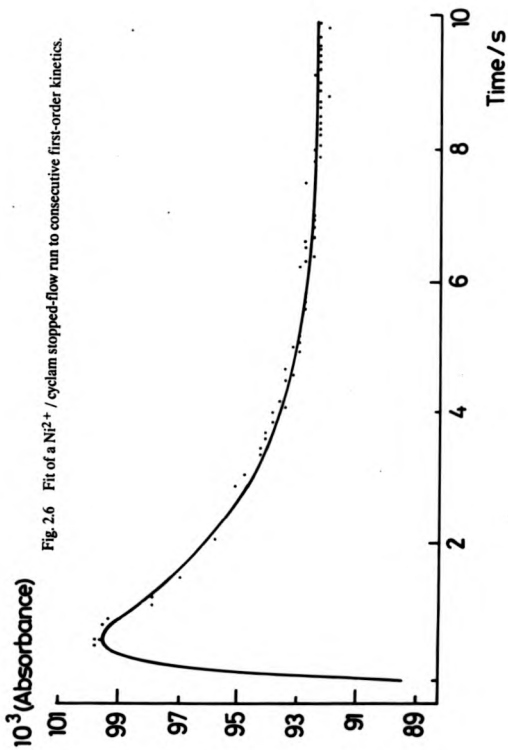
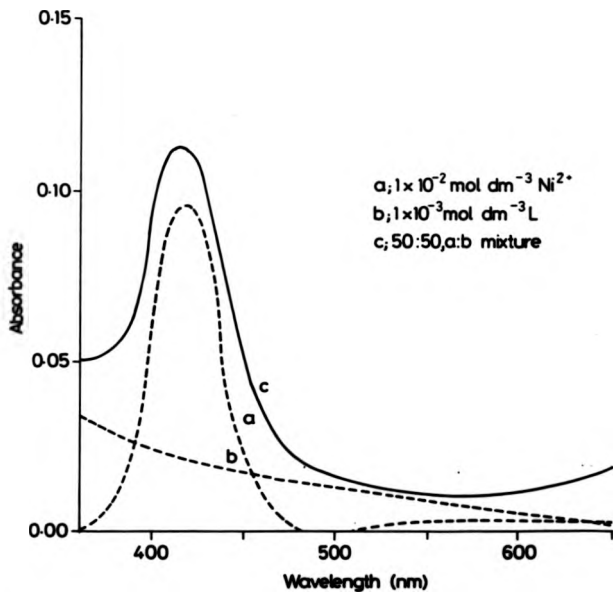


Fig. 2.6 Fit of a Ni<sup>2+</sup> / cyclam stopped-flow run to consecutive first-order kinetics.

Fig. 2.7 Electronic spectra of  $\text{Ni}^{2+}$  and [9]ane $\text{N}_3$  in dms $\text{o}$ .



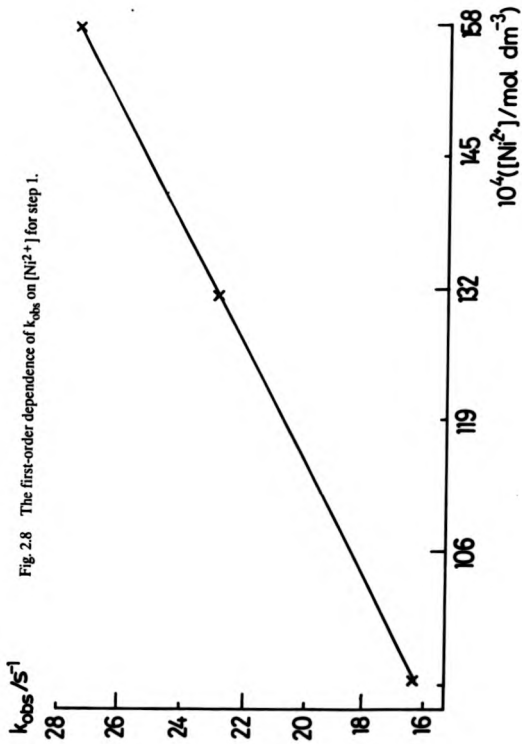
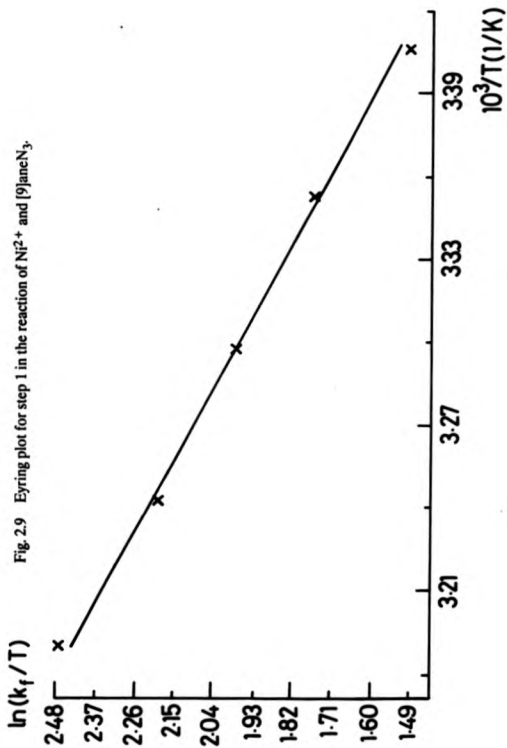


Fig. 2.9 Eyring plot for step 1 in the reaction of  $\text{Ni}^{2+}$  and  $[\text{9}]_{\text{aq}}\text{Ni}^{2+}$ .



being experimentally indistinguishable from zero. For the second, metal independent step  $k_{obs}$  was determined as  $0.4904 \pm 0.0088 \text{ s}^{-1}$  at  $25 \text{ }^\circ\text{C}$ . As in the cyclam study, the small absorbance change in this step did not facilitate a study of the activation parameters on the stopped-flow apparatus (see Appendix 1 for rate data).

### 2.3.3 The Complexation Reaction between $\text{Cu}^{2+}$ and Cyclam in dmsO.

The optimum absorbance change on mixing was considered to be at 526 nm, and so the kinetics of reaction were studied at this wavelength, though the results were checked at other wavelengths to make sure no other reactions were occurring which may have been missed at this wavelength (figure 2.10). The concentrations used were  $5 \times 10^{-4} \text{ mol dm}^{-3}$  cyclam and  $5.15 \times 10^{-3} \text{ mol dm}^{-3} \text{ Cu}^{2+}$ . Yet again, a two stage, consecutive first order process was observed, but this time the second step involved a large increase in absorbance (figure 2.11). The first step was followed over 0.1 s and  $k_f$  was calculated as  $5476 \pm 23 \text{ dm}^3 \text{ mol}^{-1} \text{ s}^{-1}$  at  $25 \text{ }^\circ\text{C}$  (figure 2.12) with activation parameters of  $\Delta H^\ddagger = 46.0 \pm 1.3 \text{ kJ mol}^{-1}$  and  $\Delta S^\ddagger = -19.0 \pm 4.3 \text{ J K}^{-1} \text{ mol}^{-1}$  (figure 2.13). The dissociation rate was indistinguishable from zero. The slower, metal independent step was followed over 100 s and gave a rate constant of  $0.0630 \pm 0.0009 \text{ s}^{-1}$  at  $25 (\pm 0.1) \text{ }^\circ\text{C}$ . This time, the large absorbance change observed for the second step allowed a study of the dependence of the rate constant on temperature. The activation parameters are  $\Delta H^\ddagger = 52.5 \pm 2.1 \text{ kJ mol}^{-1}$  and  $\Delta S^\ddagger = -92.3 \pm 7.1 \text{ J K}^{-1} \text{ mol}^{-1}$  at  $25.0 \text{ }^\circ\text{C}$  (figure 2.14). Rate data are listed in Appendix 1.

### 2.3.4 The Complexation Reaction between $\text{Cu}^{2+}$ and [9]aneN<sub>3</sub> in dmsO.

With [9]aneN<sub>3</sub> similar reactant concentrations to the  $\text{Cu}^{2+}$ /cyclam study were used, with  $4 \times 10^{-4} \text{ mol dm}^{-3}$  [9]aneN<sub>3</sub> and  $4.13 \times 10^{-3} \text{ mol dm}^{-3} \text{ Cu}^{2+}$ . This time, the reaction was followed at 610 nm (figure 2.15) and at this wavelength the two stage reaction observed involved an initial increase, followed by a decrease in absorbance. Following the first step over 0.1 s at  $25 \text{ }^\circ\text{C}$  over a range of  $\text{Cu}^{2+}$  concentrations gave

Fig. 2.10 Electronic spectra of  $\text{Cu}^{2+}$  and cyclam in dmsO.

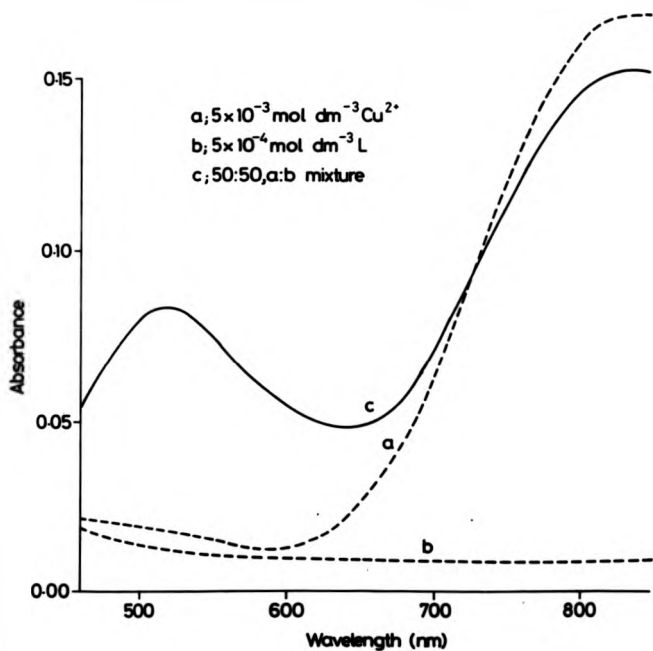
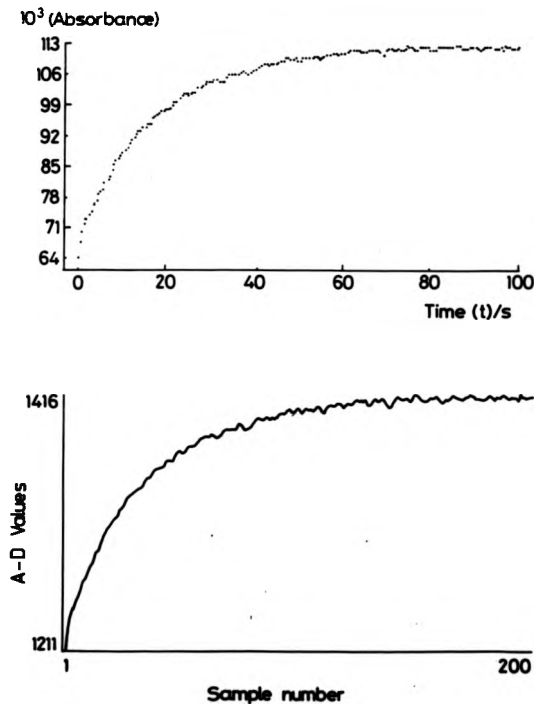
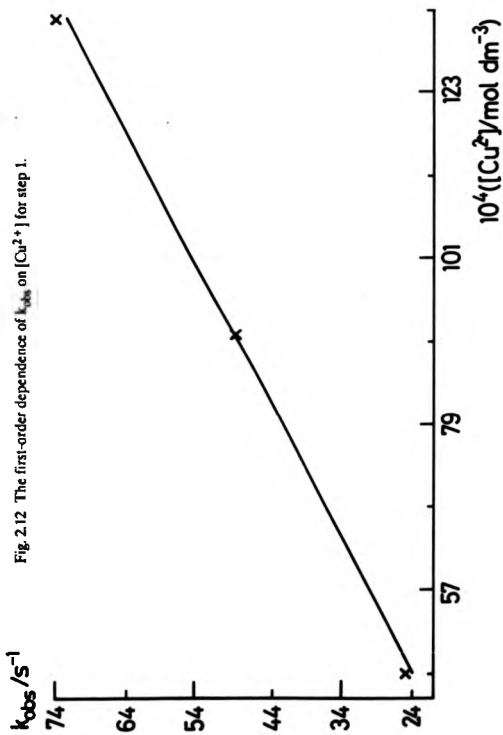


Fig. 2.11 Typical stopped-flow trace for the  $\text{Cu}^{2+}$  / cyclam reaction, top trace shows digitized data, bottom trace shows direct transmittance data.







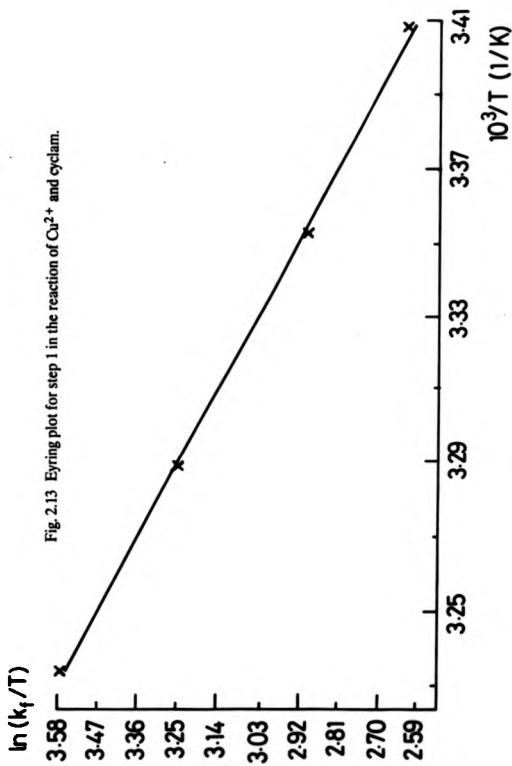


Fig. 2.14 Eyring plot for step 2 in the reaction of  $\text{Cu}^{2+}$  and cyclam.

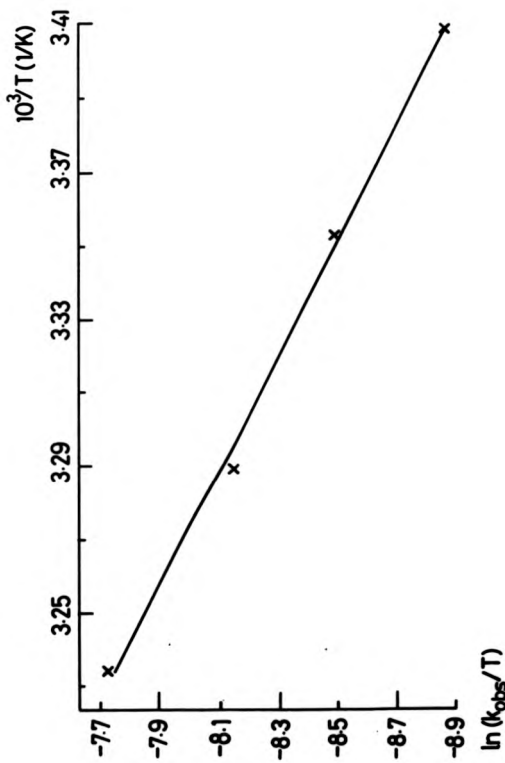
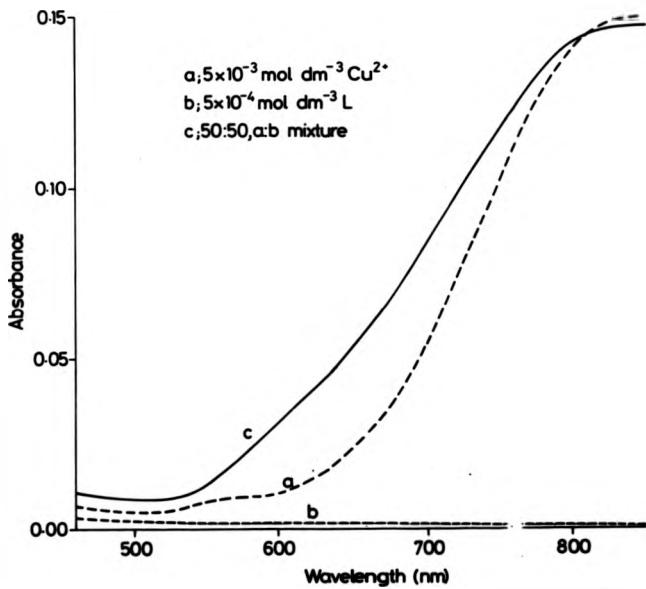


Fig. 2.15 Electronic spectra of  $\text{Cu}^{2+}$  and [9]ane  $\text{N}_3$  in dmso.

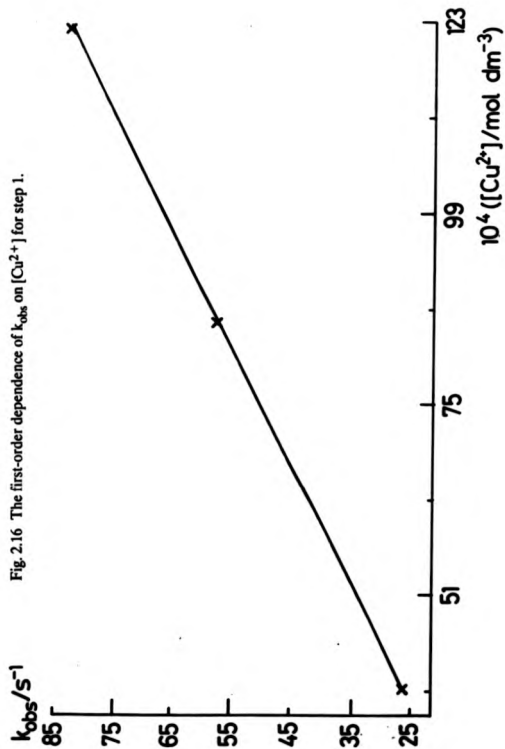


a bimolecular rate constant of  $6728 \pm 33 \text{ dm}^3 \text{ mol}^{-1} \text{ s}^{-1}$  (figure 2.16), with a dissociation rate indistinguishable from zero. A temperature dependence study showed that the first step had activation parameters of  $\Delta H^\ddagger = 42.5 \pm 1.3 \text{ kJ mol}^{-1}$  and  $\Delta S^\ddagger = -29.2 \pm 4.5 \text{ J K}^{-1} \text{ mol}^{-1}$  at 25 °C (figure 2.17). The second stage was followed over 10 s and was found to be independent of the  $\text{Cu}^{2+}$  concentration, with a rate constant of  $0.3904 \pm 0.0072 \text{ s}^{-1}$  at 25 °C. A variable temperature study on the second stage did not give reproducible results and so was not pursued. The rate data are listed in Appendix 1.

### 2.3.5 The Complexation Reaction between $\text{Co}^{2+}$ and Cyclam in dmsO.

$\text{Co}(\text{cyclam})^{2+}$  is known to be extremely oxygen sensitive in aqueous solution, and the kinetics and mechanism of this process have been studied (see section 2.4 for a discussion of this).<sup>208-210</sup> Likewise, in dmsO solution the complex was found to be extremely air sensitive and so all the solutions were deoxygenated before use. Figure 2.18 illustrates the changes in the electronic spectrum on mixing solutions of  $\text{Co}^{2+}$  and cyclam in deoxygenated dmsO under pseudo-first order conditions and also the effect of exposing the solution to the air. The kinetics were followed at 400 nm in the absence of oxygen using  $2.5 \times 10^{-4} \text{ mol dm}^{-3}$  cyclam and  $2.5\text{-}7.5 \times 10^{-3} \text{ mol dm}^{-3} \text{ Co}^{2+}$  solutions.

A two step, consecutive first order process was again observed, but this time a third step was seen to interfere with the second step (figure 2.19). This third process involved a very large and slow absorbance increase similar to that seen when the deoxygenated solutions were exposed to the air, thus this third stage of the reaction is likely to be the reaction of the product and/or intermediate with traces of oxygen remaining in the stopped-flow apparatus (see section 2.4). The initial stage was followed over 0.04 s and was seen to have a first order dependence on the  $\text{Co}^{2+}$  concentration, with a bimolecular rate constant of  $29418 \pm 44 \text{ dm}^3 \text{ mol}^{-1} \text{ s}^{-1}$  at 25 °C (figure 2.20), with a dissociation rate indistinguishable from zero. The activation parameters of this process are  $\Delta H^\ddagger = 33.7 \pm 0.9 \text{ kJ mol}^{-1}$  and  $\Delta S^\ddagger = -46.2 \pm 2.9 \text{ J}$



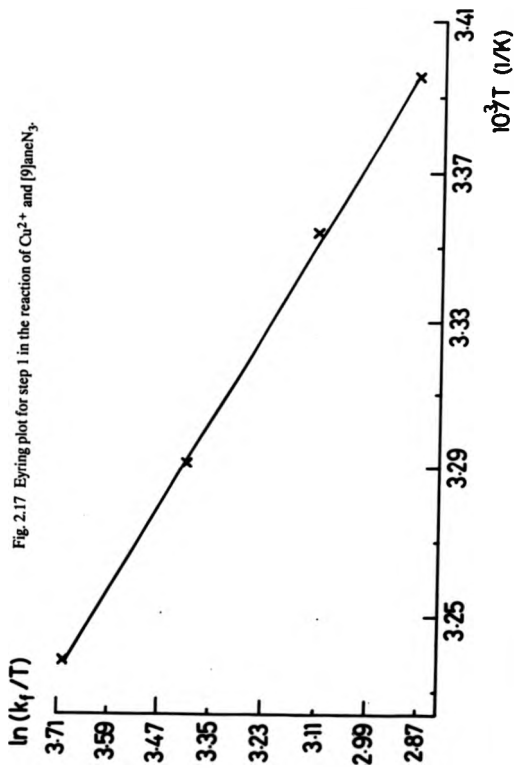
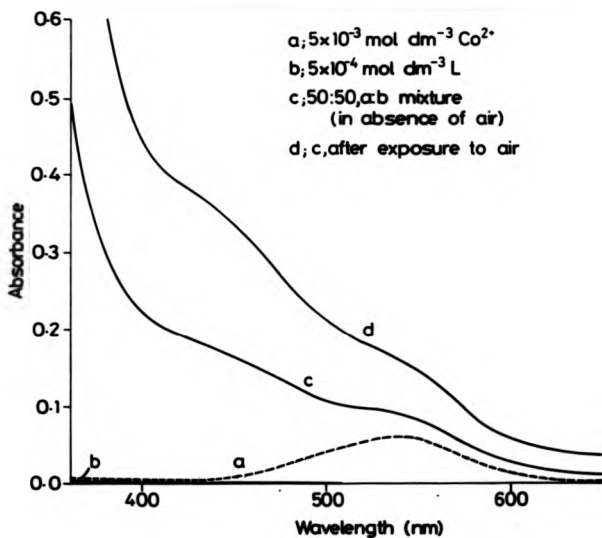


Fig. 2.18 Electronic spectra of  $\text{Co}^{2+}$  and cyclam in dmso.



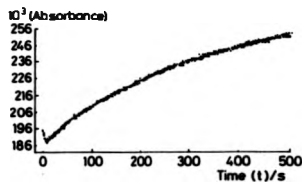
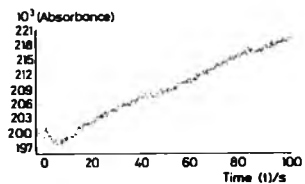
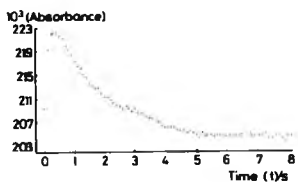
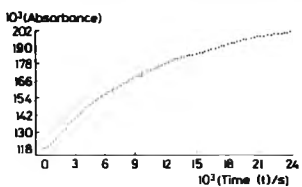
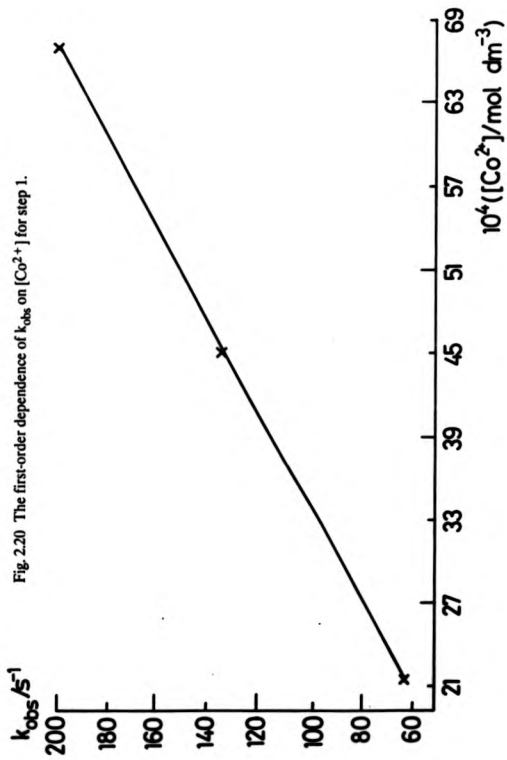


Fig. 2.19 Typical stopped-flow traces for the  $\text{Co}^{2+}$  / cyclam reaction.



$\text{K}^{-1} \text{mol}^{-1}$  at 25 °C (figure 2.21). The second stage was extremely difficult to follow due to the interference from the third stage, though curve-fit data suggested a value of  $k_{\text{obs}}$  ca.  $0.4\text{--}0.5 \text{ s}^{-1}$ . The third stage did not fit to first order kinetics when followed over 500 s (figure 2.22), and so an analysis of the data was carried out assuming second order kinetics and fitting to the equation;

$$\ln(1 + \Delta_o/[A]_o [A_o - A_\infty/A_1 - A_\infty]) = \ln [B]_o/[A]_o + \Delta_o kt$$

$$\text{where } [B]_o = [\text{CoL}^{2+}]_o \text{ ca. } 2.5 \times 10^{-4} \text{ mol dm}^{-3}$$

$$[A]_o = [\text{O}_2]_o \text{ ca. } 1 \times 10^{-4} \text{ mol dm}^{-3}$$

$$\Delta_o = [B]_o \cdot [A]_o$$

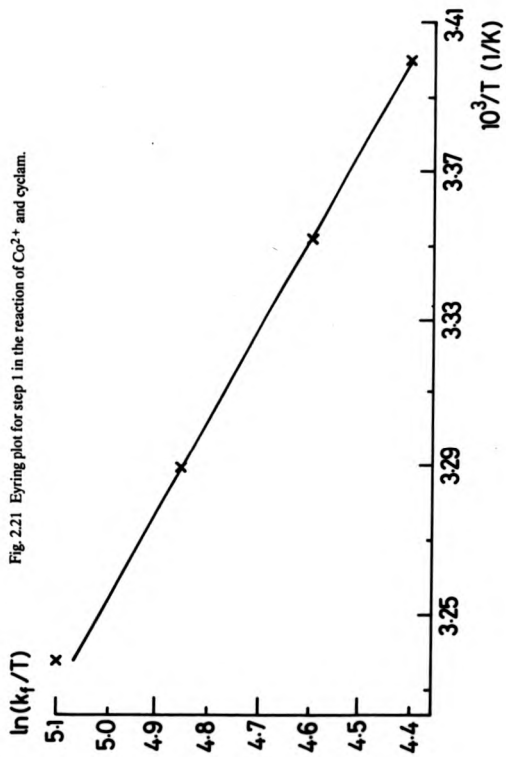
From straight line plots of time vs.  $\ln(1 + 1.5\{A_o - A_\infty/A_1 - A_\infty\})$  the data are seen to obey second order kinetics (figure 2.23), with a rate constant of ca.  $7.5\text{--}9 \times 10^5 \text{ dm}^3 \text{ mol}^{-1} \text{ s}^{-1}$ , which compares well with the measured value of  $(5.0 \pm 1.5) \times 10^5 \text{ dm}^3 \text{ mol}^{-1} \text{ s}^{-1}$  for the same reaction in water<sup>208</sup> at 25 °C. The rate data are listed in Appendix 1.

\* - If second order kinetics are present for the third stage then the concentration of oxygen must be in the order of the concentration of the complex formed in the initial stages of the reaction (ca.  $2.5 \times 10^{-4} \text{ mol dm}^{-3}$  assuming the reaction goes to completion). Air-saturated water is  $2.58 \times 10^{-4} \text{ mol dm}^{-3}$  at 25 °C.<sup>211</sup> Thus, the oxygen concentration is likely to be less than the complex concentration and so ca.  $1 \times 10^{-4} \text{ mol dm}^{-3}$  seems a reasonable estimate.

### 2.3.6 The Complexation Reaction between $\text{Co}^{2+}$ and [9]aneN<sub>3</sub> in dmsO.

Unlike  $\text{Co}(\text{cyclam})^{2+}$  the product of the reaction studied here is not air sensitive and so no complicating reactions with oxygen were observed. The reaction was studied at 360 nm under the same conditions as used in the  $\text{Co}^{2+}/\text{cyclam}$  study (2.3.5). Figure 2.24 shows the electronic spectra of the reactants before and after mixing. The two step, consecutive first order kinetics were again observed. The ini-

Fig. 2.21 Eyring plot for step 1 in the reaction of  $\text{Co}^{2+}$  and cyclam.



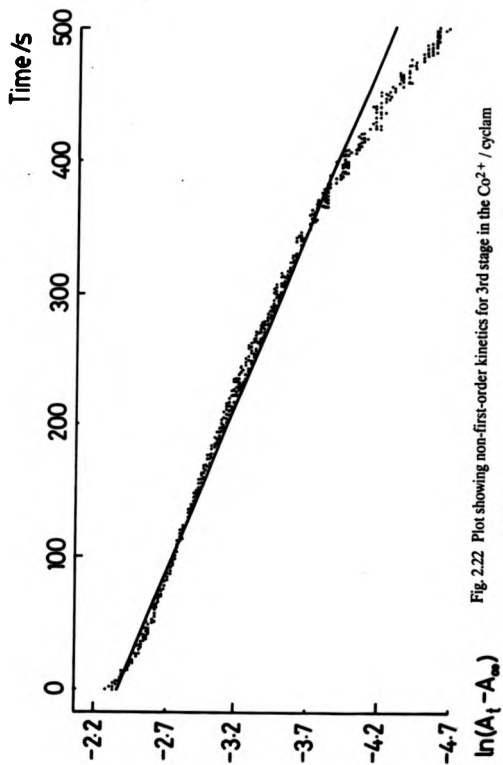


Fig. 2.22 Plot showing non-first-order kinetics for 3rd stage in the  $\text{Co}^{2+}$  / cyclam reaction.

Fig. 2.23 Linear fit of data for 3rd stage to 2nd order kinetics in the reaction of  $\text{Co}^{2+}$  and cyclam.

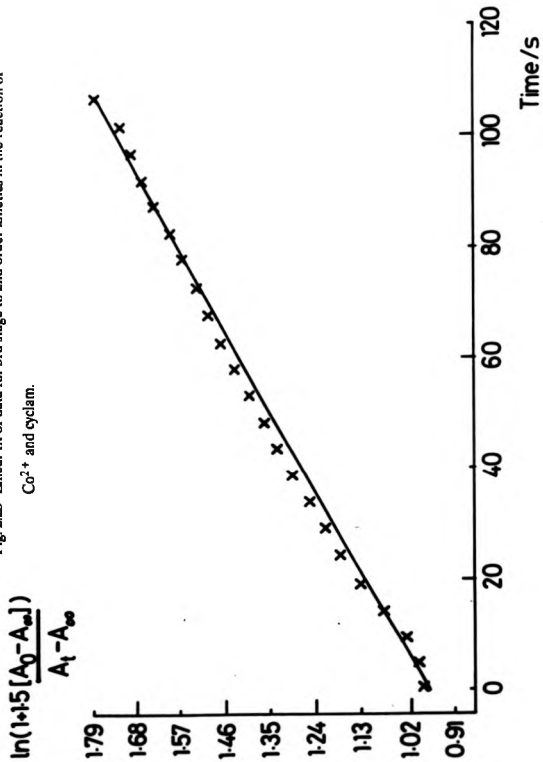
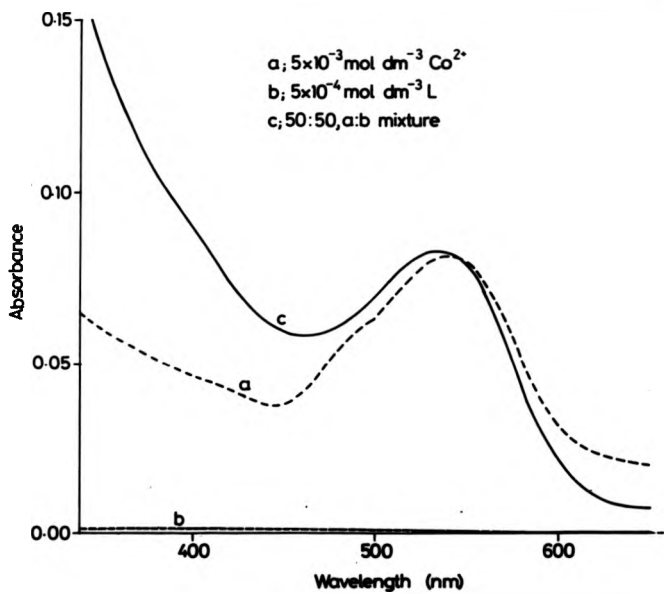


Fig. 2.24 Electronic spectra of  $\text{Co}^{2+}$  and [9]ane $\text{N}_3$  in dmsO.



tial step was followed over 0.04 s and the bimolecular rate constant was calculated to be  $31306 \pm 401 \text{ dm}^3 \text{ mol}^{-1} \text{ s}^{-1}$  at 25 °C (figure 2.25), with no detectable dissociation rate. The activation parameters are  $\Delta H^\ddagger = 39.030 \pm 0.399 \text{ kJ mol}^{-1}$  and  $\Delta S^\ddagger = -28.134 \pm 1.311 \text{ J K}^{-1} \text{ mol}^{-1}$  at 25 °C (figure 2.26). The second step is very slow and difficult to measure accurately. Curve-fit data indicate that the first order rate constant for this process is ca.  $3 \pm 1 \times 10^4 \text{ s}^{-1}$ . All rate data are listed in Appendix 1.

## 2.4 Discussion

All the reactions were studied under pseudo first-order conditions, and showed consecutive first-order kinetics of the type;



By studying the variation in the observed rate constants ( $k_1$ ,  $k_2$ ) with the concentration of excess metal ion it was deduced that in all cases the reactions displayed an initial rapid process which was directly dependent on the concentration of the metal followed by a second, slower process which was independent of the metal concentration.

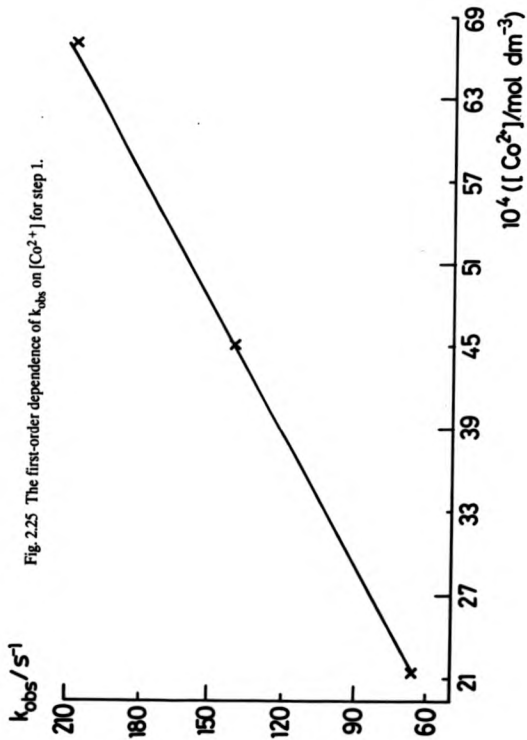


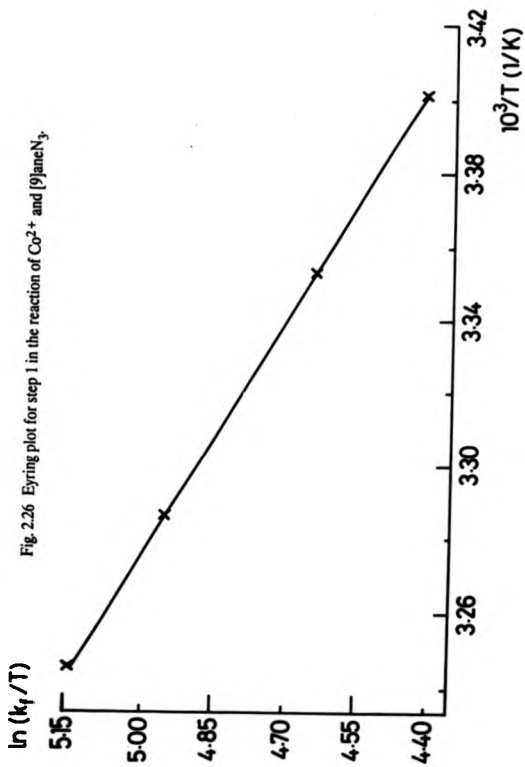
( $M^{2+} = \text{Cu}^{2+}, \text{Co}^{2+}, \text{Ni}^{2+}$ ; L = cyclam, [9]aneN<sub>3</sub>; int = intermediate;

$$k_f \gg k_{int})$$

The first step is first-order in  $[M^{2+}]$  and  $[L]$ , and the second step is first order kinetics overall. No reverse reactions were observed and thus the reactions are considered as going to completion, with no equilibria detectable. The calculated rate constants for the reactions between divalent metal ions and the macrocyclic ligands cyclam and [9]aneN<sub>4</sub> are collected in Table 2.1.

With both ligands the initial rate constant ( $k_f$ ) decreases in the order





$k_{Co} > k_{Cu} > k_{Ni}$  which parallels the rate of exchange of solvent molecules for these ions with solvent in dmsO.

Table 2.1

Measured Rate Constants for the Reaction of various Macrocylic Compounds with Labile Transition Metals, dmsO, T = 25.0 °C,  $\mu = 0.1 \text{ mol dm}^{-3}$ , for errors see 2.3.

Ligand	Metal	$k_f$ $\text{dm}^3 \text{ mol}^{-1} \text{ s}^{-1}$	$k_{int}$ $\text{s}^{-1}$
Cyclam	Ni <sup>2+</sup>	1620	0.53
	Co <sup>2+</sup>	29418	*
	Cu <sup>2+</sup>	5476	0.06
[9]aneN <sub>3</sub>	Ni <sup>2+</sup>	1747	0.49
	Co <sup>2+</sup>	31306	ca. $3 \pm 1 \times 10^{-4}$
	Cu <sup>2+</sup>	6728	0.39

\* - not measured, see 2.3.5.

Similar biphasic processes have been observed before for divalent transition metals reacting with macrocylic ligands in non-aqueous solvents, e.g. substituted cyclams with Ni<sup>2+</sup> in CH<sub>3</sub>CN,<sup>55</sup> cyclam and tmc with Ni<sup>2+</sup> in dmsO and dmf,<sup>55</sup> methylated cyclams with Ni<sup>2+</sup> and Cu<sup>2+</sup> in dmf<sup>94</sup> and N<sub>2</sub>O<sub>2</sub> macrocycles with Ni<sup>2+</sup> in methanol.<sup>123</sup> The data for the reaction between Ni<sup>2+</sup> and cyclam shown here in dmsO is a repeat of a previous study made by Kaden and Hertli.<sup>55</sup> The value of  $k_f$  obtained by Hertli and Kaden,  $(1.6 \pm 0.1) \times 10^3 \text{ dm}^3 \text{ mol}^{-1} \text{ s}^{-1}$  compares very well with our measured value. The previous authors report a value of  $2.3 \pm 0.2 \text{ s}^{-1}$  for  $k_{int}$ , which is over 4 times larger than our measured value. Since a higher concentration of ligand and therefore a stronger absorbance change was employed we believe it to be a more reliable figure. Also, the smaller value is in keeping with all other reported values for these types of reactions over a range of solvents, the highest reported value being  $0.92 \text{ s}^{-1}$  at 25 °C for an N<sub>2</sub>O<sub>2</sub> macrocycle reacting with Ni<sup>2+</sup> in

methanol.<sup>123</sup> Another difference from Kaden's results is that he reports that the intermediate possesses a lower molar absorptivity than the end product. However, figure 2.2 shows that our results indicate that the intermediate has a higher molar absorptivity than the end product. No explanation can be given to account for these differences, but the agreement between the rate constants and the activation parameters for the initial step is clear (see later).

Kaden<sup>55</sup> suggested that macrocyclic ligands reacted via the Eigen-Wilkins mechanism in non-aqueous solvents, a conclusion which was also reached by Hay and Norman.<sup>95</sup> For the reactions of cyclam and [9]aneN<sub>3</sub> with Co<sup>2+</sup>, Ni<sup>2+</sup> and Cu<sup>2+</sup> to conform to this mechanism they must obey the equation;

$$k_f = n K_{\text{ex}} k_{\text{ex}} \quad (\text{see } 1.2)$$

$$\text{where } k_{\text{ex}} = N_{\text{C}} k_{\text{ex}}^{-1}$$

and  $N_{\text{C}}$  = co-ordination number of metal ion.

and  $k_{\text{ex}}^{-1}$  = first-order rate constant associated with the exchange of a single solvent molecule.

The formation rate constant ( $k_f$ ) in this equation must be equivalent to the rate constant for initial metal attachment (previously denoted as  $k_f$  in Table 2.1). "n" is the statistical factor describing the probability that a ligand in the outer-sphere complex replaces a dissociating solvent molecule. Previous work on reaction mechanisms in dmsO have shown that the solvent has a large role to play in the value of "n". The high donor ability<sup>212</sup> of dmsO compared to water may slow down the reaction process by competing with the ligand for the vacant co-ordination sites left by dissociating solvent molecules, even to the extent of shifting the rate determining step from first bond formation to first chelate ring closure in multidentate ligands.<sup>62,64,213</sup> Langford<sup>60</sup> originally proposed that "n" depended on the number of sites in the second co-ordination sphere, and suggested values of 0.1-0.2. Nichols and Grant have published the clearest data for the value of "n" for substitution reactions in dmsO for a range of charged and uncharged, mono- and multidentate ligands reacting with Ni<sup>2+</sup>.<sup>56</sup> They found that "n" was independent of the nature of the

ligand and ranged from 0.2-0.5 for most reactions.

The value of  $K_{\text{ex}}$  is very dependent on the type of solvent used as the reaction medium, and can be calculated using the Fuoss equation (see 1.2). The centre-to-centre distance between the metal ion and the nearest donor atom of the ligand must first be determined in order to calculate  $K_{\text{ex}}$ . For uncharged ligands in dmso values of this distance (*a*) have been suggested to lie between 6 and 7 Å. Nichols and Grant<sup>56</sup> used ionic strength dependence data for the reaction between Ni(II) and dithiocarbamate ions to calculate a value of 6 Å for "a". Petrucci et al<sup>213</sup> used conductance data for the Ni(dmso)<sub>6</sub><sup>2+</sup>, NCS<sup>-</sup> ion pair to estimate a value of 6.1 Å, while molecular size parameters were used to give an estimate of 7 Å.<sup>57</sup> This range of values of "a" produces a range of  $K_{\text{ex}}$  values of 0.55-0.86 dm<sup>3</sup> mol<sup>-1</sup>. Taking into account the increased van der Waals radius for a hexadmsio ion compared to a hexa-aquo ion ("a" is normally taken as 4 Å for water)<sup>51</sup> in an analogous way to Pearson and Ellgen for methanol<sup>54</sup> we prefer the value of 6 Å, giving  $K_{\text{ex}} = 0.55$  dm<sup>3</sup> mol<sup>-1</sup>.

The value of  $k_{\text{ex}}^{-1}$  will depend on the particular metal ion and must be measured independently. Unfortunately, the values of  $k_{\text{ex}}^{-1}$  for Ni<sup>2+</sup>, Co<sup>2+</sup> and Cu<sup>2+</sup> in dmso have long been an area of considerable confusion, with much conflicting data being published. Most research has concentrated on [Ni(dmso)<sub>6</sub>]<sup>2+</sup>. The earliest reports of  $k_{\text{ex}}$  for this species used <sup>1</sup>H nmr methods but since the protons are well away from the point of co-ordination in these ions (the O atom of dmso) the data obtained are in significant error.<sup>215-218</sup> <sup>13</sup>C nmr was used to better effect.<sup>56</sup> <sup>17</sup>O nmr must surely be the most sensitive method in this respect and recent work<sup>219</sup> produced the largest value yet for  $k_{\text{ex}}^{-1}$ . However, in view of other work an approximate value of  $k_{\text{ex}}$  will be taken as  $1 \times 10^6$  s<sup>-1</sup> at 25 °C with  $\Delta H^\ddagger$  ca. 50 kJ mol<sup>-1</sup> and  $\Delta S^\ddagger$  ca. 0 J K<sup>-1</sup> mol<sup>-1</sup>. Less attention has been focussed on Co<sup>2+</sup> and Cu<sup>2+</sup>.  $k_{\text{ex}}$  for Co<sup>2+</sup> is in the region of  $1.7 \times 10^5$  s<sup>-1</sup> at 25 °C with  $\Delta H^\ddagger$  ca. 40 kJ mol<sup>-1</sup> and  $\Delta S^\ddagger$  ca. 1.6 J K<sup>-1</sup> mol<sup>-1</sup>.<sup>97</sup> For Cu<sup>2+</sup> the only published data suggest a value of  $7.95 \times 10^3$  s<sup>-1</sup> with  $\Delta H^\ddagger = 30$  kJ mol<sup>-1</sup> and  $\Delta S^\ddagger = -57$  J K<sup>-1</sup> mol<sup>-1</sup> at 25 °C.<sup>190,191</sup> which seems exceptionally low in view of the trends in solvent variation on metal exchange rates for

other divalent metals.<sup>97</sup> For  $\text{Ni}^{2+}$  and  $\text{Co}^{2+}$  the solvent exchange rates in dmsO are only an order of magnitude less than those in water, but if the reported  $\text{Cu}^{2+}$  figure is correct then the exchange rate for  $\text{Cu}^{2+}$  in dmsO is greater than five orders of magnitude less than for water. No other divalent first row transition metal displays this behaviour and it is tempting to dismiss the data as being in considerable error. Indeed the data were obtained using  $^1\text{H}$  nmr techniques which are known to be insensitive for this kind of work and metal nitrate complexes were employed; nitrate ions are known to co-ordinate to metal ions and affect exchange rates (though such co-ordination should increase the exchange rate). However, none of these can explain such a large difference in the dmsO exchange rate for  $\text{Cu}^{2+}$  compared to  $\text{H}_2\text{O}$  and so in the absence of any other data the value reported by Vigee et al must be used for our calculations. In its favour Vigee et al observed two exchange rates for  $\text{Cu}^{2+}$  in dmsO with the value quoted above corresponding to exchange of the two relatively labile axial solvent molecules in the Jahn-Teller distorted  $\text{Cu}^{2+}$  species; exchange of the equatorial molecules was only observable at temperatures above 100 °C. This behaviour is consistent with that observed by Swift and Connick in their original studies on the rates of water exchange on  $\text{Cu}^{2+}$ .<sup>220</sup>

Table 2.2

Calculated values for n, using the Eigen-Wilkins equation  
(see text), 25 °C, dmsO.

Metal	$k_{\text{ex}}^{-1}$ $\text{s}^{-1}$	$k_f$ $\text{dm}^3 \text{mol}^{-1} \text{s}^{-1}$	n
$\text{Ni}^{2+}$	$1 \times 10^4$	1620(Cyclam)	0.049
		1747([9]aneN <sub>3</sub> )	0.053
$\text{Co}^{2+}$	$1.7 \times 10^5$	29418(Cyclam)	0.052
		31306([9]aneN <sub>3</sub> )	0.056
$\text{Cu}^{2+}$	$7.95 \times 10^3$	5476(Cyclam)	0.313
		6728([9]aneN <sub>3</sub> )	0.385

Thus, having established values of  $n$ ,  $k_{\text{on}}$  and  $k_{\text{ex}}^{-1}$ , assuming the reactions follow the Eigen-Wilkins mechanism as previous studies suggest, we can calculate values for  $n$ , the statistical factor, for the reactions of the macrocyclic ligands with  $\text{Co}^{2+}$ ,  $\text{Ni}^{2+}$  and  $\text{Cu}^{2+}$  (Table 2.1). The calculated values are tabulated in Table 2.2.

For the reactions of  $\text{Ni}^{2+}$  and  $\text{Co}^{2+}$  with the macrocyclic ligands the values of  $n$  calculated using the Eigen-Wilkins equation are very similar and are ca. 0.05. This relatively small value of  $n$  reflects the bulk of dmsol molecules, which leaves a relatively small hole in the inner-sphere of the metal ion upon loss of a single solvent molecule, and is attributed to steric hindrance to first bond formation. This is in line with the observed negative values of  $\Delta S^\ddagger$  which are expected when the probability factor,  $P$ , is small, in the collision theory equation,  $k = (PZ)e^{-E/RT}$  ( $Z$  = collision frequency). A low  $A$ -factor ( $A = PZ$ ) gives rise to a negative value of  $\Delta S^\ddagger$  (see later, Table 2.3). For the  $\text{Cu}^{2+}$  reactions the value of  $n$  is  $> 0.3$ , which is ca. 6 times greater than the values for  $\text{Ni}^{2+}$  and  $\text{Co}^{2+}$ , this may well reflect the error in the value of  $k_{\text{ex}}^{-1}$  used in the calculations (see earlier). Assuming that  $n$  for the  $\text{Cu}^{2+}$  reactions is also ca. 0.05 we can thus calculate a new value for  $k_{\text{ex}}^{-1}$  for  $\text{Cu}^{2+}$ , a calculation of this sort gives  $k_{\text{ex}}^{-1} = 5.6 \times 10^4 \text{ s}^{-1}$ , which is larger than the reported figure though still seems quite low compared with the exchange rate of  $\text{Cu}^{2+}$  in other solvents.<sup>97</sup>

Further evidence that the reactions obey the Eigen-Wilkins interchange mechanism is that the two different macrocyclic ligands have very little effect on the rate constants for the initial stage of the mechanism. This would be expected for the mechanism since the rate determining step is loss of a solvent molecule and so will be independent of the ligand structure.

Another indication that the reactions follow the dissociative interchange mechanism is seen in the activation parameters, which are displayed in Table 2.3.

According to the Eigen-Wilkins mechanism the activation enthalpy for the ligand substitution process ( $\Delta H_f^\ddagger$ ) will be equal to the sum of the activation enthalpy

for the solvent exchange reaction ( $\Delta H_{ex}^\ddagger$ ) and the enthalpy of formation of the outer-sphere complex ( $\Delta H_{os}^0$ );

$$\Delta H_f^\ddagger = \Delta H_{os}^0 + \Delta H_{ex}^\ddagger$$

Since for uncharged ligands  $\Delta H_{os}^0$  will be close to zero the activation enthalpy for the reaction should equal the activation enthalpy for solvent exchange if the mechanism is obeyed. The activation enthalpies for dmso exchange on  $Ni^{2+}$ ,  $Co^{2+}$  and  $Cu^{2+}$  are ca. 50, 40 and 30  $kJ\ mol^{-1}$  (at 25 °C) respectively.

**Table 2.3**

Activation Parameters for the reactions in Table 2.1

in dmso, 25 °C,  $\mu = 0.1\ mol\ dm^{-3}$ , for errors see 2.3.

Ligand	Metal	$\Delta H_f^\ddagger$	$\Delta S_f^\ddagger$	$\Delta G_f^\ddagger$
		$kJ\ mol^{-1}$	$J\ K^{-1}\ mol^{-1}$	$kJ\ mol^{-1}$
Cyclam	$Ni^{2+}$	+49.3	-17.6	+54.2
	$Co^{2+}$	+33.7	-46.2	+47.5
	$Cu^{2+}$	+46.0	-19.0	+51.7
[9]aneN <sub>3</sub>	$Ni^{2+}$	+35.4	-64.3	+54.1
	$Co^{2+}$	+39.0	-28.1	+47.4
	$Cu^{2+}$	+42.5	-29.2	+50.7

These values compare reasonably well with the data in Table 2.3 (considering the uncertainty in the solvent exchange values) and again suggest that the Eigen-Wilkins mechanism is operative.

For the cyclam reactions the order of the initial rate constants ( $k_f$ ) decreases in the order  $k_f(Co^{2+}) > k_f(Cu^{2+}) > k_f(Ni^{2+})$ , paralleling the order of decreasing solvent exchange rate constant as would be expected on the basis of the Eigen-Wilkins mechanism. The activation enthalpies for this process increase in the order  $\Delta H^\ddagger(Co^{2+}) < \Delta H^\ddagger(Cu^{2+}) < \Delta H^\ddagger(Ni^{2+})$  and the activation entropies increase in the order  $\Delta S^\ddagger(Co^{2+}) < \Delta S^\ddagger(Cu^{2+}) < \Delta S^\ddagger(Ni^{2+})$ . Thus, the rates of substitution

are controlled by the enthalpies, with the entropies actually opposing the order. The most favourable enthalpy ( $\Delta H_f^\ddagger = 33 \text{ kJ mol}^{-1}$  for  $\text{Co}^{2+}$ ) is coupled to the least favourable entropy ( $\Delta S_f^\ddagger = -46 \text{ J K}^{-1} \text{ mol}^{-1}$ ), showing the dominance of the enthalpy in the kinetics. The loss in ligand entropy on forming the activated complex outweighs the entropy gain due to dissociation of a dmsol molecule from the metal ion (and/or from the solvated ligand), thus producing negative entropy of activation values for all the reactions. In linear polyamines this is indicative of an unfavourable ligand configuration.<sup>221</sup>

In the reactions of the smaller [9]aneN<sub>3</sub> ligand the activation enthalpy is more favourable in each case compared with the cyclam reactions, whereas the activation entropies are less favourable for each metal ion. These contributions largely cancel each other out, though the free energy of activation for the [9]aneN<sub>3</sub> systems are slightly smaller, producing slightly quicker reactions in the case of the smaller macrocycle. This again shows the dominance of the enthalpy terms. It is not unexpected that the N<sub>3</sub> macrocycle has less favourable entropy contributions in activation since it is rather more rigid in its co-ordination requirements in comparison to the larger and more flexible cyclam ligand.

Thus, the favourable enthalpy terms are governed by the dissociation of the first solvent molecule from the metal ion in accordance with the Eigen-Wilkins mechanism. The unfavourable ligand configurations of the macrocyclic amines control the entropy terms, producing adverse contributions. There are no large differences between the activation entropies of the reactions and so they are likely to involve the same metal co-ordination numbers, at least during the initial rapid process.

As to the nature of the intermediates formed in each reaction we cannot be sure of the details using only the limited data given here. Since no dissociation rate was observed under the conditions employed in measuring the reaction kinetics we can be fairly sure that the intermediates do not involve only single metal-to-ligand bonds and probably do not involve only two bonds as the low stability of such species

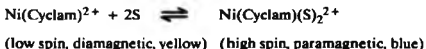
would surely be indicated by the presence of a back reaction in the initial metalation step. Thus, the intermediates are likely to contain the ligand bound to the metal ions via three or four donor atoms. In the case of the [9]aneN<sub>3</sub> ligand this would involve full co-ordination, whereas for cyclam it may involve only three metal-N bonds, though again full co-ordination is more likely as the co-ordination of the final nitrogen would undoubtedly be much quicker than is observed in the second, slower stage of the reactions due to the well established solvent labilising effect of nitrogen donor atoms, here already bound to the metal.<sup>68</sup> Kaden<sup>55</sup> suggests that the cyclam already exhibits square planar co-ordination on Ni<sup>2+</sup> from electronic spectra considerations, though the possibility of a folded structure in the cyclam intermediates cannot be ruled out. Indeed, there is already evidence that macrocycles react with metal ions via folded intermediates<sup>126,222</sup> and also that dissociation of macrocyclic complexes proceeds via folded species.<sup>14</sup>

The slower, first order process thus probably involves some kind of rearrangement within the co-ordination sphere of the metal of the already fully co-ordinated macrocycle to form the final, thermodynamically stable complex. The intermediate is likely to be a thermodynamically unstable analogue of this final complex and the rearrangement may well involve inversion of one or more of the nitrogen centres to a more stable orientation or to a mixture of isomers. This explanation is also used for the similar reaction step in the reaction of Ni<sup>2+</sup> with cyclam in acetonitrile<sup>95</sup> where the process was found to be accelerated by base, as are the isomerisations of previously characterised intermediates.<sup>144</sup> This interpretation is consistent with the observation that the rate constant for this process is independent of the metal ion concentration.

No correlation between the rate constants ( $k_{int}$ ) and the metal-ligand species is observed, indicating the complexity of this process. In one case (the reaction of Cu<sup>2+</sup> with cyclam) the activation parameters for the second step could be measured ( $\Delta H_{int}^\ddagger = 52 \text{ kJ mol}^{-1}$ ,  $\Delta S_{int}^\ddagger = -92 \text{ J K}^{-1} \text{ mol}^{-1}$  at 25 °C) and show both an unfavourable enthalpy and entropy, which combine to slow the rearrangement consider-

ably.

For the  $\text{Ni}^{2+}$ /cyclam reaction the product formed is almost certainly a mixture of square planar and tetragonally distorted octahedral species which are in rapid equilibrium with one another.

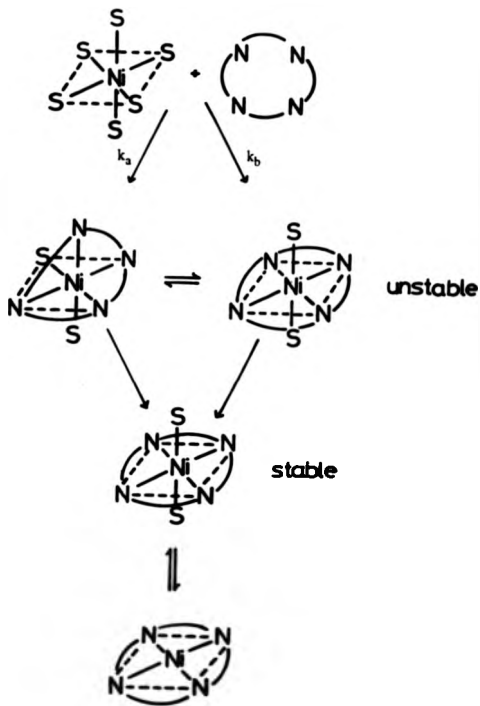


S = co-ordinating solvent molecule

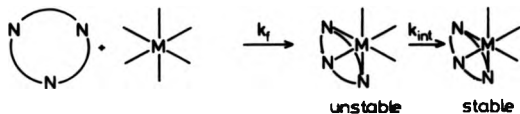
Such equilibria have been observed in a whole range of co-ordinating solvents, including dmsc. Fabbrizzi<sup>223</sup> showed that 29% of the *trans*-isomer of the octahedral species was present in aqueous solution at 25 °C. Since then a number of structural and thermodynamic studies have appeared on the subject.<sup>224,225</sup> The final stage of the complexation reaction must surely involve this process. Billo<sup>226</sup> prepared the *cis*-isomer of  $\text{Ni}(\text{cyclam})(\text{H}_2\text{O})_2^{2+}$  and studied the kinetics of its isomerisation to the *trans*-species. The violet *cis*-isomer isomerises only slowly, at pH 3 the half-life for the process is 250 days at 25 °C. Billo concluded from his work that the *cis*-isomer is a likely intermediate of both formation and dissociation reactions of  $\text{Ni}(\text{cyclam})^{2+}$ . Hay and Norman<sup>95</sup> observed a third step in the complexation reaction between  $\text{Ni}^{2+}$  and cyclam in  $\text{CH}_3\text{CN}$ , which they attributed to interconversion of the planar and octahedral species. No such process was observed in our studies and thus the second stage is likely to involve interconversions between the folded *cis*-isomer and the *trans*-octahedral and square planar species. This suggests a very complex set of processes and would explain the lack of correlation in the rate constants for the second step in all the metals studied. The other metals probably react via folded intermediates also, but no octahedral/planar equilibria are expected, thus simplifying the kinetics for the second step with  $\text{Co}^{2+}$  and  $\text{Cu}^{2+}$ .

A simplified mechanism for the complexation process of  $\text{Ni}^{2+}$  with cyclam is shown in Scheme I. In this case the initial rate constant,  $k_f$  would equal the sum of the rate constants  $k_a$  and  $k_b$ , although the relative rates are impossible to establish with the data obtained. The second, slower stage of the reaction can thus be seen to

Scheme I Mechanism for the complexation of  $\text{Ni}^{2+}$  with cyclam in dmso.

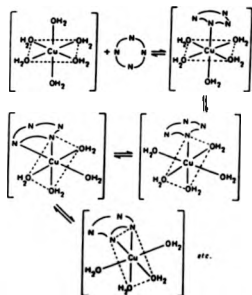


be a complicated mixture of processes, again defying serious kinetic treatment using the measured data. The reactions with  $\text{Co}^{2+}$  and  $\text{Cu}^{2+}$  are likely to proceed in an analogous manner, though the mechanism may be slightly simplified as no octahedral/planar equilibrium will be present in the final stages of the reaction. The mechanism for the [9]ane $\text{N}_3$  complexation will also be simpler, as no folded intermediates can be present. Thus, the mechanism for metalation is possibly;



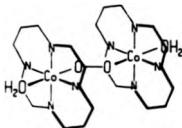
The 1:1 complex was formed in all cases (under conditions of  $[\text{M}^{2+}] \gg [\text{L}]$ ).

For the complexation reactions of  $\text{Cu}^{2+}$  the mechanisms will almost certainly involve initial attack at an axial site on the tetragonally distorted ion species (since  $k_f$  correlates to  $k_{\text{eq}}(\text{axial})$  - see earlier). From previous work with tetragonal aqua  $\text{Cu}(\text{II})$  species<sup>93,222</sup> the next step must be rapid Jahn-Teller inversion to place the substituted ligand in the equatorial plane.



This process will occur with both cyclam and [9]aneN<sub>3</sub> complexations.

The second stage of the reaction between Co<sup>2+</sup> and cyclam could not be measured as a third step interfered greatly. This process involved a large change in absorbance (see Figures 2.20 & 2.21) and was discovered to be the reaction of Co(cyclam)<sup>2+</sup> with dioxygen (see 2.3.5). As soon as the product of complexation is formed traces of oxygen in the stopped-flow apparatus immediately scavenged these species to form  $\mu$ -peroxo-bridged dimers.



The kinetics of formation and decomposition of such species has been the subject of intense study<sup>210</sup> and the systematic study of the reactions of many Co(II) macrocyclic compounds with dioxygen has been carried out<sup>208,209</sup> to determine the effect of ring size and ligand structure on these reactions. Details of the mechanism of reaction of Co(cyclam)<sup>2+</sup> with O<sub>2</sub> are given in references 208 and 209.

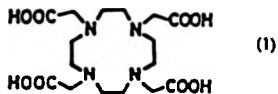
In conclusion the reactions of Co<sup>2+</sup>, Ni<sup>2+</sup> and Cu<sup>2+</sup> with cyclam and [9]aneN<sub>3</sub> proceed via an initial rapid step, which follows the Eigen-Wilkins mechanism, followed by a subsequent slow rearrangement step to the final thermodynamically stable product. More detailed structural information could be obtained for the intermediates by rapid scanning UV/visible spectrophotometry to determine the electronic spectra of these species. The stopped-flow nmr technique<sup>219</sup> could be used to follow the changes in solvation as the reactions proceed.

## Chapter 3

### Rates and Mechanism of Co-ordination of Labile Transition Metal Ions with Tri- and Tetra-aza Macrocycles Functionalised with a Single Pendent Co-ordinating 2,2'-Bipyridyl-6-yl-methyl Arm.

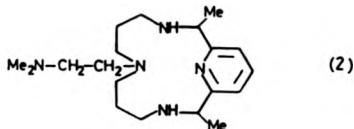
#### 3.1 Introduction

The introduction of additional ligating groups into macrocyclic ligands in the form of pendent co-ordinating arms has received a good deal of attention in recent years. This is because functionalisation at N- or C- atoms in azamacrocycles can modify the properties of the macrocycle. The effect may be a change in solubility, if hydrophilic groups like sulphonates or carboxylates are used, or an increase in metal ion binding specificity. By introducing pendent arms with hard donor atoms such as oxygen onto an azamacrocycle the ligand can thus bind alkali and alkaline earth metals. Thus, the ligand 1,4,7,10-tetraazacyclododecane-N,N',N'',N'''-tetraacetic acid (1), which has four pendent acetate arms, binds to  $\text{Ca}^{2+}$  with a stability constant of  $\log K = 15.85$ , which is one of the strongest complexes of  $\text{Ca}^{2+}$  known, with edta complexing with a  $\log K$  of only 11.00.<sup>227</sup>

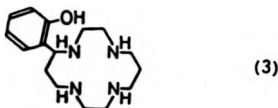


The potential uses of pendent arm macrocycles have been listed by Pilichowski et al<sup>228</sup> and include the immobilisation of macrocycles onto polymers or inorganic supports (see chapter 5). The functional group of the side chain can be used to tune the properties of a metal ion to which it is co-ordinated. Thus, with the nickel complex of (2) one can shift from an octahedral, paramagnetic, blue complex to a square

planar, diamagnetic, yellow complex by adjusting the pH to control the co-ordination of the amino side chain through protonation.<sup>229,230</sup>



Kimura et al have shown<sup>231</sup> that the redox potential of Ni(II)/Ni(III) is greatly affected by the co-ordination of the pendent arm in the Ni(II) complex of (3).

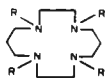


Pendent arm macrocycles can be synthesized with any number of pendent groups producing many varied properties. The synthesis of such azamacrocycles has been reviewed for triaza-,<sup>26,41</sup> tetraaza-,<sup>18</sup> and pentaaza-macrocycles.<sup>26</sup>

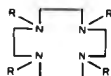
Early studies of the kinetics of pendent arm macrocycles largely concentrated on the effect that the metal ion has on the reactivity of the pendent groups in transition metal complexes. This is because the macrocycle holds the metal ion in a kinetically inert environment thus allowing the study of metal ion promoted or induced reactions under strict steric control. To this end studies have been carried out on the Cu(II) promoted hydrolysis of ester and nitrile pendent side chains.<sup>232-234</sup> The kinetics of intramolecular binding and dissociation of macrocycles with one or more pendent arms also received attention.<sup>18</sup> However, little work has been carried out on the mechanism of metal insertion reactions with pendent arm macrocycles. Studies in this area have concentrated on the tetraaza macrocycles containing four acetate or four hydroxyethyl arms.<sup>235-237</sup>

In a study of the kinetics of interaction of metal ions with DOTA and TETA

Wilkins and Kasprzyk<sup>235</sup> observed that the monoprotonated forms of the ligand were the most reactive species in aqueous solution over a wide range of pH. This behaviour is also found



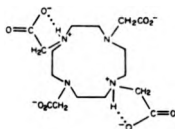
DOTA



TETA



with EDTA and the unsubstituted macrocycles (chapter 1). The unreactivity of the diprotonated ligands is thought to be due to an intramolecular hydrogen bonded structure, which again models the unsubstituted macrocycles.



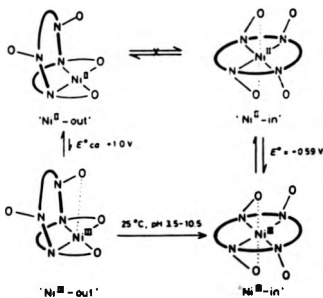
Comparison of the formation rate constants with EDTA, cyclam and cyclen (Table 3.1) suggests that the metal ions are not part of the macrocyclic ring, though the large stabilities<sup>227</sup> must mean that some interaction with the N-donors occurs.

Table 3.1

Formation rate constants for the reactions of M<sup>2+</sup> with various monoprotonated ligands, 25 °C, k<sub>f</sub> / dm<sup>3</sup> mol<sup>-1</sup> s<sup>-1</sup>, ref. 235.

Ligand	k <sub>f</sub> / Zn <sup>2+</sup>	k <sub>f</sub> / Ni <sup>2+</sup>	k <sub>f</sub> / Cu <sup>2+</sup>
H(DOTA) <sup>3-</sup>	1.1 × 10 <sup>7</sup>	3 × 10 <sup>6</sup>	1.2 × 10 <sup>9</sup>
H(TETA) <sup>3-</sup>	1.6 × 10 <sup>8</sup>	2.5 × 10 <sup>4</sup>	-
H(EDTA) <sup>3-</sup>	ca. 10 <sup>9</sup>	2 × 10 <sup>5</sup>	2 × 10 <sup>9</sup>
cyclenH <sup>+</sup>	3.3 × 10 <sup>4</sup>	66	2.9 × 10 <sup>6</sup>
cyclamH <sup>+</sup>	5.0 × 10 <sup>4</sup>	53	1.8 × 10 <sup>6</sup>

The reactions proceed with a faster rate than for the macrocycles, consistent with the observation that conversion of a "picket-fence" porphyrin into a tetracarboxylic acid derivative greatly accelerates its metalation rate.<sup>238</sup> The proposed mechanism with DOTA and TETA involves initial capture of the metal ion by one of the pendent arms, followed by transformation to the final product. In this case X-ray crystallography has shown the final product to be the metal ion being bound by two amines and two acetate groups.<sup>237,239</sup> Thus, it is difficult to compare the kinetics of these pendent arm macrocycles with the unsubstituted macrocycles. For the 14 membered macrocycle with four acetate arms the Ni(II) complex has been converted from the "metal-out" position to the "metal-in" position (figure) where the metal ion is bound inside the macrocyclic cavity by all four nitrogen donors.<sup>237</sup>

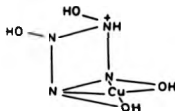


The prohibitively high kinetic barrier for metal insertion was avoided by oxidation of the Ni(II) to Ni(III), which readily forms the "metal-in" complex. Subsequent

reduction to Ni(II) thus produced the "Ni(II)-in" complex as a stable isomer. Similar tetra-acetate pendent arm species with the 13 and 15 membered tetraaza macrocycles do not undergo this process, and nor do the  $\text{Cu}^{2+}$ ,  $\text{Co}^{2+}$  and  $\text{Zn}^{2+}$  complexes of the ligand.

Replacing the acetate arms with hydroxyethyl pendent groups circumvents the problem of the metal-in/metal-out structures.<sup>236</sup> The complexes are of similar stabilities to the complexes of tmc, which are known to be five co-ordinate,<sup>240</sup> and are more stable than the "metal-out" complexes of the tetraacetate tetraaza macrocycles. Rapid metalation reactions occur with this ligand as the hydroxyethyl groups provide points of attachment outside the macrocyclic ring for the incoming metal ion. Thus, the problem of the metal-in/metal-out structures can be overcome by ensuring that the points of initial attachment do not provide a structure of such stability that, as with the tetraacetate tetraaza macrocycles, the metal ion prefers to remain outside the macrocyclic cavity.

The acid dissociation kinetics of the Cu(II) complex of the tetra-hydroxyethyl ligand have been studied.<sup>241</sup> Unlike the highly stable  $\text{Cu}(\text{cyclam})^{2+}$ <sup>145</sup> the Cu(II) complex of this ligand is readily dissociated in acidic solution, with a  $k_H$  of  $3.44 [\text{H}^+] \text{ s}^{-1}$  ( $3.15 \times 10^{-4} [\text{H}^+] \text{ s}^{-1}$  for  $\text{Cu}(\text{cyclam})^{2+}$ ). A "metal-out" structure is proposed as an intermediate in the reaction.



In the present study the effect on the kinetics of functionalising cyclam and [9]aneN<sub>3</sub> with a 2,2'-bipyridyl-6-yl-methyl pendent arm has been investigated. This is believed to be the first study of the complexation reactions of single pendent arm macrocycles. The bipyridine moiety aids the kinetic investigation by UV/visible stopped-flow methods enormously as it is a very good chromophore and large UV

changes are expected on complexation. Also, bipyridine is one of the most widely studied ligands in terms of complexation kinetics and so there is a wealth of available data for comparison to aid analysis of the results.

### 3.2 Experimental

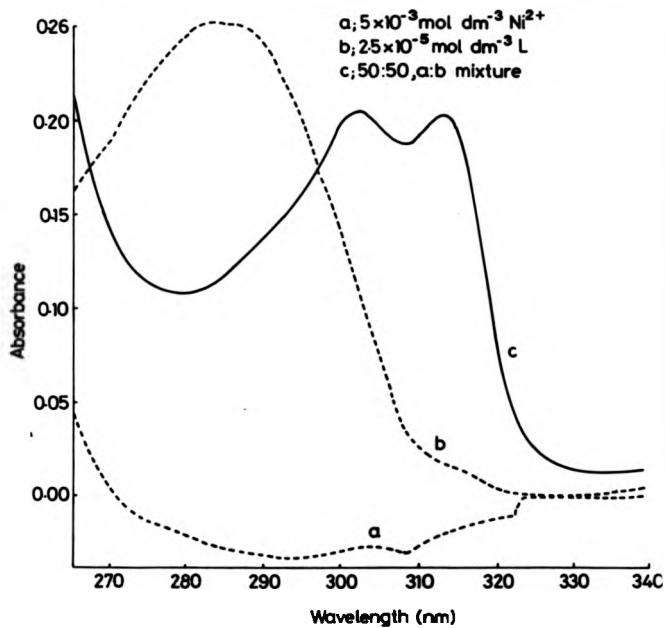
All the procedures and materials employed are as described in Chapter 2 except for the ligands used. In this study the ligands were prepared by the method of Moore et al.<sup>242</sup>

### 3.3 Results

3.3.1 The Complexation Reaction between  $Ni^{2+}$  and 1-(2,2'-bipyridyl-6-yl-methyl)-1,4,8,11-tetraazacyclotetradecane in dmso.

The effect on the electronic spectrum of mixing  $Ni^{2+}$  and the ligand in dmso is illustrated in figure 3.1 for pseudo-first order conditions. The wavelength at which the kinetics were followed by the stopped-flow method was chosen as 313.4 nm, which was considered to be the wavelength at which maximum absorbance/transmittance change occurred. The concentration of ligand used was  $2.5 \times 10^{-5} \text{ mol dm}^{-3}$ , with metal concentrations varying between  $5 \times 10^{-3}$  and  $1.5 \times 10^{-2} \text{ mol dm}^{-3}$  after mixing. Only very low concentrations of ligand were required because of the very favourable absorbance changes observed. A large excess of metal (between 200 and 600 times the ligand concentration) was required to speed the reaction to an accurately measurable level ( $k_{\text{obs}} \text{ ca. } 1-2 \text{ s}^{-1}$ ). As in the previous studies involving cyclam and [9]aneN<sub>3</sub> the stopped-flow traces revealed a two step, consecutive first order process, with both stages marked by an increase in absorbance. The first step was followed over 4 s and the observed rate constant had a first order dependence on the metal concentration. A plot of  $k_{\text{obs}}$  vs.  $[Ni^{2+}]$  gave a straight line of slope  $162.7 \pm 2.0 \text{ dm}^3 \text{ mol}^{-1} \text{ s}^{-1}$  which is the bimolecular rate constant at 24.8 °C. The

Fig. 3.1 Electronic spectra of  $\text{Ni}^{2+}$  and Cyclam-Bipy in dmso.



intercept was experimentally indistinguishable from zero, showing that the dissociation rate of the first step was immeasurable by this method (figure 3.2). The dependence of the bimolecular rate constant on temperature was measured, and analysis via an Eyring plot gave the activation parameters at 25 °C to be  $\Delta H^\ddagger = 49.0 \pm 0.9$  kJ mol<sup>-1</sup> and  $\Delta S^\ddagger = -37.9 \pm 2.8$  J K<sup>-1</sup> mol<sup>-1</sup> (figure 3.3). The second step in the reaction was slower than the first and was followed over 50 s. Analysis by a combination of first order kinetic plots and consecutive first order fits as in the previous work showed that the observed rate constant was independent of the metal ion concentration, with a rate constant of  $0.0478 \pm 0.0057$  s<sup>-1</sup> at 25 °C (figure 3.4 shows a typical first order fit of the data for the second step in the reaction). The low rate constant and the small absorbance change involved meant that no accurate temperature dependence studies could be carried out, and so the activation parameters were not measured. All rate data are listed in Appendix 2.

3.3.2 The Complexation Reaction between Ni<sup>2+</sup> and 1-(2,2'-bipyridyl-6-yl-methyl)-1,4,7-triazacyclononane in dmsu.

The point of maximum absorbance change was 314 nm (figure 3.5). Identical concentrations and conditions were used as in the previous experiment (see 3.3.1). The observed kinetics were again revealed to be a two step, consecutive first order process with identical behaviour to the previous study (figure 3.6). The first stage was slower this time and had to be followed over 10 s to determine the bimolecular rate constant from the dependence of the observed rate constant on the metal concentration. At 24.8 °C  $k_f = 41.5 \pm 0.7$  dm<sup>3</sup> mol<sup>-1</sup> s<sup>-1</sup>, with no measurable dissociation rate (figure 3.7). The activation parameters, derived from an Eyring plot (figure 3.8), were  $\Delta H^\ddagger = 62.9 \pm 2.2$  kJ mol<sup>-1</sup> and  $\Delta S^\ddagger = +4.5 \pm 11.3$  J K<sup>-1</sup> mol<sup>-1</sup> at 25 °C. The observed rate constant for the slower second step, which was again metal independent, was followed over 50 s to give a rate constant of  $(5.33 \pm 0.54) \times 10^{-2}$  s<sup>-1</sup> at 24.8 °C, with the small absorbance change involved not lending itself to an accurate study of the activation parameters. All rate data are listed in Appendix 2.

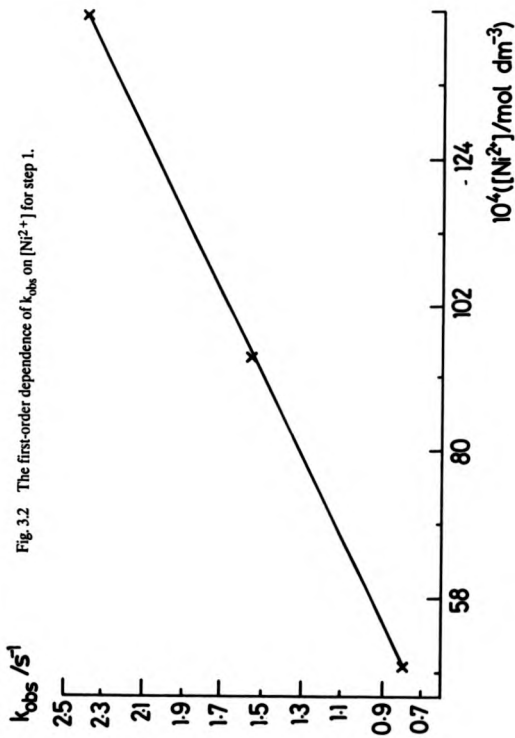
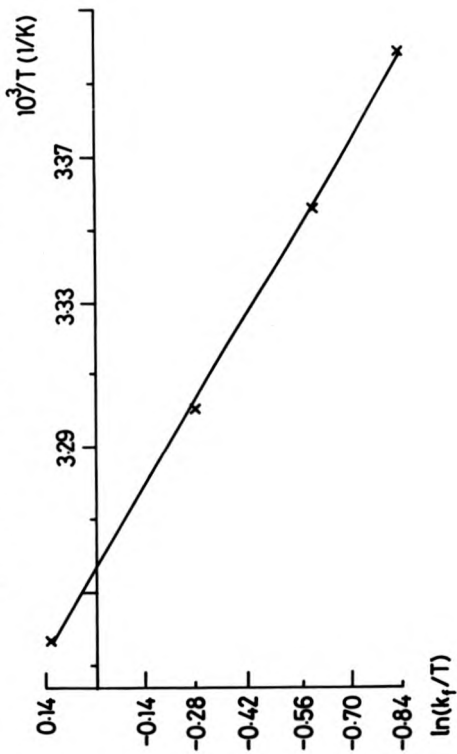


Fig. 3.3 Eyring plot for step 1 in the reaction of  $\text{Ni}^{2+}$  and Cyclam-Bipy.



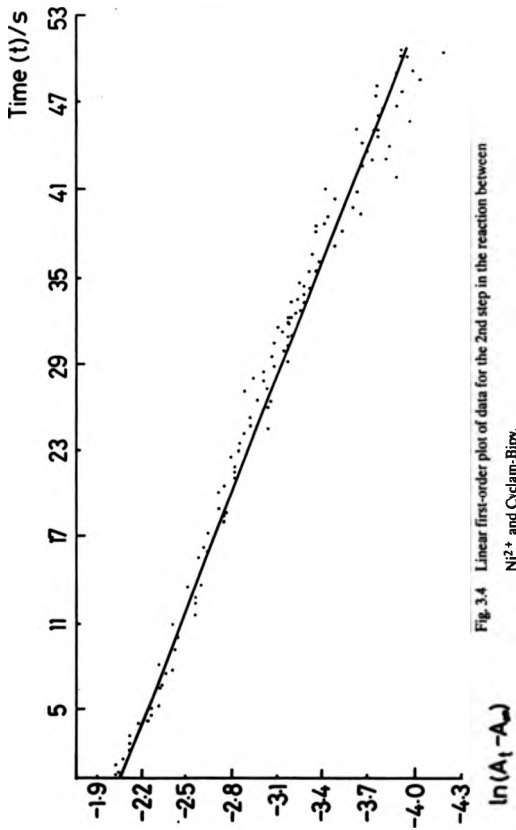


Fig. 3.4 Linear first-order plot of data for the 2nd step in the reaction between  $\text{Ni}^{2+}$  and Cyclam-Bipy

Fig. 3.5 Electronic spectra of  $\text{Ni}^{2+}$  and [9]ane $\text{N}_3$ -Bipy in dmsO.

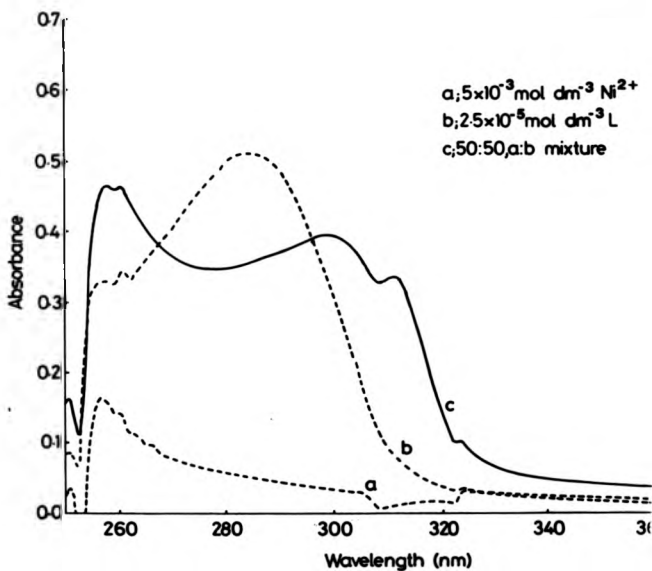
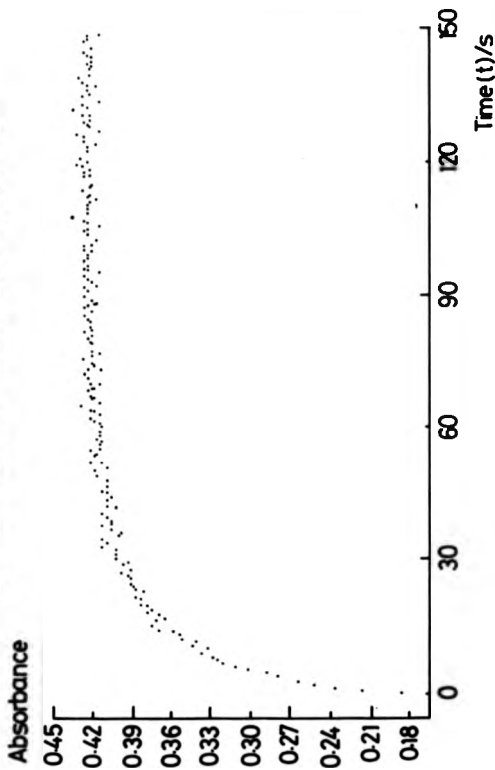
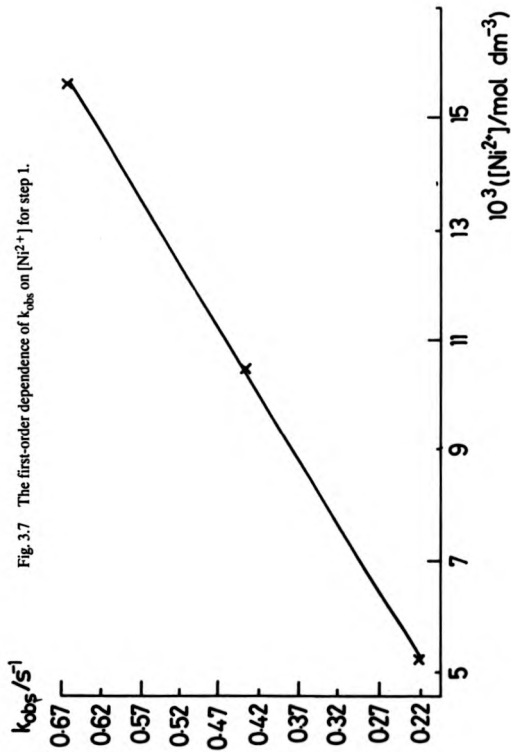


Fig. 3.6 Typical stopped-flow trace for the  $\text{Ni}^{2+}$  and  $(\text{O}^i\text{acac})_3\text{Bi}(\text{py})$  reaction.





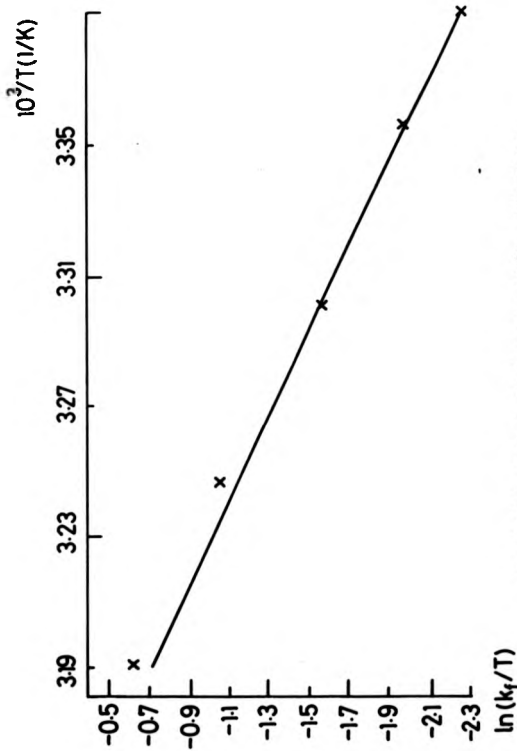


Fig. 3.8 Eyring plot for step 1 in the reaction of  $\text{Ni}^{2+}$  and [9]ane $\text{N}_3$ -Bipy.

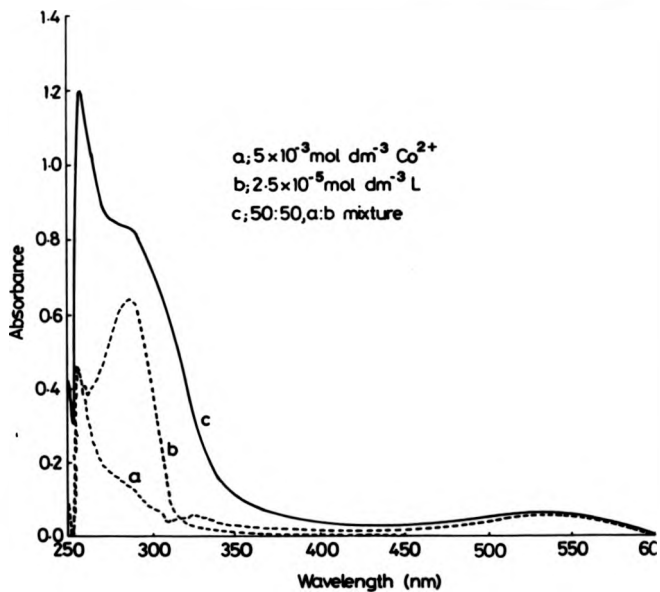
3.3.3 The Complexation Reaction between  $\text{Co}^{2+}$  and 1-(2,2'-bipyridyl-6-yl-methyl)-1,4,8,11-tetraazacyclotetradecane in dmsO.

The reaction between  $\text{Co}^{2+}$  and cyclam-6-methyl-bipyridine was found to be not appreciably air sensitive during the time taken to carry out the experiments, and solutions made up under anaerobic conditions gave identical results to solutions made up in air. The reaction was followed at 315 nm (figure 3.9) using  $2.5 \times 10^{-5}$  mol  $\text{dm}^{-3}$  ligand and  $5.15 \times 10^{-3}$  mol  $\text{dm}^{-3}$   $\text{Co}^{2+}$  (after mixing). As with the  $\text{Ni}^{2+}$  experiments a large absorbance change in this region allowed the use of a small ligand concentration and a wide range of  $\text{Co}^{2+}$  concentrations. Again a two step, consecutive first order biphasic process was observed, each step being identified by an increase in absorbance. The first step was followed over 0.4 s and a study of the dependence of the observed first order rate constant on the metal concentration yielded a value of  $918.6 \pm 10.9 \text{ dm}^3 \text{ mol}^{-1} \text{ s}^{-1}$  at  $24.9 \pm 0.2 \text{ }^\circ\text{C}$  for the bimolecular rate constant, with a first order dependence on metal (figure 3.10). This time, a small intercept was observable, but with a large error; thus the dissociation rate of the intermediate was  $0.129 \pm 0.071 \text{ s}^{-1}$  at  $24.9 \pm 0.2 \text{ }^\circ\text{C}$ . The activation parameters for the forward rate constant were measured from an Eyring plot (figure 3.11) as  $\Delta H^\ddagger = 41.4 \pm 2.7 \text{ kJ mol}^{-1}$  and  $\Delta S^\ddagger = -50.1 \pm 9.0 \text{ J K}^{-1} \text{ mol}^{-1}$  at  $25 \text{ }^\circ\text{C}$ . The errors in the small intercept did not facilitate a serious study of the activation parameters for this process. For the second, slower step the reaction was followed over 30 s, and analysis as in previous experiments gave a rate constant of  $0.0722 \pm 0.0016 \text{ s}^{-1}$  at  $24.9 \pm 0.2 \text{ }^\circ\text{C}$ , which was independent of the metal concentration. All rate data are listed in Appendix 2.

3.3.4 The Complexation Reaction between  $\text{Co}^{2+}$  and 1-(2,2'-bipyridyl-6-yl-methyl)-1,4,7-triazacyclononane in dmsO.

This reaction was followed at 323 nm (figure 3.12), and was found to be insensitive to air, as was the previous experiment (3.3.3). Identical conditions were used as in the previous study. A similar biphasic process was observed, but this time the

Fig. 3.9 Electronic spectra of  $\text{Co}^{2+}$  and Cyclam-Bipy in dmsO.



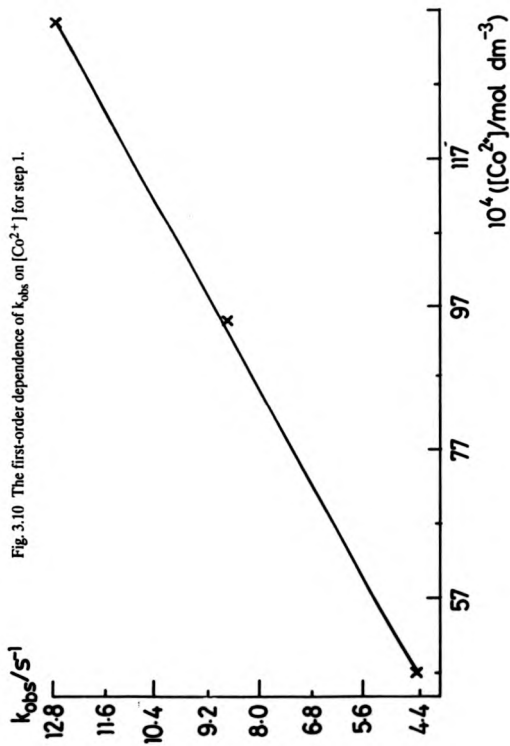


Fig. 3.11 Eyring plot for step 1 in the reaction of  $\text{Co}^{2+}$  and Cyclam-Bipy.

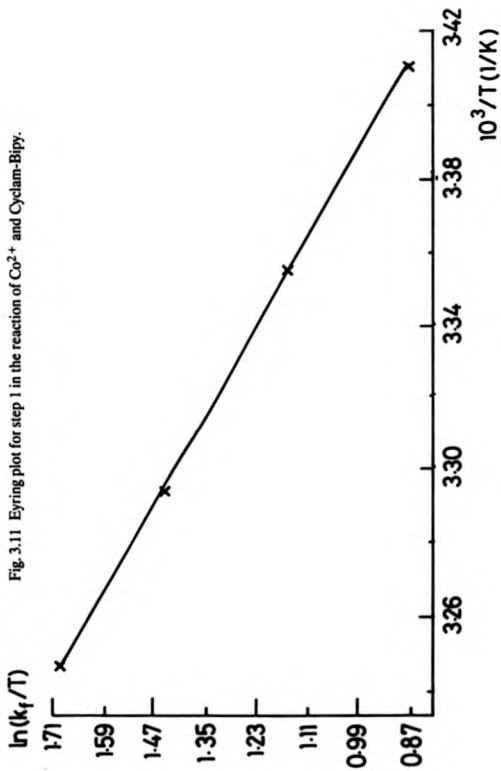
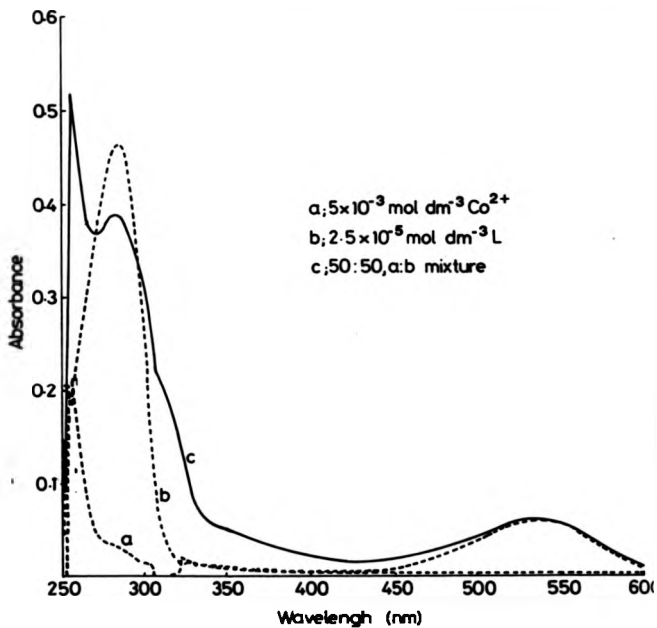


Fig. 3.12 Electronic spectra of  $\text{Co}^{2+}$  and  $[\text{9}]\text{aneN}_3$  in dmsu.



first step was quicker and had to be followed over 0.15 s. The calculated bimolecular rate constant for this process was  $2773 \pm 32 \text{ dm}^3 \text{ mol}^{-1} \text{ s}^{-1}$  at  $24.8 \pm 0.1 \text{ }^\circ\text{C}$  (figure 3.13) with a first order dependence on the metal concentration. Again, a small intercept was observed,  $0.54 \pm 0.22 \text{ s}^{-1}$ , with a large error. The activation parameters for the forward process are  $\Delta H^\ddagger = 49.4 \pm 1.0 \text{ kJ mol}^{-1}$  and  $\Delta S^\ddagger = -13.1 \pm 3.5 \text{ J K}^{-1} \text{ mol}^{-1}$  at  $25.0 \text{ }^\circ\text{C}$ , as derived from an Eyring plot (figure 3.14). The second step was followed over 20 s and was found to be independent of the metal concentration, with a rate constant of  $0.1100 \pm 0.0027 \text{ s}^{-1}$  at  $24.8 \pm 0.1 \text{ }^\circ\text{C}$ . All rate data are listed in Appendix 2.

3.3.5 The Complexation Reaction between  $\text{Cu}^{2+}$  and 1-(2,2'-bipyridyl-6-yl-methyl)-1,4,8,11-tetraazacyclotetradecane in dmsO.

Attempts to follow this reaction at both ultra-violet and visible wavelengths (figures 3.15 & 3.16) proved impossible. At ligand concentrations required to provide a large enough absorbance change on mixing, the concentrations of  $\text{Cu}^{2+}$  required to retain pseudo-first order conditions drove the reaction at a rate too rapid for the stopped-flow technique (the apparatus has a "dead time" of 2 ms, so the reaction was complete in less than 2 ms), and all that was visible was the tail end of the presumably second, slower stage of the reaction (if the reaction follows the same biphasic process as found with the other metals). This is due to the unfavourable absorbance changes on mixing.

(\* - the dead time is the time required for mixing and moving the solutions from the mixer to the observation chamber)

3.3.6 The Complexation Reaction between  $\text{Cu}^{2+}$  and 1-(2,2'-bipyridyl-6-yl-methyl)-1,4,7-triazacyclononane in dmsO.

Again, attempts to follow this reaction in the visible region (figure 3.17) with  $2.5 \times 10^{-3} \text{ mol dm}^{-3}$  ligand and  $2.5 \times 10^{-2} \text{ mol dm}^{-3} \text{ Cu}^{2+}$  pushed the reaction rate too

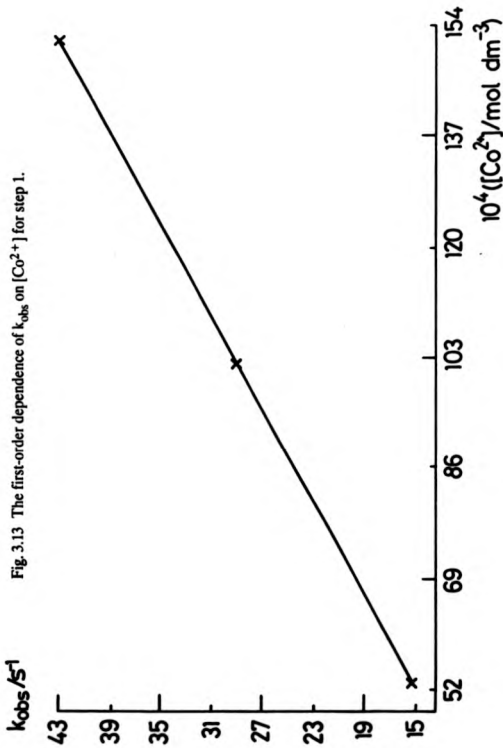


Fig. 3.14 Eyring plot for step 1 in the reaction of  $\text{Co}^{2+}$  and  $[\text{9JanetN}_5\text{Bipy}]$ .

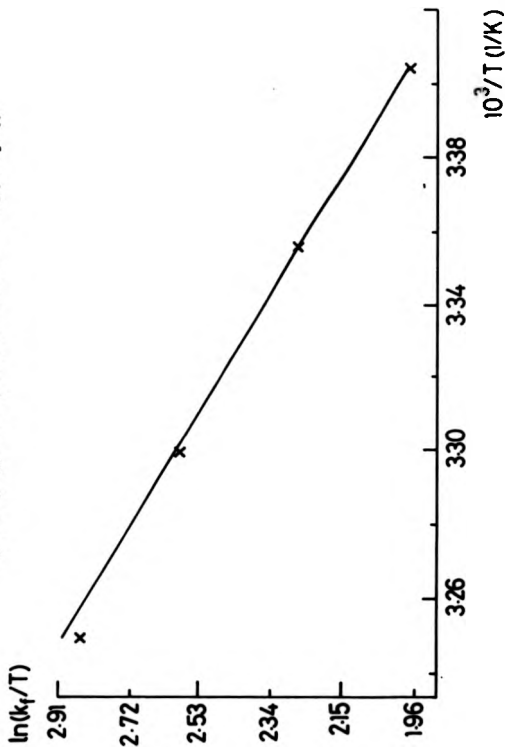


Fig. 3.15 Electronic spectra of  $\text{Cu}^{2+}$  and Cyclam-Bipy in dmso - U. V. region.

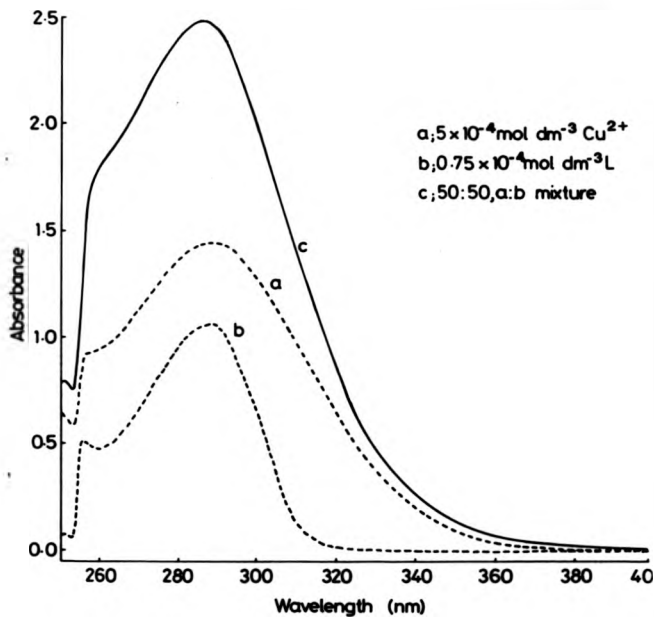


Fig. 3.16 Electronic spectra of  $\text{Cu}^{2+}$  and Cyclam-Bipy in dmso - visible region.

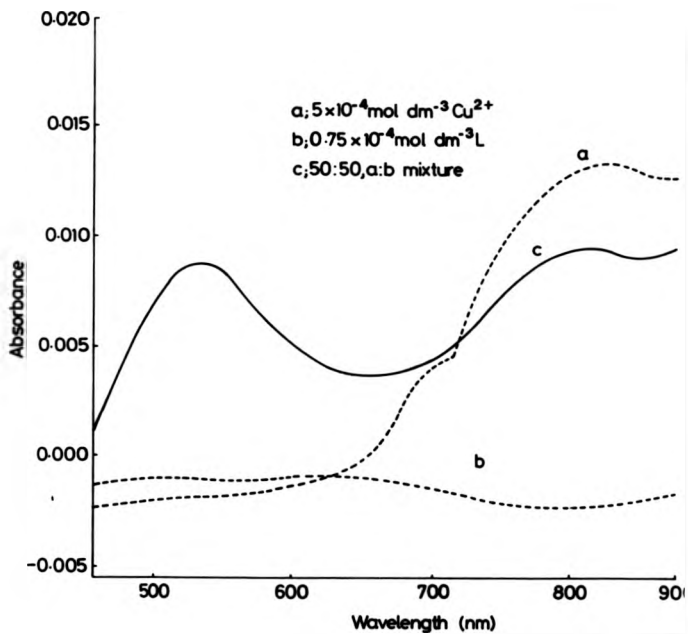
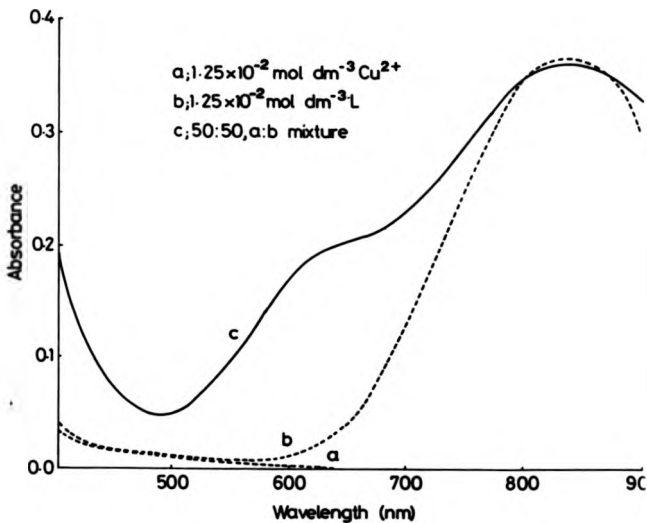


Fig. 3.17 Electronic spectra of  $\text{Cu}^{2+}$  and [9]jane $\text{N}_3$ -Bipy in dmsO - visible region.



high to be measured. However, this time the rates were just measurable by following the reaction in the ultra-violet region (figure 3.18) at 316.5 nm using  $1.25 \times 10^{-5}$  mol dm<sup>-3</sup> ligand and  $1.25$ - $3.5 \times 10^{-4}$  mol dm<sup>-3</sup> Cu<sup>2+</sup> (both after mixing). A two step, consecutive first order process was observed, with both stages displaying the now characteristic increase in absorbance for reactions followed in the ultra-violet. A study of the metal ion concentration dependence of the observed rate constant for the first step was carried out by following the reaction over 0.04 s. The calculated bimolecular rate constant at 25.0 °C was  $2.456 \times 10^5$  ( $\pm 9.2 \times 10^3$ ) dm<sup>3</sup> mol<sup>-1</sup> s<sup>-1</sup> (figure 3.19). A large intercept was observed in the plot of  $k_{\text{obs}}$  vs. [Cu<sup>2+</sup>], with the dissociation rate for the first step being  $19.99 \pm 1.29$  s<sup>-1</sup>. Unfortunately, an accurate temperature dependence study of the activation parameters proved impossible, as the investigation was limited by the value of the observed rate constants, which were too large to be accurately measured. The second stage of the reaction was followed over 2 s and proved to be independent of the metal ion concentration with an observed rate constant of  $1.34 \pm 0.01$  s<sup>-1</sup>. All rate data are listed in Appendix 2.

### 3.3.7 The Complexation Reaction between Zn<sup>2+</sup> and 1-(2,2'-bipyridyl-6-yl-methyl)-1,4,8,11-tetraazacyclotetradecane in dmsO.

The reaction was studied at 316 nm, with  $2.5 \times 10^{-5}$  mol dm<sup>-3</sup> ligand and  $5$ - $15 \times 10^{-4}$  mol dm<sup>-3</sup> Zn<sup>2+</sup> (figure 3.20), where the point of maximum absorbance change was considered to exist on mixing. A two step, consecutive first order process was observed, with both steps marked by an increase in absorbance. A study of the effect of varying the metal concentration and temperature on the observed rate constant for the first step showed a first order dependence on the metal concentration, with a bimolecular rate constant of  $1.22 \times 10^4 \pm 209$  dm<sup>3</sup> mol<sup>-1</sup> s<sup>-1</sup> at 25.0 °C and a dissociation rate of  $5.099 \pm 0.139$  s<sup>-1</sup> (figure 3.21). The activation parameters for the forward step were  $\Delta H^\ddagger = 49.8 \pm 0.8$  kJ mol<sup>-1</sup> and  $\Delta S^\ddagger = +0.3 \pm 2.6$  J K<sup>-1</sup> mol<sup>-1</sup> (figure 3.22) and for the dissociation step,  $\Delta H^\ddagger = 16.3 \pm 0.8$  kJ mol<sup>-1</sup> and  $\Delta S^\ddagger = -177.0 \pm 2.6$  J K<sup>-1</sup> mol<sup>-1</sup> (figure 3.23), all at 25.0 °C. A study of the second step over 3 s

Fig. 3.18 Electronic spectra of  $\text{Cu}^{2+}$  and Cyclam-Bipy in dmsO - U. V. region.

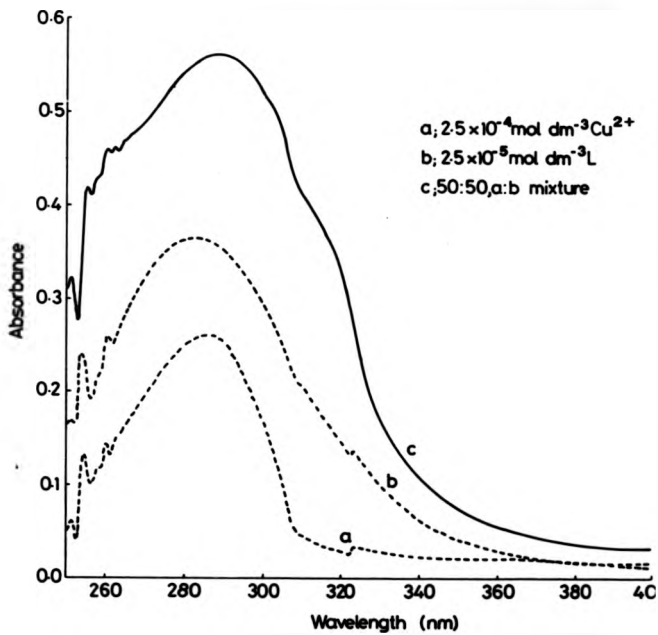


Fig. 3.19 The first-order dependence of  $k_{\text{obs}}$  on  $[\text{Cu}^{2+}]$  for step 1.

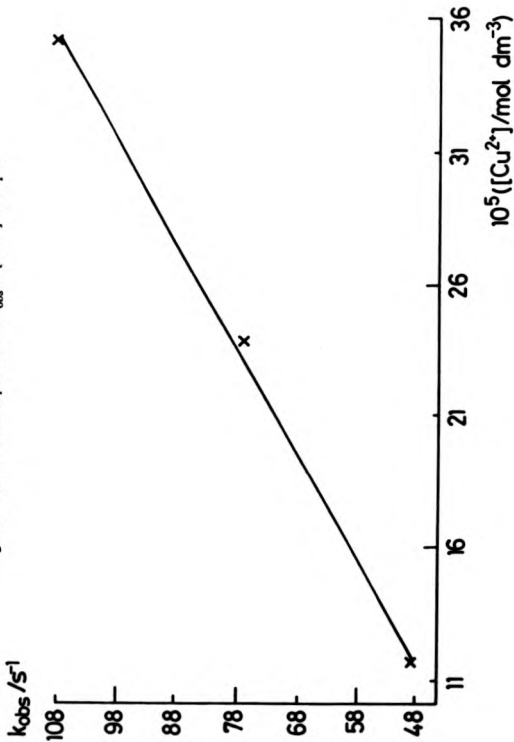
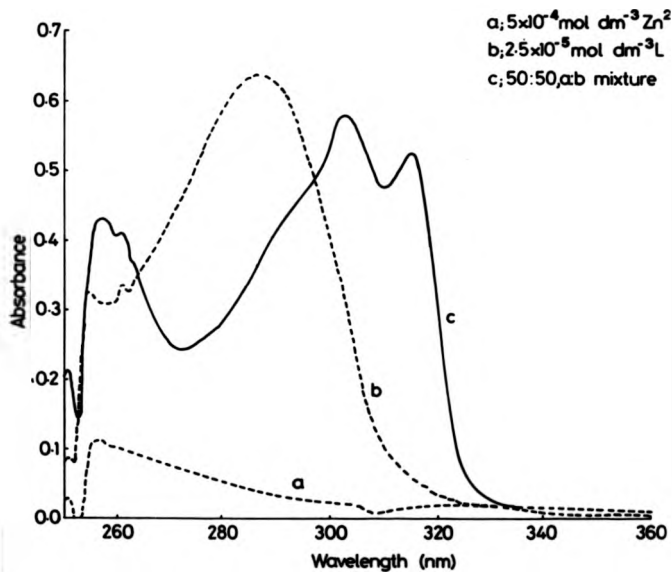


Fig. 3.20 Electronic spectra of  $Zn^{2+}$  and Cyclam-Bipy in dmso.



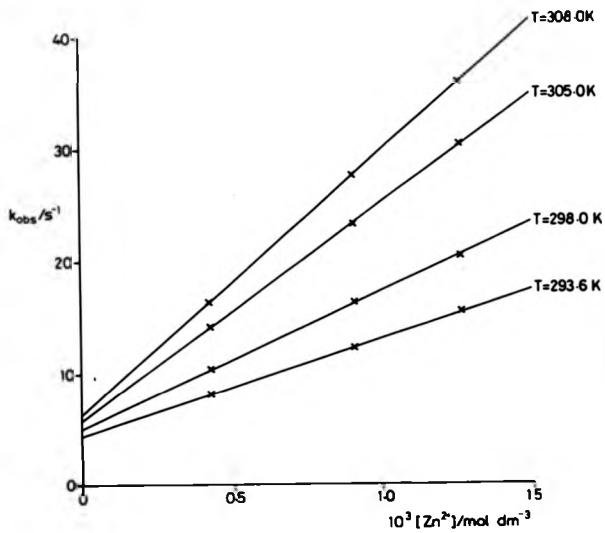
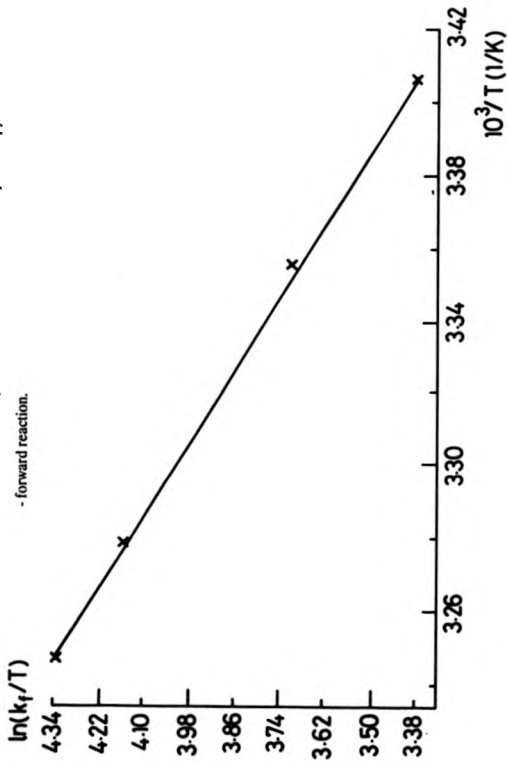


Fig. 3.21 The first-order dependence of  $k_{\text{obs}}$  on  $[\text{Zn}^{2+}]$  for step 1.

Fig. 3.22 Eyring plot for step 1 in the reaction of  $Zr^{2+}$  and Cyclam-Bipy  
- forward reaction.



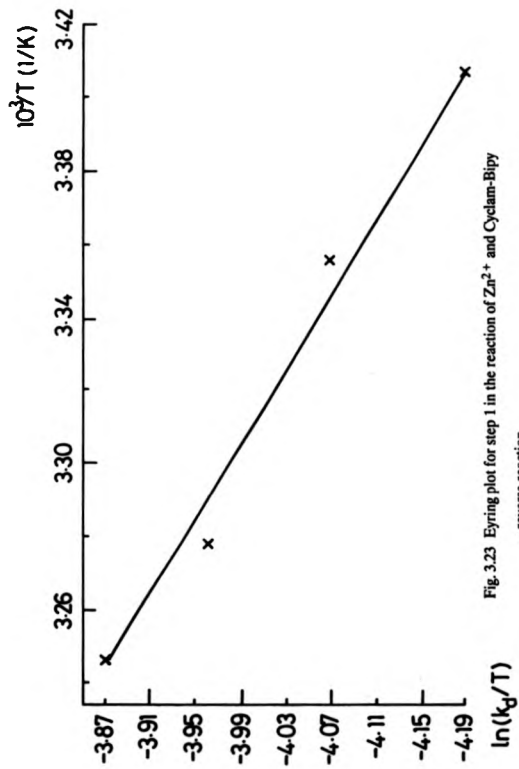


Fig. 3.23 Eyring plot for step 1 in the reaction of  $Zn^{2+}$  and Cyclam-Bipy - reverse reaction.

showed no dependence on the metal concentration, with a rate constant of  $0.768 \pm 0.016 \text{ s}^{-1}$  at  $25.0 \text{ }^\circ\text{C}$ . This time, a temperature dependence study of the second stage was possible due to a favourable absorbance change, with the derived activation parameters (figure 3.24) being  $\Delta H^\ddagger = 31.3 \pm 1.6 \text{ kJ mol}^{-1}$  and  $\Delta S^\ddagger = -142.8 \pm 5.4 \text{ J K}^{-1} \text{ mol}^{-1}$  at  $25.0 \text{ }^\circ\text{C}$ . All rate data are listed in Appendix 2.

### 3.3.8 The Complexation Reaction between $\text{Zn}^{2+}$ and 1-(2,2'-bipyridyl-6-yl-methyl)-1,4,7-triazacyclononane in dmsO.

The change in the electronic spectrum of the reactants on mixing is shown in figure 3.25. It is very similar to the reaction of  $\text{Zn}^{2+}$  with the cyclam derivative of 2,2'-bipyridine (figure 3.20) and so the same concentrations as those experiments (3.3.7) were used in this study. The reaction was followed at 313 nm and stopped-flow traces again displayed a two step, consecutive first order process. Analysis of the first step by following the reaction over 0.2 s and observing the dependence of the rate constant on metal concentration and temperature (figure 3.26) gave a calculated bimolecular rate constant of  $1.25 \times 10^5 \pm 98 \text{ dm}^3 \text{ mol}^{-1} \text{ s}^{-1}$  at  $25.0 \text{ }^\circ\text{C}$  and a dissociation rate of  $5.01 \pm 0.07 \text{ s}^{-1}$  at  $25.0 \text{ }^\circ\text{C}$ . The activation parameters, derived from Eyring plots, were  $\Delta H^\ddagger = 50.6 \pm 1.4 \text{ kJ mol}^{-1}$  and  $\Delta S^\ddagger = +3.2 \pm 4.5 \text{ J K}^{-1} \text{ mol}^{-1}$  at  $25.0 \text{ }^\circ\text{C}$  for the forward process (figure 3.27) and  $\Delta H^\ddagger = 16.9 \pm 1.0 \text{ kJ mol}^{-1}$  and  $\Delta S^\ddagger = -175.1 \pm 2.9 \text{ J K}^{-1} \text{ mol}^{-1}$  at  $25.0 \text{ }^\circ\text{C}$  for the reverse process (figure 3.28). The second stage, observed over 10 s, showed no dependence on metal ion concentration, with a rate constant of  $0.197 \pm 0.017 \text{ s}^{-1}$  at  $25.0 \text{ }^\circ\text{C}$  and activation parameters of  $\Delta H^\ddagger = 128.7 \text{ kJ mol}^{-1}$  and  $\Delta S^\ddagger = +173.0 \pm 4.0 \text{ J K}^{-1} \text{ mol}^{-1}$  at  $25.0 \text{ }^\circ\text{C}$  (figure 3.29). All rate data are listed in Appendix 2.

### 3.3.9 The Complexation Reactions between $\text{Mn}^{2+}$ and the ligands 1-(2,2'-bipyridyl-6-yl-methyl)-1,4,8,11-tetraazacyclotetradecane and 1-(2,2'-bipyridyl-6-yl-methyl)-1,4,7-triazacyclononane.

At concentrations of reactants suitable to produce a large enough absorbance

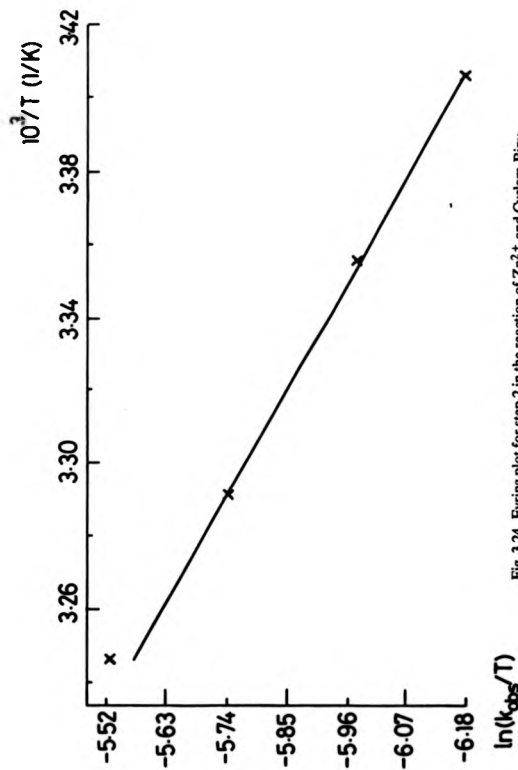
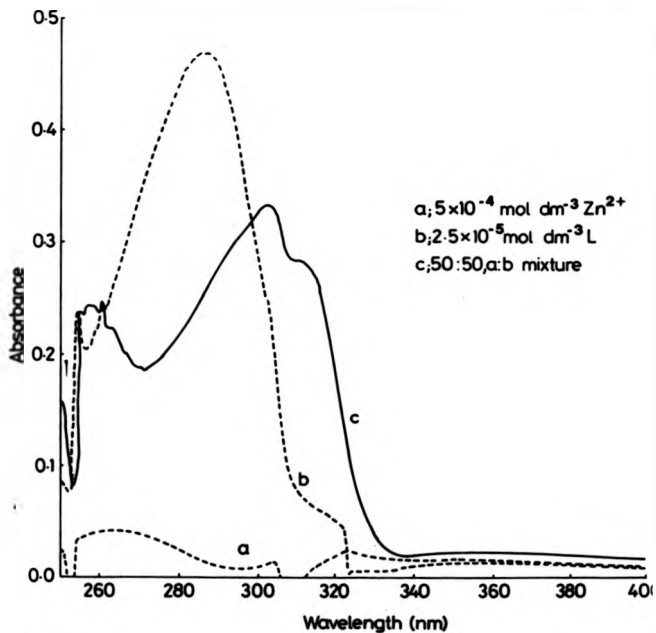


Fig. 3.24 Eyring plot for step 2 in the reaction of  $Zn^{2+}$  and Cyclam-Bipy.

Fig. 3.25 Electronic spectra of  $Zn^{2+}$  and [9]aneN<sub>3</sub>-Bipy in dmso.



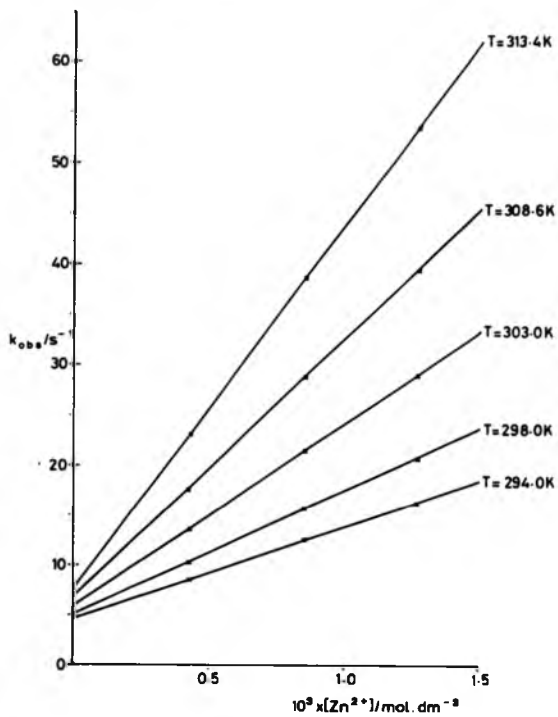
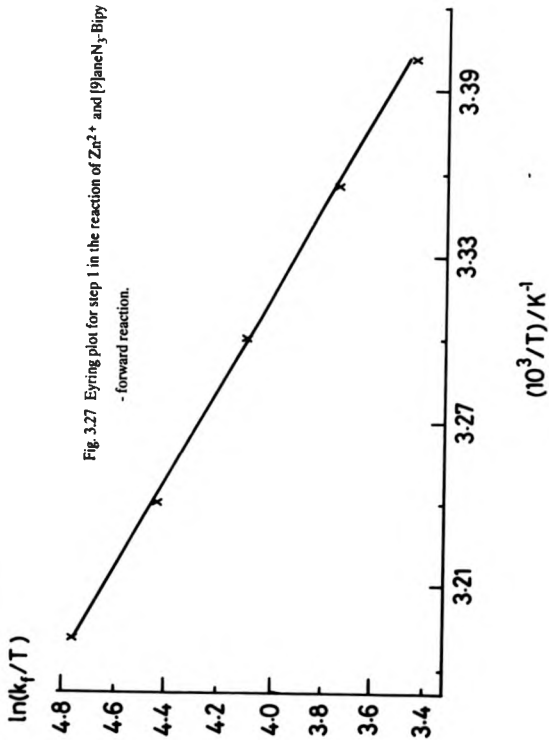


Fig. 3.26 The first-order dependence of  $k_{\text{obs}}$  on  $[\text{Zn}^{2+}]$  for step 1.



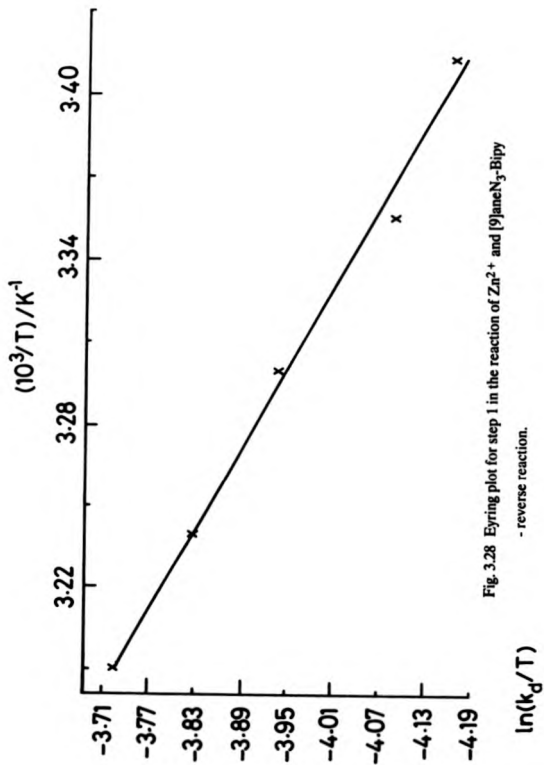


Fig. 3.28 Eyring plot for step 1 in the reaction of  $Zn^{2+}$  and [9]juncN<sub>3</sub>-Bipy - reverse reaction.

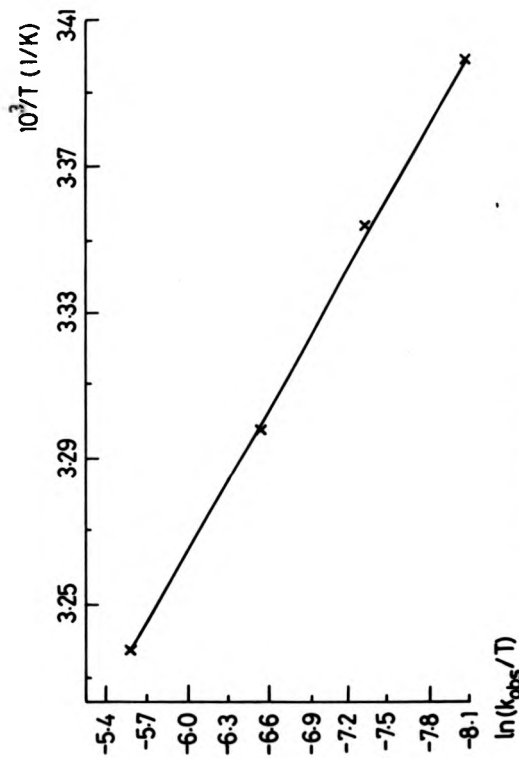
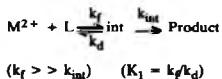


Fig. 3.29 Eyring plot for step 2 in the reaction of  $Zn^{2+}$  and [9]janeN<sub>5</sub>-Bipy.

change on mixing (e.g. figure 3.30 for [9]aneN<sub>3</sub>-Bipy) all reactions, followed at 316 nm, were too fast to measure on the stopped-flow timescale. Only the tail end of a reaction could be observed. Thus, no data was obtainable for these two reactions in dmso. Decreasing the concentrations of reactants would make the absorbance change too small to measure and decreasing the temperature to slow the reaction would be impractical as the dmso solutions freeze at just under 20 °C.

### 3.4 Discussion

As with the work discussed in the previous chapter, all the reactions studied here displayed a biphasic kinetic process, with equivalent concentration dependencies as before for the two steps (2.4). However, with the pendent arm macrocycles the initial rapid step displayed a reverse reaction for some of the metals (Zn<sup>2+</sup>, Co<sup>2+</sup> and Cu<sup>2+</sup>) studied. Thus, the complexation process is slightly more complicated than for unsubstituted cyclam and [9]aneN<sub>3</sub> with the initial step involving an equilibrium.



The pendent arm thus has the effect of destabilising the intermediate with respect to the reactions of the unsubstituted macrocycles. The measured and calculated rate constants for the complexation reactions of Ni<sup>2+</sup>, Cu<sup>2+</sup>, Co<sup>2+</sup>, Zn<sup>2+</sup> and Mn<sup>2+</sup> with cyclam and [9]aneN<sub>3</sub> functionalised with a single pendent 2,2'-bipyridyl-6-yl-methyl arm are listed in Table 3.2.

Initial attachment of the metal ion must occur through either a bipyridyl or a macrocyclic donor atom. In order to determine at which of these two moieties initial reaction occurs it is useful to compare the rate constants of complexation for bipy, cyclam, [9]aneN<sub>3</sub> and the relevant pendent arm macrocycle with each metal ion. Full

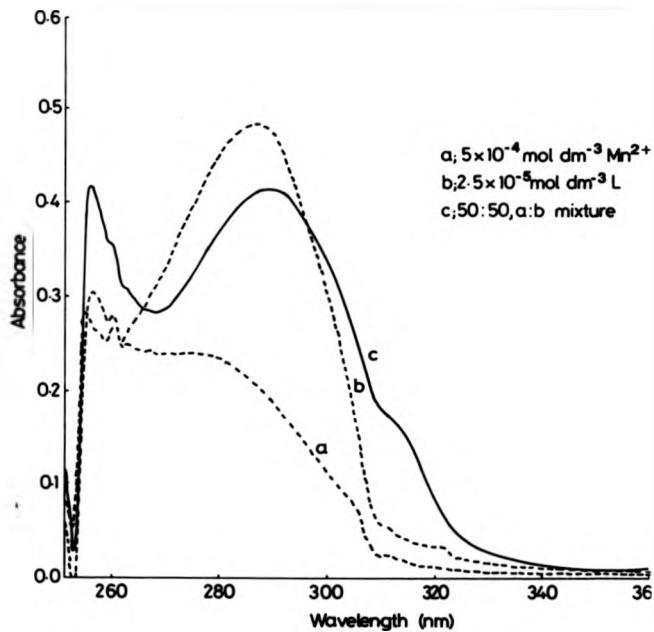


Fig. 3.30 Electronic spectra of  $Mn^{2+}$  and [9]ane $N_3$ -Bipy in dmsc.

data are only available for  $\text{Ni}^{2+}$  and  $\text{Co}^{2+}$  and values are listed in Table 3.3.

**Table 3.2**

Measured Rate Constants for the Reactions of Various Pendent arm Ligands with Labile Transition Metals, for errors see 3.3, \* - not measured, see results.

Ligand	Metal	$k_f$ $\text{dm}^3 \text{ mol}^{-1} \text{ s}^{-1}$	$k_d$ $\text{s}^{-1}$	$k_{\text{int}}$ $\text{s}^{-1}$	$\log K_1$ $= \log (k_f/k_d)$
Cyclam-Bipy	$\text{Ni}^{2+}$	162.7	*	0.047	*
	$\text{Co}^{2+}$	918.6	0.129	0.072	$3.85 \pm 2.12$
	$\text{Zn}^{2+}$	12310	5.05	0.760	$3.39 \pm 0.04$
	$\text{Mn}^{2+}$	*	*	*	*
[9]ane $\text{N}_3$ -Bipy	$\text{Ni}^{2+}$	41.5	*	0.053	*
	$\text{Cu}^{2+}$	246000	19.99	1.337	$4.09 \pm 0.42$
	$\text{Co}^{2+}$	2773	0.54	0.11	$3.71 \pm 1.55$
	$\text{Zn}^{2+}$	12510	5.01	0.196	$3.40 \pm 0.07$
	$\text{Mn}^{2+}$	*	*	*	*

**Table 3.3**

Comparison of Forward Rate Constants for the Reactions of  $\text{Ni}^{2+}$  and  $\text{Co}^{2+}$  with various Ligands.

25 °C, dmso,  $k_f / \text{dm}^3 \text{ mol}^{-1} \text{ s}^{-1}$

Reactant	$k_f / \text{Ni}^{2+}$	$k_f / \text{Co}^{2+}$
Cyclam-bipy	162.7	918.6
[9]ane $\text{N}_3$ -bipy	41.5	2773
Cyclam <sup>a</sup>	1620	29418
[9]ane $\text{N}_3$ <sup>a</sup>	1747	31306
bipy <sup>b</sup>	69	3600

refs: a - chapter 2, b - ref. 62

From comparison of the data for  $\text{Ni}^{2+}$  and  $\text{Co}^{2+}$  it is clear that the initial rate constants for the reactions with both pendent arm macrocycles resemble much more closely the corresponding values for bipy rather than the unsubstituted macrocycles, with pendent arm macrocycle/bipy values differing by less than a factor of 4 times at the very most, whereas for the free macrocycle the values are up to 30 times larger (e.g. for  $\text{Co}^{2+}$  with cyclam). Since we have already established that the free macrocycles react via the Eigen-Wilkins mechanism in dmsO (see 2.4) then the lower reactivity of the pendent arm macrocycles may suggest that these ligands do not follow this mechanism. To substantiate this claim we may calculate the values of  $n$  expected from the dissociative interchange mechanism using  $K_{\text{ex}} = 0.55$  as in chapter 2. The calculated values are tabulated in Table 3.4.

The values of  $n$  for  $\text{Ni}^{2+}$ ,  $\text{Co}^{2+}$  and  $\text{Zn}^{2+}$  are all very similar and lie in the range  $1.3 - 4.9 \times 10^{-3}$ . These values are very small and again reflect the bulk of the dmsO molecules as in Chapter 2. With  $\text{Cu}^{2+}$  the value of  $n$  is again anomalous, this

**Table 3.4**

Calculated values of  $n$  using the Eigen-Wilkins equation

25 °C, dmsO, C/B = Cyclam-Bipy, T/B = [9]aneN<sub>3</sub>,  $k_f / \text{dm}^3 \text{mol}^{-1} \text{s}^{-1}$ .

Metal	$k_f$	$k_f$	$k_{\text{ex}}^{-1}$	$n$	$n$
	C/B	T/B	$\text{s}^{-1}$		
$\text{Ni}^{2+}$	162.7	41.5	$1 \times 10^4$	$4.9 \times 10^{-3}$	$1.3 \times 10^{-3}$
$\text{Cu}^{2+}$	-	246000	$7.95 \times 10^3$	-	14.07
$\text{Co}^{2+}$	918.6	2773	$1.7 \times 10^5$	$1.6 \times 10^{-3}$	$4.9 \times 10^{-3}$
$\text{Zn}^{2+}$	12310	12510	$8.7 \times 10^{5*}$	$4.3 \times 10^{-3}$	$4.4 \times 10^{-3}$
$\text{Mn}^{2+}$	-	-	$6.3 \times 10^{6*}$	-	-

\* -  $k_{\text{ex}}^{-1} \text{Zn}^{2+}$  ref. 194,  $k_{\text{ex}}^{-1} \text{Mn}^{2+}$  ref. 243.

may be due to the error in  $k_{\text{ex}}^{-1}$  for this ion in dmsO since doubt has already been placed on the value for the rate of solvent exchange for this ion in dmsO (see chapter

2); thus, this data may substantiate this doubt somewhat. If we assume that the reaction of  $\text{Cu}^{2+}$  with [9]ane $\text{N}_3$ -bipy follows the Eigen-Wilkins mechanism we can then generate a value for  $k_{\text{ex}}^{\text{I}}(\text{Cu}^{2+})$  in dmsO from the equation used previously. This produces a value in the range  $2.3 - 8.6 \times 10^7 \text{ s}^{-1}$  at  $25.0^\circ\text{C}$ , which seems much more reasonable than the published data.<sup>190,191</sup> This value is much more in keeping with the trends in solvent exchange rate variance with metal ions<sup>97</sup> observed in many other solvents e.g.  $\text{H}_2\text{O}$ ,  $\text{MeOH}$ ,  $\text{dmf}$ ,  $\text{CH}_3\text{CN}$  etc. This value would also explain the order of the increasing rate constants ( $k_f$ ) observed in the reactions studied here ( $k_f(\text{Cu}^{2+}) > k_f(\text{Zn}^{2+}) > k_f(\text{Co}^{2+}) > k_f(\text{Ni}^{2+})$ ) as this order is now paralleled by the solvent exchange rates of the metal ions. However, with the unsubstituted macrocycles this new value could not explain the rate constants observed for the reactions with  $\text{Cu}^{2+}$  (see 2.4) in terms of the Eigen-Wilkins mechanism. There is clearly some kind of abnormal behaviour occurring in one (or both) of the systems and more work is required before this problem is resolved e.g. measuring the rate of dmsO exchange on  $\text{Cu}^{2+}$  using  $^{17}\text{O}$  nmr methods, and the rate of reaction of bipy with  $\text{Cu}^{2+}$  in dmsO.

The values of "n" calculated by assuming the Eigen-Wilkins mechanism for  $\text{Ni}^{2+}$ ,  $\text{Co}^{2+}$  and  $\text{Zn}^{2+}$  are very interesting in that they are much lower than the values calculated for "normal" substitution reactions (ca. 0.2) (see 2.4 & ref. 56). Also, they are very similar to the value calculated by Nichols and Grant<sup>56</sup> for the reaction between  $\text{Ni}^{2+}$  and bipy in dmsO (0.008); a value which the authors used to suggest anomalous behaviour for the substitution reactions of this ligand (and 1,10-phenanthroline) in dmsO. This also suggests that the initial reaction step of the biphasic process involves reaction of the bipyridyl moiety. Data from the studies of the substitution reactions of 2,2'-bipyridyl in aqueous solution suggests that in this solvent reaction occurs via the Eigen-Wilkins mechanism. For the reaction of  $\text{Ni}^{2+}$  with pyridine and with 2,2'-bipyridine the rate constants are ca.  $4\,000$  and  $1\,500 \text{ dm}^3 \text{ mol}^{-1} \text{ s}^{-1}$  respectively at  $298.1 \text{ K}$  in water<sup>86,87</sup> whereas in dmsO the same reactions have rate constants of ca.  $2\,000$  and  $69 \text{ dm}^3 \text{ mol}^{-1} \text{ s}^{-1}$  respectively.<sup>62,65</sup> This illus-

trates the reduced rate of reaction for bipy in dmsO compared with H<sub>2</sub>O, and the change from an Eigen-Wilkins mechanism to some other mechanism. A number of authors have attempted to explain this behaviour, though the most likely interpretation is that chelate ring closure becomes rate determining for bipy in dmsO.<sup>244</sup> This suggestion was supported by studies of the dissociation of Ni(bipy)<sup>2+</sup> in water and dmsO, where the rate of chelate ring closure was found to be ca. 60 times slower in dmsO than in water.<sup>244</sup> The reason for the occurrence of this SCS mechanism (see 1.3) is likely to be due to increased competition of the solvent molecules, with respect to chelate ring closure, for the intermediate, where only a single metal-donor bond is present. The dmsO molecules are known to possess a higher donor ability than water.<sup>212</sup> Also, the bulkiness of the co-ordinated dmsO molecules may hinder the approach of the donor atoms on co-ordination (the water molecules are much smaller).

Since a number of the reactions studied display an equilibrium in the initial rapid step values for the stability constants of this process may be calculated. These values, where all necessary data are available, are listed in Table 3.2. If the initial reaction step involves reaction with the bipy moiety, as the data suggests, then it would be useful to compare these stability constants with the stability constants for the 1:1 complexes of M(bipy)<sup>2+</sup> in dmsO in order to determine the extent to which the reaction intermediates match the simpler complexes. Unfortunately, the only available data for M(bipy)<sup>2+</sup> stabilities in dmsO is for the Zn<sup>2+</sup> complex.<sup>194</sup> However, by comparing this figure to that for the aqueous stability constant, where data is available for all the complexes, we can determine the difference in stability (2 log units for Zn(bipy)<sup>2+</sup>) and thus use this value to generate approximate values of the stability constants for the other metals. Data calculated in this way are compared with stability constants calculated from the rate constants for the pendent arm macrocyclic reactions in Table 3.5.

Table 3.5

Comparison of Stability Constants for bipy and bipy/macrocycle species.

dmsO,  $\mu = \text{ca. } 0.1 \text{ mol dm}^{-3}$

Metal	$\log K_1 / \text{bipy}$	$\log K_1 / \text{cyclam-bipy}$	$\log K_1 / [9]\text{aneN}_3\text{-bipy}$
$\text{Ni}^{2+}$	5.1	-	-
$\text{Co}^{2+}$	3.8	$3.85 \pm 2.12$	$3.71 \pm 1.55$
$\text{Mn}^{2+}$	0.6	-	-
$\text{Zn}^{2+}$	$3.4^{194}$	$3.39 \pm 0.04$	$3.40 \pm 0.07$
$\text{Cu}^{2+}$	4.3	-	$4.09 \pm 0.42$

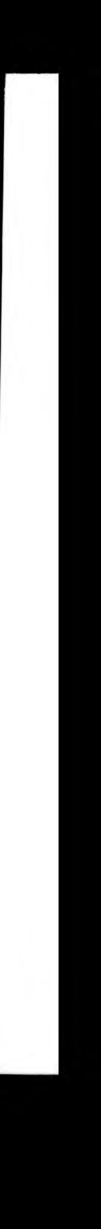
all bipy values calculated at 19.2 °C, according to the equation;

$$\log K_1 = \log K_1 \text{M}^{2+}(\text{H}_2\text{O}) - \{\log K_1 \text{Zn}^{2+}(\text{H}_2\text{O}) - \log K_1 \text{Zn}^{2+}(\text{dmsO})\}$$

Where the values can be calculated the match with the observed figures is remarkable. For  $\text{Co}^{2+}$  and  $\text{Cu}^{2+}$  the figures are in some error, but for  $\text{Zn}^{2+}$  the match is so close that the two numbers are essentially identical. This suggests that the intermediate in the reactions of  $\text{Zn}^{2+}$  with the pendent arm macrocycles involves  $\text{Zn}^{2+}$  bonded to the bipy arm only, with the macrocycle well out of the co-ordination sphere, since much higher stability constants would be expected if any of the macrocyclic nitrogen donors were co-ordinated.

The match for the  $\text{Cu}^{2+}$  and  $\text{Co}^{2+}$  data is sufficient to suggest that this form of intermediate also occurs in the reactions of these ions. If this behaviour is assumed for all the reactions, then it should be able to explain why the dissociation rate of the  $\text{Ni}^{2+}$  intermediate could not be measured and why the  $\text{Mn}^{2+}$  reactions are too fast to measure.

Using the estimated stability constant for  $\text{Ni}(\text{bipy})^{2+}$  (Table 3.5) and the formation rate constants (Table 3.2) for the reaction between  $\text{Ni}^{2+}$  and the pendent arm macrocycles it is possible to predict the rate constant of dissociation for the intermediates. Thus  $k_d$  is ca.  $1.3 \times 10^{-3} \text{ s}^{-1}$  and ca.  $3.3 \times 10^{-3} \text{ s}^{-1}$  at 25.0 °C for the cyclam and [9]aneN<sub>3</sub> containing ligands respectively. By studying the plots of  $k_{\text{obs}}$



vs.  $[\text{Ni}^{2+}]$  for these two reactions (figures 3.2 & 3.8) it is easy to see why such small values of  $k_d$  would not be observable as intercepts, since the data conform to the straight line equation  $k_{\text{obs}} = k_f[\text{M}^{2+}] + k_d$ .

For the  $\text{Mn}^{2+}$  reactions the estimated low stability constant for  $\text{Mn}(\text{bipy})^{2+}$  along with the estimated value for the formation rate constant (see earlier) generate a value of ca.  $2.5 \times 10^4 \text{ s}^{-1}$  for  $k_d$ . Thus, at a concentration of ca.  $5 \times 10^{-4} \text{ mol dm}^{-3}$  (see 3.3.9) the  $\text{Mn}^{2+}$  reaction would proceed with an observed first order rate constant of ca.  $25\,050 \text{ s}^{-1}$ , which could not possibly be observed on the stopped-flow timescale since the dead time on the instrument is 2 ms and this reaction has a half-life of 0.028 ms. Thus, the low stability of the intermediate causes the large value for  $k_d$  to become the dominant term in the kinetics. This is not unexpected since  $\text{Mn}^{2+}$  often has a high-spin  $t_{2g}^3 e_g^2$  electronic configuration and, therefore, does not have ligand field effect stabilisation in its complexes. Thus, assuming an intermediate of the form suggested for the  $\text{Zn}^{2+}$  reactions can explain the unobservable data for other metal ion reactions.

Another convincing observation to substantiate the initial reaction of the bipy moiety is found if it is considered that bipy covalently bound to a macrocycle will block attack at the adjacent bipyridyl nitrogen, whereas with free bipy the two donors are equally available for bonding. Thus, the rates of reaction of the pendent arm macrocycles should be a statistical factor of two smaller than for bipy.

By comparing the rates of reaction of the pendent arm macrocycles with  $\text{Zn}^{2+}$  with the reaction of  $\text{Zn}^{2+}$  with bipy at 292.2 K (by calculating the data at 292.2 K for the macrocyclic reactions using the relevant activation parameters (see Table 3.8)), the values of  $k_f$  are indeed roughly one half of those for the bipy reaction (Table 3.6).

However, similar comparisons for the data of the  $\text{Ni}^{2+}$  and  $\text{Co}^{2+}$  reactions (Table 3.3) are not as clear cut, and other factors may come into play here. Since the forward rate constants are expected to be halved the same factors should control the reverse process and so the dissociation rate constants ( $k_d$ ) should also be halved.

**Table 3.6**Comparison of Forward Rate Constants for various  $Zn^{2+}$  reactions.T = 292.2 K, dmsO,  $\mu = 0.1 \text{ mol dm}^{-3}$ 

Reactant	$k_f / \text{dm}^3 \text{ mol}^{-1} \text{ s}^{-1}$
bipy <sup>194</sup>	18700
cyclam-bipy	7810
[9]aneN <sub>3</sub> -bipy	8060

Again comparing the relevant values for the  $Zn^{2+}$  reactions at 292.2 K (Table 3.7) clearly demonstrates the applicability of this hypothesis.

**Table 3.7**Comparison of Reverse Rate Constants for various  $Zn^{2+}$  reactions.T = 292.2 K, dmsO,  $\mu = 0.1 \text{ mol dm}^{-3}$ 

Reactant	$k_d / \text{s}^{-1}$
bipy <sup>194</sup>	8.25
cyclam-bipy	4.77
[9]aneN <sub>3</sub> -bipy	4.02

The activation parameters for many of these processes have also been determined and are listed in Table 3.8. Examination of the activation parameters for the forward rate constant of the initial step of the reactions shows that the processes are not controlled by enthalpy alone, as was the case for the unsubstituted macrocycles (see 2.4). In fact, for the three cyclam-bipy reactions listed the fastest reaction, that of  $Zn^{2+}$ , actually has the least favourable activation enthalpy and in this case it is the much higher value of the activation entropy, compared to the  $Ni^{2+}$  and  $Co^{2+}$  reactions, which controls the kinetics. This supports the idea that the Eigen-Wilkins mechanism is inoperative at this stage as the reactions should be controlled by the enthalpy terms if the reactions undergo this mechanism, as was observed in chapter

Table 3.8

Activation Parameters for the Reactions of two Single Pendent Arm Macrocycles with Labile Transition Metals, for errors see 3.3.

25 °C,  $\mu = 0.1 \text{ mol dm}^{-3}$ , dmsO

Ligand	Metal	$\Delta H_f^\ddagger$ kJ mol <sup>-1</sup>	$\Delta S_f^\ddagger$ J K <sup>-1</sup> mol <sup>-1</sup>	$\Delta G_f^\ddagger$ kJ mol <sup>-1</sup>
Cyclam-bipy	Ni <sup>2+</sup>	49.0	-37.9	60.3
	Co <sup>2+</sup>	41.1	-50.1	56.0
	Zn <sup>2+</sup>	49.8	+0.3	49.7 <sup>*1</sup>
[9]aneN <sub>3</sub> -bipy	Ni <sup>2+</sup>	62.9	+4.5	61.6
	Co <sup>2+</sup>	49.4	-13.1	53.3
	Zn <sup>2+</sup>	50.6	+3.2	49.7 <sup>*2</sup>

$$^*1 \Delta H_d^\ddagger = 16.3 \text{ kJ mol}^{-1}, \Delta S_d^\ddagger = -177.0 \text{ J K}^{-1} \text{ mol}^{-1}, \Delta G_d^\ddagger = 68.6 \text{ kJ mol}^{-1}$$

$$^*2 \Delta H_d^\ddagger = 16.9 \text{ kJ mol}^{-1}, \Delta S_d^\ddagger = -175.1 \text{ J K}^{-1} \text{ mol}^{-1}, \Delta G_d^\ddagger = 69.2 \text{ kJ mol}^{-1}$$

$$\Delta H_{int}^\ddagger = 128.7 \text{ kJ mol}^{-1}, \Delta S_{int}^\ddagger = +173.0 \text{ J K}^{-1} \text{ mol}^{-1}, \Delta G_{int}^\ddagger = 77.4 \text{ kJ mol}^{-1}$$

2. However, the same trends are not observed for the reactions with [9]aneN<sub>3</sub>-bipy where the Ni<sup>2+</sup> data includes a favourable entropy term and an unfavourable enthalpy term, the latter controlling the reaction and causing a slow reaction rate. The data for Zn<sup>2+</sup> reacting with both ligands are very similar, suggesting that the same process is occurring in both reactions. This perhaps confirms the earlier conclusions that the first stage of the Zn<sup>2+</sup> reactions are identical, whereas for the other metals other factors, not applicable to the Zn<sup>2+</sup> systems, may affect the reactions slightly, causing deviations from the data expected on the basis of the proposed intermediate structure. For the Zn<sup>2+</sup> reactions the nature of the macrocyclic moiety contained in the ligands have no effect on the kinetics of the first reaction step as manifested by identical rate constants and activation parameters, whereas for the other metals that were studied the macrocycles clearly have some part to play in this reaction process, perhaps suggesting that the macrocycles are not fully out of the co-

ordination sphere during the formation of the initial intermediates as has been proposed for the  $Zn^{2+}$  systems.

The similarities in the initial  $Zn^{2+}$  reactions is also evident when the activation parameters for the dissociation process of the intermediates are studied (Table 3.8). As with the forward reactions, the parameters for the reverse reactions are essentially identical, with a very favourable enthalpy term, but an extremely unfavourable entropy term, which controls the processes for this reverse step. The values for  $\Delta H_d^\ddagger$  are very small and are almost identical to the energy required for the simple diffusion of two species to bring them together. Thus, the activation parameters for the reverse processes do not represent a single step and are probably associated with a multistep process that includes a pre-equilibrium. The value for the activation entropy is also strange and cannot represent a single process for reactions of this nature. Such large negative entropies must represent a severe ordering of the species and are usually only observed when two reactants of the same charge come together, causing a large increase in charge density and severe electrostriction of the solvent molecules. By the principle of microscopic reversibility the forward process must also be composed of more than one step.

Another useful exercise to determine the mechanism of these reactions may be to compare the activation enthalpies for solvent exchange, the reaction with bipy, the reactions with the free macrocycles and the reactions for the pendent arm macrocycles. Full data are only available for  $Ni^{2+}$  and  $Co^{2+}$  and are collected in Table 3.9.

Hopefully the enthalpies for the pendent arm macrocycles should be closest to the values for those for the reactions with bipy. However, Table 3.9 shows that although the values are not too far from the bipy values neither in some cases are they too far from the activation enthalpies of the reactions with the free macrocycles, nor the dmsc exchange reactions. It has already been established that the initial reactions of the pendent arm macrocycles do not follow the Eigen-Wilkins mechanism and do not react via the macrocyclic moiety and so any similarities in the above

Table 3.9

Comparison of Activation Enthalpies for various  $\text{Ni}^{2+}$  and  $\text{Co}^{2+}$  reactions in dmsO  
 25 °C,  $\mu = 0.1 \text{ mol dm}^{-3}$ , all values =  $\Delta H^\ddagger / \text{kJ mol}^{-1}$

Metal	dmsO	bipy	cyclam	[9]aneN <sub>3</sub>	C/B	T/B
$\text{Ni}^{2+}$	ca. 50 <sup>a</sup>	52.7 <sup>b</sup>	49 <sup>a</sup>	35 <sup>a</sup>	49.0	62.9
$\text{Co}^{2+}$	ca. 40 <sup>a</sup>	52.7 <sup>b</sup>	33 <sup>a</sup>	-	41.1	49.4

refs: a - chapter 2, b - ref. 62.

data are probably mere coincidence.

The entropies of activation for the initial complexation processes in the reactions of the pendent arm macrocycles vary between  $-50.1$  and  $+4.5 \text{ J K}^{-1} \text{ mol}^{-1}$ . This variation may be due to differences in co-ordination numbers for the different metal species.  $\text{Ni}^{2+}$  and  $\text{Co}^{2+}$  are certainly known to possess octahedral solvated ions in dmsO.<sup>245</sup> However,  $\text{Ni}^{2+}$  is also known for its ability to distort tetragonally and thus low concentrations of four or five co-ordinate species may co-exist with the standard six co-ordinate state. Since such low co-ordinate species may well react via an associative mechanism<sup>246</sup> only low concentrations of a more reactive species is necessary to affect the mechanism/kinetics, particularly since octahedral/square planar equilibria are known to be rapid for the  $\text{Ni}^{2+}$  ion.<sup>247,249</sup> Similarly, the co-ordination environment of  $\text{Zn}^{2+}$  in dmsO is unknown. In methanol the solvation number can vary from six at low dilution to four at higher concentrations, with co-ordination of perchlorate anions complicating the situation.<sup>193</sup> The variance in  $\Delta S_f^\ddagger$  values may thus reflect the existence of such co-ordination numbers. Certainly in the final, thermodynamically stable products of these reactions the co-ordination numbers are known to differ between the metals. In solution the  $\text{Ni}^{2+}$  complex of both ligands is octahedral, with a dmsO molecule occupying the sixth position in the [9]aneN<sub>3</sub>-bipy complex. For  $\text{Zn}^{2+}$  the final complex is five co-ordinate for the [9]aneN<sub>3</sub>-bipy complex. The crystal structures also differ, with  $[\text{Ni}(\text{[9]aneN}_3\text{-bipy})\text{OH}_2]^{2+}$  in a distorted octahedral environment. For

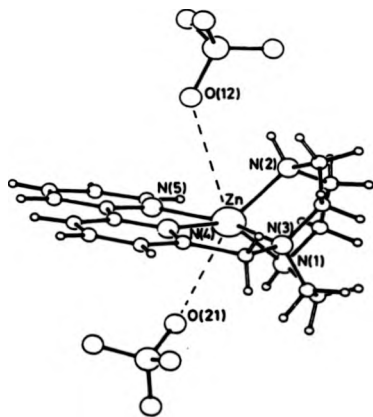
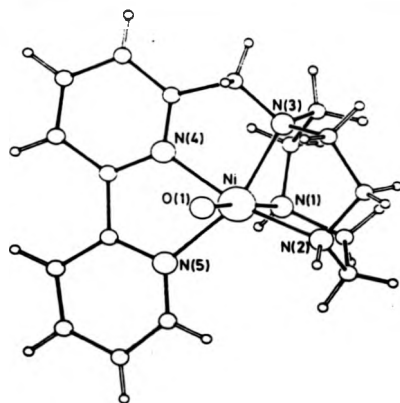


Fig. 3.31 Crystal structures of some [9]aneN<sub>3</sub>-Bipy complexes, top = [Ni((9)aneN<sub>3</sub>-bipy)OH<sub>2</sub>]<sup>2+</sup>, bottom = [Zn((9)aneN<sub>3</sub>-bipy)(OClO<sub>3</sub>)<sub>2</sub>]

[Zn(9)aneN<sub>3</sub>-bipy)(OClO<sub>3</sub>)<sub>2</sub>] the metal is seven co-ordinate, with two loosely co-ordinated perchlorate ions (figure 3.31). The effect of the ligand on solvent structure has been suggested as an important consideration in substitution reactions in non-aqueous media,<sup>62,63</sup> though here the equivalence of the Zn<sup>2+</sup> activation parameters for the initial step suggests this is unimportant in these reactions.

The rate constants for the slower, second process decrease in the order  $k_{Cu} > k_{Zn} > k_{Co} > k_{Ni}$  (Table 3.2), paralleling the proposed order of solvent exchange. Thus, solvent exchange may well be involved in this process. Certainly, where the activation parameters for  $k_{int}$  could be measured (Table 3.8) the  $\Delta S_{int}^\ddagger$  suggests a dissociative process. However, the second step is likely to represent a number of configurational/conformational/co-ordination number changes as did the reactions of the unsubstituted macrocycles (see 2.4).

In terms of configurational changes there are two basic processes which both pendent arm macrocycles must undergo before final complexation can occur. 2,2'-bipyridine is known to exist in a *trans*- configuration in solution<sup>250</sup> and for maximum ligand solvation the attached macrocycle will probably lie pointing away from the bipy moiety with the macrocyclic cavity "open" - particularly in a strong donor solvent like dmso, where the dipole moment of a dmso molecule is 4.11 D at 25 °C.

Thus, for complete co-ordination to a metal ion the bipy must rotate to produce a *cis*-configuration and the methylene arm must rotate to bring the macrocycle round to attach to the metal ion (see figure 3.31). The former process must occur during the initial stage of the reaction to form the proposed intermediate and this configurational change may well contribute to the "abnormally" slow substitution reactions of bipy in dmso, as the vacant site left after solvent dissociation will be less accessible with a bulky aromatic ring in the way. The latter process will certainly occur after the intermediate is formed for the Zn<sup>2+</sup> reaction, in the second, slower reaction; but for the other metals, where data are not as clear cut, differing degrees of this process may be involved prior to the formation of the intermediate. As previously discussed (2.4) once the macrocycle has bonded conformational rear-

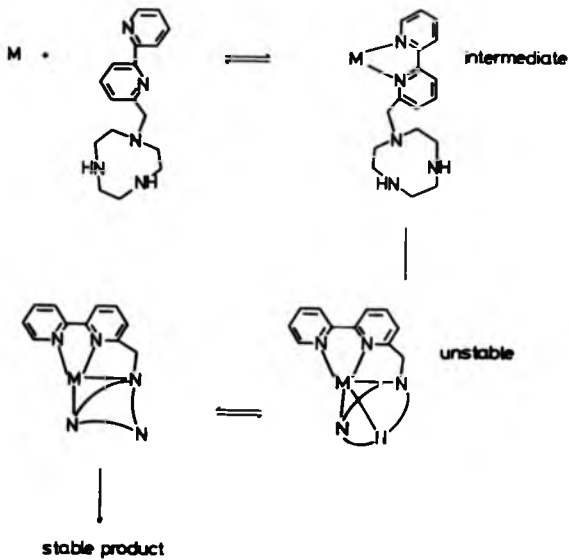
rangements may be necessary, in the form of nitrogen inversions, to form the final product and these processes will also contribute to the second step in the reactions. Thus the values of  $k_{\text{int}}$  represent composite quantities which are impossible to investigate using the techniques employed here.

Scheme I shows the proposed reaction mechanism for the pendent arm macrocycles reacting with first row transition metals in dmsO.

For the cyclam containing ligand the second reaction stage will contain an extra step as an extra donor atom is present for co-ordination.

Therefore, the study of the complexation reactions of cyclam and [9]aneN<sub>3</sub> functionalised with a pendent 2,2'-bipyridyl-6-yl-methyl arm illustrates that initial reaction of pendent arm macrocycles occurs via the pendent arm, at least for these ligands, as has been postulated by previous studies in macrocycles containing four pendent arms,<sup>235,236,241</sup> despite the fact that in their unfunctionalised forms the macrocyclic moieties react much faster than 2,2'-bipyridine. The presence of the pendent arm also enhances the stabilities of the final products. This is illustrated by the fact that no metal-metal exchange reactions were observed with any of the metal complexes, using Cu<sup>2+</sup> or Hg<sup>2+</sup> as scavenger ions, over a period of several hours, even at elevated temperatures.

Further studies need to be carried out on pendent arm systems to see if this mechanism is a general one.



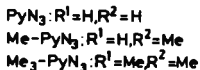
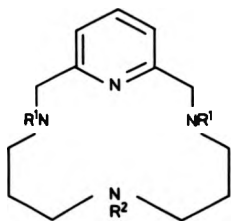
Scheme 1 Mechanism for the complexation of  $M^{2+}$  with [9]aneN<sub>3</sub>-bipy in dmsO.

## Chapter 4

### Rates and Mechanism of Co-ordination of Labile Transition Metal Ions with Tetra-aza Macrocycles Containing a Pyridine Group

#### 4.1 Introduction

The effect of increasing rigidity and degree of alkylation on the kinetics of complexation of aza macrocycles with transition metals has been actively studied over the years (see 1.5). The effect of substituting a pyridine group for a secondary amine has already been the subject of a limited study.<sup>112</sup> This chapter deals with the effect that a pyridine group has on the kinetics of aza macrocycles and also the effect of increasing methylation by studying the kinetics of complexation of  $Ni^{2+}$ ,  $Co^{2+}$  and  $Cu^{2+}$  with the ligands  $PyN_3$ ,  $Me-PyN_3$  and  $Me_3-PyN_3$  in dmso.



#### 4.2 Experimental

All procedures and materials are as described in Chapter 2 except for the ligands used. In this study the ligands were prepared by the methods of Moore et al: for  $PyN_3$ ,<sup>251</sup>  $Me-PyN_3$ ,<sup>252</sup> and  $Me_3-PyN_3$ .<sup>253</sup>

### 4.3 Results

#### 4.3.1 The Complexation Reaction between $\text{Ni}^{2+}$ and $\text{PyN}_3$ in *dmso*.

The reaction was followed at 308 nm, at the point where maximum absorbance change was observed on mixing solutions of the reactants (figure 4.1). The ligand concentration was  $5 \times 10^{-4} \text{ mol dm}^{-3}$  after mixing and the metal concentration was varied between  $5 \times 10^{-3}$  and  $1.5 \times 10^{-2} \text{ mol dm}^{-3}$  (after mixing). The stopped-flow data did not conform to first order kinetics and are interpreted as a two step, consecutive first order reaction (figure 4.2). A study of the dependence of the observed rate constant for the first step on metal ion concentration was carried out by following the reaction over 1 s. A first order dependence was found (figure 4.3) with a calculated bimolecular rate constant of  $441.6 \pm 1.8 \text{ dm}^3 \text{ mol}^{-1} \text{ s}^{-1}$  at 25 °C. The dissociation rate for the first step was experimentally indistinguishable from zero. Determination of the activation parameters for this process from an Eyring plot (figure 4.4) yielded  $\Delta H^\ddagger = 83.6 \pm 0.9 \text{ kJ mol}^{-1}$  and  $\Delta S^\ddagger = +86.0 \pm 3.2 \text{ J K}^{-1} \text{ mol}^{-1}$  at 25 °C. The second step was followed over 60 s and the observed first order rate constant was found to be independent of the metal ion concentration, with a rate constant of  $0.0354 \pm 0.0020 \text{ s}^{-1}$  at 25 °C. The small absorbance change involved in the second step did not allow a serious study of the temperature dependence of this process. All rate data are listed in Appendix 3.

#### 4.3.2 The Complexation Reaction between $\text{Ni}^{2+}$ and *Me-PyN<sub>3</sub>* in *dmso*.

The effect of mixing the reactants on the electronic spectrum of the system is shown in figure 4.5. The reaction was studied at 310 nm, using the same reactant concentrations as for the previous study (4.3.1). Again, stopped-flow traces revealed data which gave non-linear fits to linear first order kinetic plots (figure 4.6), the reaction displaying a two step, consecutive first order process. Analysis as before yielded a bimolecular rate constant of  $443.0 \pm 3.4 \text{ dm}^3 \text{ mol}^{-1} \text{ s}^{-1}$  at 25 °C for the first step, the observed rate constant possessing a first order dependence on the metal ion

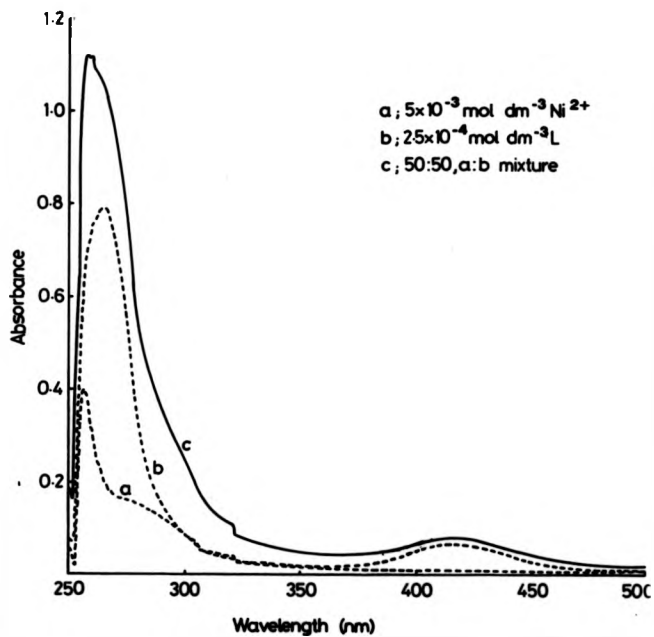
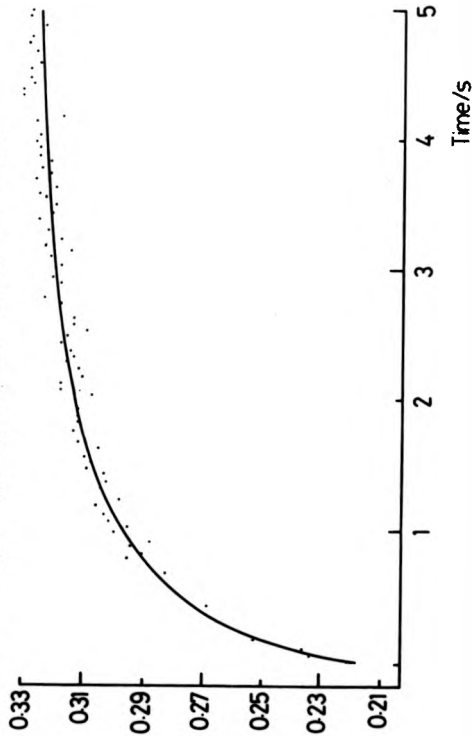
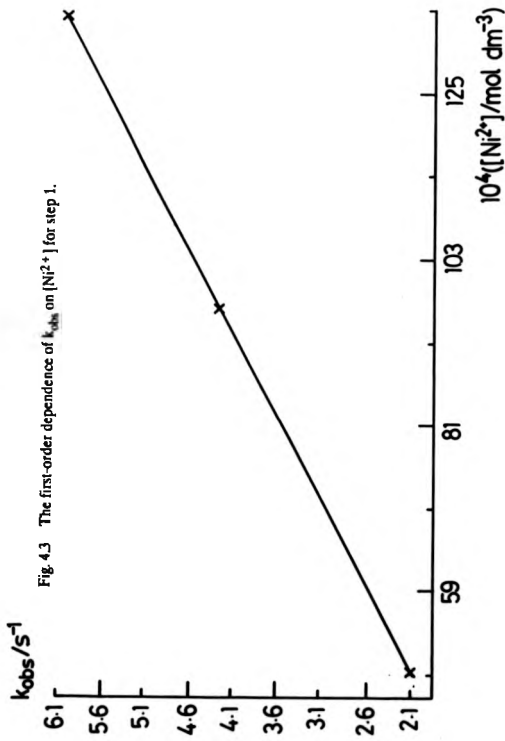


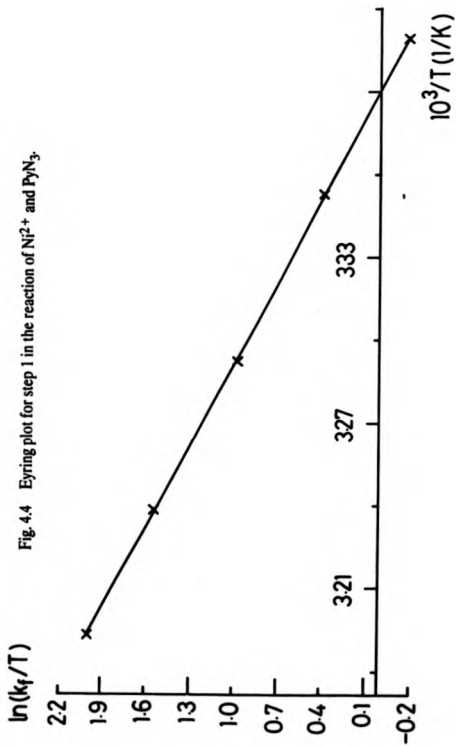
Fig. 4.1 Electronic spectra of  $\text{Ni}^{2+}$  and  $\text{PyN}_3$  in dmsc.

Absorbance

Fig. 4.2 Typical stopped-flow trace for the reaction of  $\text{Ni}^{2+}$  and  $\text{PyN}_3$ .







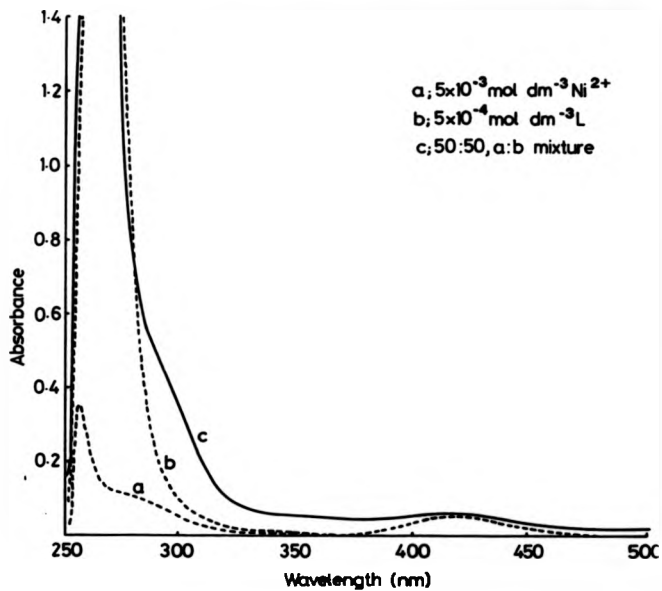


Fig. 4.5 Electronic spectra of  $\text{Ni}^{2+}$  and  $\text{Me-PyN}_3$  in  $\text{dmsu}$ .

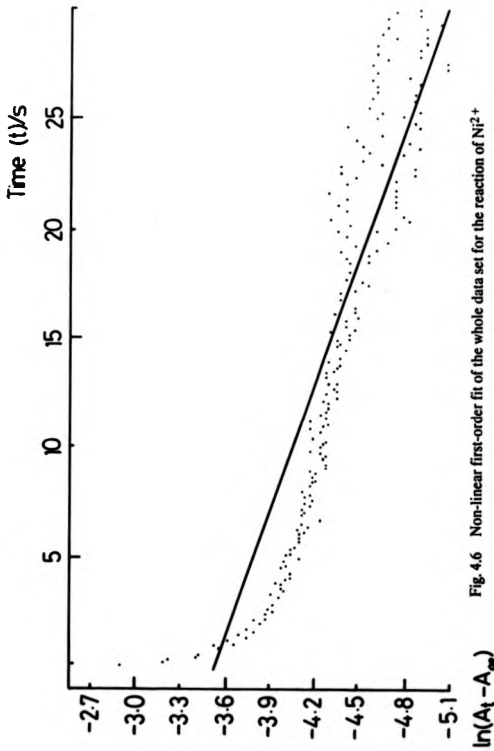


Fig. 4.6 Non-linear first-order fit of the whole data set for the reaction of  $\text{Ni}^{2+}$  and  $\text{Me-PyN}_3$ .

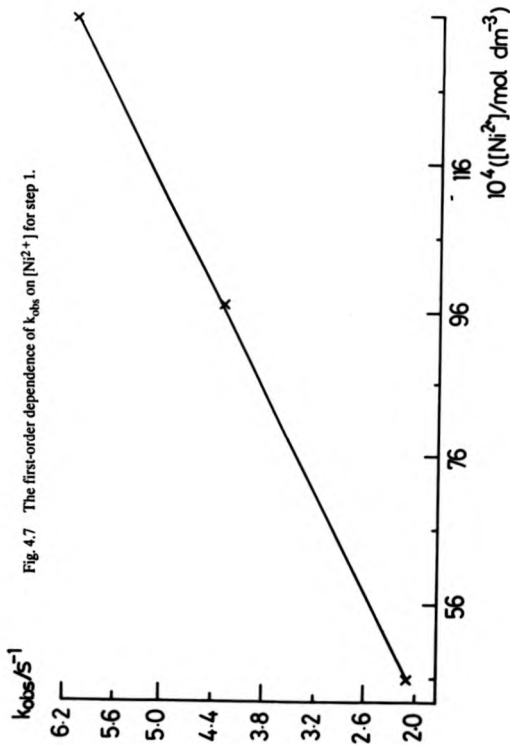
concentration (figure 4.7), with activation parameters, derived from an Eyring plot (figure 4.8) of  $\Delta H^\ddagger = 77.1 \pm 0.3 \text{ kJ mol}^{-1}$  and  $\Delta S^\ddagger = +64.2 \pm 1.0 \text{ J K}^{-1} \text{ mol}^{-1}$  at 25 °C. The slower, second stage of the reaction was followed over 200 s to give an observed rate constant of  $0.0127 \pm 0.0004 \text{ s}^{-1}$ , at 25 °C, the rate constant displaying no dependence on the concentration of metal present. Activation parameters were difficult to determine for this process owing to the small absorbance change involved. All rate data are listed in Appendix 3.

#### 4.3.3 The Complexation Reaction between $\text{Ni}^{2+}$ and $\text{Me}_3\text{-PyN}_3$ in dmso.

This reaction was initially followed in the visible region (figure 4.9) at 384 nm, where the usual two step, consecutive first order process was observed using the same reaction concentrations as in the previous two studies. Following the reaction over 0.3 s showed that the first stage had a first order dependence on the metal ion concentration with a bimolecular rate constant of  $1849.8 \pm 3.2 \text{ dm}^3 \text{ mol}^{-1} \text{ s}^{-1}$  at 25 °C (figure 4.10), with activation parameters of  $\Delta H^\ddagger = 85.4 \pm 1.7 \text{ kJ mol}^{-1}$  and  $\Delta S^\ddagger = +104.1 \pm 5.6 \text{ J K}^{-1} \text{ mol}^{-1}$  at 25 °C (figure 4.11). The rate constant for the slower, second stage could not be measured at this wavelength as very little absorbance change was involved. Thus, the reaction was then followed in the ultra-violet region at 290 nm (figure 4.12) using the same reactant concentrations. The second stage was involved with a larger percentage of the total absorbance change at this wavelength, so that the rate constant was just measurable, though the change was not good enough to allow an accurate temperature dependence study. The observed rate constant for the second, metal independent step was  $0.0132 \pm 0.0004 \text{ s}^{-1}$  at 25 °C. All rate data are listed in Appendix 3.

#### 4.3.4 The Complexation Reaction between $\text{Co}^{2+}$ and $\text{PyN}_3$ in dmso.

A very favourable absorbance change was observed in the electronic spectrum when the reactants were mixed, under pseudo first order conditions (figure 4.13). The reaction was followed at 333 nm, with  $2.5 \times 10^{-4} \text{ mol dm}^{-3} \text{ PyN}_3$  and  $0.5\text{-}1.5 \times$



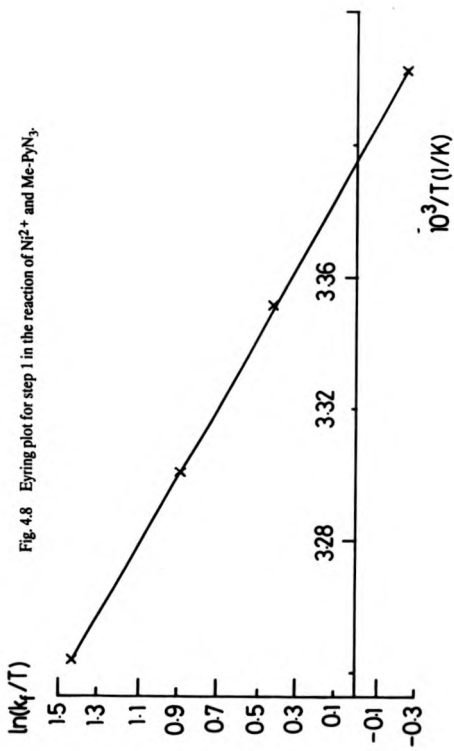


Fig. 4.8 Eyring plot for step 1 in the reaction of  $Ni^{2+}$  and  $Me-PyN_3$ .

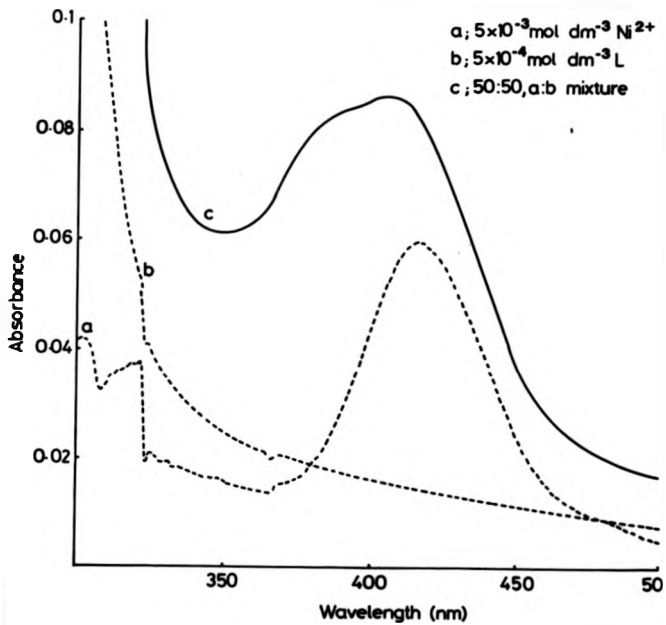
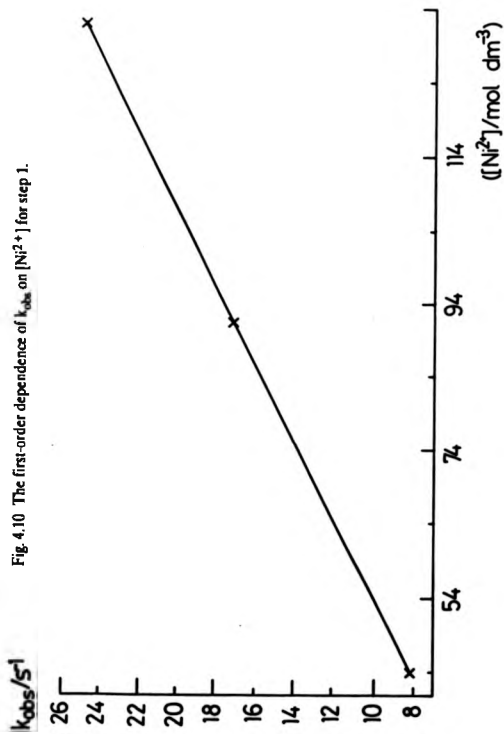
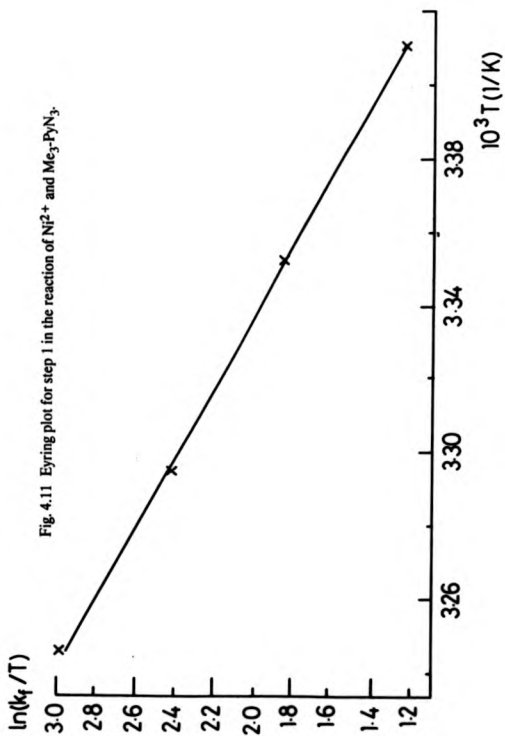


Fig. 4.9 Electronic spectra of  $\text{Ni}^{2+}$  and  $\text{Me}_3\text{-PyN}_3$  in dmsO - visible region.

Fig. 4.10 The first-order dependence of  $k_{obs}$  on  $[Ni^{2+}]$  for step 1.





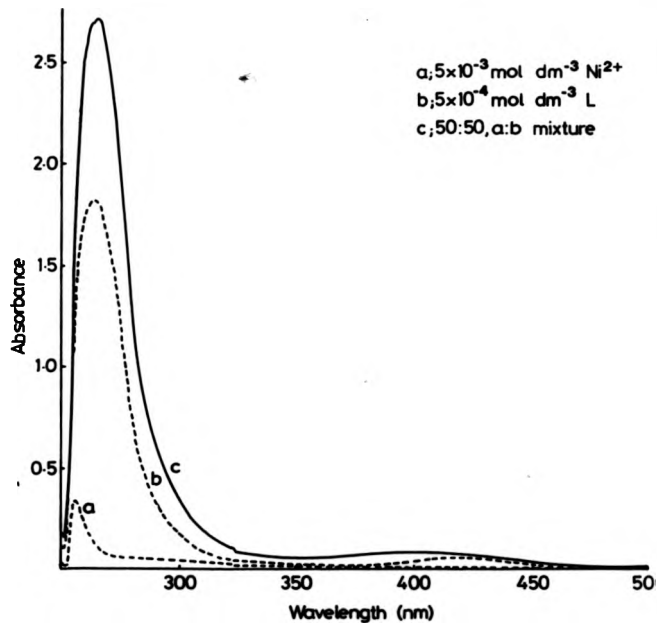


Fig. 4.12 Electronic spectra for  $\text{Ni}^{2+}$  and  $\text{Me}_3\text{PyN}_3$  in  $\text{dmso}$  - U. V. region.

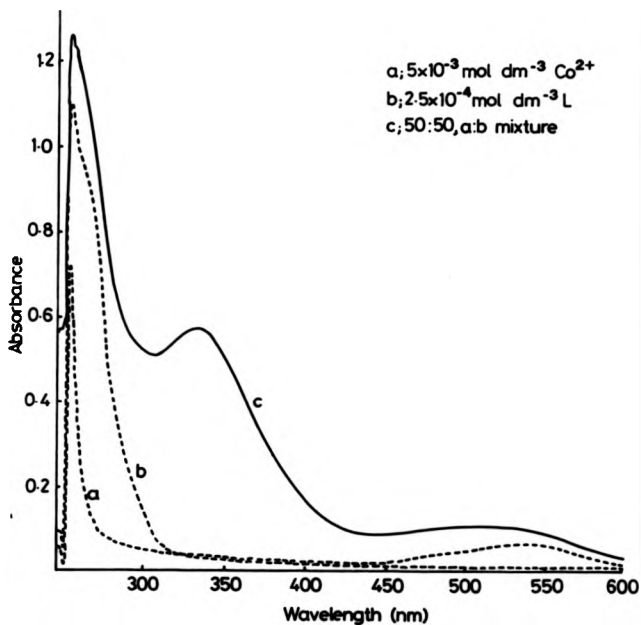


Fig. 4.13 Electronic spectra of  $\text{Co}^{2+}$  and  $\text{PyN}_3$  in dmsa.

$10^{-2} \text{ mol dm}^{-3} \text{ Co}^{2+}$  after mixing. A two step, consecutive first order process was observed, with both steps involving an increase in absorbance. Following the first step over 0.2 s, a first order dependence on the metal ion concentration was seen (figure 4.14), with a bimolecular rate constant of  $1887 \pm 51 \text{ dm}^3 \text{ mol}^{-1} \text{ s}^{-1}$  at  $25.0 \text{ }^\circ\text{C}$ , and activation parameters (figure 4.15) of  $\Delta H^\ddagger = 50.4 \pm 1.2 \text{ kJ mol}^{-1}$  and  $\Delta S^\ddagger = -13.1 \pm 3.9 \text{ J K}^{-1} \text{ mol}^{-1}$  at  $25.0 \text{ }^\circ\text{C}$ . The second step was followed over 50 s, and an observed rate constant of  $0.0511 \pm 0.0042 \text{ s}^{-1}$  was measured at  $25 \text{ }^\circ\text{C}$  for the process, with no dependence on the metal concentration being observed. A temperature dependence study of this process proved too inaccurate to follow due to the small absorbance change involved. The reaction was not found to be affected by oxygen within the timescale of the measurements, as solutions prepared under  $\text{N}_2$  and in air gave identical results when the experiments were carried out under  $\text{N}_2$  and in air respectively. However, small changes in the electronic spectrum were observed after leaving a solution of the product in air for 2 hours. All rate data are listed in Appendix 3.

#### 4.3.5 The Complexation Reaction between $\text{Co}^{2+}$ and $\text{Me-PyN}_3$ in dmsO.

Unlike the  $\text{Ni}^{2+}$  systems, incorporating a single methyl group onto the ligand causes a much more favourable absorbance change in the electronic spectrum on mixing the reactants (figure 4.16); with half the ligand concentration producing an equivalent absorbance change. The kinetics of complexation were followed at 323 nm, with equivalent concentrations to the previous  $\text{Co}^{2+}$  study being used, where a biphasic process was again observed (figure 4.17), the data not fitting to a linear first order plot (figure 4.18). The bimolecular rate constant for the initial step was calculated as  $1852 \pm 14 \text{ dm}^3 \text{ mol}^{-1} \text{ s}^{-1}$  at  $25.0 \text{ }^\circ\text{C}$  (figure 4.19), with no observable dissociation rate, the activation parameters being  $\Delta H^\ddagger = 63.5 \pm 3.2 \text{ kJ mol}^{-1}$  and  $\Delta S^\ddagger = +30.1 \pm 10.6 \text{ J K}^{-1} \text{ mol}^{-1}$  at  $25.0 \text{ }^\circ\text{C}$  (figure 4.20). The second step was independent of the metal concentration, with an observed rate constant of  $0.3347 \pm 0.0085 \text{ s}^{-1}$  at  $25.0 \text{ }^\circ\text{C}$ , the activation parameters being  $\Delta H^\ddagger = 72.9 \pm 1.1 \text{ kJ mol}^{-1}$  and  $\Delta S^\ddagger = -9.4$

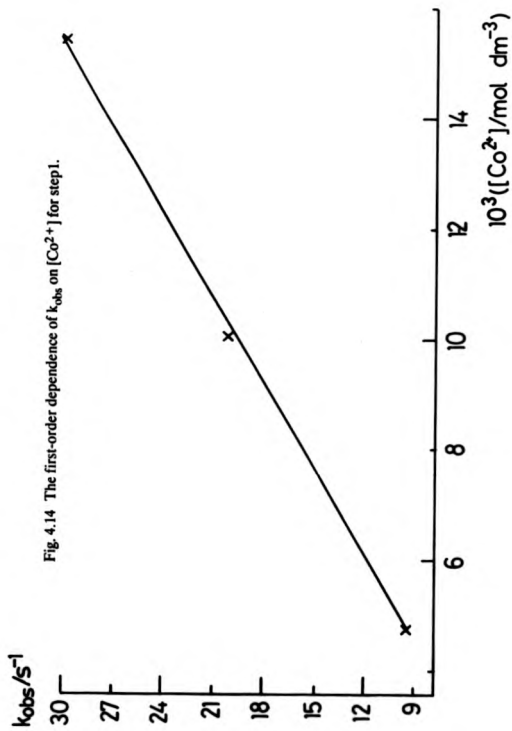
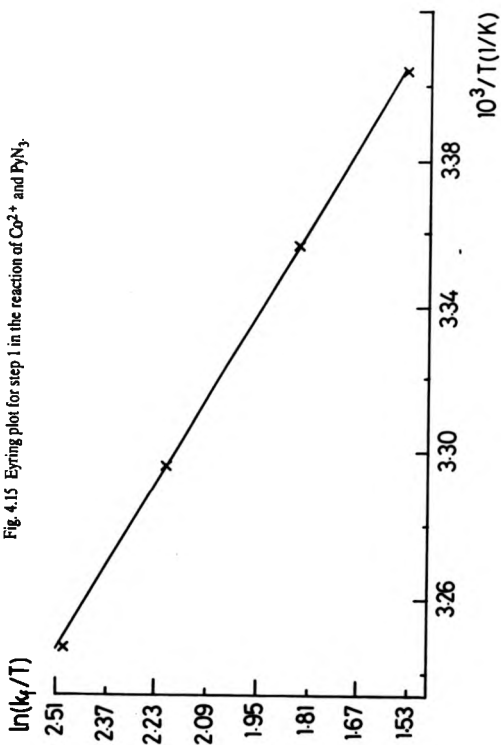


Fig. 4.15 Eyring plot for step 1 in the reaction of  $\text{Co}^{2+}$  and  $\text{PyN}_3$ .



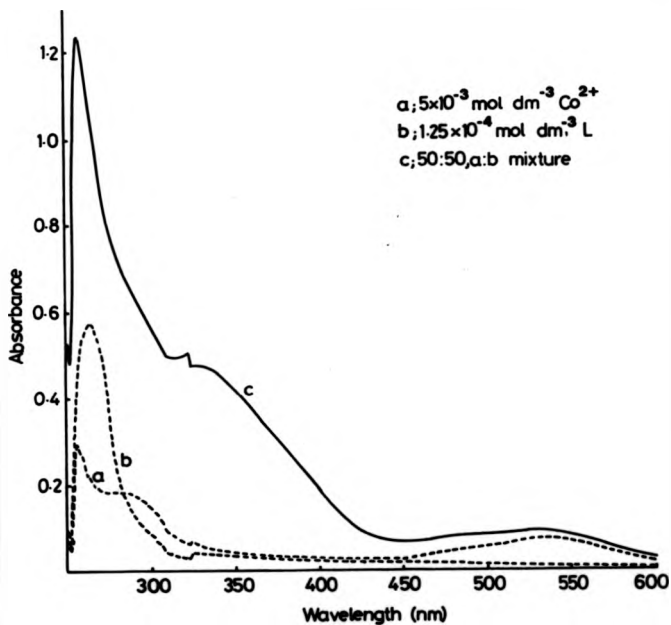
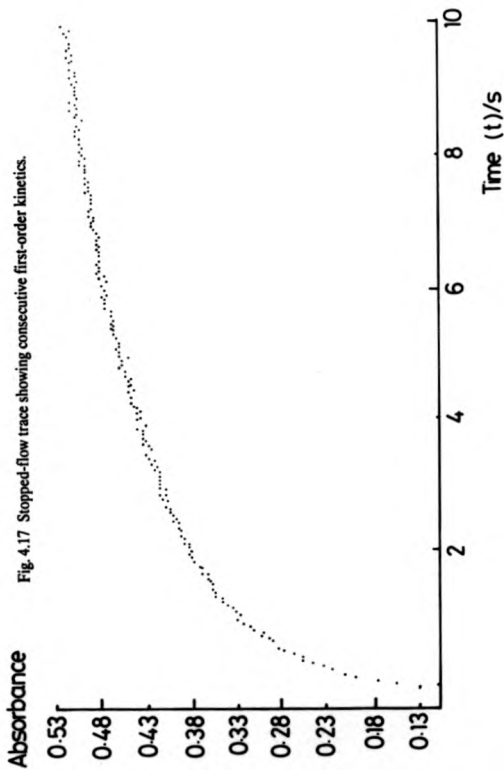


Fig. 4.16 Electronic spectra of  $\text{Co}^{2+}$  and  $\text{Me-PyN}_3$  in  $\text{dmso}$ .



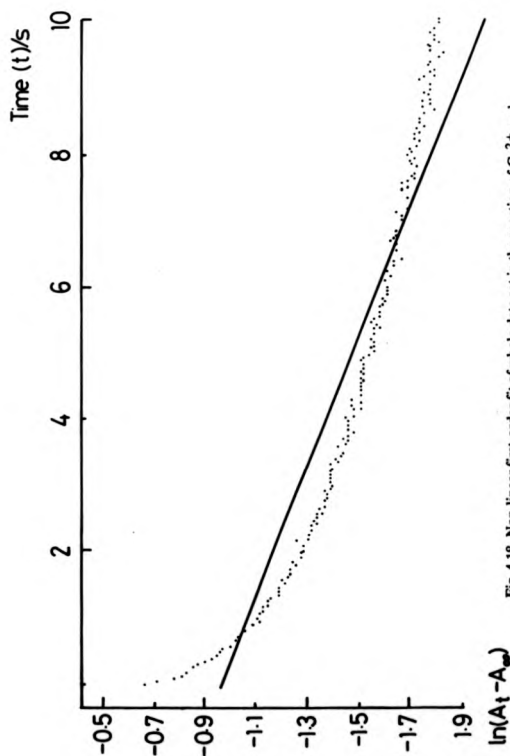


Fig. 4.18 Non-linear first-order fit of whole data set in the reaction of  $\text{Co}^{2+}$  and  $\text{Me-PyN}_3$

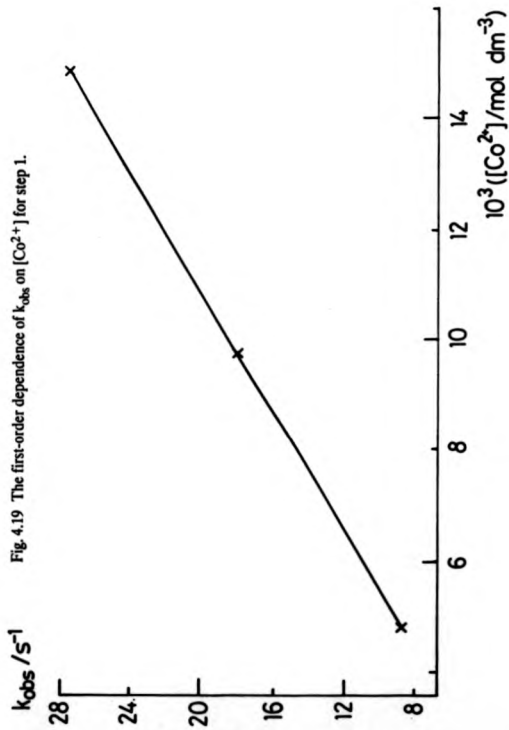
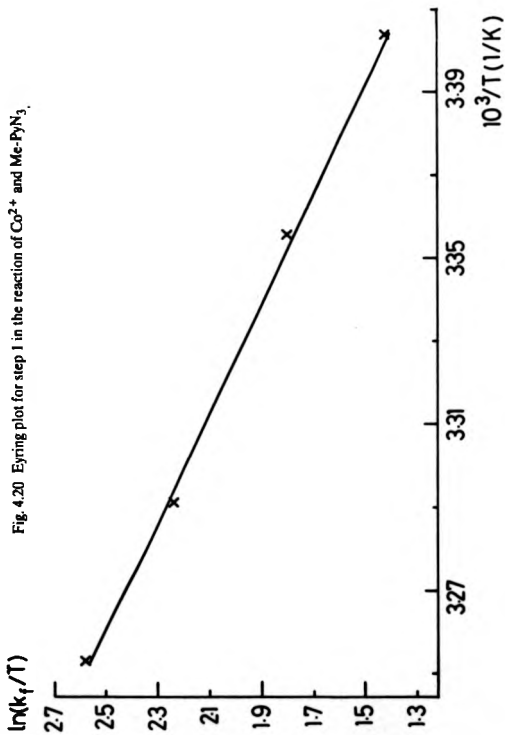


Fig. 4.20 Eyring plot for step 1 in the reaction of  $\text{Co}^{2+}$  and  $\text{Me-PyN}_3$ .



$\approx 3.6 \text{ J K}^{-1} \text{ mol}^{-1}$  at  $25.0 \text{ }^\circ\text{C}$ , derived from an Eyring plot (figure 4.21). The effect of oxygen on the reaction was identical to the previous  $\text{Co}^{2+}$  study (4.3.4). All rate data are listed in Appendix 3.

#### 4.3.6 The Complexation Reaction between $\text{Co}^{2+}$ and $\text{Me}_3\text{-PyN}_3$ in dmsO.

This time the absorbance change on mixing the reactants was far less favourable than for the mono-methylated ligand (figure 4.22). A biphasic process was again observed, the reaction being followed at  $318 \text{ nm}$ , with  $2.5 \times 10^{-4} \text{ mol dm}^{-3}$   $\text{Me}_3\text{-PyN}_3$  and  $0.5\text{-}1.5 \times 10^{-2} \text{ mol dm}^{-3}$   $\text{Co}^{2+}$  (after mixing). The calculated bimolecular rate constant for step 1 is  $349 \pm 4 \text{ dm}^3 \text{ mol}^{-1} \text{ s}^{-1}$  at  $25.0 \text{ }^\circ\text{C}$  (figure 4.23), with no observable dissociation rate, and activation parameters of  $\Delta H^\ddagger = 88.1 \pm 2.3 \text{ kJ mol}^{-1}$  and  $\Delta S^\ddagger = +99.2 \pm 7.4 \text{ J K}^{-1} \text{ mol}^{-1}$  at  $25.0 \text{ }^\circ\text{C}$  (figure 4.24), the process displaying a first order dependence on the  $\text{Co}^{2+}$  concentration. The second step was independent of the metal concentration, with an observed rate constant of  $0.0199 \pm 0.0003 \text{ s}^{-1}$  at  $25.0 \text{ }^\circ\text{C}$ , the small absorbance change not facilitating an accurate temperature dependence study. The effect of oxygen on the reaction is the same for the previous experiments (4.3.4 & 4.3.5). All rate data are listed in Appendix 3.

#### 4.3.7 The Complexation Reaction between $\text{Cu}^{2+}$ and $\text{PyN}_3$ in dmsO.

The change in the visible spectrum on mixing solutions of the reactants under pseudo first order conditions is shown in figure 4.25. Little change occurred in the ultra-violet region. The reaction was followed at  $568 \text{ nm}$ , which was considered to be the point of maximum absorbance change. Concentrations studied were  $5 \times 10^{-4} \text{ mol dm}^{-3}$  ligand and  $0.5\text{-}1.5 \times 10^{-2} \text{ mol dm}^{-3}$   $\text{Cu}^{2+}$  (after mixing). A two step, consecutive first order reaction was observed. The observed rate constants for the first step were very fast and it was difficult to obtain consistent results, thus many more data were collected than usual in order to get accurate, averaged results. A study of the metal ion concentration variation for the first step, studied over  $0.03 \text{ s}$ , displayed a first order dependence on the  $\text{Cu}^{2+}$  concentration, with a bimolecular

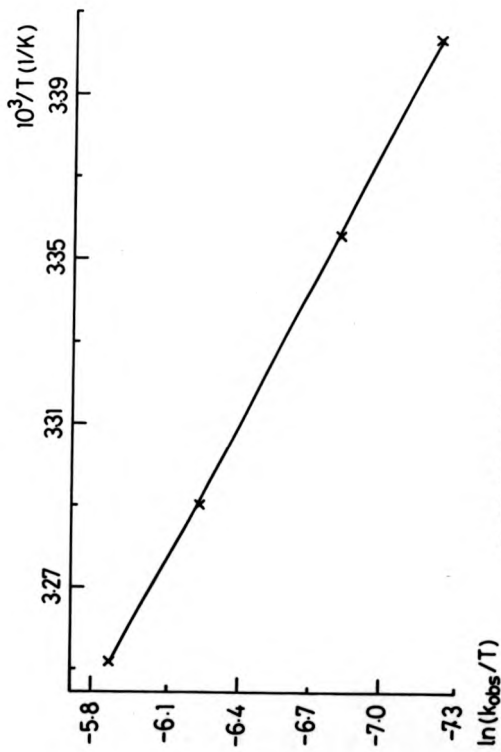


Fig. 4.21 Eyring plot for step 2 in the reaction of  $\text{Co}^{2+}$  and  $\text{Me-PyN}_3$ .

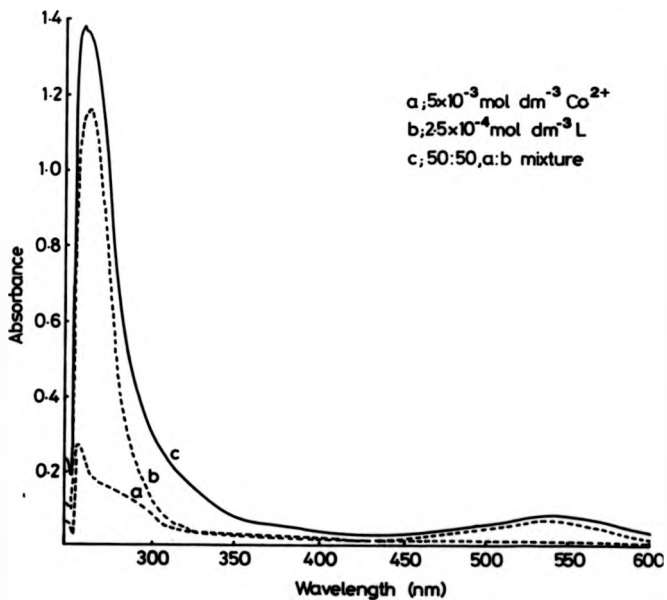
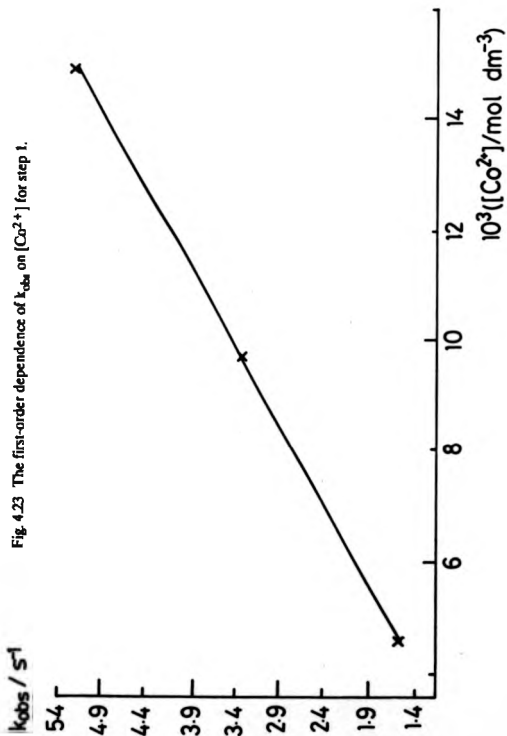
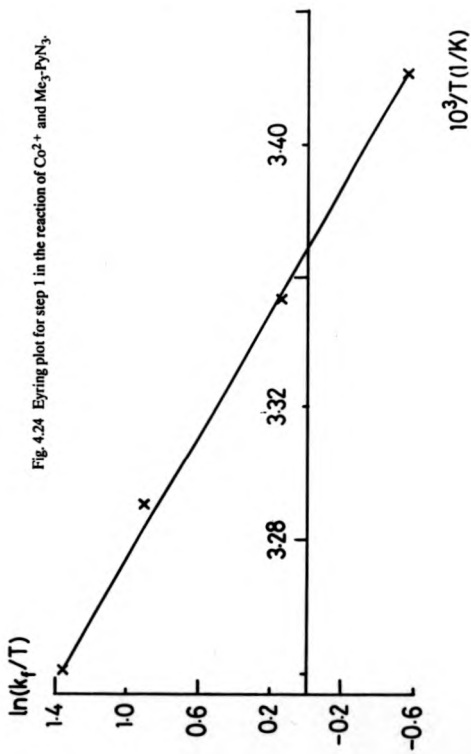


Fig. 4.22 Electronic spectra of  $\text{Co}^{2+}$  and  $\text{Me}_3\text{-PyN}_3$  in  $\text{dmso}$ .





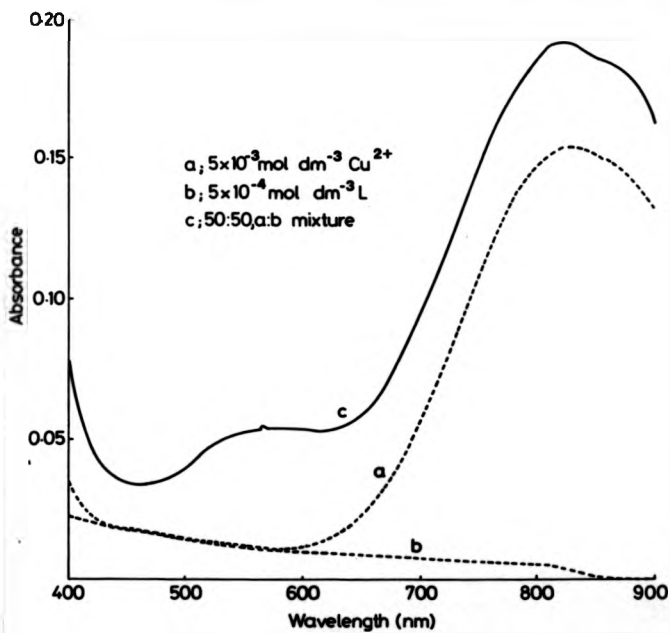
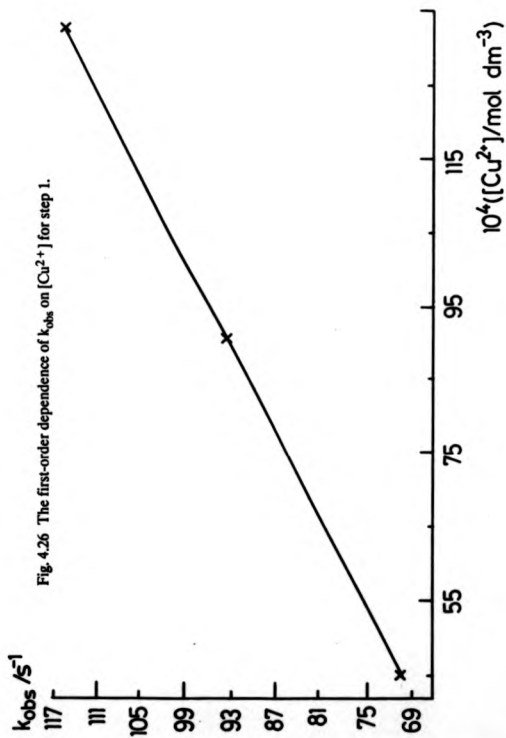


Fig. 4.25 Electronic spectra of  $\text{Cu}^{2+}$  and  $\text{PyN}_3$  in dmso.

forward rate constant of  $5070 \pm 12 \text{ dm}^3 \text{ mol}^{-1} \text{ s}^{-1}$  and a large dissociation rate of  $47.7 \pm 0.2 \text{ s}^{-1}$ , both at  $25.0 \text{ }^\circ\text{C}$  (figure 4.26). A temperature dependence study on step 1 proved impossible to carry out as the readings fluctuated wildly at elevated temperatures. It was not possible to reduce the reactant concentrations to help measurements as decreasing the ligand concentration meant that there was insufficient absorbance change to measure, and reducing the  $\text{Cu}^{2+}$  concentration any further would produce second order kinetics. It was not possible to measure the rate constant for the second, slower step in the reaction owing to a very small absorbance change being involved. All rate data are listed in Appendix 3.

#### 4.3.8 The Complexation Reaction between $\text{Cu}^{2+}$ and Me-PyN<sub>3</sub> in dmsO.

The monomethylated ligand produced a much more favourable absorbance change in the visible region on mixing with  $\text{Cu}^{2+}$  in dmsO than the unsubstituted ligand (4.3.7)(figure 4.27). The reaction was followed at 568 nm, the same wavelength as before, using identical reactant concentrations as for the reaction of the parent macrocycle. A two step, consecutive first order process was again observed (figure 4.28), with both steps marked by an increase in absorbance, the first stage covering approximately 40% of the total change in absorbance. However, at 700 nm, the process displayed an increase in absorbance for the first stage, followed by a decrease in absorbance for the second, this time the first step covered approximately 70% of the total absorbance change (figure 4.29). At 568 nm the first step of the reaction was found to possess a first order dependence on the  $\text{Cu}^{2+}$  concentration, with a bimolecular rate constant of  $4274 \pm 59 \text{ dm}^3 \text{ mol}^{-1} \text{ s}^{-1}$ , and a dissociation rate of  $44.9 \pm 0.5 \text{ s}^{-1}$ , both at  $25.0 \text{ }^\circ\text{C}$  (figure 4.30). The activation parameters for these processes were  $\Delta H^\ddagger = 59.4 \pm 0.3 \text{ kJ mol}^{-1}$  and  $\Delta S^\ddagger = +23.8 \pm 1.1 \text{ J K}^{-1} \text{ mol}^{-1}$  at  $25.0 \text{ }^\circ\text{C}$  for the forward reaction (figure 4.31) and  $\Delta H^\ddagger = 44.4 \pm 0.9 \text{ kJ mol}^{-1}$  and  $\Delta S^\ddagger = -64.6 \pm 3.0 \text{ J K}^{-1} \text{ mol}^{-1}$  at  $25.0 \text{ }^\circ\text{C}$  for the reverse reaction (figure 4.32). The second step in the reaction proceeded very slowly, and had to be followed over 200 s. The observed rate constant was independent of the metal ion concentration, with a



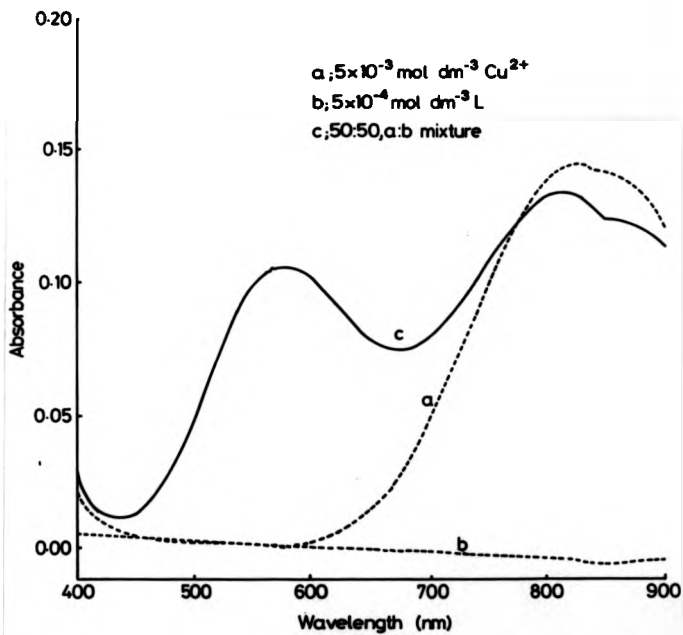


Fig. 4.27 Electronic spectra of  $\text{Cu}^{2+}$  and Me-PyN<sub>3</sub> in dmao.

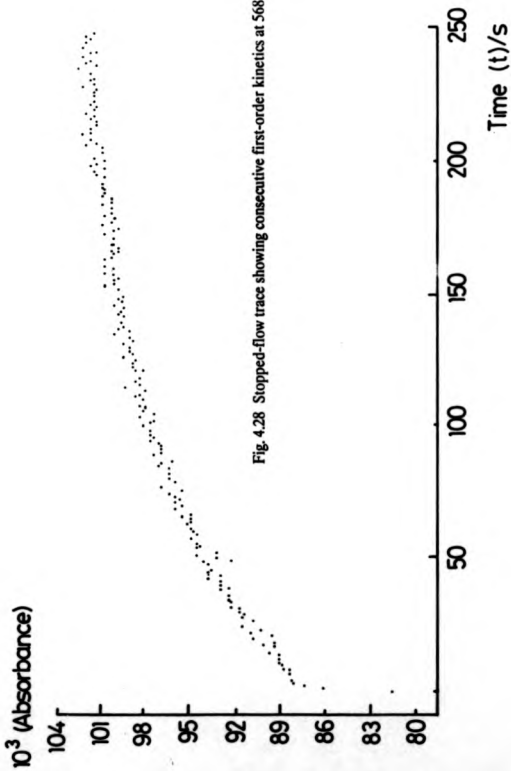
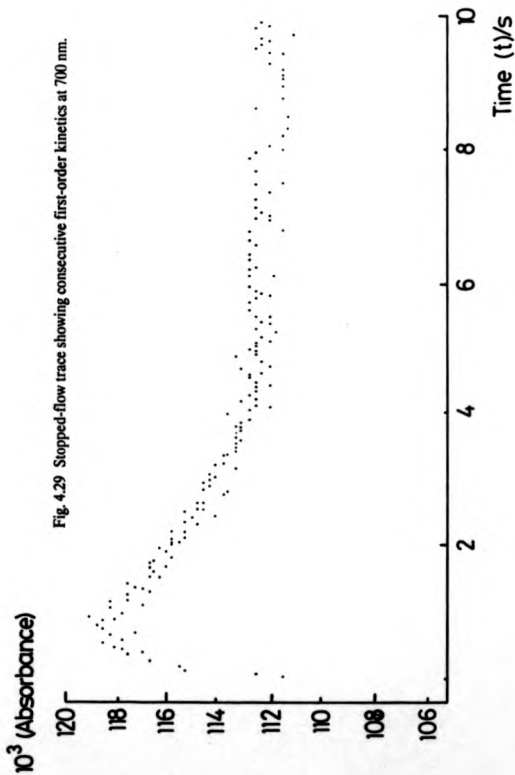


Fig. 4.28 Stopped-flow trace showing consecutive first-order kinetics at 568 nm.



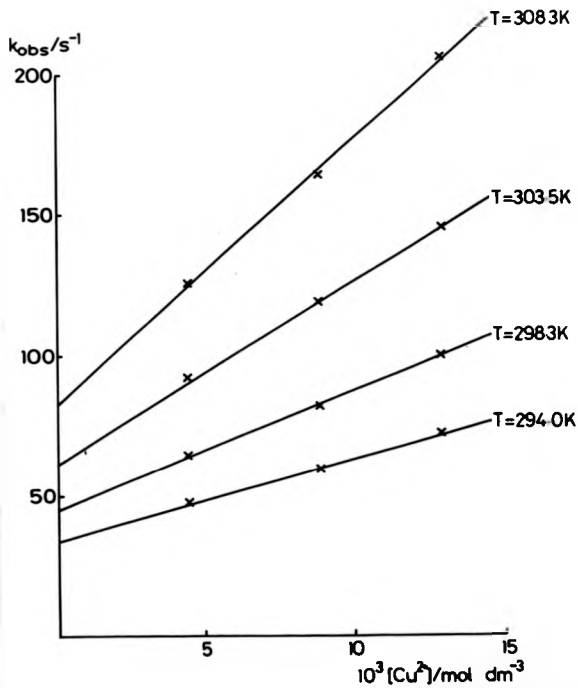
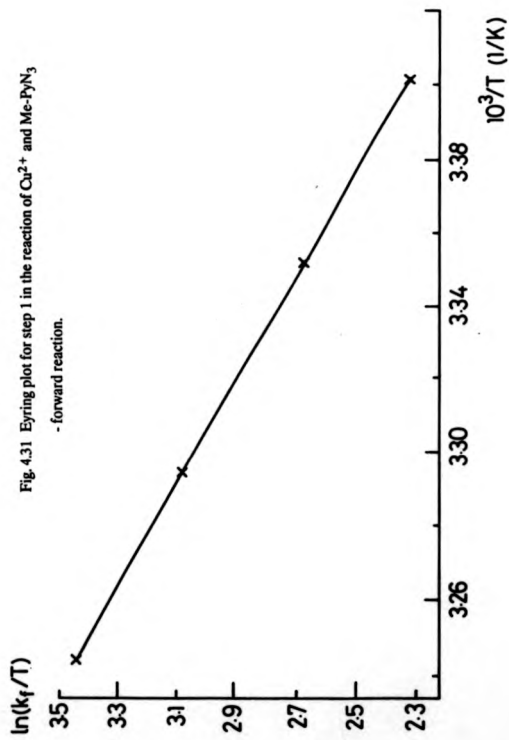


Fig. 4.30 The first-order dependence of  $k_{\text{obs}}$  on  $[\text{Cu}^{2+}]$  for step 1.

Fig. 4.31 Eyring plot for step 1 in the reaction of  $\text{Cu}^{2+}$  and Me-PyN<sub>3</sub>  
- forward reaction.



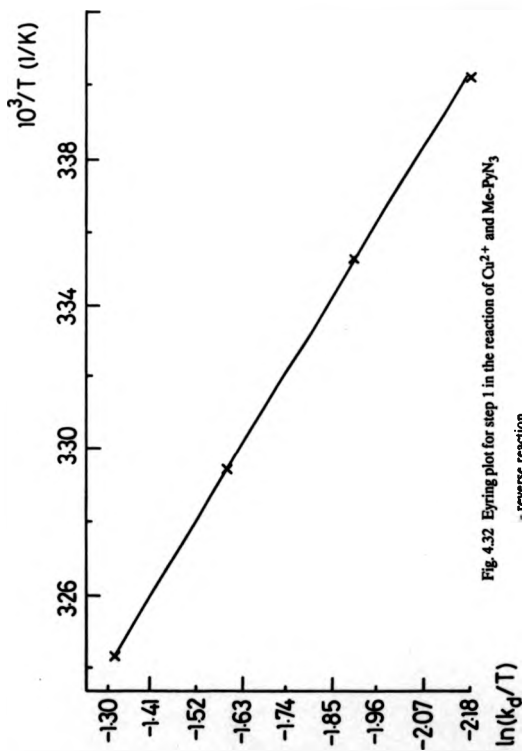


Fig. 4.32 Eyring plot for step 1 in the reaction of  $\text{Cu}^{2+}$  and Me-pyN<sub>3</sub>

- reverse reaction.

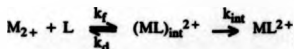
value of  $0.0098 \pm 0.0014 \text{ s}^{-1}$  at  $25.0 \text{ }^\circ\text{C}$ . All rate data are listed in Appendix 3.

#### 4.3.9 The Complexation Reaction between $\text{Cu}^{2+}$ and $\text{Me}_3\text{-PyN}_3$ in dmsO.

The fully methylated ligand produces an even more favourable absorbance change on mixing the reactants than those found in the less alkylated ligands (figure 4.33). The peak in absorbance was slightly shifted this time, with the reaction being followed at  $606 \text{ nm}$ , though concentrations identical to those in the two previous studies were used again here. A two step, consecutive first order process was again observed, with both stages involving an increase in absorbance. At  $700 \text{ nm}$  the absorbance change for the second step again decreased, with the first step involving a higher percentage of the total absorbance change than at  $606 \text{ nm}$  (see 4.3.8). At  $606 \text{ nm}$ , the first step was found to possess a first order dependence on the  $\text{Cu}^{2+}$  concentration, with a bimolecular rate constant of  $6276 \pm 118 \text{ dm}^3 \text{ mol}^{-1} \text{ s}^{-1}$  and a dissociation rate of  $18.6 \pm 1.1 \text{ s}^{-1}$ , both at  $25.0 \text{ }^\circ\text{C}$  (figure 4.34). The derived activation parameters are  $\Delta H^\ddagger = 29.4 \pm 0.7 \text{ kJ mol}^{-1}$  and  $\Delta S^\ddagger = -73.8 \pm 2.4 \text{ J K}^{-1} \text{ mol}^{-1}$  at  $25.0 \text{ }^\circ\text{C}$  for the forward process (figure 4.35), and  $\Delta H^\ddagger = 10.6 \pm 0.4 \text{ kJ mol}^{-1}$  and  $\Delta S^\ddagger = -185.1 \pm 1.3 \text{ J K}^{-1} \text{ mol}^{-1}$  at  $25.0 \text{ }^\circ\text{C}$  for the reverse process (figure 4.36). The second stage of the reaction was much quicker than for the previous ligand, and could be followed over  $10 \text{ s}$ . The observed rate constant is  $0.2589 \pm 0.0051 \text{ s}^{-1}$  at  $25.0 \text{ }^\circ\text{C}$ , the process being independent of the metal ion concentration. All rate data are listed in Appendix 3.

#### 4.4 Discussion

The kinetics of complexation of  $\text{PyN}_3$ ,  $\text{Me-PyN}_3$  and  $\text{Me}_3\text{-PyN}_3$  all follow the typical biphasic process observed in the previous chapters.



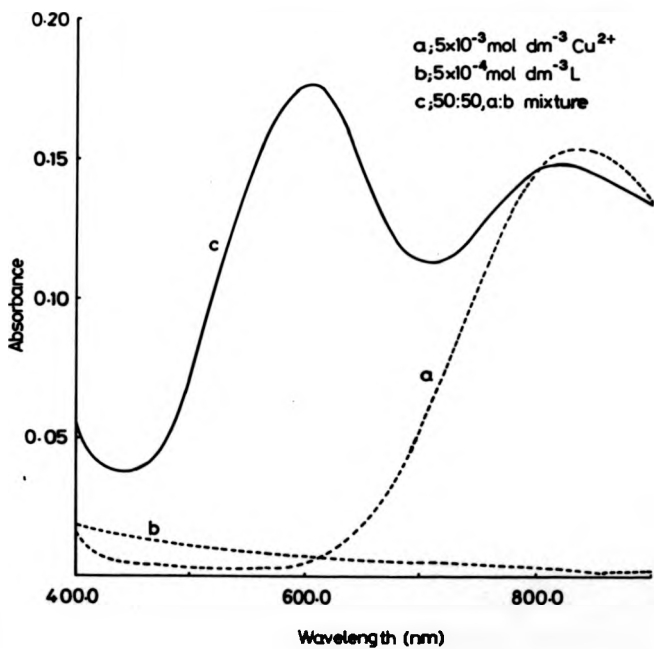


Fig. 4.33 Electronic spectra of  $\text{Cu}^{2+}$  and  $\text{Me}_3\text{-PyN}_3$  in dmsol.

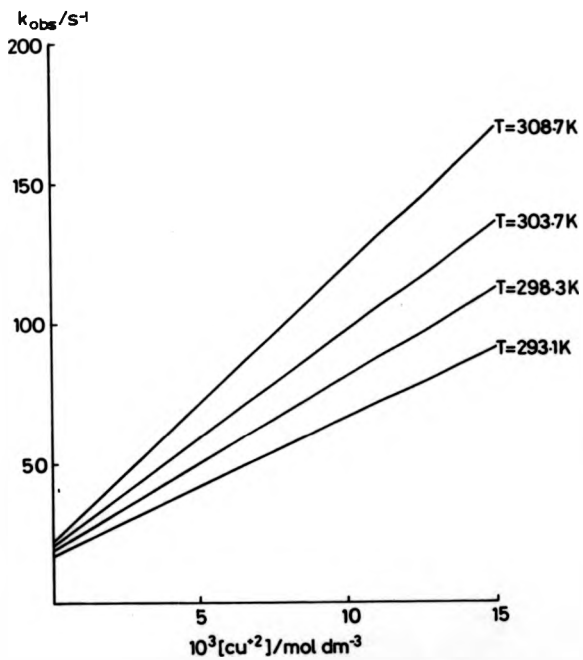
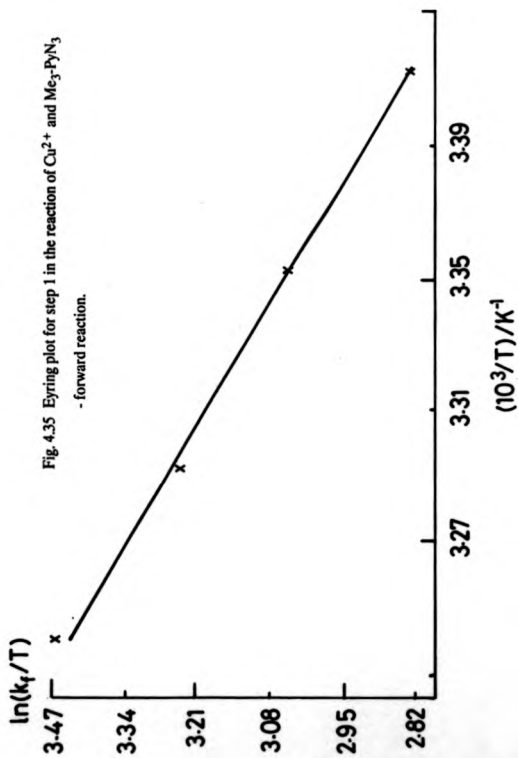


Fig. 4.34 The first-order dependence of  $k_{\text{obs}}$  on  $[\text{Cu}^{2+}]$  for step 1.



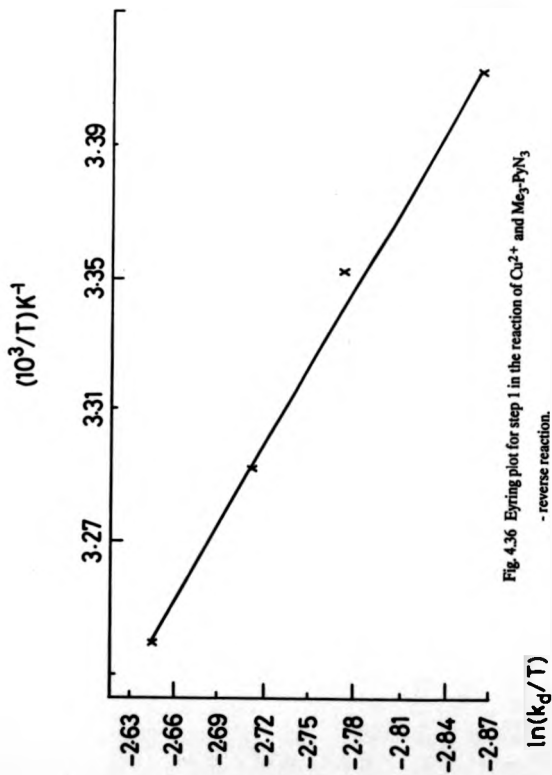


Fig. 4.36 Eyring plot for step 1 in the reaction of  $Cu^{2+}$  and  $Me_3PN_3$   
- reverse reaction.

For the  $\text{Ni}^{2+}$  and  $\text{Co}^{2+}$  reactions no  $k_d$  was observed, whereas for the  $\text{Cu}^{2+}$  reactions a large  $k_d$  was seen.

The measured rate constants and activation parameters for the reaction of  $\text{Co}^{2+}$  with the three ligands under study are shown in Table 4.1.

Comparison of the data for  $\text{PyN}_3$  with that for cyclam (chapter 2), which has no rigid pyridine moiety, shows that the initial rate of reaction decreases by over 15 times. This may be due to the decreased flexibility of the pyridine containing macrocycle or to steric effects. The much faster reaction rate of cyclam is due to a more favourable activation enthalpy ( $33 \text{ kJ mol}^{-1}$ ). The more favourable entropy observed in the  $\text{PyN}_3$  system may be due to differences in ligand solvation; the structural differences between the two ligands will certainly play a part in the entropy values, though the entropy does not control either reaction.

Table 4.1

Rate Constants and Activation Parameters for the Reactions of  $\text{Co}^{2+}$  with  $\text{PyN}_3$ 's,  $25.0^\circ$ ,  $\text{dmso}$ ,  $\mu = 0.1 \text{ mol dm}^{-3}$ , for errors see 4.3.

	$\text{PyN}_3$	$\text{Me-PyN}_3$	$\text{Me}_3\text{-PyN}_3$
$k_t / \text{dm}^3 \text{ mol}^{-1} \text{ s}^{-1}$	1887	1852	349
$k_{\text{int}} / \text{s}^{-1}$	0.05	0.335	0.02
$\Delta H_t^\ddagger / \text{kJ mol}^{-1}$	50.4	63.4	88.1
$\Delta S_t^\ddagger / \text{J K}^{-1} \text{ mol}^{-1}$	-13.1	+30.0	+99.2
$\Delta G_t^\ddagger / \text{kJ mol}^{-1}$	53.9	54.1	58.5
$\Delta H_{\text{int}}^\ddagger / \text{kJ mol}^{-1}$	-	72.9	-
$\Delta S_{\text{int}}^\ddagger / \text{J K}^{-1} \text{ mol}^{-1}$	-	-9.5	-
$\Delta G_{\text{int}}^\ddagger / \text{kJ mol}^{-1}$	-	74.8	-

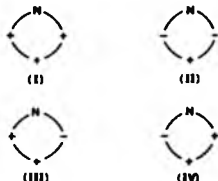
The main enthalpy effects will be due to changing a secondary amine donor to a pyridine donor, this will undoubtedly affect the bond strength, ligand field and conformational enthalpies. Since cyclam reacts with  $\text{Co}^{2+}$  via the Eigen-Wilkins mech-

anism in dmsO the much reduced reaction rate of  $\text{PyN}_3$  may indicate that this mechanism is inoperative, perhaps with the SCS mechanism coming into effect due to the increased difficulty of conformational/configurational changes in  $\text{PyN}_3$ .

The effect of alkylation on the reactions of  $\text{PyN}_3$  with  $\text{Co}^{2+}$  in dmsO can be seen in Table 4.1. Methylation of the nitrogen in the *trans*-position to the pyridine moiety has no effect on the initial reaction rate. The activation enthalpy for this reaction becomes less favourable on methylation. This trend is again observed on complete methylation of the ligand, where the very large enthalpy of activation controls the reaction, reducing the initial reaction rate 5 times, despite a very favourable increase in the activation entropy. Thus, for the  $\text{Co}^{2+}$  reactions the change in activation enthalpy controls the reactions for  $\text{PyN}_3$ ,  $\text{Me-PyN}_3$  and  $\text{Me}_3\text{-PyN}_3$  with increasing methylation favouring the entropy term but having an adverse effect on the enthalpy term, causing a marked drop in reaction rate on complete methylation. According to the  $\Delta S_i^\ddagger$  values increasing methylation also produces increasing dissociative character in the reactions. On this basis it would be expected that simple methylation would have little effect on the rate of a dissociative reaction, but this is not observed for the  $\text{Me}_3\text{-PyN}_3$  reaction. Thus, considering the great effect on the initial reaction rate of methylation at the amines in the *cis*-position to the pyridine moiety the rate determining step in the reaction mechanism may well involve the bonding between the  $\text{Co}^{2+}$  and these amines. Whether this involves initial binding or binding at the point of closing the first chelate ring is difficult to say. However, Schröder has recently published the crystal structure of a ligand very similar to those studied here (see later), and has shown that the lone pairs at the two equivalent N-atoms point out of the macrocyclic ring, whereas the pyridine and the remaining amine lone pairs point into the ring. If this arrangement is still found in solution then it would be easy to see that initial binding might occur at the nitrogens where the lone pairs are most accessible, followed by configurational changes to facilitate further bonding.

The structure of the intermediate is difficult to determine. Certainly more

than two nitrogen donors must be bonded to the  $\text{Co}^{2+}$  as the intermediate is stable enough to display no  $k_d$ . On the basis of the cyclam results (chapter 2) it is tempting to suggest full ligand-to-metal co-ordination for the intermediate in a thermodynamically unstable arrangement, requiring one or more N-inversions to produce the final, stable product. The exact nature of the final product has not been studied, but the electronic spectra suggest an octahedral environment for  $\text{Co}^{2+}$  for each of the ligands, and it is most likely that the macrocycles will bond in a square planar arrangement in keeping with other tetraaza macrocycles. A number of different isomers are possible for the final product, with two being an enantiomeric pair (III & IV).



Thus, due to the lack of knowledge concerning the structures of these complexes in dmso solution it is difficult to decide exactly what rearrangements occur in the second, slower step. Certainly  $k_{int}$  shows no correlation with the degree of ligand methylation and this may suggest a number of reaction steps and/or more than one type of reaction. Perhaps the intermediate has more than one path for rearrangement, the exact isomer formed depending on which N-inverts. The possibility of folded macrocycle intermediates cannot be ruled out (see chapter 2) as the ligand must surely form such a species at some stage during the reaction. A change of co-ordination number may also occur, with a square pyramidal intermediate being formed. The second reaction step almost certainly involves different processes for the reactions of the three ligands and so the possibility of more than one type of intermediate arises. Probing the mechanism of these reactions beyond the initial, rapid step is clearly a very demanding task.

The results for the reactions of  $\text{Ni}^{2+}$  with the three ligands are listed in Table 4.2.

**Table 4.2**

Rate Constants and Activation Parameters for the Reactions of  $\text{Ni}^{2+}$  with  $\text{PyN}_3$ 's.

25.0 °C, dmsO,  $\mu = 0.1 \text{ mol dm}^{-3}$ , for errors see 4.3.

	$\text{PyN}_3$	$\text{Me-PyN}_3$	$\text{Me}_3\text{-PyN}_3$
$k_f / \text{dm}^3 \text{ mol}^{-1} \text{ s}^{-1}$	442	443	1850
$k_{\text{int}} / \text{s}^{-1}$	0.0354	0.0127	0.0132
$\Delta H_f^\ddagger / \text{kJ mol}^{-1}$	83.6	77.1	85.4
$\Delta S_f^\ddagger / \text{J K}^{-1} \text{ mol}^{-1}$	+86.0	+64.2	+104.1
$\Delta G_f^\ddagger / \text{kJ mol}^{-1}$	58.0	57.9	54.0

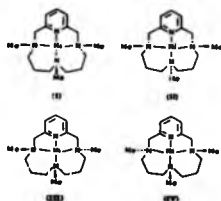
Comparison of the rate constant for reaction of  $\text{Ni}^{2+}$  with  $\text{PyN}_3$  to the same reaction with cyclam (chapter 2) shows that the replacement of a secondary amine with a pyridine moiety only reduces the rate by 3.7 times which is not as great as the effect found for the  $\text{Co}^{2+}$  system. As with the  $\text{Co}^{2+}$  reaction the activation enthalpy and entropy here are both greater than the reaction with cyclam, though the differences are much greater for the  $\text{Ni}^{2+}$  reactions, with the enthalpy being less favourable by  $34.6 \text{ kJ mol}^{-1}$  and the entropy being more favourable by  $103.6 \text{ J K}^{-1} \text{ mol}^{-1}$ . Thus the steric and flexibility constraints of  $\text{PyN}_3$  have only a small effect on the rate constant, at 25 °C, but a very large effect on the activation parameters.

Considering the small effect on the reaction rate from the increased rigidity the Eigen-Wilkins mechanism may still be operative for the  $\text{Ni}^{2+}$  reaction. The reaction is certainly dissociative in character, though the large enthalpy required for activation reflects the energetic expense of the more rigid ligand compared to cyclam.

Methylation of the amine in the *trans*-position to the pyridine moiety has little effect on the reaction rate with  $\text{Ni}^{2+}$ , as was observed with  $\text{Co}^{2+}$ . The activation

enthalpy is slightly more favourable than for  $\text{PyN}_3$ , and the entropy is slightly less favourable, with the result that the reaction rate constant for the  $\text{Me-PyN}_3$  reaction is unchanged. On full methylation the activation enthalpy is little affected, but the entropy term becomes dominant and actually causes a large increase in the reaction rate compared to the less methylated ligands. The rate constant for the  $\text{Me}_3\text{-PyN}_3$  reaction is actually slightly larger than that for the reaction with cyclam. This behaviour seems very strange at first as  $\text{Ni}^{2+}$  is reacting faster than  $\text{Co}^{2+}$  with this ligand in the initial stage of the reaction, and it is difficult to conceive increasing steric hindrance by methylation causing an increase in reaction rate.

An explanation for this apparent anomaly lies in the structural changes involved during the reactions. The  $\text{Ni}^{2+}$  complexes of  $\text{PyN}_3$  and  $\text{Me-PyN}_3$  are known to be low-spin square planar complexes,<sup>251,252</sup> whereas the  $\text{Me}_3\text{-PyN}_3$  complex is a paramagnetic square pyramidal structure in co-ordinating solvents, with a solvent molecule taking up one of the equatorial positions and the macrocycle having a folded arrangement.<sup>253</sup> In terms of isomers, four are again possible for the  $\text{Ni}^{2+}$  complexes.



Moore et al.<sup>253</sup> concluded that isomer (I) was a kinetically formed first product, which underwent slow isomerisation to isomer (II) in co-ordinating solvents and in the presence of other monodentate ligands. Barefield et al.<sup>253</sup> studied this isomerisation process in aqueous solution. They suggested that the reaction occurred via inversion of a tertiary nitrogen and observed various effects on addition of base or  $\text{NaClO}_4$ . They noted that there may be alternative pathways for isomerisation depending on the base used.

The rate constant for this process in 1:10 (v/v) acetone/water at  $\mu = 0.1$  mol  $\text{dm}^{-3}$  ( $\text{NaClO}_4$ ) and 298 K is ca.  $0.01 \text{ s}^{-1}$ . This is the same as the rate constant for the second stage of the  $\text{Me}_3\text{-PyN}_3$  reaction under similar conditions in dmsO and so may suggest that isomer (I) is the intermediate formed in this reaction. This would certainly account for the fact that no dissociation process was measurable for the initial reaction step. The rate constants for the second step in the reactions of  $\text{PyN}_3$  and  $\text{Me-PyN}_3$  with  $\text{Ni}^{2+}$  are also similar to the value for the N-inversion process. The structures of these complexes are likely to be similar to isomer (I) with the N-H/N-Me's all on the same side of the macrocyclic plane.<sup>252,256</sup> Thus, the second reaction steps for the reactions with  $\text{PyN}_3$  and  $\text{Me-PyN}_3$  may involve isomerisations of the type III or IV to I, alternatively a folded macrocyclic intermediate may occur which isomerises to the final product. Thus, the effect of methylation on the reactions with  $\text{Ni}^{2+}$  indicates that the reaction with  $\text{Me}_3\text{-PyN}_3$  must react via a different pathway to the  $\text{PyN}_3$  and  $\text{Me-PyN}_3$  ligands, thus causing an apparent anomaly in the reaction rates.

With the reactions of  $\text{PyN}_3$ ,  $\text{Me-PyN}_3$  and  $\text{Me}_3\text{-PyN}_3$  with  $\text{Cu}^{2+}$  in dmsO different kinetic behaviour is observed from the  $\text{Ni}^{2+}$  and  $\text{Co}^{2+}$  systems. A large contribution from the dissociation rate on the kinetics of the initial, rapid process is observed, indicating the formation of a much less stable intermediate. The rate constants and activation parameters are listed in Table 4.3.

The reaction of  $\text{Cu}^{2+}$  with  $\text{PyN}_3$  has a rate constant almost the same as that for the reaction with cyclam (chapter 2). Thus, the pyridine ring seems to have no effect on the reaction rate with  $\text{Cu}^{2+}$  in dmsO. This seems startling, unless the reaction proceeds via a truly dissociative process. Whether or not cyclam reacts via the Eigen-Wilkins mechanism with  $\text{Cu}^{2+}$  in dmsO has already been discussed in chapter 2. Unfortunately, the activation parameters for the  $\text{PyN}_3$  reaction could not be measured (see 4.3.7) and so no comparison can be made with cyclam regarding this information.

The effect of methylation on the reactions of  $\text{PyN}_3$  is tabulated in Table 4.3.

Table 4.3

Rate Constants and Activation Parameters for the Reactions of  $\text{Cu}^{2+}$  with  $\text{PyN}_3$ 's.  
 25.0 °C, dmsO,  $\mu = 0.1 \text{ mol dm}^{-3}$ , for errors see 4.3.

	$\text{PyN}_3$	$\text{Me-PyN}_3$	$\text{Me}_3\text{-PyN}_3$
$k_f / \text{dm}^3 \text{ mol}^{-1} \text{ s}^{-1}$	5070	4243	6196
$k_d / \text{s}^{-1}$	47.7	44.5	18.3
$k_{\text{int}} / \text{s}^{-1}$	-	0.0098	0.259
$\Delta H_f^\ddagger / \text{kJ mol}^{-1}$	-	59.4	29.4
$\Delta S_f^\ddagger / \text{J K}^{-1} \text{ mol}^{-1}$	-	+23.8	-73.8
$\Delta G_f^\ddagger / \text{kJ mol}^{-1}$	-	51.8	51.5
$\Delta H_d^\ddagger / \text{kJ mol}^{-1}$	-	44.4	10.6
$\Delta S_d^\ddagger / \text{J K}^{-1} \text{ mol}^{-1}$	-	-64.6	-185.1
$\Delta G_d^\ddagger / \text{kJ mol}^{-1}$	-	63.4	65.8

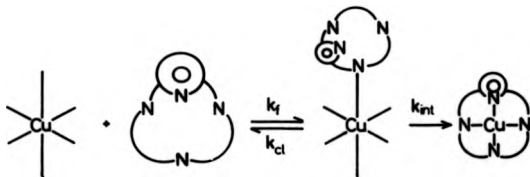
Increasing methylation seems to have little effect on the rate constants of complexation for the reactions. The dissociation rate constants observed are equivalent for  $\text{PyN}_3$  and  $\text{Me-PyN}_3$  but the value is reduced by more than half for the fully methylated ligand. Thus, although methylation at the two equivalent nitrogens seems to have little effect on the forward rate constants, a noticeable effect is present in the reverse rate constants, again displaying the importance of this site in the kinetics.

The activation parameters for the  $\text{Me-PyN}_3$  and  $\text{Me}_3\text{-PyN}_3$  reactions show great diversity. For both forward and reverse processes the  $\text{Me-PyN}_3$  reactions are marked by favourable entropies of activation and unfavourable enthalpies of activation compared to the  $\text{Me}_3\text{-PyN}_3$  reactions. Large differences in the values may indicate the presence of different pathways in the mechanisms of the two ligand reactions, perhaps with different co-ordination number changes. A multistep process is indicated by the activation parameters of the dissociation rate constant for the  $\text{Me}_3\text{-PyN}_3$  reaction (see 3.4).

The stability constants calculated for the initial reaction are all very similar,

with  $\log_{10}K$  ca. 2.0 for  $\text{PyN}_3$  and  $\text{Me-PyN}_3$  and ca. 2.5 for  $\text{Me}_3\text{-PyN}_3$  (at 25.0 °C and  $\mu = 0.1$ ). This suggests a similar intermediate for all the reactions. With such low values the intermediate cannot involve  $\text{Cu}^{2+}$  bonding to more than one nitrogen atom as the chelate effect would produce higher stabilities. The apparent lack of any large effect of ligand methylation on the stability constants might indicate that the intermediate involves bonding to the pyridine nitrogen, since this is not methylated. However, since 2,6-lutidine is well known as being too sterically hindered to bond to  $\text{Cu}^{2+}$ , such an intermediate is extremely unlikely to form considering the even greater 2,6-steric hindrance involved in these ligands. Thus, the intermediate must involve co-ordination to one of the other two types of amine present in the macrocycles. In view of the effect of methylation at the amines in the *cis*-position to the pyridine on the dissociation rate it is therefore suggested that the intermediate involves co-ordination at this point, with methylation making dissociation more difficult and producing a slightly more stable intermediate. In view of the lack of trend in the formation constants the rate determining step is probably not bonding of the  $\text{Cu}^{2+}$  to these nitrogens as occurs with the  $\text{Ni}^{2+}$  and  $\text{Co}^{2+}$  reactions.

Thus, the initial reaction probably involves attack at the axial position of a  $\text{Cu}^{2+}$  ion by the appropriate nitrogen.



The visible spectra of the final products are as expected for planar  $\text{CuN}_4^{2+}$  chromophores, with the magnetic moment of  $[\text{Cu}(\text{Me}_3\text{-PyN}_3)]^{2+}$  in the range

expected for high-spin Cu(II) complexes.<sup>251-253</sup> Thus, the second stage of these reactions represent a number of steps in the mechanism, probably involving the formation of folded intermediates (see chapter 2). Due to the complexity of these processes the rate constants for the second step show no real trend on increasing ligand methylation. The first step in the process designated by  $k_{int}$  may be Jahn-Teller inversion to bring the bound nitrogen into the equatorial plane of the  $Cu^{2+}$  ion. Such inversions are usually rapid<sup>257</sup> although in the case of  $Cu(OH)_3^-$  reacting with cyclic and open-chain polyamines in basic aqueous media Jahn-Teller inversion following the first bond formation was proposed as the rate determining step.<sup>93</sup> The slow inversion was considered to be due to inhomogeneity in the inner co-ordination sphere. Thus, this is unlikely to occur here, and so rapid inversion may occur prior to formation of the intermediate so that the intermediate involves a Cu-N equatorial bond. Presumably the closing of the first chelate ring is therefore very favourable in the reactions of the ligands with the  $Ni^{2+}$  and  $Co^{2+}$  reactions and so these ions do not experience such mechanistic problems.

The range of mechanistic behaviour displayed by the three ions reacting with  $PyN_3$ ,  $Me-PyN_3$  and  $Me_3-PyN_3$  is illustrated in Figure 4.37. The  $Co^{2+}$  reactions are the most straightforward, with methylation at the amines in the *cis*-position to the pyridine moiety causing a severe drop in initial reaction rate. For  $Ni^{2+}$  the same ligand ( $Me_3-PyN_3$ ) reacts with a much larger rate than for the lesser methylated ligands and this can be explained by a change in complex geometry. For the  $Cu^{2+}$  reactions an unstable intermediate is formed, with  $Me_3-PyN_3$  producing the most stable intermediate. The importance of methylation at the amines in the *cis*-position to the pyridine is apparent for all three ions. This suggests initial attack at these two equivalent nitrogens for all three metals. Crystal structures of a related dimethylated ligand show lone pairs pointing out of the macrocyclic cavity for the two amines *cis*-to the pyridine, but lone pairs pointing into the cavity for the pyridine and the amine *trans*-to the pyridine (figure 4.38).<sup>254,258</sup>

There are no data regarding the conformations of these ligands in solution but

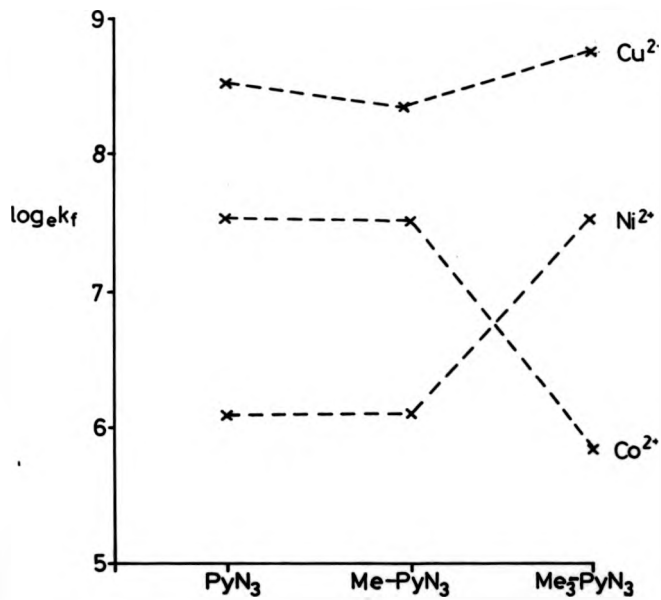


Fig. 4.37 Variation of  $k_f$  for initial reaction on ligand methylation.

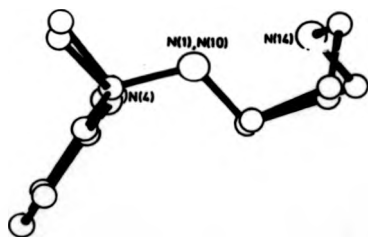
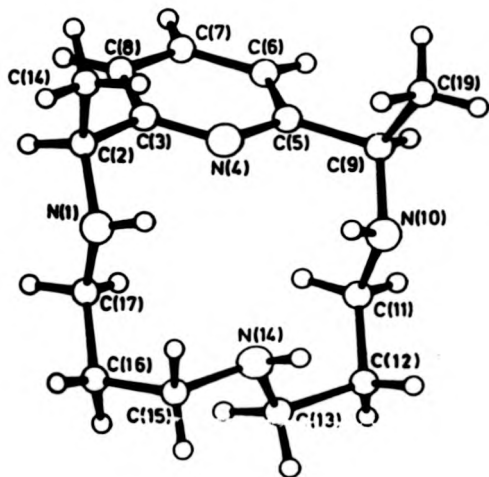


Fig. 4.38 Crystal structure of free ligand related to  $\text{PyN}_3$ <sup>258</sup>

Moore et al noted that benzylation of  $\text{PyN}_3$  occurred preferentially at the two nitrogens *cis*-to pyridine.<sup>251</sup> The steric hindrance of the nitrogen *trans*-to pyridine is clear from the crystal structures and thus this is good evidence for retention of conformation on solvation, though the conformation may well be solvent dependent. The kinetic data discussed in this chapter also lend weight to the idea of retention of conformation in solution.

Kaden and Schultz-Grünow<sup>112</sup> concluded that the introduction of a pyridine ring into an  $\text{N}_4$  macrocycle did not produce a dramatic effect on the reaction rates with  $\text{Co}^{2+}$ ,  $\text{Ni}^{2+}$ ,  $\text{Cu}^{2+}$  and  $\text{Zn}^{2+}$  in water, with rates being only 10-100 times smaller than cyclam. These authors were studying mainly monoprotonated ligands, the effects of protonation differing for the pyridine containing and the pyridine absent  $\text{N}_4$  macrocycles. Our results, being carried out in dmsO, have no such protonation problems and show that for the unprotonated ligands the effect of introducing a pyridine ring is much smaller, with no effect on the forward rate constant observed for the  $\text{Cu}^{2+}$  reactions, and a variety of mechanisms required to explain the kinetic behaviour.

Further work which could be carried out on these systems would be to investigate the structures of the intermediates using rapid scanning UV/visible spectrometry. It would be interesting to study the kinetics of the more substituted ligands such as the di- and tri-benzyl substituted  $\text{PyN}_3$ . These ligands are known to bond to  $\text{Ni}^{2+}$  in a square pyramidal form with folded macrocycles as  $\text{Me}_3\text{-PyN}_3$  does with  $\text{Ni}^{2+}$ . Thus, the kinetics of complexation may well follow the behaviour of the anomalous  $\text{Ni}^{2+}/\text{Me}_3\text{-PyN}_3$  reaction. The  $\text{Cu}^{2+}$  complexes of these ligands are still square planar<sup>251</sup> and so should follow the behaviour of reactions with less substituted ligands.

$\text{PyN}_3$  and related ligands have formed the basis for the preparation of a number of pendent arm macrocycles, with arms capable of co-ordination to a metal ion.<sup>259-263</sup> Thus, the knowledge of the kinetics of pendent arm ligands (chapter 3) and  $\text{PyN}_3$  ligands (chapter 4) could be extended to a study of the kinetics of pendent

arm  $\text{PyN}_3$  ligands to see if any similarities or deviations arise.

The  $\text{PyN}_3$  work could also be extended to a study of the  $\text{PyN}_4$  ligands which have recently been reported<sup>264,265</sup> to study the effects of larger ring size and extra donor atoms on the kinetics of complexation.

## Chapter 5

### A Study of Amine Modified Silica Gels

#### 5.1 Introduction

Silica gel ( $\text{SiO}_2$ ) is one of the most versatile and widely used materials for the support of metal complexes for catalysis. Like most inorganic oxide supports it relies on its surface covering of hydroxyl-groups to attach metals and ligands. The highly polar surface of  $\text{SiO}_2$  is usually undesirable in a catalyst and the surface hydroxyls can be removed by reaction of a suitable non-polar lipophilic molecule, such as t-butyltrimethylchlorosilane, which makes the surface highly stable to hydrolysis.<sup>266</sup> In this fashion  $\text{SiO}_2$  can be modified using a wide variety of silanes, and these silanes can be modified further, thus providing the ability to tailor the surface to specific purposes. Understandably modified silicas are of great importance in a variety of fields including phase-transfer catalysis,<sup>267</sup> preconcentration of trace metals,<sup>268</sup> enzyme immobilisation,<sup>269</sup> chromatography<sup>270-272</sup> and chemical photoconversion.<sup>273,274</sup> Due to the unquestionable importance of  $\text{SiO}_2$  and its derivatives there has been a considerable amount of work devoted to understanding the surface processes involved.

##### 5.1.1 Silica Gel:- Surface Structure and Metal Binding.

The exact nature of the surface of a silica gel depends largely on its chemical and physical history, in particular the method and conditions used to prepare the gel and any modifications, either by thermal or chemical means. The heterogeneity of the surface is due to a variety of surface adsorption sites. Thermodynamic aspects of this heterogeneity have been studied.<sup>275,276</sup>

The surface-active groups on silica are of two distinct types; siloxanes (Si-O-Si) and silanols (Si-OH),<sup>277,278</sup> though the latter are the most important on the majority

of synthetically prepared silica gels, in terms of reactivity and surface accessibility. I.R. and nmr studies have identified a number of different types of silanol groups. There are the "free" Si-OH groups, which are physically and chemically active since they are isolated from other species and so are incapable of significant surface hydrogen-bonding. These possess a sharp peak at ca.  $3750\text{ cm}^{-1}$  in the infra-red (figure 5.1). They are mainly single hydroxy silanol sites (Si-OH) but also include geminal hydroxyl silanol sites (Si(OH)<sub>2</sub>).<sup>279</sup> These two types of silanol can be distinguished using <sup>29</sup>Si CP/MAS nmr<sup>280</sup> (figure 5.2). "Bound" Si-OH groups are strongly hydrogen-bonded to water on the gel surface. Since these will be involved in varying degrees of hydrogen-bonding the I.R. spectrum shows a broad band around  $3400\text{ cm}^{-1}$ , which includes the stretching modes from the physically adsorbed water (figure 5.1). <sup>29</sup>Si CP/MAS nmr makes no distinction between these two types of single hydroxy silanol groups. A third type of silanol group is the "inner" or "intrastructural" silanol, which lies inside the closed pores and/or in the gel matrix. These are chemically inactive and the exact frequency at which they resonate in the I.R. spectrum very much depends upon the conditions of synthesizing the gel.<sup>279,281-284</sup> Proton nmr has also been used to distinguish between the different types of silanols.<sup>285</sup> Using various sophisticated nmr techniques Maciel et al observed that there were three types of protons present in untreated silica gels, corresponding to the H-bonded SiOH, the isolated SiOH and physically adsorbed water (figure 5.3), the water could be removed simply by evacuating the gel at room temperature.

Since the exact nature and abundance of silanol sites on the surface of silica gels differs depending on the type of gel used and these sites are of great importance in the chemistry of the surfaces, work has been carried out to find a convenient method of determining the surface concentrations of the silica hydroxyl-groups. Early attempts included measuring the amount of methane gas given off when CH<sub>3</sub>MgI or LiCH<sub>3</sub> was reacted with the silica gel surface.<sup>286,287</sup> Other methods include deuterium exchange mass spectrometry<sup>288</sup> and infra-red spectroscopy.<sup>289</sup> More recent work has largely centred on nmr techniques. Davydov et al<sup>290</sup> used

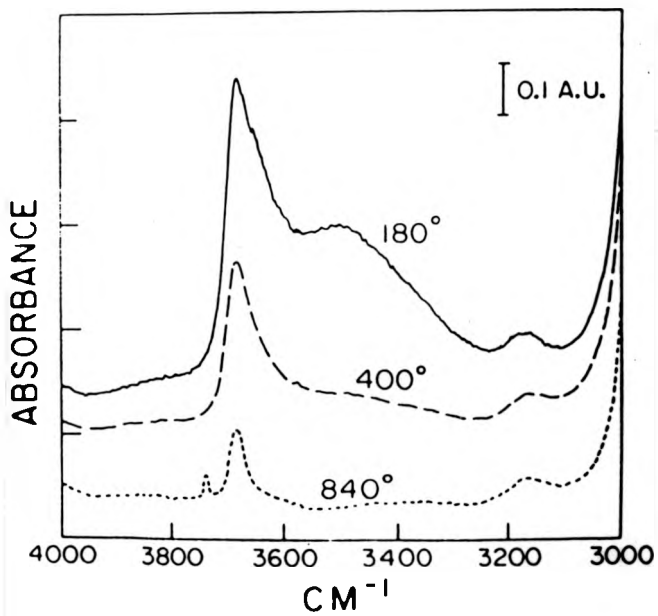


Fig. 5.1 I. R. spectra of heat treated silica gel.<sup>276</sup>

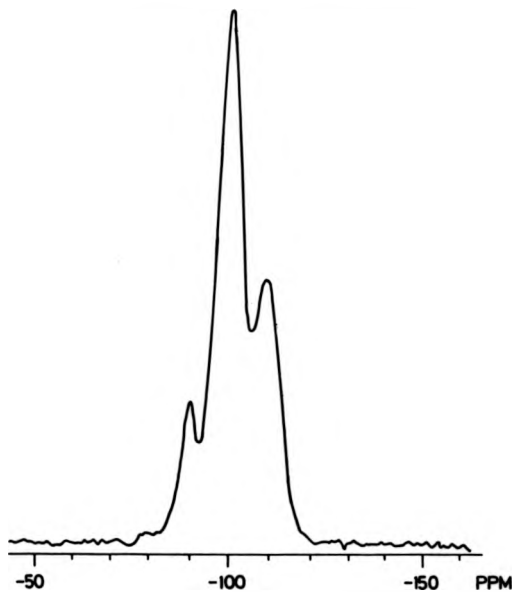


Fig. 5.2 CP / MAS  $^{29}\text{Si}$  nmr spectrum of Fisher S-157 silica gel.<sup>292</sup>

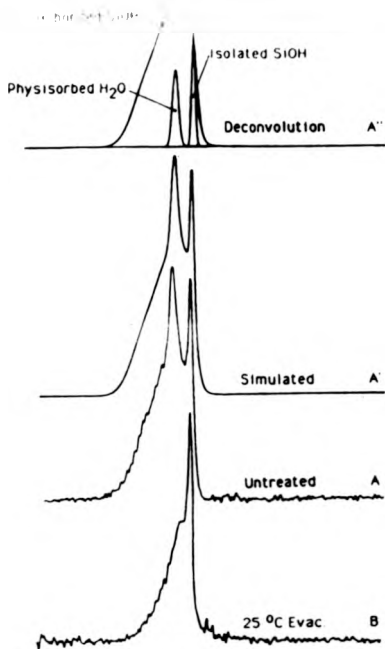


Fig. 5.3 187 MHz  $^1\text{H}$  CRAMPS spectra of Fisher S-679 silica gel.<sup>285</sup>

proton nmr to measure the total content of hydroxy-groups in a sample of silica gel. This value could be split into contributions from surface and intraskeletal groups by reacting the surface groups with heavy water vapour, and measuring the change in the nmr signals. Maciel et al have used  $^{29}\text{Si}$  CP/MAS nmr to determine the surface OH content in various silicas<sup>291</sup> by reacting the hydroxyls with a silylating agent (HMDS - hexamethyldisilazine).<sup>292,293</sup> However, Fyfe et al recently challenged some of Maciel's results,<sup>294</sup> claiming that the resonances of bulk silicons with four siloxane bonds are not quantitative due to the excessively long cross polarization relaxation times, although the data concerning the surface groups are still valid. In this case the authors used the MAS technique on its own to produce quantitatively reliable data concerning both surface and bulk structures (MAS is required for the resolution of the peak structures). A typical value for silanol group concentration is in the order of  $7.5 \mu\text{mol m}^{-2}$  or  $4.2\text{-}5.7 \text{ hydroxyls nm}^{-2}$ .<sup>295</sup> Using  $^{29}\text{Si}$  nmr also has the added advantage that structural information about the silicon atoms is obtained. The relative intensities of  $(\text{HO})_2\text{Si}^+(\text{OSi})_2$ ;  $(\text{HO})\text{Si}^+(\text{OSi})_3$  and  $\text{Si}^+(\text{OSi})_4$  can easily be determined by Gaussian deconvolution of the spectra (figure 5.4). Thus, an "average" structure of a silica gel can be determined (figure 5.5).

Also of paramount importance in the chemistry of silica gel is the effect that temperature has on the number of surface silanol sites. This is because simply by heating gels a weight loss occurs due to the evolution of water, both from physically adsorbed water molecules and from condensation reactions of adjacent hydroxyl groups. Thus, a study of the processes of dehydration and rehydration can give vital clues for the development of a theoretical model to describe the  $\text{SiO}_2$  surface.

There are three temperature regions of importance in the thermal modification of silica surfaces.<sup>278</sup> Heating of silica gels up to  $115^\circ\text{C}$  or evacuation at room temperature removes the majority of physically adsorbed water, though complete removal of the bound water does not occur until heating to higher temperatures. The exact temperature involved depends largely on the pore structure of the gel, with narrow pore silicas requiring the most extreme conditions, up to  $300^\circ\text{C}$  in some

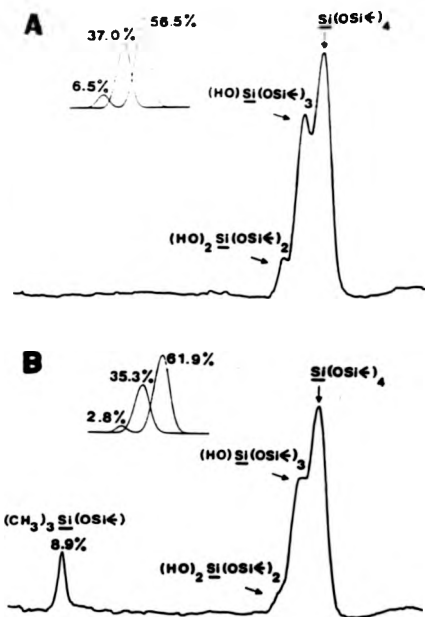


Fig. 5.4 Quantitative  $^{29}\text{Si}$  MAS nmr spectra of surface treated silica gel.<sup>294</sup>

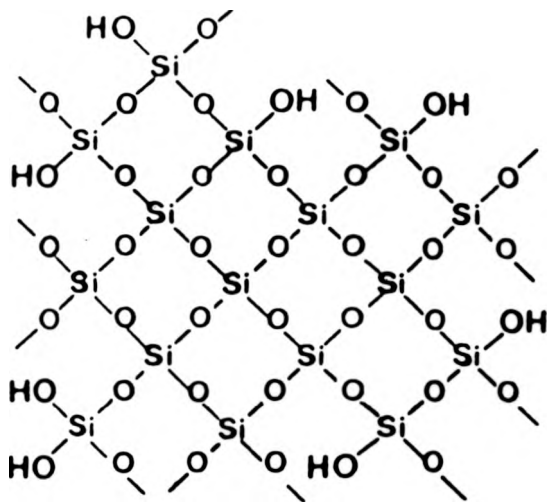
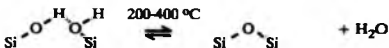


Fig. 5.5 Average structure of Fisher S-157 silica gel.<sup>294</sup>

cases<sup>296</sup> (experimental data suggest the presence of a strongly bound monolayer of water, directly interacting with the silanols, covered by two or more weakly bound water layers which interact through the primary layer<sup>319</sup>). At around 200 °C the reversible condensation of adjacent hydroxyl groups occurs, forming siloxane species and molecular water;



This dehydration occurs progressively from the strongest to the weakest hydrogen-bonded silanols with increasing temperature. The rehydration of the siloxanes is relatively easy at these temperatures, though the siloxane bonds are known to be hydrophobic<sup>298</sup> and probably act as poor sites for the initial adsorption of water. Rehydration may thus occur via initial association of water molecules with neighbouring (uncondensed) hydroxyl groups, and so the kinetics of rehydration would be dependent on the extent of condensation.<sup>298,299</sup> Thus, at temperatures higher than 400 °C rehydration becomes very slow and the reaction becomes essentially irreversible; indeed, Agzamkhodzhaev et al<sup>300</sup> found that a surface dehydrated at 900 °C for 10 hours required several years of standing in liquid water at ambient temperature to become fully rehydrated. An alternative explanation of this behaviour is that at 200-400 °C the condensation reaction forms "strained" siloxane species which are easily rehydrated to the silanols. At temperatures greater than 400 °C these "strained" species rearrange to a more stable configuration, which is thus harder to rehydrate.<sup>301</sup>

Although thermal modification below 400 °C occurs with little change in specific surface area, at temperatures between 600 and 1100 °C, the silica gels begin to sinter and become fluid-like, causing a loss of specific surface area. This occurs at between 600 and 800 °C,<sup>302</sup> thus making silica gels thermodynamically less stable than more crystalline silicas, such as aerosil, carboasil and quartz. In this temperature region further dehydroxylation of previously unreacted silanols has been suggested, perhaps with migration of internal silanol groups to the surface.<sup>286,296</sup> However, in a

more recent investigation, using  $^{29}\text{Si}$  CP/MAS nmr, Maciel and Sindorf established that a significant density of hydroxyl groups remain at temperatures up to 1100 °C, with about 90% of the original hydroxyl groups being removed by condensation.<sup>291</sup> Figure 5.6 shows the effect of heating on the bulk hydroxyl density in a sample of silica gel, determined by  $^{29}\text{Si}$  nmr and by direct weight loss measurement. The difference in the two sets of data at low temperatures probably indicates the presence of tightly bound, physically adsorbed water molecules even at temperatures up to 250 °C.

Boudreau and Cooper<sup>276</sup> used pyridine as a basic probe on unsilanized and silanized (HMDS) silica gel to show that gels pretreated at 400 °C were much more chemically reactive than those pretreated at 180 °C, due to the removal of hydrogen-bonding interactions; and thus increasing the surface homogeneity for a more efficient bonded liquid chromatography stationary phase. Thermal pretreatment at 840 °C also produced increased reactivity, but the sintering that occurred meant that the gel was no longer useful for chromatography.

These studies of de/rehydration have helped to determine an accurate model of silica gel surfaces. Original X-ray work on silicas suggested that the structure most closely resembled  $\beta$ -cristobalite and similar crystalline phases<sup>303</sup> and thus all proposed models use this similarity as a basis. The first model of the silica surface was based on the 111 face of  $\beta$ -cristobalite. DeBoer and Vleeskins<sup>304</sup> suggested an ideal surface, with hydroxyl groups about 5 Å apart and arranged in a hexagonal array (figure 5.7). They suggested that by dehydrating and rehydrating reorganization would cause any surface irregularities to be removed thus producing a thermally stable surface structure. Hockey<sup>305</sup> later revised this model to try to explain measured hydroxyl densities. He suggested a more varied structure, composed of both geminal and single hydroxyl groups. On dehydration the geminal hydroxyls would be easily condensed to form a more regular, though more strained, surface (figure 5.8). At sufficiently higher temperatures the lattice strain could be relaxed. These models do not explain the presence of substantial amounts of "paired" hydroxyls, which exist

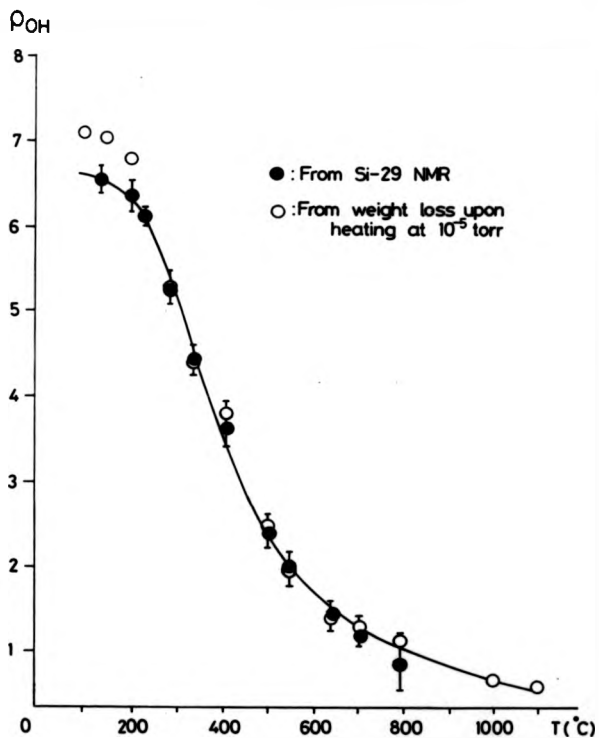


Fig. 5.6 Bulk hydroxyl density as a function of temperature.<sup>291</sup>

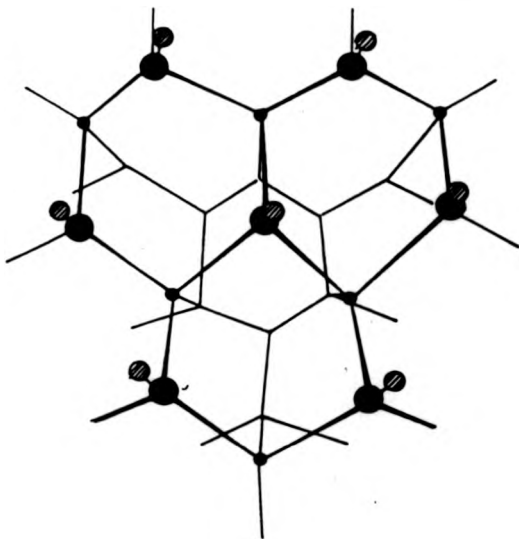


Fig. 5.7 DeBoer and Vleeskins model of the surface of silica gel.<sup>292</sup>

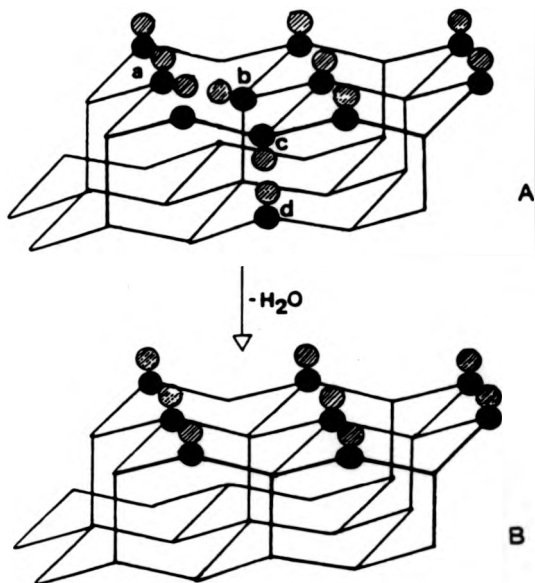


Fig. 5.8 Hockey model of the surface of silica gel.<sup>292</sup>

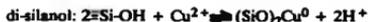
even at higher temperatures, since all OH's are separated by at least 5 Å. Thus, Peri and Hensley<sup>306</sup> proposed a surface which was similar to the 100 face of  $\beta$ -cristobalite, where each surface silicon is connected to a geminal pair of hydroxyl groups (figure 5.9). They proposed the random condensation of hydroxyl groups along surface rows on dehydration, forming both geminal and vicinal hydroxyl pairs. However, this model does not suggest a mechanism for the formation of isolated single hydroxyls. An alternative suggestion was for a surface similar to the 111 face of  $\beta$ -cristobalite. This could account for the presence of single hydroxyls, vicinal hydroxyl pairs and condensation of adjacent hydroxyl groups, but does not account for the existence of geminal hydroxyl groups. To clear up these inconsistencies Sindorf and Maciel<sup>292</sup> have recently proposed, on the basis of <sup>29</sup>Si CP/MAS nmr data, that the surface of silica is more heterogeneous than previously suggested, and may contain segments resembling both the 111 and 100 faces of  $\beta$ -cristobalite (figure 5.10). This explanation seems to fit the available data well, and suggests that for surfaces heated to moderate temperatures, the elimination/restoration of geminal sites by de/rehydration is a reversible process.

Silanol groups are capable of complexing a variety of metal ions. They are acidic, with a  $pK_a$  of between 4 and 7,<sup>307</sup> and can thus cause precipitation of metal hydroxides in some cases. The precise amount of metal ion taken up onto the silica gel surface depends greatly on the pH, in aqueous solution (figure 5.11).

A good deal of work has been done on the complex formation between inorganic oxides and various  $Cu^{2+}$  complexes in water.<sup>308-310</sup> With silica gel and aquated  $Cu^{2+}$  ions, both mono- and di-silanol complexes are formed;



$$\log^* K_1^s = -4.89 \pm 0.23 \text{ (Aerosil 300, } S = 248 \pm 5 \text{ m}^2 \text{ g}^{-1}, 25 \text{ }^\circ\text{C, 0.1 M NaNO}_3\text{)}.$$



$$\log^* \beta_2^s = -10.18 \pm 0.04 \text{ (identical conditions)}^{309}$$

(total amount of copper attached =  $3.9 \mu\text{mol g}^{-1}$  at pH 7).

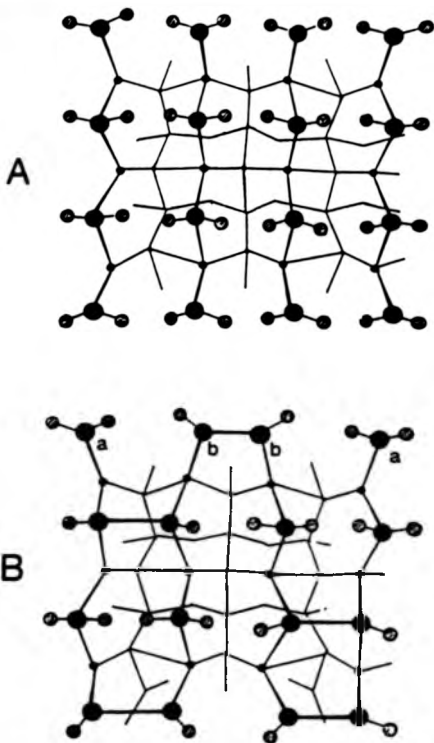


Fig. 5.9 Peri and Hensley model of the surface of silica gel.<sup>292</sup>

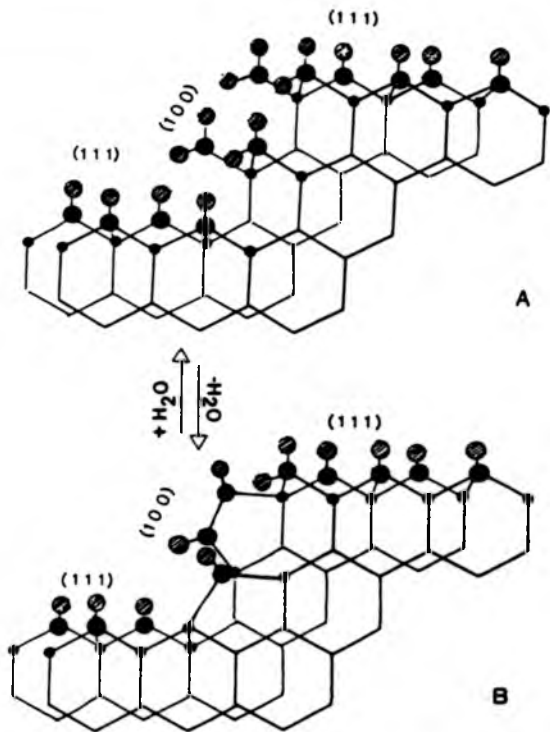


Fig. 5.10 Sinforf and Maciel model of the surface of silica gel.<sup>292</sup>

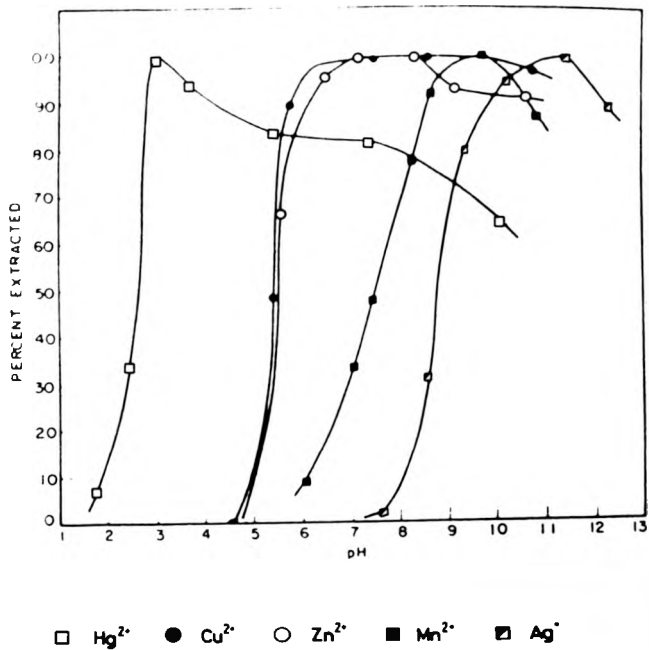


Fig. 5.11 Metal extraction onto silica gel as a function of pH.

Three-site attachment is extremely unlikely due to the low surface density of hydroxyl groups. Using ligands like en and bipy tends to stabilise the surface complexes. Recently, Zelewsky and Bemtgen<sup>311</sup> used esr spectroscopy to carry out a thorough study of  $\text{Cu}^{2+}$  complexes on silica gel surfaces. They found that esr can easily distinguish between the freely tumbling complexes in solution and the immobilised adsorbed species. Using Aerosil 300 they discovered that the adsorption of  $\text{Cu}^{2+}$  followed the deprotonation curve of the  $\text{SiOH}$  groups (figure 5.12), with the amount of  $\text{Cu}^{2+}$  adsorption being  $1.5 \times 10^{-5} \text{ mol g}^{-1}$  at pH 7 (this value is about 4 times higher than that found by Bourg et al<sup>309</sup>). Using different ligands affected greatly the adsorption of  $\text{Cu}^{2+}$ . N-chelating ligands with conjugated  $\pi$  systems (bipy, phen, terpy) were found to enhance the adsorption of  $\text{Cu}^{2+}$  by the formation of ternary surface complexes (figure 5.13), whereas aliphatic amines, such as en, were found to reduce the adsorption.

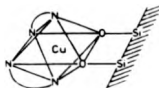


Fig. 5.13 Proposed structure of  $\text{Cu}(\text{bipy})_2(\text{SiO}^-)_2$  surface complex.<sup>311</sup>

Unsaturated N/O containing ligands (e.g.  $\alpha$ -picolinate) formed less stable surface complexes than the N chelating ligands, though generally neutral or negatively charged complexes were not absorbed at all at high pH values. The observations could be explained by four different modes of adsorption. For the ligands with conjugated  $\pi$  systems a co-ordinate bond formation between  $\text{Cu}^{2+}(\text{aq})$  and  $\text{SiO}^-$  groups is proposed. At low pH, bonds between *cis*- $\text{CuL}_2^{n+}$  complexes and  $\text{SiOH}$  are formed for bipy and phen (with 2 donors). Hydrogen bonds are also formed, between  $\text{SiOH}$  and suitable groups in  $\text{CuL}$  complexes, e.g. the oxime oxygens in  $\text{Cu}(\text{DOHDO-pn})^+$  (3,9-dimethyl-4,8-diazaundeca-3,8-diene-2,10-dionedioxime). Purely electrostatic binding also occurs, between  $\text{SiO}^-$  and  $\text{CuL}_x^{2+}$  complexes, such

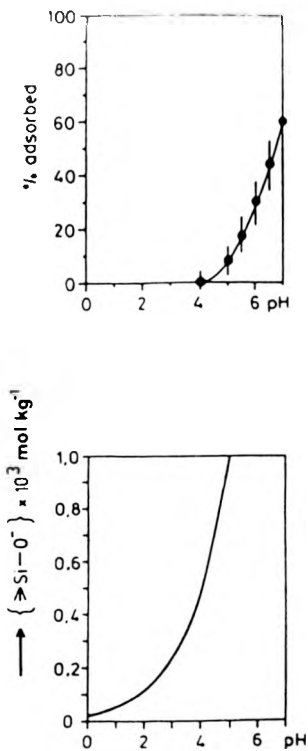
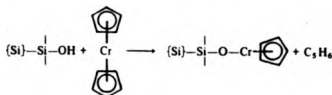


Fig. 5.12 Adsorption of  $\text{Cu}^{2+}$  (top) and  $\text{SiO}^-$  concentration (bottom) as a function of pH.<sup>311</sup>

as  $\text{Cu}(\text{cyclam})^{2+}$  and  $\text{Cu}(\text{terpy})_2^{2+}$ , where *cis*- $\text{Cu}^{2+}$  sites are not available for bonding.

Many metal complexes bound to the surface of silica gel have found great use in catalytic processes. Organometallic compounds such as Zr, Hf, Cr, Ni allyls, Ti, Zr, Hf benzyls, Ti, Zr neopentyls, Cr cyclopentadienyls and Cr arenes reacted with silanol groups form  $\text{Si-O-M}_{n-1}$  bonds and supported metals of this kind are used to great effect in the catalysis of the Ziegler-Natta polymerisation of olefins. Only a fraction of the metal atoms on the surface generate catalytically active sites, and so it is the nature rather than the number of immobilised species that is important. The exact nature of the support is also of paramount importance in the process of catalysis. With chromocene the silica stabilises the chromium in a co-ordinatively unsaturated state thus producing a highly active catalyst.<sup>312</sup>

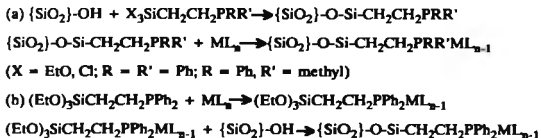


$[\text{Zr}(\text{C}_3\text{H}_5)_4]$  reacts with silanol groups to form a mixture of mono- and di-silanol complexes, in the same way that  $\text{Cu}^{2+}$  does. A variety of metal carbonyls can also bond to the surface of silica to form active catalysts,<sup>313,314</sup> forming many types of subcarbonyl species. The structures and mechanisms involved in all these processes are beyond the scope of this thesis, for a more detailed account of this subject see references 315 and 316.

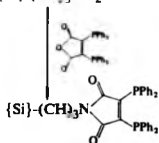
### 5.1.2 Modified Silica Gels:- Syntheses and Metal Binding.

The importance of unmodified silica gel is unquestionable (5.1.1), but the chemically active surface silanols allow modification of the gel surface via silylating agents thereby opening up a whole new field of study. These modified silica gels offer a number of important technical properties such as non-swelling, thermal and mechanical stability and high rates of equilibrium attainment. A large variety of

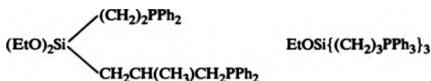
silanes and ligating silanes have now been attached to silica gel. Many research groups have concentrated on the introduction of phosphine groups onto the surface of silica for the subsequent attachment of metal complexes. Work has centred on two basic approaches, which differ only in the order of the steps;<sup>315</sup>



Numerous patents have been taken out on these types of materials. The first approach was reaction (a), because it has many advantages; the range of bridging groups can easily be varied from the simple  $\text{-CH}_2\text{CH}_2\text{-}$  to higher aliphatics or aromatics, also, by bonding ligating molecules onto a surface they become rigidly orientated preventing molecular interactions, thus any metal complexes which are unstable in solution will be stable on the modified surface as dimerisation etc. cannot occur. Finally, the environment of the catalytic sites can be controlled in terms of polarity by either leaving unreacted silanol groups or by "end-capping" using other silylating agents. Reaction (b) was introduced to try to get around the difficulty of determining the precise nature of the catalytic site in reaction (a). The theory was that the complex can be isolated and characterised by standard methods prior to bonding to the silica surface, though in practice the complexes tend to be oils rather than crystalline. The preparation of the phosphinated silylating agents in both of these reactions can often be quite demanding,<sup>317</sup> particularly when chiral centres on multidentates are involved. Indeed, much difficulty was experienced initially in purifying simple bidentate phosphines with  $\text{-SiR}_3$  groups. One route suggested to obviate this problem was;<sup>318</sup>



though a number of multidentate phosphinated silylating agents have now been synthesized,<sup>319</sup> including:



Many other strategies have been devised for the phosphino-modification of silica gel. One method involves building the -Si-O-Si- backbone around a trialkoxysilylphosphine to produce a non-linear polymer;<sup>316</sup>



Alternatively, silica gel may be phosphinated using phosphorus trichloride to produce a silica containing -PCl<sub>2</sub> groups on the surface, subsequent treatment with RXH (R = alkyl, aryl, X = O, S, NHR') yields a silica with a donor surface. Silica may also be derivatised to contain hydroxyl groups as a glycofase (e.g. {Si}-OCH<sub>2</sub>C(OH)<sub>2</sub>CH<sub>2</sub>OH). These groups can then be functionalised using multidentate phosphines.

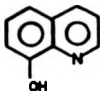
A more general route is available through the chloromethylation of the silica surface using Me<sub>2</sub>ClSiCH<sub>2</sub>Cl, in a manner analogous to chloromethylation of polystyrene.<sup>320</sup> Subsequent reaction with NaCH(CH<sub>2</sub>PPh<sub>2</sub>)<sub>2</sub> yields a supported bidentate phosphine.

Although much of the early work on silica supported ligating groups was carried out on phosphines, most of the above syntheses can be used to attach a variety of donors to the silica surface. There has been a lot of interest in recent years in the modification of silica gel using amine containing ligands due to their great affinity for metal complexation and their high complex stabilities. Simple amino-functionalised silica gels are usually prepared from the reaction between an amino containing silylating agent and  $\{\text{Si}\}\text{-OH}$ , in an analogous manner to the phosphines (reaction (a)). Though again alternative synthetic routes have appeared. A large number of different functional groups have been attached to silica, including pyridyl, morpholino, piperidino, pyrrolidino, Schiff base, cyano, thiol and cyclopentadienyl.<sup>315</sup>

Amine-modified silica gels have been found to be particularly useful as pre-concentration agents for trace metals when chelating groups are used. Leyden and Luttrell<sup>268</sup> studied a range of immobilised chelating functional groups. Primary and secondary amines and ethylenediamine were bound to silica gel via silylating reagents and subsequently further functionalised to their dithiocarbamate derivatives. The syntheses were simple to carry out and the resulting reagents were tested for stability, metal capacity, rate of metal uptake and pH dependence of metal uptake. All the materials were found to be stable in water at room temperature in a mid-pH range. The silanol groups themselves are unstable at very low and very high pH values, undergoing acid and base hydrolysis. The amine-modified silica gels become unstable when heated for over an hour at temperatures of 150 °C, the resins becoming yellow, probably due to oxidation to some kind of bound nitrogen oxide. The dithiocarbamate derivatives are much more unstable. In acidic solution, below pH 2.5, carbon disulphide is released. The gel containing two dithiocarbamates per ligand was considered to be more stable than the gel with only one dithiocarbamate per ligand.

- (1)  $\{\text{Si}\}-(\text{CH}_2)_3\text{-N}(\text{CH}_3)\text{H}$       (4)  $\{\text{Si}\}-(\text{CH}_2)_3\text{-N}(\text{CS}_2^-)\text{-CH}_3$   
 (2)  $\{\text{Si}\}-(\text{CH}_2)_3\text{-NH}_2$       (5)  $\{\text{Si}\}-(\text{CH}_2)_3\text{-NH}-(\text{CH}_2)_2\text{-NH-CS}_2^-$   
 (3)  $\{\text{Si}\}-(\text{CH}_2)_3\text{NH}(\text{CH}_2)_2\text{NH}_2$       (6)  $\{\text{Si}\}-(\text{CH}_2)_3\text{N}(\text{CS}_2^-)\text{-(CH}_2)_2\text{NHCS}_2^-$

The capacity of the modified gels for  $\text{H}_2$ ,  $\text{Zn}^{2+}$  and  $\text{Cu}^{2+}$  was measured. The amount of dithiocarbamate ligands was determined by an iodine titration. The amount of  $\text{H}^+$ /metal uptake in gels (1)-(5) varied little, being 0.47-0.53  $\text{mmol g}^{-1}$ , whereas for gel (6) the amount was almost doubled, with 0.94  $\text{mmol g}^{-1}$   $\text{Zn}^{2+}$ , 0.97  $\text{mmol g}^{-1}$   $\text{Cu}^{2+}$  and 1.00  $\text{mmol g}^{-1}$  dithiocarbamate groups. The rate of metal uptake in the gels varied greatly depending on the metal ion studied, though even the most inert metal ion,  $\text{Cr}^{3+}$ , was 90% extracted in 40 minutes with gel (4). The effect of varying the pH on the amount of metal extracted was investigated to find the conditions necessary for quantitative removal of a particular metal ion from solution using a particular gel. The percentage extraction of  $\text{Cu}^{2+}$  using the range of modified gels is shown in figure 5.14. The investigations showed that the properties of the gels were more than adequate for their use as preconcentration aids in X-ray fluorescence analysis. Similar conclusions were determined from a study of 8-hydroxyquinoline immobilised silica gel.<sup>271</sup> This material is stable down to pH 0,<sup>321</sup> and is inert to a number of solvents.



Its use is limited to trace or low levels of metal concentrations due to the small capacity of the material, which is a common feature of these gels. However, one major advantage with these modified gels is that they can easily be recycled, by leaching out the metals with dilute acid, with no effect on their performance; which is much more convenient than the careful washing procedures required in the most common chelating resin for removal of trace heavy metals from seawater, Che-

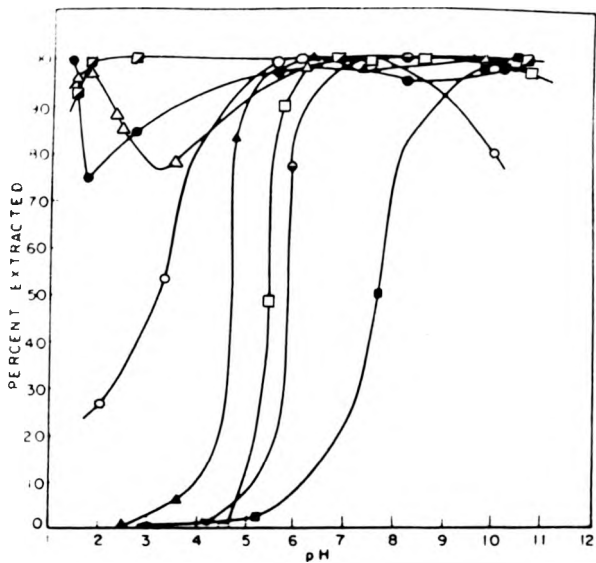
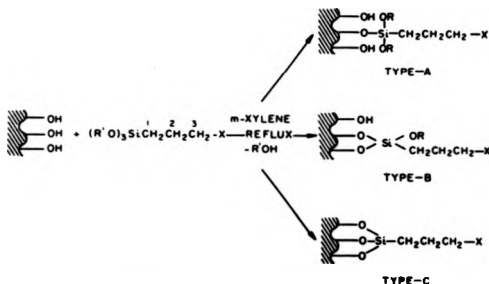


Fig. 5.14 Extraction of  $\text{Cu}^{2+}$  onto various functionalised silica gels.<sup>268</sup>

● bis-dithiocarbamate, Δ dithiocarbamate, ◻ dithiocarbamate, ○ silyl xanthate, □ silica gel, ▲ diamine, ⊖ amine, ■ amine.

Precise characterisation of the bonding modes and structures involved in the amine modification of silica gel surfaces is by no means simple, as the chemistry of immobilised ligands and metal complexes will not necessarily be that of the analogous moieties in solution. A variety of analytical techniques have been applied to the problem and comparisons with the data of model compounds in solution can prove invaluable. Understandably most systematic studies of the bonding on silylated silica surfaces have focussed on simple silanes reacting with silica gel. Solid-state  $^{29}\text{Si}$  and  $^{13}\text{C}$  CP/MAS nmr spectroscopy has proved invaluable in this area, though electronic absorption, electron spin resonance, photoacoustic and infra-red spectroscopy have all been applied. One very useful tool is simple elemental analysis, from which data concerning surface concentrations of species can be calculated.

In principle, an organotrialkyl- or trichloro-silane can react with a silica gel surface to form three types of bonding.



Type-A bonds involve condensation to form only one silanol-to-silane bond. Type-B involves two silanol groups bonding with one organosilane molecule and type-C corresponds to three silanol groups per organosilane molecule. Sudhalter et al.<sup>323</sup> found that  $^{29}\text{Si}$  CP/MAS nmr could distinguish between the three bonding

modes. For 3-chloropropyl modified silica gel, 3 peaks were found in the spectrum, which were assigned to the three different types of bonding, while in the spectrum of 3-aminopropyl modified silica only two peaks were observed, which was attributed to an absence of type-A bonding (figure 5.15). The  $^{13}\text{C}$  CP/MAS nmr spectra of the same samples were found to be highly dependent on the solvent that was used to wash them, with interferences from absorbed methanol which must be bound to the modified silica and be immobilised enough to be detected by the cross polarization techniques. Type-B bonds were considered to be the most common in these systems.

$^{13}\text{C}$  spin-lattice relaxation data gathered by Shinoda and Saito<sup>324</sup> suggested that hydrogen-bonding was important in the structures of silica gels modified with  $-\text{Si}(\text{CH}_2)_3\text{NH}_2$  and  $-\text{Si}(\text{CH}_2)_3\text{NH}(\text{CH}_2)_2\text{NH}_2$ . The spectral resolution was dependent on the solvent used to suspend the samples, with more polar solvents producing better resolution. By studying the effect of protonation on the relaxation times of the amine-modified silicas Shinoda and Saito deduced that the internal motion of the surface bonded amino groups is more restricted in the unprotonated state, suggesting hydrogen-bonding between the amino groups. Evidence for the former type of hydrogen-bonding exists in infra-red studies,<sup>325</sup> and for the latter, site-site interaction has been observed between amino and picramid groups on a silica surface.<sup>326</sup>

Explaining silane-to-silica surface bonding in terms of three bonding modes (Types A, B and C) is probably quite a naive oversimplification as additional chemical processes could easily lead to a variety of structures. For unreacted Cl's or OR's on the silane, hydrolysis by the solvent could introduce new atoms or moieties into the bonding, and the condensation of silanes to form "polymers" cannot be disregarded. Certainly any realistic model of the bonding at silica surfaces must take into account a certain amount of surface water as it has already been shown (see 5.1.1) that small amounts of water remain even after extensive heat treatment. A number of possible bonding structures is shown below for  $\text{RSiCl}_3$  reacted with a silica surface.

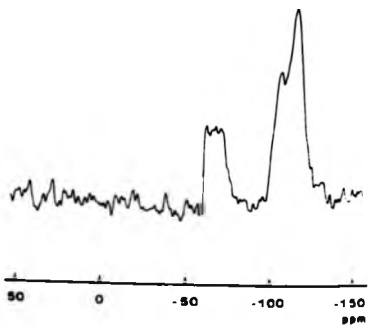
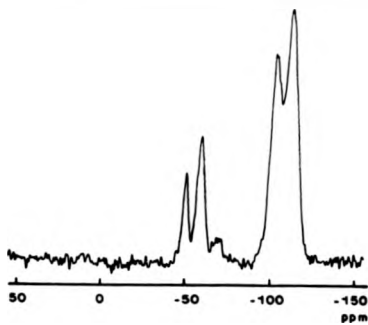
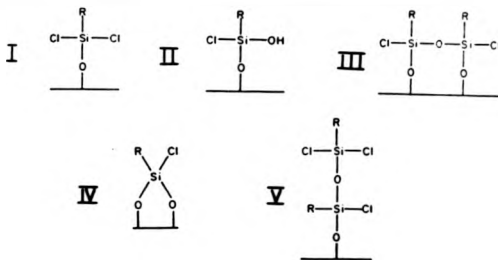


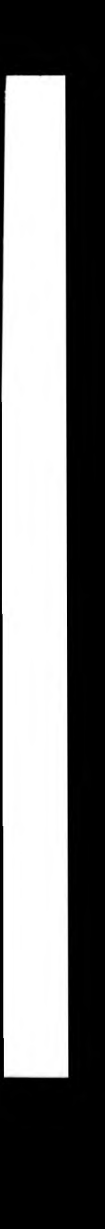
Fig. 5.15 CP / MAS  $^{29}\text{Si}$  nmr spectra of modified silica gels,<sup>323</sup>

top = 3-chloropropyl silica, bottom = 3-aminopropyl silica.



Taking into account many of these possible interactions Maciel and Sindorf<sup>327</sup> carried out a detailed study of the reactions of silica surfaces with polyfunctional chloromethyl silanes and ethoxymethyl silanes, using solid-state nmr techniques. They found that the presence of molecular water was actually instrumental in determining the course and extent of silylation. The chemistry of the chlorosilane and ethoxysilane reactions was shown to be very similar, with single silanol-to-silane bonds characterising the silane environments in materials prepared from near-anhydrous gels. The authors offered substantial evidence that for materials prepared with absorbed surface water present silane species with two or more siloxane bonds were formed, and that these species were not as in structure IV, but were formed from the pairwise cross-linking of mono-silanol structures, as in structure III. Simply by exposing anhydrous modified-gels to the air caused direct hydrolysis of unreacted Cl groups and silane-to-silane condensation reactions, though the ethoxysilanes required more water and heating to produce these reactions. An example of this behaviour is shown in the <sup>29</sup>Si CP/MAS nmr spectra in figure 5.16 for the reaction products of dimethyldichlorosilane and silica gel. More highly functionalised silanes will produce higher degrees of "horizontal" polymerisation.

Since reaction conditions, stoichiometry, and reagent type (both silane and silica gel) can all affect the bonding in these modified silica surfaces it is impossible to produce a general model of the bonding modes for these systems. Thus, other



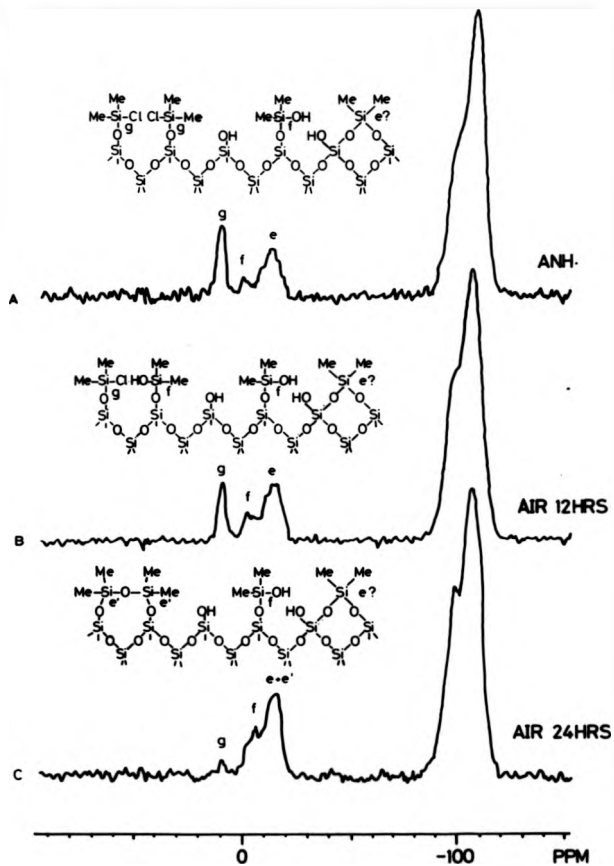
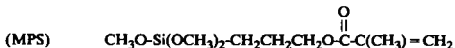


Fig. 5.16 CP / MAS  $^{29}\text{Si}$  nmr spectra of silica gel reacted with  $\text{Si}(\text{CH}_3)_2\text{Cl}_2$ .<sup>327</sup>

studies may well come to different conclusions unless all conditions are copied exactly. However, Leyden et al<sup>328</sup> also found evidence for "horizontal polymerisation" on the surface of silane-modified silica gel, using silica gel with less than half the surface area of that used by Maciel and Sindorf. Leyden et al probed the surface bonding using salicylaldehyde. They formed the Schiff's base species by reaction with (aminopropyl)silane immobilised on silica gel and then studied the uptake of  $\text{Cu}^{2+}$  ions. They observed that oven curing of their amine-modified gels increased the stability of their products, and suggested that this was due to some of the silane being simply hydrogen-bonded to the surface on reaction, the curing forming additional covalent bonds between these species and the silanol groups.

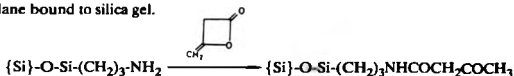
The structures of more complicated amine-modified silica gels have also been reported. De Haan et al<sup>329</sup> studied the bonding of 3-aminopropyltriethoxysilane and 3-methacryloxypropyltrimethoxysilane (MPS) with silica gel. Again using <sup>29</sup>Si and <sup>13</sup>C CP/MAS nmr, this time in conjunction with data from F.T. I.R. spectroscopy.



They proposed bonding modes and solvation processes very similar to those previously described. They suggested that a strong preference for reactions between silanes over those between silanes and the surface existed, thus accounting for the horizontal polymers described earlier. With MPS a lower surface coverage was observed compared to the simpler amine, probably due to more folding of the longer organic chains and interaction between the keto groups and the silanol groups on the silica surface. The surface bonding for the larger silane involved mono- and bidentate silanol bonds, whereas for the simpler amine tridentate bonds and cross-linking was evident, these higher modes of bonding being favoured by higher temperatures.

A variety of analytical techniques were used in the characterisation of a silica

immobilised acetoacetamide,<sup>330</sup> made from the reaction of diketene with aminopropylsilane bound to silica gel.



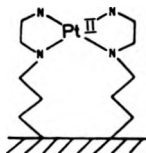
The amide NH and CO groups are strongly hydrogen-bonded and are in the normal *trans*- configuration. At the surface the ligand is mainly in the keto form, and this has been shown to complex with several metal ions under weakly acidic conditions.

The nature of metal complexes of amine-modified silica gels has also been studied. The copper (II) complexes of various Schiff base ligands anchored to silica gel were studied by Shields and Boucher.<sup>331</sup> They used a combination of I.R., electronic absorption and electron paramagnetic resonance spectroscopy along with elemental analyses to derive structural information about the complexes they formed. They prepared the Schiff base ligands from simple primary amines bound to silica gel. They then prepared a range of green Cu(II) complexes using  $\text{Cu}(\text{OOCCH}_3)_2 \cdot \text{H}_2\text{O}$ . A complex with the predominant form Cu(anchored Schiff base)( $\text{CH}_3\text{CO}_2$ ) was observed. Two Schiff base ligands bonding to the Cu(II) ions was considered unlikely as a low surface density of ligands was deliberately prepared, with an average distance of  $10 \text{ \AA}$  between them.

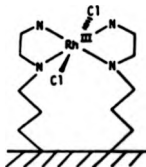
Electron paramagnetic resonance spectroscopy also featured highly in a recent Russian study of copper(II) complexes of modified silica gels.<sup>332</sup> The Cu(II) complex of simple propylamino-groups grafted onto the surface of silica gel was found to be composed of an  $\text{N}_2\text{O}_2$  donor set, with two amino groups and two water molecules binding to the Cu(II) ion in a distorted tetrahedral environment. With dithiocarbamate ligands, prepared from the amino ligands on silica gel, the geometry of the Cu(II) complexes depended greatly on the solvent used. In acid solution, with Cu(II) thiuram disulphide added, a surface complex containing an  $\text{S}_4\text{N}$  donor set was observed, while in chloroform square planar Cu(II) dithiocarbamate complexes

occurred.

$^{13}\text{C}$  nmr was used to study the complexes of Pt(II) and Rh(III) with aminated silica surfaces.<sup>333</sup> Spectra were obtained from both the suspended state (in water) using ordinary high resolution nmr and in the dry state using CP/MAS techniques. Figure 5.17 shows the  $^{13}\text{C}$  nmr of the Pt(II) complex of  $\text{NH}_2\text{CH}_2\text{CH}_2\text{NHCH}_2\text{CH}_2\text{CH}_2\text{Si}-(\text{Si})$  suspended in water. The broadened peaks at 46.2 and 55.0 ppm correspond to the co-ordinated species, whereas the sharper peaks are due to the unco-ordinated species. No line broadening due to the exchange of co-ordinated and unco-ordinated ligands was observed up to 80 °C. A square planar Pt(II) complex is proposed.



For Rh(III) an octahedral environment is suggested with the same ligand on the basis of diffuse reflectance spectra.



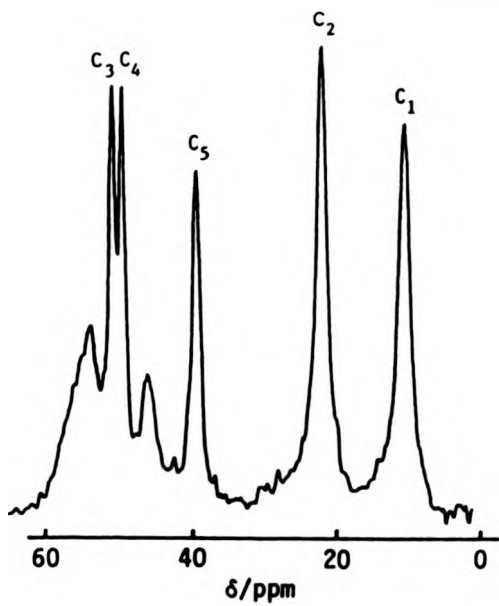


Fig. 5.17  $^{13}\text{C}$  nmr spectrum of a diamine modified silica gel.<sup>333</sup>

The amount of metal ion uptake by a silica surface modified with an imidazopylpropyl group has been studied.<sup>334</sup> A variety of divalent transition metal halides were considered using acetone or ethanol as solvent. The metal adsorption was shown to fit the Langmuir Isotherm<sup>335</sup> using the equation;

$$C_2/n_2^a = 1/n^a b + C_2/n^a$$

where;  $C_2$  = metal concentration (mol dm<sup>-3</sup>)

$n_2^a$  = uptake of metal (mol g<sup>-1</sup>)

$n^a$  = no. of absorption sites per gramme (mol g<sup>-1</sup>)

$b$  = constant

(1 denotes solvent, 2 denotes solute)

( $b = K/a_1$  where  $K$  = equilibrium constant for the process;

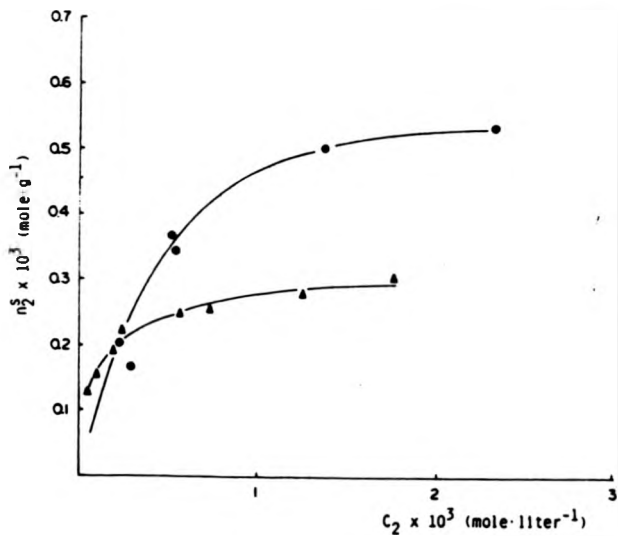


and  $a_1$  = activity of solvent)

Figure 5.18 illustrates the fit of the data for CuCl<sub>2</sub> to this equation. Increasing the average number of ligand groups per unit surface did not cause a significant increase in the adsorption capacity, probably due to increasing surface density causing blocking of certain ligands. High values of the constant "b" were used to suggest that adsorption occurs with the metal directly co-ordinating with the unsubstituted imidazole nitrogen.

### 5.1.3 Macrocycles Bonded to Silica Gel.

The excellent metal ion selectivity observed for macrocyclic compounds makes them ideal candidates for use as selective metal extractors in the form of polymers, resins or surface-bonded species, and this has been exploited for a number of years. Most attention has focussed on the application of immobilised crown ethers in this field and there are a number of reviews on this subject.<sup>88,336,337</sup> Generally, the work has concerned the polymerisation of functionalised macrocycles and the bonding of crown ethers to functionalised polystyrene, with the subsequent analysis of selectivity



$\blacktriangle$   $\text{CuCl}_2$ /ethanol;  $\bullet$   $\text{CuCl}_2$ /acetone.

Fig. 5.18 Metal adsorption for a modified silica gel.<sup>334</sup>

patterns for alkali and alkaline earth metals. Increasingly these cyclic ethers are now being surface-bonded on to silica gel due to the chemical and technical advantages this inorganic support offers, particularly in aqueous media. These materials have achieved much success, especially in the area of chromatography. Kimura et al<sup>338</sup> have shown that alkali metal halides can be separated on poly(benzo-15-crown-5)-modified silica gel by elution with water or water/methanol mixtures. These stationary phases were prepared with the crown ethers bound to the silica gel through amide linkages. The crown ethers form sandwich-type 2:1 crown ether unit-to-cation complexes. Cram et al<sup>339</sup> prepared a silica-immobilised optically active crown ether and achieved enantiomeric resolution of amino acid ester salts using solid-liquid chromatography.

Bradshaw et al<sup>340</sup> has pointed out that if linkage of a macrocycle to silica gel is achieved via a donor atom then the selectivity patterns found for that macrocycle in solution will almost certainly be affected. Thus, they prepared a series of crown ethers and diaza-crown ethers which were functionalised with an (alkoxy)methyl sidearm on the carbon framework,<sup>341</sup> which they bonded to silica gel. They showed that the values of logK for the association of several metal cations with these materials were very similar to the values found for the analogous free complexes i.e. not bound to silica gel. It was suggested that the silica gel bound macrocycles formed complexes in the same manner as do the free macrocycles in aqueous media. Thus, the prediction of metal selectivity patterns seems possible in silica gel systems where the macrocycle is not bonded through a donor atom. This is in contrast to polystyrene bound macrocycles, where the hydrophobic nature of the support means that the materials are not wetted by water, and so solvation of the macrocycles will not be equivalent for bound and free ligands. The stability of Bradshaw's materials are exceptional, with the modified-gels being used between pH values of -0.5 and 11.0 for 6 months with no measurable decrease in activity.

The major drawback in Bradshaw's approach is the difficult task of synthesising a macrocycle with a suitable functional group attached via the carbon framework.



tinuation of earlier work carried out on a series of  $O_2N_2$  and  $O_2N_3$  macrocycles immobilised on polystyrene,<sup>343</sup> which were found to be unsuitable for metal uptake in aqueous media.

#### 5.1.4 Introduction to the Present Study.

The work presented in this chapter involves a study of amine-modified silica gels. The attached ligands are dien and its macrocyclic analogue [9]aneN<sub>3</sub>, tren, 3,2,3-tet and its macrocyclic analogue cyclam. This study is designed to extend the knowledge already obtained for simple bound open-chain amine ligands such as  $\{Si\}-(CH_2)_3NH_2$  and  $\{Si\}-(CH_2)_2NH(CH_2)_2NH_2$  (see 5.1.2) by looking at higher amines, and to assess the advantages and disadvantages of using a macrocyclic polyamine.

Macrocycles containing only nitrogen donors have been little used in the modification of silica surfaces. Tetraphenylporphyrin has been bonded to a silica bound 3-imidazolylpropyl group and its Fe(II) complex used for oxygen absorption.<sup>344</sup> The simple nitrogen macrocycle cyclam has not yet been bonded to silica gel. French workers have prepared a polymer supported cyclam by the reaction of cyclam with chloromethylated polystyrene resin. The material extracted up to 2.0 mmol g<sup>-1</sup> of Cu<sup>2+</sup> from solution, whereas for Ni<sup>2+</sup> and Co<sup>2+</sup> the capacity was < 0.085 mmol g<sup>-1</sup>. However, total extraction required heating at 80 °C for 2 days, at which temperature the lifetime of the support is very short. Thus, a study of cyclam supported on silica gel is reported here, as the hydrophilic nature of the support should be beneficial in the metal uptake kinetics and the material should be able to be reused many times if the bound macrocycle conforms to previous studies.

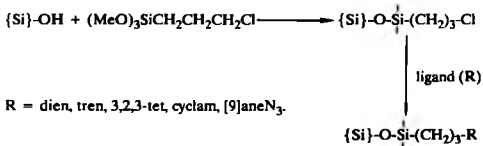
## 5.2 Experimental

### 5.2.1 Materials and Syntheses.

The hydrated tetrafluoroborate salts of Cu<sup>2+</sup>, Ni<sup>2+</sup> and Co<sup>2+</sup> used in the

metal uptake studies were purchased from Alfa-Inorganics and were used without further purification. The open-chain amines used in the preparation of the modified silica gels (dien, tren, 3,2,3-tet) were obtained from Aldrich. Purity was checked using  $^1\text{H}$  nmr and was considered to be satisfactory. The macrocycles used (cyclam and [9]aneN<sub>3</sub>) were prepared according to literature methods.<sup>200-202</sup> Three grades of silica gel were used in the syntheses, with increasing pore size. The smallest pore size was obtained using Kieselgel 60 (Merck) with a pore size of 60 Å (surface area = 500 m<sup>2</sup> g<sup>-1</sup>, pore volume = 0.75 cm<sup>3</sup> g<sup>-1</sup>, mesh = 230-400). 100 Å pore size was obtained using HPLC sorbent (Sigma, No. H-7631) (surface area = 300 m<sup>2</sup> g<sup>-1</sup>, average particle size = 10 μm). The largest pore size was achieved by using Davisil Grade 643 (Aldrich) with a pore size of 150 Å (surface area = 300 m<sup>2</sup> g<sup>-1</sup>, pore volume = 1.15 cm<sup>3</sup> g<sup>-1</sup>, mesh = 200-425, pH (5% slurry) = 7.0) [all manufacturer's specifications].

A summary of the procedure for preparing the modified silica gels is outlined below.



Two different methods were used to prepare the amine-modified silica gel, both using the basic route outlined in Scheme I.

#### Method 1;

Silica gel (2 g) was stirred in distilled water (20 ml) for two hours. The gel was filtered off and suspended in 15 ml xylene containing 1.2 ml (3-chloropropyl)trimethoxysilane (Aldrich), and stirred at 80 °C under nitrogen for 8 hours. The silylated silica gel was then filtered off and washed with acetone, followed by dichlo-

romethane. The silylated gel was dried in a vacuum desiccator (at this stage some workers prefer to protect the unreacted silanol groups by reaction with  $\text{Me}_3\text{SiCl}$ , however this still does not "end-cap" all of the unreacted silanol groups and so we decided not to include this procedure). To attach the amine ligands to the modified silica gel a solution of the appropriate ligand (ca.  $5 \times 10^{-2}$  mol) in xylene (50 ml) was added to 2.2 g of the modified silica gel and the mixture placed in an ultrasonic bath for 30 min. The mixture was then refluxed at 150 °C for 15 hr under  $\text{N}_2$  without stirring. The product was isolated by filtration and repeatedly washed with hot methanol to remove any unreacted or physisorbed ligand. The amine-modified gel was then dried in a vacuum desiccator. In the case of cyclam and [9]ane $\text{N}_3$  the pure unreacted ligand could easily be reclaimed by removing some of the methanol from the washings on a rotary evaporator, the solid crystallising out. The other amines are all liquids and so reclaiming the pure unreacted ligands would be much more difficult and was not attempted. The products were characterised by elemental analysis (obtained commercially from Butterworth Laboratories Ltd.) and solid-state  $^{13}\text{C}$  CP/MAS nmr spectroscopy (see results section).

#### Method 2;

Silica gel (4 g) was heated at 320 °C for 5 hours in a stream of dry  $\text{N}_2$ . This was then poured directly into 10 ml of (3-chloropropyl)trimethoxysilane and stirred at 80 °C for 8 hours under dry  $\text{N}_2$ . The solid product was then isolated by filtration and dried under vacuum. The functionalised gel (2.6 g) was then placed in a solution of 0.98 g cyclam in 100 ml xylene and suspended in an ultrasonic bath for 30 mins, followed by refluxing the suspension (without stirring) at 150 °C for 15 hrs. The product was washed repeatedly with hot methanol and dried in vacuo. This procedure was only carried out with cyclam using the 60 Å silica gel.

Solid-state  $^{13}\text{C}$  CP/MAS nmr spectra were obtained on a Bruker MSL360 F.T. nmr spectrometer, using a 7 mm bore zirconia sample holder with a Kel-F stopper. The spin rate was ca. 3.5 kHz. At least 2000 scans were collected for each compound

using a contact time of 5 ms and a recycle time of 2 s. The  $^1\text{H}$  channel was set up with reference to tetramethylsilane. The  $^{13}\text{C}$  cross-polarization experiments were set up using adamantane.

#### 5.2.2 Metal Uptake Studies.

An aqueous solution of metal tetrafluoroborate (20 ml) of previously determined concentration (ca.  $10^{-3}$ - $10^{-1}$  mol  $\text{dm}^{-3}$ ) was added to the amine-modified silica gel (150-200 mg) and the mixture shaken overnight in a sealed flask on a platform shaker. The solid was removed by filtration and the concentration of the metal ions in the filtrate was obtained using a combination of edta titration and atomic absorption spectroscopy for reproducibility. All experiments were carried out at near neutral pH. At least six different metal concentrations were studied for each modified gel and in all cases the initial metal present was never less than the amount required to occupy all the sites on the functionalised silica. The uptake of the metal ions was determined from the difference in the metal ion concentration before and after shaking. This procedure was based on the results from a number of previous metal uptake studies.

(a) In order to determine the time required to achieve complete metal ion binding  $\text{Cu}(\text{BF}_4)_2$  was reacted with cyclam functionalised silica gel in a series of experiments. Each experiment was terminated at a different time 3 hrs, 6 hrs, 9 hrs etc. There was no increase in metal uptake after 3 hrs, and so shaking overnight was more than adequate. For the copper experiments the blue colouration of the products was clearly visible in a matter of minutes, and sometimes quicker. For modified gels previously wetted in distilled water the uptake of copper appeared to be visibly faster than for the unwetted gels. Thus, the kinetics of metal uptake seem to be controlled by the rate of swelling of the silica gel beads.

(b) To determine the reproducibility of the experimental procedure the level of saturation of a gel using  $\text{Cu}^{2+}$  was duplicated by using the same batch of cyclam modified gel. Reproducibility appeared to be about 8%.

The metal complexes of the amine-modified silica gels were characterised using diffuse reflectance and infra-red spectroscopy. Diffuse reflectance spectra were obtained on a Shimadzu UV-365 spectrophotometer fitted with an integrating sphere attachment using a packed magnesium oxide powder as standard, samples were ground to a powder and then wetted with distilled water (2 drops to 0.3 g of gel) to make them stick to the sample holder. Infra-red spectra were obtained as nujol mulls on a Perkin-Elmer 580B spectrometer.

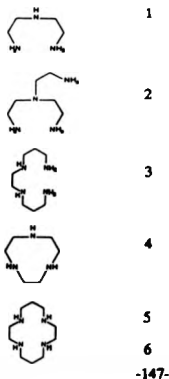
For the determination of metal ion concentrations edta titrations were carried out as described earlier (2.2.1). Atomic absorption spectroscopy was carried out on a Varian Techtron AA6 atomic absorption spectrometer using an air-acetylene flame and taking readings at the following wavelengths, 324.7 nm ( $\text{Cu}^{2+}$ ), 240.7 nm ( $\text{Co}^{2+}$ ) and 341.5 nm ( $\text{Ni}^{2+}$ ) using edta titrated solutions as standards.

### 5.3 Results and Discussion

Six surface modified silica gels were prepared;

$(\text{Si})\text{-O-Si}(\text{CH}_2)_3\text{-L}$

where L =



Gels 1 - 5 were prepared by method 1 and gel 6 by method 2, all using silica gel of 60 Å pore size. The polyamines in gels 1 - 3 can also bond via the secondary amines, rather than through the primary amines as shown, and a mixture of these two species is likely to exist for these ligands. All other ligands used have only a single secondary or primary nitrogen site available for bonding.

The elemental analyses for gels 1 - 6 are listed in Table 5.1. Using the nitrogen value we can calculate the amount of polyamine present on the gel, since this is the only source of nitrogen present in these species. The type of bonding present for the spacer groups (see 5.1.2) can also be probed by examining the ratio of %C / %N and comparing it to the theoretical ratio assuming three silanol linkages per silane modification. These figures are given in Table 5.2.

**Table 5.1**  
Elemental Analyses for gels 1 - 6.

Gel	% C	% H	% N
1	9.78	2.16	3.36
2	9.33	2.20	3.56
3	11.88	2.45	3.02
4	10.98	2.21	2.99
5	10.91	2.06	1.88
6	15.70	3.31	4.33

For gels prepared by method 1 the bulk and rigidity of the ligands may well control the amount of ligand bonded to the spacer groups. The largest amount of ligand present is found with the smaller dien and [9]aneN<sub>3</sub> ligands, with the cyclic ligand having a lower value, presumably because of the conformational and configurational constraints present in the cyclic system. The bonding of tren in gel 2 is more favourable than for 3,2,3-tet in gel 3. This seems strange as tren would appear to present more steric constraints than the flexible 3,2,3-tet. Localised molecular sur-

Table 5.2

Comparison of Observed and Calculated C/N ratios.

Gel	amount of L / mmol g <sup>-1</sup>	C/N (measured)	C/N (calculated)
1	0.800	2.91	2.33
2	0.636	2.62	2.25
3	0.540	3.93	2.75
4	0.712	3.67	3.00
5	0.336	5.80	3.25
6	0.773	3.63	3.25

face structures on the gels must therefore favour the binding of tren over 3,2,3-tet. Certainly with gel 5, the most constrained ligand, cyclam, has the greatest difficulty in binding to the modified gel surfaces, as would be expected. Interestingly, the same gel, prepared by method 2, shows a greatly increased level of cyclam binding to the modified surfaces, illustrating the effectiveness of the thermal pretreatment used in this method for removing interfering water molecules bound to the gel surfaces. These water molecules will certainly have a large influence on the binding of polyamines, and this effect will be heightened in the cyclic cyclam system, as the level of binding for gel 5 displays. Thus, method 2 may well increase the level of binding for the other polyamines, but method 1 gives a good degree of ligand binding already, and so this was not pursued.

The amount of these ligands bound to the surface of silica gel is less than that found for previously prepared gels containing  $\text{-NH}_2$  and  $\text{-NH(CH}_2)_2\text{NH}_2$  (2.8 and 2.0 mmol g<sup>-1</sup> respectively)<sup>333</sup>, although this is expected since these are prepared via a single reaction using the already aminated silylating reagent. For more complex chelating ligands, such as the dithiocarbamates prepared by Leyden and Luttrell<sup>268</sup>, attachment is of the order of 0.54 - 0.58 mmol g<sup>-1</sup>. For the much studied 8-hydroxy-quinoline/silica gel derivative, the ligand is present in quantities of only 0.149 mmol g<sup>-1</sup><sup>345</sup>. Lindoy et al<sup>342</sup> produced an attachment of 0.41 mmol g<sup>-1</sup> using an  $\text{N}_3\text{O}_2$

macrocyclic. Thus, the levels of attachment found for the chelating polyamines studied here seems very good, considering the useful possibilities they may possess in terms of selectivity of metal uptake, especially for macrocyclic systems. However, the ultimate criterion for the usefulness of these compounds is the accessibility of the binding sites to various metals, and this is discussed later.

The C/N ratios are larger in every case than the values calculated assuming binding of three silanol groups per silane reagent, for gel 5 the difference is quite considerable. Thus, the amount of carbon present may be larger than expected due to incomplete hydrolysis of the methoxy groups on the silylating reagent, evidence for this is also seen in the solid state nmr spectra shown later. The values also give good evidence for cross-polymerisation reactions between silanes prior to reaction at the gel surface, as suggested by previous workers, producing bonding modes of the type illustrated in section 5.1.2.

Some of the silanol groups may also have reacted with the methanol produced during the initial reactions to form surface methoxy-groups. Thus, there is likely to be a variety of silane species present on the gel surfaces. The C/N ratios could also be produced by a lower N value than expected, and the very high C/N found for gel 5 is good evidence for the incomplete reaction of the polyamines with the spacer groups.

The modified surfaces will thus contain a mixture of chlorinated and ligand bearing silane groups, which will be bound to the gel surface in a variety of ways. The surface will also contain methoxy-groups and unreacted silanols, which may interfere with metal uptake. Studying the true nature of these modified surfaces requires sophisticated techniques and has only been attempted with simple silylating agents (see 5.1.2).

Previous authors have attempted to analyse the attachment of the silanes quantitatively, but they have to assume a mode of bonding (e.g. 1 silanol to 1 silane). However, the variety of surface species clearly present on modified silica gels invalidates this approach. Leyden et al<sup>30</sup> suggested that silica gels possess in the order of

7.5  $\mu\text{mol m}^{-2}$  of silanol groups, which for the 60 Å gel used in our studies (500  $\text{m}^2 \text{g}^{-1}$ ) corresponds to 3.75  $\text{mmol g}^{-1}$  of silanols. They also suggested that after modification with silanes there is about 3.5  $\mu\text{mol m}^{-2}$  of unreacted silanols present. These can participate in hydrogen bonding and may affect the subsequent attachment of the polyamine ligands in our study. Proton transfer from silanols to amines is thought responsible for the "tailing" that is observed when amines are separated by chromatography.<sup>346</sup> Sindorf and Maciel<sup>293</sup> reported that the silanols were present in the order of 5 silanol groups per  $\text{nm}^2$ . Thus, combining this figure with the known amount of ligand present on each gel and with the surface area of the gel we can calculate the number of silanol groups per ligand (Table 5.3).

**Table 5.3**

Calculated Surface Density and Silanol Coverage.

Gel	no. molecules of ligand $\text{nm}^{-2}$	no. silanols / ligand
1	0.964	5.17
2	0.766	6.53
3	0.650	7.69
4	0.860	5.81
5	0.404	12.38
6	0.93	5.38

For a straightforward bonding mode of the type;



we would expect three silanol groups per ligand, but the values in Table 5.3 indicate that this is not the case, which is again evidence for incomplete reaction of the ligands with the chloro-silane modified gel surface. The density of the ligands is quite low, but models indicate that the ligands are still sufficiently close to interact with one another e.g. in terms of hydrogen-bonding and metal ion binding, even for

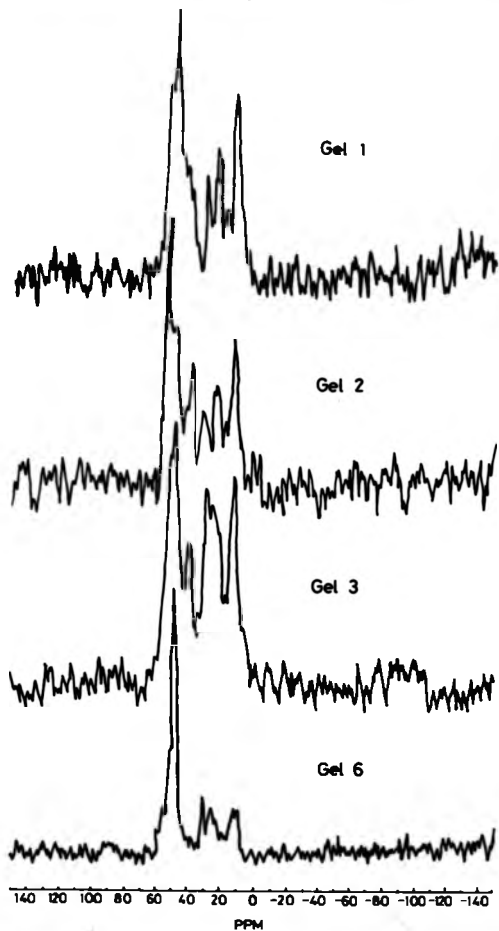
the smallest ligand on gel 1. The question of proximity of ligands is an important one. For heterogeneous catalysis applications of these systems it would be advantageous to prepare a surface where the ligands are very far apart, avoiding interactions, since many catalysts are deactivated by dimerisation. For preconcentration and trace metal uptake it may be more preferable to attach as many ligands as possible to the gel surface, with a high density, so that the amount of metal ion taken up may be increased, thus increasing efficiency.

Similar calculations for determining the density etc. of the spacer groups is only possible if the relative proportions of each type of bonding mode is known.

Characterisation of surface modified materials is notoriously complex and difficult due to the diversity of surface species. A number of techniques can be usefully used however. The  $^{13}\text{C}$  CP/MAS spectra for some of the gels are shown in Figure 5.19. Full assignment of all the peaks is impossible without some very sophisticated nmr experiments. All four spectra show peaks for the three carbons of the spacer group, with  $\delta$  /ppm = 10.5 - 12.1 ( $\text{C}_1$ ), 22.1 - 25.6 ( $\text{C}_2$ ) and 45.1 - 48.4 ( $\text{C}_3$ ) (numbers designated from the silicon atom). The carbon atoms of the polyamine ligands produce large peaks, some showing minor structure. One notable feature is that the ligand peak for gel 6 is very much sharper than in the other spectra, suggesting that the cyclam exists in far fewer environments than for the other ligands and the large height, relative to the minor peaks, illustrates the large quantity of ligand which was attached using method 2. Certainly for the gels 1 and 3 the ligands could bind via two different nitrogen atoms, each arrangement producing new chemical environments for the carbon framework and causing a broadening of the peaks. Another common peak is observed at  $\delta$  = 51.4 - 52.1 ppm and can be assigned to the presence of  $-\text{OCH}_3$  groups on the gel surfaces, either from unhydrolysed silanes or from methanol reacting with unreacted silanol groups. A sharp singlet exists, at  $\delta$  = 27.8 - 30.2 ppm, in each spectrum, but cannot be assigned to any of the carbon atoms common to all the gels.

Thus, although  $^{13}\text{C}$  CP/MAS nmr spectroscopy has been used successfully to

Fig. 5.19  $^{13}\text{C}$  CP / MAS nmr spectra of modified silica gels.



analyse simple surface structures (see 5.1.2), much more sophisticated techniques are required for the more complex structures observed in these polyamine modified gels. Natural abundance  $^{15}\text{N}$  CP/MAS nmr spectroscopy may be of some use in these systems, particularly in determining relative amounts of structures when more than one is possible.  $^{14}\text{N}$  CP/MAS would be useless in this respect since  $^{14}\text{N}$  has spin 1 and so all resonances would be broadened out into the noise level under CP/MAS conditions.

Attempts were made to measure the I.R. spectra of the gels, but the peaks were very broad. More sensitive techniques, such as F.T.-I.R. would be useful here.

Surface modified silica gels are more often characterised by studying their ability to complex metal ions. To this effect the uptake of  $\text{Cu}^{2+}$ ,  $\text{Ni}^{2+}$  and  $\text{Co}^{2+}$  was studied for gel 5. Figure 5.20 shows the results obtained. Even though all experiments were carried out using more than enough metal ions to fill all the available binding sites "saturation level" for each ion was not reached until the concentration of the metal ion was ca.  $0.05 \text{ mol dm}^{-3}$ , which corresponds to ca. 15 times more metal than binding sites under the conditions employed. This is presumably due to a build up of charge on the surface of the gel as the cations are complexed and thus a large excess of metal is required to "saturate" the binding sites. The maximum level of loading is different for each metal, with each level less than the total amount possible assuming 1:1 binding of ligand to metal (Table 5.4).

This is presumably due to a combination of the stability of the complex formed (the levels follow the order of the Irving-Williams stability sequence) and the different stereochemistries adopted by the metal ions. The steric effect of the polymeric gel matrix will also have a large effect, perhaps hindering certain ligand conformational changes, thus reducing the ability of certain metals to bind. It may also limit access of the metal ions to particular binding sites. Similarly the initial binding of a metal ion may block access to other, deeper binding sites. Very similar results were obtained by Lindoy et al<sup>342</sup> in their studies of a silica immobilized  $\text{N}_3\text{O}_2$  macrocycle (Table 5.4).

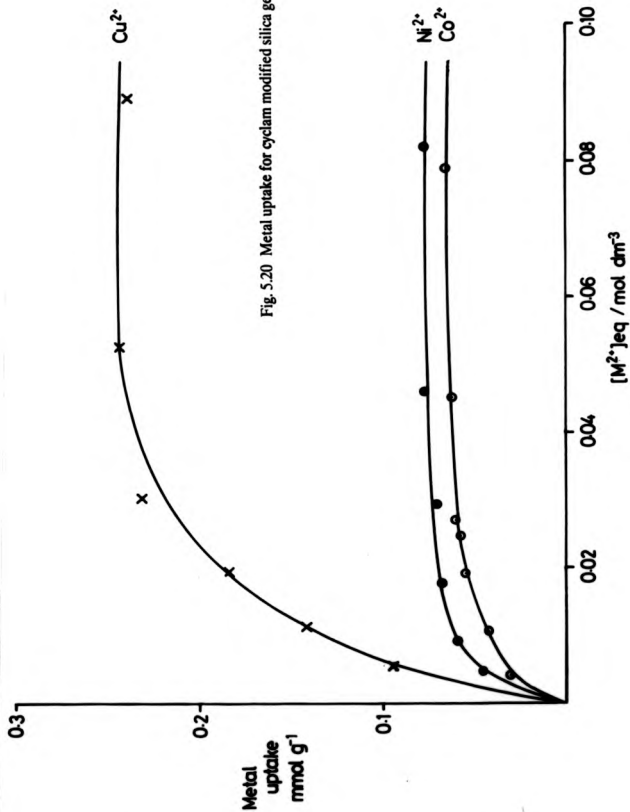


Fig. 5.20 Metal uptake for cyclam modified silica gel.

Table 5.4

Metal Uptake Data for Gel 5		
Metal	max. uptake / mmol g <sup>-1</sup>	% of sites filled
Cu <sup>2+</sup>	0.24	72
Ni <sup>2+</sup>	0.077	23
Co <sup>2+</sup>	0.066	20
cf. ref. 363		
Cu <sup>2+</sup>	0.29	71
Ni <sup>2+</sup>	0.11	27
Co <sup>2+</sup>	0.090	22

These authors also observed a change in binding order for Zn<sup>2+</sup> and Cd<sup>2+</sup> when compared with the free ligand complexes. Thus, it is clear that the solid support has an important effect on the metal binding ability of supported ligands. This factor will certainly be exploited in the future though the preparation of a desired reagent may be difficult to control until the exact nature of the effect of the surfaces is known. Thus, the blocking properties of the surfaces could be used in conjunction with macrocycles, some of which already possess metal ion selectivity, to produce highly selective reagents for particular metals. Indeed, when gel 5 was shaken with an equimolar mixture of Cu<sup>2+</sup>, Ni<sup>2+</sup> and Co<sup>2+</sup> no uptake of Ni<sup>2+</sup> or Co<sup>2+</sup> was detectable, only Cu<sup>2+</sup>. This also suggests that Cu<sup>2+</sup> ions take up the same binding sites as Ni<sup>2+</sup> and Co<sup>2+</sup> or at least restrict access of these ions to other sites. The control of complexation sites on surface supported materials is clearly an important problem to solve as the applications in terms of trace metal uptake, heterogeneous catalysis, chromatography etc. should prove extremely fruitful.

The effect of changing the pore size of the gel used to prepare the silica supported cyclam using method 1 was studied using gels of pore size 60, 100 and 150 Å. Surprisingly little change was observed on the saturation level for Cu<sup>2+</sup> for the three gels with the maximum uptake for the 100 and 150 Å gels both being 0.26 mmol g<sup>-1</sup>.

The reusability of the  $\text{Cu}^{2+}$  complexed cyclam gel 5 was tested by leaching the  $\text{Cu}^{2+}$  out using very strong acid over a number of days at 50 °C. The gel was slightly discoloured after this procedure but repeating the  $\text{Cu}^{2+}$  uptake experiment showed that the level of maximum  $\text{Cu}^{2+}$  uptake was identical to before. The main problem in the rejuvenation of supported macrocyclic ligands is that the very high stability constants of the complexes (free  $\text{Cu}(\text{cyclam})^{2+}$  has  $\log K = 27.2$  in  $\text{H}_2\text{O}$  at 25 °C - see chapter 1) means that severe conditions are required for leaching out of the metal ions to allow reuse of the gels; if this is required, as it would be in heavy metal uptake for waste water treatment. For heterogeneous catalysis the high complex stabilities would prove very advantageous as they would minimise "bleeding" of the metal ions into the reaction medium. Thus, if reusable reagents are required then less stable species may be more usefully studied.

The maximum level of  $\text{Cu}^{2+}$  uptake was measured for all the gels prepared (Table 5.5).

**Table 5.5**

Gel	Maximum Uptake of $\text{Cu}^{2+}$ in gels 1 - 6		
	max. $\text{Cu}^{2+}$ uptake / mmol $\text{g}^{-1}$	% filling of available sites	log K of "free" complexes
1	0.34	42.5	15.8 ( <sup>178</sup> )
2	0.256	40	18.8 ( <sup>162</sup> )
3	0.326	60	21.8 ( <sup>178</sup> )
4	0.551	77	16.2 ( <sup>178</sup> )
5	0.24	72	27.2 ( <sup>178</sup> )
6	0.66	85	27.2 ( <sup>178</sup> )

The percentage of the available binding sites taken up by the  $\text{Cu}^{2+}$  ions did not follow the order of the stabilities of the "free" 1:1 complexes, except that the most stable complex has the biggest uptake of metal at saturation. The low values

for the percentage uptake of  $\text{Cu}^{2+}$  in gels 1 and 2 may indicate that each ion is bound to more than one ligand, which is certainly conceivable for the dien ligand of gel 1. These results again indicate the important effect that the gel surface has on the metal complexations.

Table 5.6 shows the  $\text{Cu}^{2+}$  capacity of various other silica gel immobilized ligands.

The  $\text{Cu}^{2+}$  capacities of the polyamine gels 1 - 6 compare well with previously prepared silica immobilized ligands. Gel 6 in particular shows a large  $\text{Cu}^{2+}$  capacity compared with other complex chelating ligands and in view of the known selectivity patterns of many macrocyclic ligands such supported macrocycles prepared by method 2 may display useful selective metal uptake properties, though these will undoubtedly be affected by the gel surface and the bonding of the ligands through a donor atom. Therefore, selectivity patterns observed in the "free" complexes may be altered in the "bound" complexes. This warrants further investigation.

Table 5.6

$\text{Cu}^{2+}$  capacity of various surface modified silica gels, {Si}-Si-R  
pH 5 - 7, pore size of gel may vary slightly

R =	max. $\text{Cu}^{2+}$ uptake / mmol $\text{g}^{-1}$	ref.
$-(\text{CH}_2)_3\text{NH}_2$	0.56	347
$-\text{Si}(\text{Me})-(\text{CH}_2)_3\text{NH}_2$	0.79	347
$-(\text{CH}_2)_3\text{NH}(\text{CH}_2)_2\text{NH}_2$	0.82	347
$-(\text{CH}_2)_3\text{N}(\text{Me})\text{CS}_2^-$	0.53	268
$-(\text{CH}_2)_3\text{N}(\text{CS}_2)(\text{CH}_2)_2\text{NH}(\text{CS}_2)$	0.97	268
$-(\text{CH}_2)_3\text{NH}(\text{CH}_2)_2\text{NHCOCH}_2\text{COCH}_3$	0.52	330
$-(\text{CH}_2)_3\text{NHCOCH}_2\text{COCH}_3$	0.43	330
$-\text{C}_6\text{H}_4\text{-N} = \text{N-HOQ}$	0.226	348
$-(\text{CH}_2)_3\text{NH-CO-C}_6\text{H}_4\text{-N} = \text{N-HOQ-N}_2\text{C}(\text{NH}_2) = \text{S}$	0.225	349

The metal uptake data can be shown to fit to the Langmuir isotherm. A plot of  $[M^{2+}]_{eq}/\text{uptake}$  vs.  $[M^{2+}]_{eq}$  gives a straight line in all cases, except for gel 6 with  $\text{Cu}^{2+}$ , e.g. figure 5.21, of slope  $1/(\text{total no. of sites})$  and intercept  $1/K(\text{total no. of sites})$  according to the equation;

$$\theta = K [M^{2+}]_{eq} / K [M^{2+}]_{eq} + 1 = \text{uptake of metal}(U) / \text{total no. of sites}(T)$$

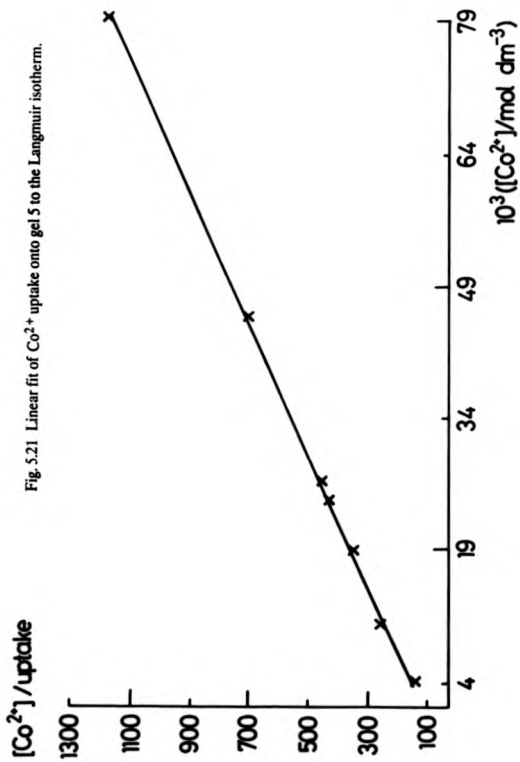
where K is an equilibrium constant relating to the adsorption process.<sup>335</sup> Table 5.7 shows the values of K and T calculated in this way.

Values of T calculated in from the Langmuir isotherm are slightly larger than those measured experimentally in every case. There seems to be no trend between the values of K and T. This is perhaps not too surprising as for K to have any real significance the system under study would have to comply closely with the conditions used in defining the Langmuir isotherm. These state that all adsorption sites are equivalent and that occupied sites do not affect binding in neighbouring sites. K for this process describes a simple adsorbed solvent/solute equilibrium which is clearly inadequate to describe the complicated processes going on the surfaces of the polyamine modified gels.

**Table 5.7**

Data calculated from the Langmuir Isotherm Equation.

Gel	Metal	K $\text{dm}^3 \text{mol}^{-1}$	T <sub>calc</sub> $\text{mmol g}^{-1}$	T <sub>meas</sub> $\text{mmol g}^{-1}$
1	$\text{Cu}^{2+}$	$380.7 \pm 48.4$	$0.346 \pm 0.002$	0.34
2	$\text{Cu}^{2+}$	$282.8 \pm 36.4$	$0.266 \pm 0.003$	0.256
3	$\text{Cu}^{2+}$	$142.7 \pm 26.4$	$0.340 \pm 0.020$	0.326
4	$\text{Cu}^{2+}$	$17.3 \pm 6.1$	$0.583 \pm 0.024$	0.5507
5	$\text{Cu}^{2+}$	$90.3 \pm 15.2$	$0.290 \pm 0.010$	0.24
5	$\text{Ni}^{2+}$	$307.1 \pm 31.0$	$0.080 \pm 0.001$	0.077
5	$\text{Co}^{2+}$	$138.5 \pm 18.0$	$0.073 \pm 0.002$	0.066
6	$\text{Cu}^{2+}$	"Anti-Langmuirian"		0.66



The Langmuir isotherm also assumes surface homogeneity, which is certainly not the case with these systems. Also, the wide range of metal concentrations studied moves out of the region of dilute concentrations required for the Langmuir isotherm. Thus, although like many systems, e.g. adsorption of polymers, gels 1 - 6 display experimental isotherms which can be fitted to the Langmuir equation, the significance of the data yielded is dubious due to the non-conformity of the "real" systems to the Langmuir assumptions. Interestingly gel 6 with  $\text{Cu}^{2+}$  shows anti-Langmuirian characteristics (figure 5.22), perhaps indicating that the initial adsorption of metal ions facilitates the sorption of additional species, suggesting interaction between binding sites, which is conceivable considering the proximity of the ligands on this gel (see Table 5.3).

The U.V./visible diffuse reflectance spectra of the metal/modified gel complexes were measured. Table 5.8 lists the data observed.

Table 5.8

U.V./visible diffuse reflectance data for complexes of gels 1 - 6.

Gel	Metal	$\lambda_{\text{max}} / \text{nm} (\bar{\nu} / \text{cm}^{-1})$
1	$\text{Cu}^{2+}$	628 (15920)
2	$\text{Cu}^{2+}$	658 (15200)
3	$\text{Cu}^{2+}$	590 (16950)
4	$\text{Cu}^{2+}$	652 (15340)
5	$\text{Cu}^{2+}$	530 (18670)
5	$\text{Ni}^{2+}$	458 (21830), 650, 665, 695 (sh)
5	$\text{Co}^{2+}$	460 (21740), 605, 655 (sh)
6	$\text{Cu}^{2+}$	530 (18670)

All the peaks observed were very broad, suggesting that many different but similar environments are present. This may be due to a range of co-ordinating ions being present, apart from the amine ligands, such as  $\text{H}_2\text{O}$ ,  $\text{OH}^-$ ,  $\text{Cl}^-$  (from the synthe-

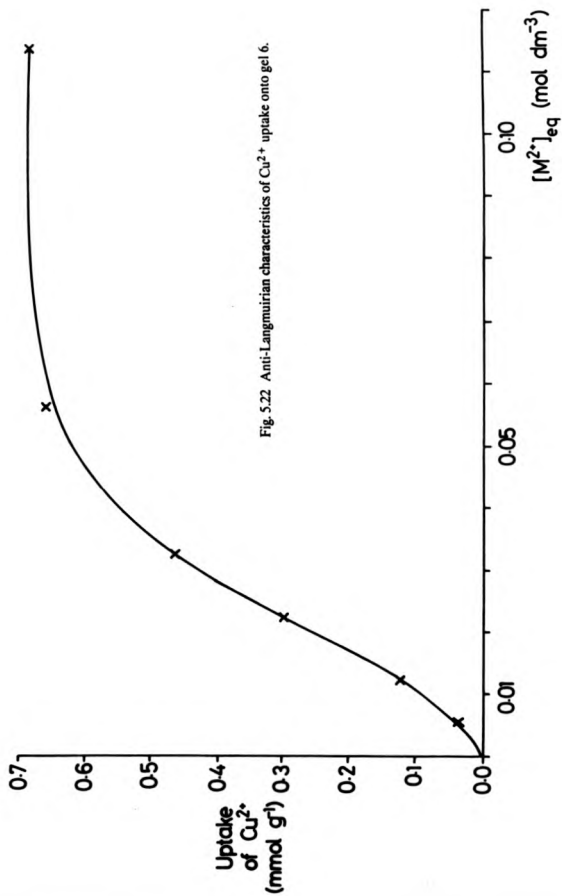
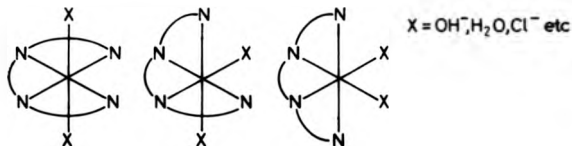


Fig. 5.22 Anti-Langmuirian characteristics of  $\text{Cu}^{2+}$  uptake onto gel 6.

sis) or co-ordinating  $\text{BF}_4^-$ , as well as a range of possible conformations of the various amine ligands, e.g. fac and mer in gel 1. All the environments of the metal complexes studied are consistent with octahedral geometry, except for gel 2. The spectrum for gel 1 suggests that two dien ligands are co-ordinated to each  $\text{Cu}^{2+}$  metal,<sup>350</sup> which is certainly possible considering the proximity of the ligands (see Table 5.3), and also explains the low figure for the percentage filling of the available binding sites (Table 5.5). Since two ligands are co-ordinated to one metal ion then 85 % of the available sites are actually occupied at saturation, showing that the sites are much more accessible than in the other gels prepared by method 1. Gel 2 also show a low figure for the percentage filling of the available binding sites. The reflectance spectrum of the  $\text{Cu}^{2+}$  complex is consistent with the trigonal bipyramidal environment displayed by complexes of the free ligand. However, there is a close similarity between the observed data and the data for an  $(\text{N}_3\text{N})(\text{N}')$  chromophore,<sup>351</sup> suggesting that the fifth, axial co-ordination site is taken up by a nitrogen from an adjacent tren ligand on the modified gel surface. Thus, two ligands are again co-ordinated to one  $\text{Cu}^{2+}$  ion, but this time one of the ligands is not completely bound to the same  $\text{Cu}^{2+}$  ion and may co-ordinate in a similar way to two or three different  $\text{Cu}^{2+}$  ions, each already fully co-ordinated to a tren ligand. Thus, the percentage filling of available sites in Table 5.5 is incorrect as co-ordination is likely to involve a complicated mixture of co-ordination environments, with some tren ligands co-ordinating to different  $\text{Cu}^{2+}$  ions via single nitrogen atoms.

The gel 3 complex with  $\text{Cu}^{2+}$  displays a reflectance spectrum consistent with all four nitrogens from one ligand being bound to one  $\text{Cu}^{2+}$  ion, which is in an octahedral environment. There is no evidence here to suggest interactions between different co-ordination sites, as found for gels 1 and 2, which is in keeping with the low ligand density suggested in Table 5.3. Octahedral 3,2,3-tet complexes possess three different isomers, which may explain the broadness of the peak in the reflectance spectrum.



For gel 4 with Cu<sup>2+</sup> the N<sub>3</sub> macrocyclic ligands can only co-ordinate facially to the metal ion. The reflectance spectrum of this complex suggests that only three nitrogen atoms are bonded per Cu<sup>2+</sup> ion, so that only one ligand is bound to a single Cu<sup>2+</sup> ion, unlike the open-chain analogue in gel 1. This illustrates the inherent steric restraints involved in cyclic systems, making co-ordination of one Cu<sup>2+</sup> ion to two ligands very difficult, despite the reasonably high density of ligands (Table 5.3). Over 3/4 of the sites are occupied by Cu<sup>2+</sup> in this gel, which is consistent with the fairly easy formation of 1:1 complexes compared to 1:2 (metal:ligand).

The reflectance spectrum of the Cu<sup>2+</sup> complex of gel 5 suggests an N<sub>4</sub> chromophore with a strong ligand field complexing with octahedral Cu<sup>2+</sup>. This suggests that cyclam is co-ordinating in the "normal" planar N<sub>4</sub> arrangement, found in the "free" complex. The same characteristics are displayed by the Cu<sup>2+</sup> complex of gel 6, which suggests that no interaction is occurring between the co-ordination sites, which is strange in view of the proximity of the ligands and the anti-Langmuirian metal uptake data. Thus, although site-site interaction probably aids the uptake of Cu<sup>2+</sup> ions, the final, stable complexes may not interact much, suggesting a complex series of processes involved in the complexation reaction.

The Ni<sup>2+</sup> complex of gel 5 displays a reflectance spectrum consistent with the "free" complex except that the peaks are considerably broadened in the solid state. Thus, as in solution (see chapter 2), the complex is a mixture of square planar and octahedral Ni<sup>2+</sup> species, with a planar cyclam co-ordinating. Heating the sample of Ni<sup>2+</sup>/gel caused a decrease in the absorption of the peaks corresponding to the octahedral sites and an increase in the peaks corresponding to the square planar environment, and a yellowing of the material, which is in keeping with the behaviour of the "free" complex, where heating causes loss of the axial monodentate ligands.

The  $\text{Co}^{2+}$  complex of gel 5 displayed an octahedral environment in the reflectance spectrum, and suggested a typical planar co-ordinating cyclam. The "free"  $\text{Co}(\text{cyclam})^{2+}$  complex is very oxygen sensitive (see chapter 2), however, the lack of clarity in the very broad peaks of the reflectance spectrum makes it difficult to decide if the immobilized species is also reacting with oxygen; further work is required to determine this. Certainly if the co-ordination sites were fixed a sufficient distance from each other on the gel surface then the formation of  $\mu$ -peroxo-bridged dimers would be impossible, though the formation of superoxo adducts may still occur.

The surface of the support material can affect the subsequent chemistry carried out on it using immobilized species. The nature of the spacer group will also have an effect, in terms of length and rigidity. Thus, the control of these factors will be of major importance in the surface immobilization of molecules. The choice of support and the conditions of preparation can be used to produce surface modified reagents containing "dilute" or "concentrated" surface species which have important consequences on their chemical behaviour. The use of macrocyclic ligands to modify inorganic oxide surfaces will undoubtedly become important in the future considering the high degrees of stability and selectivity inherent in these ligands. These subjects deserve further study as the reagents formed have a wide range of applications. Environment friendly materials could be prepared for the extraction of toxic metals from waste water, and by using macrocycles some degree of metal selectivity may be achieved which would be of great importance in situations where some metals need to be extracted but others left behind. Similarly the recovery of expensive trace metals used in industry may prove far easier using these kinds of supported chelating ligands. One advantage here being the ease of extraction of the metals from the recovery materials. An important application will be in the field of heterogeneous catalysis, where using "dilute" surface species will avoid reduction in catalytic activity from dimerisation. Many other applications are already being investigated, such as metal ion chromatography,<sup>338</sup> preconcentration of trace metals to aid

sample preparation in X-ray fluorescence spectrometry,<sup>268</sup> and organic synthesis of oligonucleotides.<sup>352</sup> Thus, there is a lot of work remaining to be carried out on these systems, which should prove of great practical value in the future.

### Appendix 1 Rate Data for Chapter 2

All av.  $k_{\text{obs}}$  values are the average of 3 - 14 readings,  $\sigma$  = standard deviation.

$k_{\text{obs1}}$  = observed rate constant for step 1,  $k_{\text{obs2}}$  = observed rate constant for step 2.

#### Data for 2.3.1.

T = 25.0 ± 0.1 °C

[Ni <sup>2+</sup> ] / mol dm <sup>-3</sup>	av. $k_{\text{obs1}} \pm \sigma / \text{s}^{-1}$	av. $k_{\text{obs2}} \pm \sigma / \text{s}^{-1}$
9.3603 × 10 <sup>-3</sup>	15.1867 ± 0.0793	0.5176 ± 0.0735
1.3126 × 10 <sup>-2</sup>	21.2775 ± 0.0823	0.5539 ± 0.0403
1.5748 × 10 <sup>-2</sup>	25.5200 ± 0.3436	0.5221 ± 0.0075

#### Temperature Dependence of Step 1:

[Ni<sup>2+</sup>] = 9.3603 × 10<sup>-3</sup> mol dm<sup>-3</sup>

T / K	av. $k_{\text{obs1}} \pm \sigma / \text{s}^{-1}$
293.2 ± 0.1	11.7317 ± 0.4010
298.2 ± 0.1	15.6400 ± 0.4882
303.4 ± 0.1	23.0333 ± 0.8643
308.6 ± 0.1	32.5488 ± 1.2580
313.2 ± 0.2	44.3700 ± 1.0401

#### Data for 2.3.2.

T = 25.0 ± 0.1 °C

[Ni <sup>2+</sup> ] / mol dm <sup>-3</sup>	av. $k_{\text{obs1}} \pm \sigma / \text{s}^{-1}$	av. $k_{\text{obs2}} \pm \sigma / \text{s}^{-1}$
9.3603 × 10 <sup>-3</sup>	16.2860 ± 0.4082	0.5029 ± 0.0193
1.3126 × 10 <sup>-2</sup>	22.8763 ± 1.6781	0.4847 ± 0.0706
1.5748 × 10 <sup>-2</sup>	27.4400 ± 1.3395	0.4837 ± 0.0997

Temperature Dependence of Step 1:

$$[\text{Ni}^{2+}] = 9.3603 \times 10^{-3} \text{ mol dm}^{-3}$$

T / K	av. $k_{\text{obs1}} \pm \sigma / \text{s}^{-1}$
293.6 $\pm$ 0.2	12.2317 $\pm$ 0.9505
298.2 $\pm$ 0.1	16.2860 $\pm$ 0.4082
303.2 $\pm$ 0.1	20.5160 $\pm$ 0.7887
308.3 $\pm$ 0.1	25.8325 $\pm$ 0.6758
313.4 $\pm$ 0.1	34.8050 $\pm$ 1.3967

Data for 2.3.3.

$$T = 25.0 \pm 0.1 \text{ } ^\circ\text{C}$$

$[\text{Cu}^{2+}] / \text{mol dm}^{-3}$	av. $k_{\text{obs1}} \pm \sigma / \text{s}^{-1}$	av. $k_{\text{obs2}} \pm \sigma / \text{s}^{-1}$
4.6119 $\times 10^{-3}$	24.7283 $\pm$ 1.9972	0.0618 $\pm$ 0.0035
9.1212 $\times 10^{-3}$	48.6500 $\pm$ 0.4228	0.0636 $\pm$ 0.0008
1.3328 $\times 10^{-2}$	73.1150 $\pm$ 2.6841	0.0637 $\pm$ 0.0012

Temperature Dependence of Steps 1 and 2:

$$[\text{Cu}^{2+}] = 4.6119 \times 10^{-3} \text{ mol dm}^{-3}$$

T / K	av. $k_{\text{obs1}} \pm \sigma / \text{s}^{-1}$	av. $k_{\text{obs2}} \pm \sigma / \text{s}^{-1}$
293.4 $\pm$ 0.1	18.5175 $\pm$ 1.3891	4.198 $\times 10^{-2} \pm 4.736 \times 10^{-3}$
298.2 $\pm$ 0.1	24.7283 $\pm$ 1.9972	6.177 $\times 10^{-2} \pm 3.494 \times 10^{-3}$
304.0 $\pm$ 0.1	35.8240 $\pm$ 2.2289	8.857 $\times 10^{-2} \pm 6.089 \times 10^{-3}$
309.2 $\pm$ 0.1	50.7200 $\pm$ 2.6369	1.356 $\times 10^{-1} \pm 1.122 \times 10^{-2}$

Data for 2.3.4.

T = 25.0 ± 0.2 °C

[Cu <sup>2+</sup> ] / mol dm <sup>-3</sup>	av. k <sub>obs1</sub> ± σ / s <sup>-1</sup>	av. k <sub>obs2</sub> ± σ / s <sup>-1</sup>
3.9345 × 10 <sup>-3</sup>	26.1683 ± 1.2307	0.3817 ± 0.0121
8.5421 × 10 <sup>-3</sup>	57.0967 ± 1.0541	0.3994 ± 0.0409
1.2246 × 10 <sup>-2</sup>	82.4450 ± 4.1595	0.3902 ± 0.0294

Temperature Dependence of Step 1:

[Cu<sup>2+</sup>] = 3.9345 × 10<sup>-3</sup> mol dm<sup>-3</sup>

T / K	av. k <sub>obs1</sub> ± σ / s <sup>-1</sup>
294.5 ± 0.1	20.6067 ± 1.7765
298.2 ± 0.2	26.1683 ± 1.2307
303.8 ± 0.1	35.7317 ± 2.0496
308.8 ± 0.2	49.1643 ± 3.7022

Data for 2.3.5.

T = 25.0 ± 0.2 °C

[Co <sup>2+</sup> ] / mol dm <sup>-3</sup>	av. k <sub>obs1</sub> ± σ / s <sup>-1</sup>
2.1446 × 10 <sup>-3</sup>	63.2833 ± 1.5864
4.5286 × 10 <sup>-3</sup>	133.4660 ± 2.2499
6.7282 × 10 <sup>-3</sup>	197.7825 ± 9.4221

Temperature Dependence of Step 1:

[Co<sup>2+</sup>] = 2.1446 × 10<sup>-3</sup> mol dm<sup>-3</sup>

T / K	av. k <sub>obs1</sub> ± σ / s <sup>-1</sup>
294.1 ± 0.1	51.7600 ± 1.2813
298.2 ± 0.2	63.2833 ± 1.5864
304.0 ± 0.1	83.2900 ± 1.4423
308.9 ± 0.1	108.4425 ± 8.4763

Data for 2.3.6.

T = 25.0 ± 0.1 °C

[Co <sup>2+</sup> ] / mol dm <sup>-3</sup>	av. k <sub>obs1</sub> = σ / s <sup>-1</sup>
2.1446 × 10 <sup>-3</sup>	65.8750 ± 1.5230
4.5286 × 10 <sup>-3</sup>	140.8800 ± 1.8929
6.7282 × 10 <sup>-3</sup>	205.7383 ± 9.5301

Temperature Dependence of Step 1:

[Co<sup>2+</sup>] = 2.1446 × 10<sup>-3</sup> mol dm<sup>-3</sup>

T / K	av. k <sub>obs1</sub> = σ / s <sup>-1</sup>
294.0 ± 0.1	51.8960 ± 1.9543
298.2 ± 0.1	65.8750 ± 1.5230
304.2 ± 0.1	91.2540 ± 2.0533
308.1 ± 0.2	113.4640 ± 4.4098

Appendix 2 Rate Data for Chapter 3

Data for 3.3.1.

$$T = 24.8 \pm 0.2 \text{ } ^\circ\text{C}$$

$[\text{Ni}^{2+}] / \text{mol dm}^{-3}$	av. $k_{\text{obs}1} \pm \sigma / \text{s}^{-1}$	av. $k_{\text{obs}2} \pm \sigma / \text{s}^{-1}$
$4.7664 \times 10^{-3}$	$0.7867 \pm 0.0206$	$4.0016 \times 10^{-2} \pm 1.0796 \times 10^{-3}$
$9.4493 \times 10^{-3}$	$1.5633 \pm 0.0741$	$5.0101 \times 10^{-2} \pm 8.1650 \times 10^{-3}$
$1.4584 \times 10^{-2}$	$2.3733 \pm 0.0946$	$5.3333 \times 10^{-2} \pm 4.7140 \times 10^{-3}$

Temperature Dependence of Step 1:

$$[\text{Ni}^{2+}] = 4.7664 \times 10^{-3} \text{ mol dm}^{-3}$$

T / K	av. $k_{\text{obs}1} \pm \sigma / \text{s}^{-1}$
$294.3 \pm 0.1$	$0.6140 \pm 0.0314$
$298.0 \pm 0.2$	$0.7867 \pm 0.0206$
$303.0 \pm 0.1$	$1.0933 \pm 0.0624$
$309.0 \pm 0.1$	$1.6701 \pm 0.0374$

Data for 3.3.2.

$$T = 24.8 \pm 0.1 \text{ } ^\circ\text{C}$$

$[\text{Ni}^{2+}] / \text{mol dm}^{-3}$	av. $k_{\text{obs}1} \pm \sigma / \text{s}^{-1}$	av. $k_{\text{obs}2} \pm \sigma / \text{s}^{-1}$
$5.2120 \times 10^{-3}$	$0.2222 \pm 0.0045$	$0.0533 \pm 0.0021$
$1.0495 \times 10^{-2}$	$0.4350 \pm 0.0101$	$0.0467 \pm 0.0018$
$1.5707 \times 10^{-2}$	$0.6601 \pm 0.0111$	$0.0602 \pm 0.0015$

Temperature Dependence of Step 1:

$$[\text{Ni}^{2+}] = 5.2120 \times 10^{-3} \text{ mol dm}^{-3}$$

T / K	av. $k_{\text{obs1}} \pm \sigma / \text{s}^{-1}$
295.0 $\pm$ 0.1	0.1667 $\pm$ 0.0047
298.0 $\pm$ 0.1	0.2222 $\pm$ 0.0045
303.0 $\pm$ 0.1	0.3333 $\pm$ 0.0047
308.0 $\pm$ 0.1	0.5633 $\pm$ 0.0171
313.4 $\pm$ 0.1	0.8767 $\pm$ 0.1464

Data for 3.3.3.

$$T = 24.9 \pm 0.2 \text{ }^\circ\text{C}$$

$[\text{Co}^{2+}] / \text{mol dm}^{-3}$	av. $k_{\text{obs1}} \pm \sigma / \text{s}^{-1}$	av. $k_{\text{obs2}} \pm \sigma / \text{s}^{-1}$
4.7146 $\times 10^{-3}$	4.4633 $\pm$ 0.0206	0.0703 $\pm$ 0.0011
9.5046 $\times 10^{-3}$	8.7333 $\pm$ 0.0852	0.0733 $\pm$ 0.0013
1.3591 $\times 10^{-2}$	12.6467 $\pm$ 0.0602	0.0733 $\pm$ 0.0013

Temperature Dependence of Step 1:

$$[\text{Co}^{2+}] = 4.7146 \times 10^{-2} \text{ mol dm}^{-3}$$

T / K	av. $k_{\text{obs1}} \pm \sigma / \text{s}^{-1}$
293.1 $\pm$ 0.1	3.3233 $\pm$ 0.3219
298.1 $\pm$ 0.2	4.4633 $\pm$ 0.0206
303.5 $\pm$ 0.2	6.0901 $\pm$ 0.1849
308.0 $\pm$ 0.2	7.8903 $\pm$ 0.2299

**Data for 3.3.4.**

$T = 24.8 \pm 0.1 \text{ }^\circ\text{C}$

$[\text{Co}^{2+}] / \text{mol dm}^{-3}$	av. $k_{\text{obs}1} \pm \sigma / \text{s}^{-1}$	av. $k_{\text{obs}2} \pm \sigma / \text{s}^{-1}$
$5.2991 \times 10^{-3}$	$15.2202 \pm 0.0909$	$0.1100 \pm 0.0082$
$1.0188 \times 10^{-2}$	$29.0233 \pm 0.2696$	$0.1133 \pm 0.0047$
$1.5237 \times 10^{-2}$	$42.6133 \pm 0.3387$	$0.1067 \pm 0.0047$

**Temperature Dependence of Step 1:**

$[\text{Co}^{2+}] = 5.2991 \times 10^{-3} \text{ mol dm}^{-3}$

$T / \text{K}$	av. $k_{\text{obs}1} \pm \sigma / \text{s}^{-1}$
$293.8 \pm 0.1$	$11.2400 \pm 0.0735$
$298.0 \pm 0.1$	$15.2202 \pm 0.0909$
$303.0 \pm 0.1$	$21.1925 \pm 1.5416$
$307.8 \pm 0.1$	$28.0605 \pm 0.7636$

**Data for 3.3.5.**

no data obtained, see 3.3.5.

**Data for 3.3.6.**

$T = 25.2 \pm 0.2 \text{ }^\circ\text{C}$

$[\text{Cu}^{2+}] / \text{mol dm}^{-3}$	av. $k_{\text{obs}1} \pm \sigma / \text{s}^{-1}$	av. $k_{\text{obs}2} \pm \sigma / \text{s}^{-1}$
$1.1630 \times 10^{-4}$	$48.5970 \pm 1.7199$	$1.3267 \pm 0.0135$
$2.3861 \times 10^{-4}$	$76.6261 \pm 7.8386$	$1.3533 \pm 0.0101$
$3.5221 \times 10^{-4}$	$107.6253 \pm 8.2791$	$1.3301 \pm 0.0118$

**Data for 3.3.7.**

Temperature Dependence of Step 1:

Values of  $k_{\text{obs}1}$  at various temperatures.

$[\text{Zn}^{2+}] / \text{mol dm}^{-3}$	$4.2522 \times 10^{-4}$	$9.0801 \times 10^{-4}$	$1.2629 \times 10^{-3}$
T / K			
$293.6 \pm 0.1$	$8.1567 \pm 0.9832$	$12.2683 \pm 0.5801$	$15.3600 \pm 0.4462$
$298.0 \pm 0.1$	$10.2567 \pm 0.2894$	$16.2475 \pm 0.5712$	$20.3250 \pm 0.7694$
$305.0 \pm 0.1$	$14.1517 \pm 0.6664$	$23.3325 \pm 0.8352$	$30.4280 \pm 0.3887$
$308.0 \pm 0.1$	$16.3525 \pm 0.3548$	$27.5367 \pm 0.8416$	$35.9780 \pm 0.9318$

Step 2:

$[\text{Zn}^{2+}] / \text{mol dm}^{-3}$	av. $k_{\text{obs}2} \pm \sigma / \text{s}^{-1}$
$4.2522 \times 10^{-4}$	$0.7604 \pm 0.0495$
$8.5354 \times 10^{-4}$	$0.7902 \pm 0.0245$
$1.2619 \times 10^{-3}$	$0.7533 \pm 0.0171$

**Data for 3.3.8.**

Temperature Dependence of Step 1:

Values of  $k_{\text{obs}1}$  at various temperatures.

$[\text{Zn}^{2+}] / \text{mol dm}^{-3}$	$4.2522 \times 10^{-4}$	$8.5352 \times 10^{-4}$	$1.26189 \times 10^{-3}$
T / K			
$294.0 \pm 0.1$	$8.5425 \pm 0.2496$	$12.6200 \pm 0.6036$	$16.3340 \pm 0.2651$
$298.0 \pm 0.1$	$10.3233 \pm 0.3058$	$15.7520 \pm 0.5683$	$20.7633 \pm 0.6074$
$303.0 \pm 0.1$	$13.6802 \pm 0.0572$	$21.5261 \pm 0.5355$	$28.9475 \pm 0.7566$
$308.6 \pm 0.1$	$17.7567 \pm 0.0896$	$28.8020 \pm 1.0775$	$39.4701 \pm 0.6732$
$313.4 \pm 0.1$	$23.0267 \pm 0.7519$	$38.7433 \pm 0.1489$	$53.5751 \pm 0.8191$

Step 2:

$T = 24.8 \pm 0.1 \text{ } ^\circ\text{C}$

$[\text{Zn}^{2+}] / \text{mol dm}^{-3}$	av. $k_{\text{obs}2} \pm \sigma / \text{s}^{-1}$
$4.2522 \times 10^{-4}$	$0.1967 \pm 0.0125$
$8.5352 \times 10^{-4}$	$0.2067 \pm 0.0125$
$1.2619 \times 10^{-3}$	$0.1833 \pm 0.0125$

Temperature Dependence of Step 2:

T / K	av. $k_{\text{obs}2} \pm \sigma / \text{s}^{-1}$
$294.0 \pm 0.1$	$0.0925 \pm 0.0025$
$298.0 \pm 0.1$	$0.1967 \pm 0.0170$
$303.0 \pm 0.1$	$0.4431 \pm 0.0276$
$308.6 \pm 0.1$	$1.1789 \pm 0.0595$

**Data for 3.3.9.**

no data obtained, see 3.3.9.

Appendix 3 Rate Data for Chapter 4

Data for 4.3.1.

T = 25.0 ± 0.1 °C

[Ni <sup>2+</sup> ]/mol dm <sup>-3</sup>	av. $k_{\text{obs1}} \pm \sigma / \text{s}^{-1}$	av. $k_{\text{obs2}} \pm \sigma / \text{s}^{-1}$
4.8253 × 10 <sup>-3</sup>	2.1075 ± 0.0981	0.0357 ± 0.0015
9.6809 × 10 <sup>-3</sup>	4.2575 ± 0.1096	0.0377 ± 0.0019
1.3569 × 10 <sup>-2</sup>	5.9540 ± 0.2778	0.0329 ± 0.0021

Temperature Dependence of Step 1:

[Ni<sup>2+</sup>] = 4.8253 × 10<sup>-3</sup> mol dm<sup>-3</sup>

T / K	av. $k_{\text{obs1}} \pm \sigma / \text{s}^{-1}$
293.3 ± 0.1	1.1720 ± 0.0977
298.2 ± 0.1	2.1075 ± 0.0981
303.7 ± 0.1	3.8183 ± 0.2696
308.7 ± 0.1	6.9600 ± 0.6923

Data for 4.3.2.

T = 25.0 ± 0.2 °C

[Ni <sup>2+</sup> ]/mol dm <sup>-3</sup>	av. $k_{\text{obs1}} \pm \sigma / \text{s}^{-1}$	av. $k_{\text{obs2}} \pm \sigma / \text{s}^{-1}$
4.6176 × 10 <sup>-3</sup>	2.0867 ± 0.1637	0.0127 ± 0.0047
9.6809 × 10 <sup>-3</sup>	4.2701 ± 0.4179	0.0132 ± 0.0047
1.3569 × 10 <sup>-2</sup>	6.0525 ± 0.1445	0.0123 ± 0.0047

Temperature Dependence of Step 1:

$$[\text{Ni}^{2+}] = 4.6176 \times 10^{-3} \text{ mol dm}^{-3}$$

T / K	av. $k_{\text{obs1}} \pm \sigma / \text{s}^{-1}$
292.2 $\pm$ 0.1	1.0533 $\pm$ 0.0386
298.2 $\pm$ 0.2	2.0867 $\pm$ 0.1637
303.0 $\pm$ 0.1	3.3680 $\pm$ 0.1588
308.4 $\pm$ 0.1	5.9451 $\pm$ 0.2471

Data for 4.3.3.

$$T = 25.0 \pm 0.1 \text{ } ^\circ\text{C}$$

$[\text{Ni}^{2+}] / \text{mol dm}^{-3}$	av. $k_{\text{obs1}} \pm \sigma / \text{s}^{-1}$	av. $k_{\text{obs2}} \pm \sigma / \text{s}^{-1}$
4.4157 $\times 10^{-3}$	8.1617 $\pm$ 0.7031	0.0134 $\pm$ 0.0005
9.1635 $\times 10^{-3}$	16.9538 $\pm$ 0.6640	0.0136 $\pm$ 0.0004
1.3255 $\times 10^{-2}$	24.4863 $\pm$ 1.9272	0.0127 $\pm$ 0.0005

Temperature Dependence of Step 1:

$$[\text{Ni}^{2+}] = 4.4157 \times 10^{-3} \text{ mol dm}^{-3}$$

T / K	av. $k_{\text{obs1}} \pm \sigma / \text{s}^{-1}$
293.2 $\pm$ 0.1	4.4900 $\pm$ 0.3315
298.2 $\pm$ 0.1	8.1617 $\pm$ 0.7031
303.5 $\pm$ 0.1	14.9173 $\pm$ 1.200
308.2 $\pm$ 0.1	27.1017 $\pm$ 1.5224

Data for 4.3.4.

$$T = 25.0 \pm 0.1 \text{ } ^\circ\text{C}$$

$[\text{Co}^{2+}] / \text{mol dm}^{-3}$	av. $k_{\text{obs1}} \pm \sigma / \text{s}^{-1}$	av. $k_{\text{obs2}} \pm \sigma / \text{s}^{-1}$
4.7335 $\times 10^{-3}$	9.5510 $\pm$ 0.0302	0.0467 $\pm$ 0.0047
1.0116 $\times 10^{-2}$	20.0102 $\pm$ 0.4253	0.0567 $\pm$ 0.0047
1.5550 $\times 10^{-2}$	29.4867 $\pm$ 0.6512	0.0501 $\pm$ 0.0082

Temperature Dependence of Step 1:

$$[\text{Co}^{2+}] = 8.3928 \times 10^{-3} \text{ mol dm}^{-3}$$

T / K	av. $k_{\text{obs1}} \pm \sigma / \text{s}^{-1}$
293.8 $\pm$ 0.1	11.4922 $\pm$ 1.2214
298.2 $\pm$ 0.1	15.7833 $\pm$ 1.1345
303.4 $\pm$ 0.1	23.3003 $\pm$ 1.4287
308.1 $\pm$ 0.1	31.2475 $\pm$ 1.6281

Data for 4.3.5.

$$T = 25.0 \pm 0.1 \text{ } ^\circ\text{C}$$

$[\text{Co}^{2+}] / \text{mol dm}^{-3}$	av. $k_{\text{obs1}} \pm \sigma / \text{s}^{-1}$	av. $k_{\text{obs2}} \pm \sigma / \text{s}^{-1}$
4.8222 $\times 10^{-3}$	8.6667 $\pm$ 0.4725	0.3275 $\pm$ 0.0540
9.7072 $\times 10^{-3}$	17.9281 $\pm$ 1.6106	0.3300 $\pm$ 0.0163
1.4914 $\times 10^{-2}$	27.3275 $\pm$ 0.9149	0.3467 $\pm$ 0.0047

Temperature Dependence of Steps 1 and 2:

$$[\text{Co}^{2+}] = 4.8222 \times 10^{-3} \text{ mol dm}^{-3}$$

T / K	av. $k_{\text{obs1}} \pm \sigma / \text{s}^{-1}$	av. $k_{\text{obs2}} \pm \sigma / \text{s}^{-1}$
293.8 $\pm$ 0.1	5.8567 $\pm$ 0.3363	0.2167 $\pm$ 0.0094
298.2 $\pm$ 0.1	8.6666 $\pm$ 0.4725	0.3275 $\pm$ 0.0540
303.9 $\pm$ 0.1	13.6567 $\pm$ 0.3654	0.5950 $\pm$ 0.0229
307.5 $\pm$ 0.2	19.4620 $\pm$ 0.4511	0.8667 $\pm$ 0.0451

Data for 4.4.6.

$$T = 25.0 \pm 0.1 \text{ } ^\circ\text{C}$$

$[\text{Co}^{2+}] / \text{mol dm}^{-3}$	av. $k_{\text{obs1}} \pm \sigma / \text{s}^{-1}$	av. $k_{\text{obs2}} \pm \sigma / \text{s}^{-1}$
4.6071 $\times 10^{-3}$	1.5840 $\pm$ 0.1728	0.0202 $\pm$ 0.0029
9.7072 $\times 10^{-3}$	3.3367 $\pm$ 0.3091	0.0202 $\pm$ 0.0017
1.4914 $\times 10^{-2}$	5.1933 $\pm$ 0.4251	0.0196 $\pm$ 0.0031

Temperature Dependence of Step 1:

T / K	av. $k_{\text{obs1}} \pm \sigma / \text{s}^{-1}$
292.3 $\pm$ 0.1	0.7762 $\pm$ 0.1432
298.2 $\pm$ 0.1	1.5840 $\pm$ 0.1728
303.9 $\pm$ 0.1	3.4082 $\pm$ 0.3855
308.6 $\pm$ 0.1	5.5485 $\pm$ 0.0621

Data for 4.3.7.

T = 25.0  $\pm$  0.1 °C

[Cu <sup>2+</sup> ] / mol dm <sup>-3</sup>	av. $k_{\text{obs1}} \pm \sigma / \text{s}^{-1}$
4.5013 $\times$ 10 <sup>-3</sup>	70.5269 $\pm$ 3.8490
9.0874 $\times$ 10 <sup>-3</sup>	93.6322 $\pm$ 4.4908
1.3316 $\times$ 10 <sup>-2</sup>	115.1850 $\pm$ 1.6358

Data for 4.3.8.

Temperature Dependence of Step 1:

Values of  $k_{\text{obs1}}$  at various temperatures.

[Cu <sup>2+</sup> ] / mol dm <sup>-3</sup>	4.4793 $\times$ 10 <sup>-3</sup>	8.8437 $\times$ 10 <sup>-3</sup>	1.2860 $\times$ 10 <sup>-2</sup>
T / K			
294.0 $\pm$ 0.1	47.1520 $\pm$ 2.0821	59.5191 $\pm$ 1.9702	72.6067 $\pm$ 3.5798
298.3 $\pm$ 0.1	64.1175 $\pm$ 2.8922	82.4101 $\pm$ 4.0388	100.1040 $\pm$ 5.0714
303.5 $\pm$ 0.1	92.4257 $\pm$ 11.5672	119.2633 $\pm$ 4.5320	146.2133 $\pm$ 3.0461
308.3 $\pm$ 0.1	126.5667 $\pm$ 7.5489	164.6527 $\pm$ 6.9683	206.4560 $\pm$ 6.1747

Step 2:

[Cu <sup>2+</sup> ] / mol dm <sup>-3</sup>	av. $k_{\text{obs2}} \pm \sigma / \text{s}^{-1}$
4.4793 $\times$ 10 <sup>-3</sup>	8.2403 $\times$ 10 <sup>-3</sup> $\pm$ 1.1501 $\times$ 10 <sup>-3</sup>
8.8437 $\times$ 10 <sup>-3</sup>	1.1617 $\times$ 10 <sup>-2</sup> $\pm$ 4.4900 $\times$ 10 <sup>-4</sup>
1.2860 $\times$ 10 <sup>-2</sup>	9.5423 $\times$ 10 <sup>-3</sup> $\pm$ 1.3865 $\times$ 10 <sup>-3</sup>

Data for 4.3.9.

Temperature Dependence of Step 1:

Values of  $k_{\text{obs1}}$  at various temperatures.

$[\text{Cu}^{2+}] / \text{mol dm}^{-3}$	$4.5013 \times 10^{-3}$	$8.8437 \times 10^{-3}$	$1.2860 \times 10^{-2}$
T / K			
293.1 ± 0.1	39.1018 ± 2.1981	60.4543 ± 2.2732	80.6640 ± 3.5509
298.3 ± 0.1	47.1802 ± 3.1426	73.7521 ± 2.5164	99.7301 ± 3.4496
303.7 ± 0.1	55.0767 ± 0.5056	89.6920 ± 1.9772	119.7950 ± 1.2680
308.7 ± 0.1	66.1233 ± 1.7291	110.1325 ± 1.9811	148.2302 ± 2.8478

Step 2:

$[\text{Cu}^{2+}] / \text{mol dm}^{-3}$	av. $k_{\text{obs2}} \pm \sigma / \text{s}^{-1}$
$4.5013 \times 10^{-3}$	0.2525 ± 0.0262
$8.8437 \times 10^{-3}$	0.2594 ± 0.0088
$1.2860 \times 10^{-2}$	0.2648 ± 0.0177

### References

- 1 J. J. Christensen, D. J. Eatough, and R. M. Izatt, *Chem. Rev.*, 1974, **74**, 351.
- 2 G. R. Newkome, J. D. Sauer, J. M. Roper, and D. C. Hager, *Chem. Rev.*, 1977, **77**, 513.
- 3 J. S. Bradshaw, G. E. Maas, R. M. Izatt, and J. J. Christensen, *Chem. Rev.*, 1979, **79**, 37.
- 4 J. S. Bradshaw and J. Y. K. Hui, *J. Heterocyclic Chem.*, 1974, **11**, 649.
- 5 D. St. C. Black and A. J. Hartshorn, *Coord. Chem. Rev.*, 1972/3, **9**, 219.
- 6 L. F. Lindoy, *Chem. Soc. Rev.*, 1975, **4**, 421.
- 7 R. M. Izatt and J. J. Christensen (Eds.), *Synthetic Multidentate Macrocyclic Ligands*, Academic Press, New York, 1978.
- 8 F. Vögtle and E. Weber (Eds.), *Host Guest Complex Chemistry*, Springer-Verlag, Berlin, 1985.
- 9 G. A. Melson (Ed.), *Co-ordination Chemistry of Macrocyclic Compounds*, Plenum, New York, 1979.
- 10 R. M. Izatt and J. J. Christensen (Eds.), *Progress in Macrocyclic Chemistry* Vol. I, Wiley, New York, 1985.
- 11 R. M. Izatt and J. J. Christensen (Eds.), *Progress in Macrocyclic Chemistry* Vol. II, Wiley, New York, 1986.
- 12 R. M. Izatt and J. J. Christensen (Eds.), *Progress in Macrocyclic Chemistry*, Vol. III, Wiley, New York, 1987.
- 13 D. H. Busch, *Science*, 1971, **171**, 241.
- 14 D. H. Busch, K. Farmery, U. Goedken, U. Katovic, A. C. Melnyk, C. R. Sperati, and N. Tokel, *Adv. Chem. Ser.*, 1971, **100**, 44.
- 15 J. J. Christensen, J. O. Hill, and R. M. Izatt, *Science*, 1971, **174**, 459.
- 16 N. F. Curtis, *Coord. Chem. Rev.*, 1968, **3**, 3.
- 17 D. E. Fenton, *Adv. Inorg. Bioinorg. Mech.*, Vol. 2, A. G. Sykes, Ed., Academic Press, London, 1983, 187.

- 18 T. A. Kaden, *Top. Curr. Chem.*, 1984, 121, 157.
- 19 J. M. Lehn, *Struct. Bond.*, 1973, 16, 1.
- 20 J. M. Lehn, *Pure Appl. Chem.*, 1977, 49, 857.
- 21 J. M. Lehn, *Pure Appl. Chem.*, 1978, 50, 871.
- 22 J. M. Lehn, *Acc. Chem. Res.*, 1978, 11, 49.
- 23 J. M. Lehn, *Pure Appl. Chem.*, 1980, 52, 2441.
- 24 T. J. Meade and D. H. Busch, *Prog. Inorg. Chem.*, 1985, 33, 59.
- 25 C. J. Pedersen and H. K. Frensdorff, *Angew. Chem., Int. Ed. Engl.*, 1972, 11, 16.
- 26 R. Bhula, P. Osvath, and D. C. Weatherburn, *Coord. Chem. Rev.*, 1988, 91, 89.
- 27 L. Fabbrizzi, *Comments Inorg. Chem.*, 1985, 4, 33.
- 28 G. W. Gokel, D. M. Dishong, R. A. Schultz, and V. J. Gotto, *Synthesis*, 1982, 997.
- 29 S. M. Nelson, *Pure Appl. Chem.*, 1980, 52, 2461.
- 30 B. Dietrich, *J. Chem. Educat.*, 1985, 62, 954.
- 31 E. Kimura, *J. Coord. Chem.*, 1986, 15, 1.
- 32 E. Kimura, *Top. Curr. Chem.*, 1985, 128, 114.
- 33 S. T. Jolley, J. S. Bradshaw, and R. M. Izatt, *J. Heterocycl. Chem.*, 1982, 19, 3.
- 34 J. B. Bremner, E. J. Browne, and I. W. K. Gunawardana, *Heterocycles*, 1982, 19, 709.
- 35 G. W. Gokel and S. H. Korzeniowski, *Macrocyclic Polyether Synthesis*, Springer, Heidelberg, 1982.
- 36 M. Nonoyama and K. Nonoyama, *Kagaku (Kyoto)*, 1980, 35, 884.
- 37 E. Kimura, *Kagaku No Ryoiki*, 1981, 35, 865.
- 38 E. Kimura, *Yakugaku Zasshi*, 1982, 102, 701.
- 39 E. Kimura, *Kuki Gosei Kagaku Kyokaiishi*, 1986, 44, 871.
- 40 M. Nonoyama and J. Fujita, *Kagaku (Kyoto)*, 1982, 37, 250.
- 41 P. Chaudhuri and K. Wieghardt, *Prog. Inorg. Chem.*, 1987, 35, 329.
- 42 M. Eigen, *Pure Appl. Chem.*, 1963, 6, 97.
- 43 M. Eigen in 'Advances in the Chemistry of Co-ordination Compounds', S.

- Kirschner, Ed., The Macmillan Co., New York, 1961, 373.
- 44 M. Eigen and K. Tamm, *Z. Electrochem.*, 1962, 66, 93 and 107.
- 45 M. Eigen and R. G. Wilkins, *Adv. Chem. Ser.*, 1965, 42, 55.
- 46 R. G. Wilkins, *Acc. Chem. Res.*, 1970, 3, 408.
- 47 R. M. Fuoss, *J. Am. Chem. Soc.*, 1958, 80, 5059.
- 48 H. Hoffmann, *Pure Appl. Chem.*, 1975, 41, 327.
- 49 R. M. Fuoss and F. Accascina, *Electrolytic Conductance*, Interscience, New York, 1959.
- 50 R. W. Gurney, *Ionic Processes in Solutions*, Dover Publications, New York, 1953.
- 51 D. B. Rorabacher, *Inorg. Chem.*, 1966, 5, 1891.
- 52 G. G. Hammes and J. I. Steinfeld, *J. Am. Chem. Soc.*, 1962, 84, 4639.
- 53 R. G. Wilkins, *Inorg. Chem.*, 1964, 3, 520.
- 54 R. G. Pearson and P. Ellgen, *Inorg. Chem.*, 1967, 6, 1379.
- 55 L. Hertli and T. A. Kaden, *Helv Chim. Acta*, 1981, 64, 33.
- 56 P. J. Nichols and M. W. Grant, *Aust. J. Chem.*, 1978, 31, 2581.
- 57 J. F. Coetzee and E. Hsu, *J. Solution Chem.*, 1975, 4, 45.
- 58 J. Williams, S. Petrucci, B. Sesta, and M. Battistini, *Inorg. Chem.*, 1974, 13, 1968.
- 59 D. B. Rorabacher and C. A. Melendez-Cepeda, *J. Am. Chem. Soc.*, 1971, 93, 6071.
- 60 W. R. Muir and C. H. Langford, *J. Am. Chem. Soc.*, 1967, 89, 3141.
- 61 J. Neely and R. E. Connick, *J. Am. Chem. Soc.*, 1970, 92, 3476.
- 62 E. F. Caldin and H. P. Bennetto, *J. Chem. Soc. (A)*, 1971, 2191.
- 63 E. F. Caldin and H. P. Bennetto, *J. Chem. Soc. (A)*, 1971, 2198.
- 64 H. P. Bennetto and Z. S. Imani, *J. Chem. Soc., Faraday Trans. 1*, 1975, 71, 1143.
- 65 P. K. Chattopadhyay and J. F. Coetzee, *Inorg. Chem.*, 1973, 12, 113.
- 66 J. Burgess, *Ions in Solution*, Ellis Horwood Ltd., Chichester, 1988.

- 67 K. Kustin, R. F. Pasternack, and E. M. Weinstock, *J. Am. Chem. Soc.*, 1966, 88, 4610.
- 68 D. W. Margerum, G. R. Cayley, D. C. Weatherburn, and G. K. Pagenkopf, *ACS Monogr.* No. 174, 1978, 1.
- 69 D. W. Margerum, D. B. Rorabacher, and J. F. G. Clarke, Jr., *Inorg. Chem.*, 1963, 2, 667.
- 70 T. S. Turan and D. B. Rorabacher, *Inorg. Chem.*, 1972, 11, 288.
- 71 F. Basolo and R. G. Pearson, *Mechanisms of Inorganic Reactions*, John Wiley and Sons, Inc., New York, 1967.
- 72 C. K. Ingold, R. S. Nyholm, and M. L. Tobe, *Nature*, (London), 1962, 194, 344.
- 73 T. S. Turan, *Inorg. Chem.*, 1974, 13, 1584.
- 74 R. B. Jordan, *Inorg. Chem.*, 1976, 15, 748.
- 75 R. W. Taylor, H. K. Stepion, and D. B. Rorabacher, *Inorg. Chem.*, 1974, 13, 128.
- 76 R. F. Pasternack, M. Angwin, L. Gripp, and R. Reingold, *J. Inorg. Nucl. Chem.*, 1972, 34, 2329.
- 77 A. Kowalak, K. Kustin, R. F. Pasternack, and S. Petrucci, *J. Am. Chem. Soc.*, 1967, 89, 3126.
- 78 W. B. Makinen, A. F. Pearlmutter and J. Stuehr, *J. Am. Chem. Soc.*, 1969, 91, 4083.
- 79 C. Lin and D. B. Rorabacher, *Inorg. Chem.*, 1973, 12, 2402.
- 80 R. G. Wilkins, *Acc. Chem. Res.*, 1970, 3, 408.
- 81 J. P. Jones, E. J. Billo, and D. W. Margerum, *J. Am. Chem. Soc.*, 1970, 92, 1875.
- 82 A. G. Desai, H. W. Dodgen, and J. P. Hunt, *J. Am. Chem. Soc.*, 1970, 92, 798.
- 83 A. G. Desai, H. W. Dodgen, and J. P. Hunt, *J. Am. Chem. Soc.*, 1969, 91, 5001.
- 84 J. P. Hunt, *Coord. Chem. Rev.*, 1971, 7, 1.
- 85 R. L. Wilder, D. A. Kamp, and C. S. Garner, *Inorg. Chem.*, 1971, 10, 1393.
- 86 R. Holyer, C. D. Hubbard, S. F. A. Kettle, and R. G. Wilkins, *Inorg. Chem.*, 1965, 4, 929.

- 87 R. Holyer, C. D. Hubbard, S. F. A. Kettle, and R. G. Wilkins, *Inorg. Chem.*, 1966, 5, 622.
- 88 M. Hiraoka, *Crown Compounds*, Kodansha, Tokyo, 1982.
- 89 ref. 10, chapter 4.
- 90 D. W. Margerum and H. M. Rosen, *Inorg. Chem.*, 1968, 7, 299.
- 91 G. K. Pagenkopf and D. W. Margerum, *Inorg. Chem.*, 1968, 7, 2514.
- 92 C. K. Poon, *Coord. Chem. Rev.*, 1973, 10, 1.
- 93 C. Lin, D. B. Rorabacher, G. R. Cayley, and D. W. Margerum, *Inorg. Chem.*, 1975, 14, 919.
- 94 J. Roper and H. Elias, *Abstracts of the 12th International Symposium on Macrocyclic Chemistry*, Hiroshima, Japan, July 1987, Paper P4.10.
- 95 R. W. Hay and P. R. Norman, *Inorg. Chim. Acta*, 1980, 45, L139.
- 96 A. P. Leugger, L. Hertli, and T. A. Kaden, *Helv Chim. Acta*, 1978, 61, 2296.
- 97 J. Burgess, *Metal Ions in Solution*, Ellis Horwood Ltd., Chichester, 1978.
- 98 M. Kodama and E. Kimura, *J. Chem. Soc., Chem. Commun.*, 1975, 326.
- 99 M. Kodama and E. Kimura, *J. Chem. Soc., Chem. Commun.*, 1975, 891.
- 100 M. Kodama and E. Kimura, *J. Chem. Soc., Dalton Trans.*, 1976, 1720.
- 101 M. Kodama and E. Kimura, *J. Chem. Soc., Dalton Trans.*, 1976, 2341.
- 102 M. Kodama and E. Kimura, *J. Chem. Soc., Dalton Trans.*, 1977, 1473.
- 103 M. Kodama and E. Kimura, *J. Chem. Soc., Dalton Trans.*, 1976, 116.
- 104 M. Kodama and E. Kimura, *J. Chem. Soc., Dalton Trans.*, 1977, 2269.
- 105 T. J. Riedo and T. A. Kaden, *Helv Chim. Acta*, 1979, 62, 1089.
- 106 M. Kodama and E. Kimura, *J. Chem. Soc., Dalton Trans.*, 1978, 104.
- 107 W. Steinmann and T. A. Kaden, *Helv Chim. Acta*, 1975, 58, 1358.
- 108 R. Buxtorf and T. A. Kaden, *Helv Chim. Acta*, 1974, 57, 1035.
- 109 E. K. Barefield and F. Wagner, *Inorg. Chem.*, 1973, 12, 2435.
- 110 M. J. D'Aniello, Jr., M. T. Mocella, F. Wagner, E. K. Barefield, and I. C. Paul, *J. Am. Chem. Soc.*, 1975, 97, 192.
- 111 D. K. Cabbiness and D. W. Margerum, *J. Am. Chem. Soc.*, 1970, 92, 2151.

- 112 P. Schultz-Grunow and T. A. Kaden, *Helv Chim. Acta*, 1978, 61, 2291.
- 113 D. Klaehn, H. Paulus, R. Grewe, and H. Elias, *Inorg. Chem.*, 1984, 23, 483.
- 114 P. Tschudi, PhD thesis, Universita t Basel, 1976.
- 115 L. Fabbrizzi, T. A. Kaden, A. Perotti, B. Seghi, and L. Siegfried, *Inorg. Chem.*, 1986, 25, 321.
- 116 M. Kodama and E. Kimura, *J. Chem. Soc., Dalton Trans.*, 1979, 325.
- 117 M. Kodama and E. Kimura, *Yuki Gosei Kagaku*, 1977, 35, 632.
- 118 T. A. Kaden, *Helv Chim. Acta*, 1970, 53, 617.
- 119 B. Bosnich, C. K. Poon, and M. L. Tobe, *Inorg. Chem.*, 1965, 4, 1102.
- 120 C. S. Kallianou and T. A. Kaden, *Helv Chim. Acta*, 1979, 62, 2562.
- 121 L. L. Diaddario, L. L. Zimmer, T. E. Jones, L. S. W. L. Sokol, R. B. Cruz, E. L. Lee, L. A. Ochrymowycz, and D. B. Rorabacher, *J. Am. Chem. Soc.*, 1979, 101, 3511.
- 122 R. G. Wilkins, *Pure Appl. Chem.*, 1973, 33, 583.
- 123 A. Ekstrom, L. F. Lindoy, H. C. Lip, R. J. Smith, H. J. Goodwin, M. McPartlin, and P. A. Tasker, *J. Chem. Soc., Dalton Trans.*, 1979, 1027.
- 124 R. Buxtorf, W. Steinmann, and T. A. Kaden, *Chimia*, 1974, 28, 15.
- 125 T. A. Kaden, *Chimia*, 1976, 30, 207.
- 126 T. A. Kaden, *Helv Chim. Acta*, 1971, 54, 2307.
- 127 L. Hertli and T. A. Kaden, *Helv Chim. Acta*, 1974, 57, 1328.
- 128 R. W. Hay, *Bio-inorganic Chemistry*, Ellis Horwood Ltd., London, 1984.
- 129 D. B. Rorabacher, M. M. Bernardo, A. M. O. Vande Linde, G. H. Leggett, B. C. Westerby, M. J. Martin, and L. A. Ochrymowycz, *Pure Appl. Chem.*, 1988, 60, 501.
- 130 T. E. Jones, L. L. Zimmer, L. L. Diaddario, D. B. Rorabacher, and L. A. Ochrymowycz, *J. Am. Chem. Soc.*, 1975, 97, 7163.
- 131 R. F. Pasternack and K. Kustin, *J. Am. Chem. Soc.*, 1968, 90, 2295.
- 132 E. Grell, T. Funck, and F. Eggers, *Membranes*, 1975, 3, 1.
- 133 M. Eigen and R. Winkler, *The Neurosciences*, F. O. Schmitt, Ed., Rockefeller

- Univ. Press, New York, 1970.
- 134 P. B. Chock, *Proc. Natl. Acad. Sci. U.S.A.*, 1972, **69**, 1939.
- 135 G. W. Liesegang, M. M. Farrow, A. Vazquez, N. Purdie, and E. M. Eyring, *J. Am. Chem. Soc.*, 1977, **99**, 3240.
- 136 J. M. Lehn, *Pure Appl. Chem.*, 1979, **51**, 979.
- 137 C. H. Park and H. E. Simmons, *J. Am. Chem. Soc.*, 1968, **90**, 2428.
- 138 J. M. Lehn, J. P. Sauvage, and B. Dietrich, *J. Am. Chem. Soc.*, 1970, **92**, 2916.
- 139 J. M. Lehn, J. Simon, and J. Wagner, *Angew. Chem., Int. Ed. Engl.*, 1973, **12**, 578.
- 140 V. M. Loyola, R. G. Wilkins, and R. Pizer, *J. Am. Chem. Soc.*, 1975, **97**, 7382.
- 141 B. Liang and C. Chung, *Inorg. Chem.*, 1981, **20**, 2152.
- 142 B. Liang and C. Chung, *Inorg. Chem.*, 1983, **22**, 1017.
- 143 J. Chen, D. Wu, and C. Chung, *Inorg. Chem.*, 1986, **25**, 1940.
- 144 R. Clay, J. Murray-Rust, and P. Murray-Rust, *J. Chem. Soc., Dalton Trans.*, 1979, 1135.
- 145 L. Chen and C. Chung, *Inorg. Chem.*, 1988, **27**, 1880.
- 146 R. A. Read and D. W. Margerum, *Inorg. Chem.*, 1981, **20**, 3143.
- 147 P. G. Graham and D. C. Weatherburn, *Aust. J. Chem.*, 1981, **34**, 291.
- 148 P. G. Graham and D. C. Weatherburn, *Aust. J. Chem.*, 1984, **37**, 2243.
- 149 L. J. Murphy, Jr., and L. J. Zompa, *Inorg. Chem.*, 1979, **18**, 3278.
- 150 R. F. Childers and R. A. D. Wentworth, *Inorg. Chem.*, 1969, **8**, 2218.
- 151 L. J. Zompa and T. N. Margulis, *Inorg. Chim. Acta*, 1978, **28**, L157.
- 152 L. J. Zompa, *Inorg. Chem.*, 1978, **17**, 2531.
- 153 R. W. Hay, R. Bembi, W. T. Moodie, and P. R. Norman, *J. Chem. Soc., Dalton Trans.*, 1982, 2131.
- 154 R. W. Hay, R. Bembi, F. McLaren, and W. T. Moodie, *Inorg. Chim. Acta*, 1984, **85**, 23.
- 155 N. F. Curtis and S. R. Osvath, *Inorg. Chem.*, 1988, **27**, 306.
- 156 R. W. Hay and R. Bembi, *Inorg. Chim. Acta*, 1982, **62**, 89.

- 157 D. A. Buckingham, D. M. Foster, and A. M. Sargeson, *J. Am. Chem. Soc.*, 1969, **91**, 3451.
- 158 M. T. Barnet, H. C. Freeman, D. A. Buckingham, I. Hsu, and D. van der Helm, *J. Chem. Soc., Chem. Commun.*, 1970, 367.
- 159 A. Ekstrom, L. F. Lindoy, and R. J. Smith, *Inorg. Chem.*, 1980, **19**, 724.
- 160 K. R. Adam, L. F. Lindoy, R. J. Smith, G. Anderegg, K. Henrick, M. McPartlin, and P. A. Tasker, *J. Chem. Soc., Chem. Commun.*, 1979, 812.
- 161 F. Wagner and E. K. Barefield, *Inorg. Chem.*, 1976, **15**, 408.
- 162 D. K. Cabbiness and D. W. Margerum, *J. Am. Chem. Soc.*, 1969, **91**, 6540.
- 163 A. E. Martell, *Adv. Chem. Ser.*, 1967, **62**, 272.
- 164 R. T. Meyers, *Inorg. Chem.*, 1978, **17**, 952.
- 165 F. A. Cotton and G. Wilkinson, *Advanced Inorganic Chemistry*, 4th Edn., John Wiley and Sons, Inc., New York, 1980, 72.
- 166 P. O. Whimp, M. F. Bailey, and N. F. Curtis, *J. Chem. Soc. (A)*, 1970, 1956.
- 167 F. P. Hinz and D. W. Margerum, *J. Am. Chem. Soc.*, 1974, **96**, 4993.
- 168 F. P. Hinz and D. W. Margerum, *Inorg. Chem.*, 1974, **13**, 2941.
- 169 G. R. Hedwig, J. L. Love, and H. K. J. Powell, *Aust. J. Chem.*, 1970, **23**, 981.
- 170 A. Dei and R. Gori, *Inorg. Chim. Acta*, 1975, **14**, 157.
- 171 A. Anichini, L. Fabbri, P. Paoletti, and R. M. Clay, *J. Chem. Soc., Chem. Commun.*, 1977, 244.
- 172 A. Anichini, L. Fabbri, P. Paoletti, and R. M. Clay, *Inorg. Chim. Acta*, 1977, **22**, L25.
- 173 A. Anichini, L. Fabbri, P. Paoletti, and R. M. Clay, *J. Chem. Soc., Dalton Trans.*, 1978, 577.
- 174 L. Fabbri, M. Micheloni, and P. Paoletti, *J. Chem. Soc., Dalton Trans.*, 1979, 1581.
- 175 L. Fabbri, P. Paoletti, and R. M. Clay, *Inorg. Chem.*, 1978, **17**, 1042.
- 176 R. M. Clay, M. Micheloni, P. Paoletti, and W. V. Steele, *J. Am. Chem. Soc.*, 1979, **101**, 4119.

- 177 R. D. Hancock and M. P. Ngwenya, *J. Chem. Soc., Dalton Trans.*, 1987, 2911.
- 178 M. Kodama and E. Kimura, *J. Chem. Soc., Dalton Trans.*, 1978, 1081.
- 179 M. Micheloni, P. Paoletti, L. Siegfried-Hertli, and T. A. Kaden, *J. Chem. Soc., Dalton Trans.*, 1985, 1169.
- 180 L. S. W. L. Sokol, L. A. Ochrymowycz, and D. B. Rorabacher, *Inorg. Chem.*, 1981, **20**, 3189.
- 181 L. L. Diaddario, PhD dissertation, Wayne State University, 1979.
- 182 R. D. Hancock and A. E. Martell, *Comments Inorg. Chem.*, 1988, **6**, 237.
- 183 K. Burger, *Solvation, Ionic, and Complex Formation Reactions in Non-Aqueous Solvents*, Elsevier, Amsterdam, 1983.
- 184 O. Popovych and R. P. T. Tomkins, *Non-Aqueous Solution Chemistry*, John Wiley and Sons, Inc., New York, 1981.
- 185 N. M. Karayannis, C. Owens, L. L. Pytlewski, and M. M. Labes, *J. Inorg. Nucl. Chem.*, 1969, **31**, 2059.
- 186 J. Selbin, W. E. Bull, and L. H. Holmes, *J. Inorg. Nucl. Chem.*, 1961, **16**, 219.
- 187 N. M. Karayannis, C. Owens, L. L. Pytlewski, and M. M. Labes, *J. Inorg. Nucl. Chem.*, 1969, **31**, 2059.
- 188 W. L. Reynolds, *Prog. Inorg. Chem.*, 1970, **12**, 1.
- 189 M. Elleb, J. Meullemeestre, M. Schwing-Weill, and F. Vierling, *Inorg. Chem.*, 1982, **21**, 1477.
- 190 G. S. Vigeo and P. Ng, *J. Inorg. Nucl. Chem.*, 1971, **33**, 2477.
- 191 C. L. Watkins and G. S. Vigeo, *J. Phys. Chem.*, 1976, **80**, 83.
- 192 S. Ishiguro, H. Suzuki, B. G. Jeliakova, and H. Ohtaki, *Bull. Chem. Soc. Jpn.*, 1989, **62**, 39.
- 193 S. A. Al-Baldawi and T. E. Gough, *Can. J. Chem.*, 1969, **47**, 1417.
- 194 D. M. W. Buck and P. Moore, *J. Chem. Soc., Dalton Trans.*, 1976, 638.
- 195 H. B. Silber, L. U. Kromer, and F. Gaizer, *Inorg. Chem.*, 1981, **20**, 3323.
- 196 D. D. Perrin, W. L. F. Armarego, and D. R. Perrin, *Purification of Laboratory Chemicals*, Pergamon Press, Oxford, 1980.

- 197 W. O. Gilmour, PhD thesis, University of Warwick, 1980.
- 198 G. Schwarzenbach and H. Flaschka, *Complexometric Titrations*, Methuen and Co. Ltd., London, 1969.
- 199 J. Bassett, R. C. Denney, G. H. Jeffery, and J. Mendham, *Vogel's Textbook of Quantitative Inorganic Analysis*, Longman, London, 1978.
- 200 E. K. Barefield, F. Wagner, A. W. Herlinger, and A. R. Dahl, *Inorg. Synth.*, 1976, **16**, 220.
- 201 J. E. Richman and T. J. Atkins, *J. Am. Chem. Soc.*, 1974, **96**, 2268.
- 202 H. Koyama and T. Yoshino, *Bull. Chem. Soc. Jpn.*, 1972, **45**, 481.
- 203 J. H. Espenson, *Chemical Kinetics and Reaction Mechanisms*, McGraw-Hill, Inc., New York, 1981.
- 204 E. S. Swinbourne, *J. Chem. Soc.*, 1960, 2371.
- 205 P. Moore and S. Moore, University of Warwick, 1986.
- 206 Apple Corp. Inc., 1979.
- 207 D. W. Marquardt, *J. Soc. Ind. Appl. Math.*, 1963, **11**, 431.
- 208 C. Wong, J. A. Switzer, K. P. Balakrishnan, and J. F. Endicott, *J. Am. Chem. Soc.*, 1980, **102**, 5511.
- 209 R. Machida, E. Kimura, and M. Kodama, *Inorg. Chem.*, 1983, **22**, 2055.
- 210 S. Fallab and P. R. Mitchell, *Adv. Inorg. Bioinorg. Mech.*, Vol. 3, A. G. Sykes, Ed., Academic Press, 1984.
- 211 S. Minakami, *Igaku No Ayumi*, 1965, **54**, 551.
- 212 V. Gutmann, *Rec. Chem. Progr.*, 1969, **30**, 171.
- 213 J. Williams, S. Petrucci, B. Sesta, and M. Battishini, *Inorg. Chem.*, 1974, **13**, 1968.
- 214 W. J. MacKellar and D. B. Rorabacher, *J. Am. Chem. Soc.*, 1971, **93**, 4379.
- 215 S. Thomas and W. L. Reynolds, *J. Chem. Phys.*, 1967, **46**, 4164.
- 216 S. Blackstaffe and R. A. Dwek, *Mol. Phys.*, 1968, **15**, 279.
- 217 N. S. Angerman and R. B. Jordan, *Inorg. Chem.*, 1969, **8**, 2579.
- 218 L. S. Frankel, *Inorg. Chem.*, 1971, **10**, 814.

- 219 C. H. McAteer, PhD thesis, University of Warwick, 1981.
- 220 T. J. Swift and R. E. Connick, *J. Chem. Phys.*, 1962, 37, 307.
- 221 T. S. Roche and R. G. Wilkins, *J. Am. Chem. Soc.*, 1974, 96, 5082.
- 222 R. W. Hay and C. R. Clark, *J. Chem. Soc., Dalton Trans.*, 1977, 1148.
- 223 A. Anichini, L. Fabbrizzi, P. Paoletti, and R. M. Clay, *Inorg. Chim. Acta*, 1977, 24, L21.
- 224 G. S. Vigee, C. L. Watkins, and H. F. Bowen, *Inorg. Chim. Acta*, 1979, 35, 255.
- 225 N. Heron and P. Moore, *Inorg. Chim. Acta*, 1979, 36, 89.
- 226 E. J. Billo, *Inorg. Chem.*, 1981, 20, 4019.
- 227 H. Stetter and W. Frank, *Angew. Chem., Int. Ed. Engl.*, 1976, 15, 686.
- 228 J. F. Pilichowski, J. M. Lehn, J. P. Sauvage, and J. C. Gramain, *Tetrahedron*, 1985, 41, 1959.
- 229 T. J. Lotz and T. A. Kaden, *J. Chem. Soc., Chem. Commun.*, 1977, 15.
- 230 T. J. Lotz and T. A. Kaden, *Helv Chim. Acta*, 1978, 61, 1376.
- 231 Y. Itaka, T. Koike, and E. Kimura, *Inorg. Chem.*, 1986, 25, 402.
- 232 T. A. Kaden, *Pure Appl. Chem.*, 1988, 60, 1117.
- 233 D. Tschudin and T. A. Kaden, *Pure Appl. Chem.*, 1988, 60, 489.
- 234 D. Tschudin, A. Riesen, and T. A. Kaden, *Helv Chim. Acta*, 1989, 72, 131.
- 235 S. P. Kasprzyk and R. G. Wilkins, *Inorg. Chem.*, 1982, 21, 3349.
- 236 C. M. Madeyski, J. P. Michael, and R. D. Hancock, *Inorg. Chem.*, 1984, 23, 1487.
- 237 E. Kimura, T. Koike, M. Yamaoka, and M. Kodama, *J. Chem. Soc., Chem. Commun.*, 1985, 1341.
- 238 D. A. Buckingham, C. R. Clark, and W. S. Webley, *J. Chem. Soc., Chem. Commun.*, 1981, 192.
- 239 H. Hafliger and T. A. Kaden, *Helv Chim. Acta*, 1979, 62, 683.
- 240 B. S. Nakani, J. J. B. Welsh, and R. D. Hancock, *Inorg. Chem.*, 1983, 22, 2956.
- 241 R. W. Hay, M. P. Pujari, W. T. Moodie, S. Craig, D. T. Richens, A. Perotti, and L. Ungaretti, *J. Chem. Soc., Dalton Trans.*, 1987, 2605.

- 242 N. W. Alcock, F. McLaren, P. Moore, G. A. Pike, and S. M. Roe, *J. Chem. Soc., Chem. Commun.*, 1989, 629.
- 243 J. C. Boubel and J. J. Delpuech, *Adv. Mol. Relaxation Processes*, 1975, 7, 209.
- 244 P. Moore and D. M. W. Buck, *J. Chem. Soc., Dalton Trans.*, 1973, 1602.
- 245 F. A. Cotton and R. Francis, *J. Am. Chem. Soc.*, 1960, 82, 2986.
- 246 R. G. Wilkins, *The Study of Kinetics and Mechanism of Reactions of Transition Metal Complexes*, Allyn and Bacon, 1974, Boston.
- 247 R. G. Wilkins, R. Yelin, D. W. Margerum, and D. C. Weatherburn, *J. Am. Chem. Soc.*, 1969, 91, 4326.
- 248 K. J. Ivin, R. Jamison, and J. J. McGarvey, *J. Am. Chem. Soc.*, 1972, 94, 1764.
- 249 C. Creutz and N. Sutin, *J. Am. Chem. Soc.*, 1973, 95, 7177.
- 250 W. R. McWhinnie and J. D. Miller, *Adv. Inorg. Chem. Radiochem.*, 1969, 12, 135.
- 251 N. W. Alcock, K. P. Balakrishnan, P. Moore, and G. A. Pike, *J. Chem. Soc., Dalton Trans.*, 1987, 889.
- 252 N. W. Alcock, P. Moore, and H. A. A. Omar, *J. Chem. Soc., Dalton Trans.*, 1986, 985.
- 253 N. W. Alcock, P. Moore, and H. A. A. Omar, *J. Chem. Soc., Dalton Trans.*, 1987, 1107.
- 254 A. J. Blake, R. O. Gould, T. I. Hyde, and M. Schroder, *Acta Crystallogr.*, 1988, C44, 1325.
- 255 K. A. Foster, E. K. Barefield, and D. G. Van Derveer, *J. Chem. Soc., Chem. Commun.*, 1986, 680.
- 256 N. W. Alcock, P. Moore, and C. Pierpoint, *J. Chem. Soc., Dalton Trans.*, 1984, 2371.
- 257 D. B. Moss, C. Lin, and D. B. Rorabacher, *J. Am. Chem. Soc.*, 1973, 95, 5179.
- 258 M. G. B. Drew, D. A. Rice, S. bin Silong, and P. C. Yates, *J. Chem. Soc., Dalton Trans.*, 1986, 1081.
- 259 N. W. Alcock, R. G. Kingston, P. Moore, and C. Pierpoint, *J. Chem. Soc., Dal-*

- ton Trans., 1984, 1937.
- 260 N. W. Alcock, K. P. Balakrishnan, P. Moore, and H. A. A. Omar, *J. Chem. Soc., Dalton Trans.*, 1987, 545.
- 261 T. J. Lotz and T. A. Kaden, *Helv Chim. Acta*, 1978, 61, 1376.
- 262 N. W. Alcock, K. P. Balakrishnan, A. Berry, P. Moore, and C. J. Reader, *J. Chem. Soc., Dalton Trans.*, 1988, 1089.
- 263 N. W. Alcock, P. Moore, and H. A. A. Omar, *J. Chem. Soc., Chem. Commun.*, 1985, 1058.
- 264 N. W. Alcock, P. Moore, H. A. A. Omar, and C. J. Reader, *J. Chem. Soc., Dalton Trans.*, 1987, 2643.
- 265 N. W. Alcock, P. Moore, C. J. Reader, and S. M. Roe, *J. Chem. Soc., Dalton Trans.*, 1988, 2959.
- 266 E. J. Corey and A. Venkateswarlu, *J. Am. Chem. Soc.*, 1972, 94, 6190.
- 267 P. Tundo, *J. Chem. Soc., Chem. Commun.*, 1977, 641.
- 268 D. E. Leyden and G. H. Luttrell, *Anal. Chem.*, 1975, 47, 1612.
- 269 P. W. Carr and L. D. Bowers, *Immobilized Enzymes in Analytical and Clinical Chemistry*, Wiley, New York, 1980.
- 270 J. R. Jezorek and H. Freiser, *Anal. Chem.*, 1979, 51, 366.
- 271 R. E. Sturgeon, S. S. Berman, S. N. Willie, and J. A. H. Desaulniers, *Anal. Chem.*, 1981, 53, 2337.
- 272 M. Novotny, *Bonded Stationary Phases in Chromatography*, E. Grushka, Ed., Ann Arbor Science, New York, 1974.
- 273 D. C. Bookbinder, J. A. Bruce, R. N. Dominey, N. S. Lewis, and M. S. Wrighton, *Proc. Natl. Acad. Sci. U.S.A.*, 1980, 77, 6280.
- 274 D. E. Leyden and W. Collins (Eds.), *Silylated Surfaces*, Gordon and Breach, New York, 1980.
- 275 S. P. Boudreau and W. T. Cooper, *Anal. Chem.*, 1987, 59, 353.
- 276 S. P. Boudreau and W. T. Cooper, *Anal. Chem.*, 1989, 61, 41.
- 277 L. R. Snyder, *Principles of Adsorption Chromatography*, Dekker, New York,

1968.

- 278 K. K. Unger, *Porous Silica, Its Properties and Uses as a Support in Liquid Chromatography*, *Journal of Chromatography Library Vol. 16*, Elsevier, New York, 1979.
- 279 S. Kondo, H. Yamauchi, Y. Kajiyama, and T. Ishikawa, *J. Chem. Soc., Faraday Trans. I*, 1984, **80**, 2033.
- 280 G. E. Maciel and D. W. Sindorf, *J. Am. Chem. Soc.*, 1980, **102**, 7606.
- 281 S. Kondo and M. Muroya, *Bull. Chem. Soc. Jpn.*, 1974, **47**, 553.
- 282 S. Kondo, K. Tomoi, and C. Pak, *Bull. Chem. Soc. Jpn.*, 1979, **52**, 2046.
- 283 S. Kondo, H. Fujiwara, and M. Muroya, *J. Colloid Interface Sci.*, 1976, **55**, 421.
- 284 S. Kondo, H. Fujiwara, T. Ichii, and I. Tsuboi, *J. Chem. Soc., Faraday Trans. I*, 1979, **75**, 646.
- 285 C. E. Bronnimann, R. C. Zeigler, and G. E. Maciel, *J. Am. Chem. Soc.*, 1988, **110**, 2023.
- 286 J. J. Fripiat and J. Uytterhoeven, *J. Phys. Chem.*, 1962, **66**, 800.
- 287 J. Uytterhoeven, M. Sleex, and J. J. Fripiat, *Bull. Soc. Chim. Fr.*, 1965, 1800.
- 288 L. T. Zhuravlev, A. V. Kiselev, V. P. Naidina, and A. L. Polyakov, *Russ. J. Phys. Chem.*, 1963, **37**, 1113.
- 289 V. Ya. Davydov, A. V. Kiselev, and S. A. Kiselev, *Kolloid Zhur.*, 1979, **41**, 227.
- 290 V. Ya. Davydov, A. V. Kiselev, H. Pfeifer, and I. Junger, *Russ. J. Phys. Chem.*, 1983, **57**, 1527.
- 291 D. W. Sindorf and G. E. Maciel, *J. Phys. Chem.*, 1983, **87**, 5516.
- 292 D. W. Sindorf and G. E. Maciel, *J. Am. Chem. Soc.*, 1983, **105**, 1487.
- 293 D. W. Sindorf and G. E. Maciel, *J. Phys. Chem.*, 1982, **86**, 5208.
- 294 C. A. Fyfe, G. C. Gobbi, and G. J. Kennedy, *J. Phys. Chem.*, 1985, **89**, 277.
- 295 L. Boksanyi, O. Liardon, and E. Kovats, *Adv. Colloid Interface Sci.*, 1976, **6**, 95.
- 296 A. C. Zettlemoyer and H. H. Hsing, *J. Colloid Interface Sci.*, 1977, **58**, 263.
- 297 R. P. W. Scott, *J. Chromatogr. Sci.*, 1980, **18**, 297.
- 298 A. V. Volkov, A. V. Kiselev, and V. I. Lygin, *Zh. Fiz. Khim.*, 1974, **48**, 1214.

- 299 R. K. Iler, *The Chemistry of Silica, Solubility, Polymerisation, and Surface Properties and Biochemistry*, Wiley, New York, 1979.
- 300 A. A. Agzamkhodzhaev, L. T. Zhuravlev, A. V. Kiselev, and K. Ya. Shengeliya, *Kolloidn. Zh.*, 1974, **36**, 1145.
- 301 G. J. Young, *J. Colloid Sci.*, 1958, **13**, 67.
- 302 J. El Rassi and C. Gonnet, *J. Liq. Chromatogr.*, 1980, **3**, 179.
- 303 C. Frondel, *The System of Mineralogy of Dana*, 7th Ed., Wiley, New York, 1962, Vol. 3 (Silica Minerals), 154.
- 304 J. H. DeBoer and J. M. Vleeskins, *Proc. K. Ned. Akad. Wet., Ser. b, Palaentol., Geol., Phys., Chem.*, 1958, **B61**, 85.
- 305 J. A. Hockey, *Chem. Ind. (London)*, 1965, 57.
- 306 J. B. Peri and A. L. Hensley, Jr., *J. Phys. Chem.*, 1968, **72**, 2926.
- 307 H. A. Bebesi and B. H. C. Winquist, *Adv. Catal.*, 1978, **27**, 98.
- 308 R. Kummert and W. Stumm, *J. Colloid Interface Sci.*, 1980, **75**, 373.
- 309 A. C. M. Bourg, S. Joss, and P. W. Schindler, *Chimia*, 1979, **33**, 19.
- 310 A. C. M. Bourg and P. W. Schindler, *Inorg. Nucl. Chem. Lett.*, 1979, **15**, 225.
- 311 A. von Zelesky and J. M. Bemtgen, *Inorg. Chem.*, 1982, **21**, 1771.
- 312 F. J. Karol, C. Wu, W. T. Reichle, and N. J. Maraschin, *J. Catal.*, 1979, **60**, 68.
- 313 D. C. Bailey and S. H. Langer, *Chem. Rev.*, 1981, **81**, 109.
- 314 J. Evans, *Chem. Soc. Rev.*, 1981, **10**, 159.
- 315 F. R. Hartley, *Supported Metal Complexes*, Reidel, Holland, 1985.
- 316 Y. Iwasawa (Ed.), *Tailored Metal Catalysts*, Reidel, Holland, 1986.
- 317 J. M. Moreto, J. Albaiges, and P. Camps in, 'Catalysis: Homogeneous and Heterogeneous', Ed. B. Delmon and G. Jannes, Elsevier, Amsterdam, 1975, 339.
- 318 M. K. Neuberg, *Diss. Abs.*, 1979, **B39**, 5929.
- 319 V. A. Semikolenov, D. Mikhailova, and J. W. Sobczak, *React. Kinet. Catal. Lett.*, 1979, **10**, 105.
- 320 S. Lamalle, H. Mortreux, M. Evrard, F. Petit, J. Grimblot, and J. P. Bonnelle, *J. Mol. Catal.*, 1979, **6**, 11.

- 321 J. M. Hill, *J. Chromatogr.*, 1973, 76, 455.
- 322 R. E. Sturgeon, S. S. Berman, A. Desautniers, and D. S. Russel, *Talanta*, 1980, 27, 85.
- 323 E. J. R. Sudhiter, R. Huis, G. R. Hays, and N. C. M. Alta, *J. Colloid Interface Sci.*, 1985, 103, 554.
- 324 S. Shinoda and Y. Saito, *J. Colloid Interface Sci.*, 1982, 89, 293.
- 325 F. J. Boerio and J. W. Williams, *Appl. Surf. Sci.*, 1981, 7, 19.
- 326 R. S. Davidson, W. J. Lough, S. A. Matlin, and C. L. Morrison, *J. Chem. Soc., Chem. Commun.*, 1981, 517.
- 327 D. W. Sindorf and G. E. Maciel, *J. Am. Chem. Soc.*, 1983, 105, 3767.
- 328 T. G. Waddell, D. E. Leyden, and M. T. DeBello, *J. Am. Chem. Soc.*, 1981, 103, 5303.
- 329 J. W. DeHaan, H. M. Van Den Bogaert, J. J. Ponjae, and L. J. M. Van de Ven, *J. Colloid Interface Sci.*, 1986, 110, 591.
- 330 D. E. Leyden, D. S. Ken, *J. Chem. Soc., Dalton Trans.*, L. W. Burggraf, F. J. Pern, and M. DeBello, *Anal. Chem.*, 1982, 54, 101.
- 331 G. D. Shields and L. J. Boucher, *J. Inorg. Nucl. Chem.*, 1978, 40, 1341.
- 332 P. M. Solozhenkin, A. I. Semikopyri, V. Z. Shart, and G. V. Lisichkin, *Russ. J. Phys. Chem.*, 1988, 62, 218.
- 333 S. Shinoda and Y. Saito, *Inorg. Chim. Acta*, 1982, 63, 23.
- 334 Y. Gushikem and J. C. Moreira, *J. Colloid Interface Sci.*, 1984, 70.
- 335 P. C. Hiemenz, *Principles of Colloid and Surface Chemistry*, Dekker, New York, 1977.
- 336 I. M. Kolthoff, *Anal. Chem.*, 1979, 51, 1R.
- 337 M. Takagi and H. Nakamura, *J. Coord. Chem.*, 1986, 15, 53.
- 338 M. Nakajima, K. Kimura, and T. Shono, *Anal. Chem.*, 1983, 55, 463.
- 339 G. Donevi, G. D. Y. Sogah, and D. J. Cram, *J. Am. Chem. Soc.*, 1975, 97, 1259.
- 340 J. S. Bradshaw, R. L. Bruening, K. E. Krakowiack, B. J. Tarbet, M. L. Bruening, R. M. Izatt, and J. J. Christensen, *J. Chem. Soc., Chem. Commun.*, 1988,

- 341 J. S. Bradshaw, K. E. Krakowiak, R. L. Bruening, B. J. Tarbet, P. B. Savage, and R. M. Izatt, *J. Org. Chem.*, 1988, 53, 3190.
- 342 V. Dudler, I. F. Lindoy, D. Sallin, and C. W. Schlaepfer, *Aust. J. Chem.*, 1987, 40, 1557.
- 343 R. S. Paredes, N. S. Valera, and L. F. Lindoy, *Aust. J. Chem.*, 1986, 39, 1071.
- 344 O. Leal, D. L. Anderson, R. G. Bowman, F. Basolo, and R. L. Burwell, Jr., *J. Am. Chem. Soc.*, 1975, 97, 5125.
- 345 M. R. Weaver and J. M. Harris, *Anal. Chem.*, 1989, 61, 1001.
- 346 E. Papp and G. Vigh, *J. Chromatogr.*, 1983, 259, 49.
- 347 I. S. Khatib and R. V. Parish, *J. Organomet. Chem.*, 1989, 2, 369.
- 348 M. A. Marshall and H. A. Mottola, *Anal. Chem.*, 1983, 55, 2089.
- 349 A. A. Audu, *Reactive Polymers*, 1989, 10, 3.
- 350 B. J. Hathaway and A. A. G. Tomlinson, *Coord. Chem. Rev.*, 1970, 5, 1.
- 351 R. Kuroda, S. F. Mason, T. Prosperi, S. Savage, and G. E. Tranter, *J. Chem. Soc., Dalton Trans.*, 1981, 2565.
- 352 J. Katzhendler, S. Cohen, E. Rahamim, M. Weisz, I. Ringel, and J. Deutsch, *Tetrahedron*, 1989, 45, 2777.

D94923